

University of Alberta

**Rapid SAGD Simulation  
Considering Geomechanics for  
Closed Loop Reservoir Optimization**

by

Ali Azad

A thesis submitted to the Faculty of Graduate Studies and Research  
in partial fulfillment of the requirements for the degree of

Doctor of Philosophy

in

Geotechnical Engineering

Civil and Environmental Engineering Department

©Ali Azad  
Spring 2012  
Edmonton, Alberta

Permission is hereby granted to the University of Alberta Libraries to reproduce single copies of this thesis and to lend or sell such copies for private, scholarly or scientific research purposes only. Where the thesis is converted to, or otherwise made available in digital form, the University of Alberta will advise potential users of the thesis of these terms.

The author reserves all other publication and other rights in association with the copyright in the thesis and, except as herein before provided, neither the thesis nor any substantial portion thereof may be printed or otherwise reproduced in any material form whatsoever without the author's prior written permission.

To IRAN

## ABSTRACT

While numerical modeling and coupling techniques have been continuously studied, analytical solution or proxy modeling for geomechanical coupling of the steam assisted gravity drainage (SAGD) has not been clearly addressed in the literature. Simulations aside, there is no particular study on the use of geomechanics in closed loop reservoir optimization. Past studies have focused mostly on two separate research areas: (a) SAGD and geomechanics and (b) intelligent optimization algorithms for smart fields.

This research has been carried out to cover two major objectives; providing a low order model to work with real-time data, and also investigating high-resolution geomechanical-flow simulation to work with data assimilation algorithms for history matching and reservoir characterization.

As the first step, a physics-based semi-analytical model was proposed based on the original Butler/Reis SAGD theory. The model was proposed for linear steam chamber geometry by modifying the variation of oil saturation in advance of the steam chamber. The model was then verified with the past experimental lab test results and numerical simulation results. Geomechanics was incorporated using the classical limit equilibrium theory. Although the results of the linear geometry model with geomechanical consideration are promising for the available case studies, application of such a theory needs to be further investigated and improved.

The linear geometry model was then replaced by circular geometry model to better simulate the rising and depletion stages of SAGD process. For the circular geometry model, a multiplier coefficient was defined to consider geomechanics called the geomechanical impact factor (GIF). Based on the results from a numerical study, GIF can be effectively employed for the variation in rock properties such as permeability and porosity. The final version of the proposed model was used for history matching two SAGD projects, UTF phases A and B. The results show that the proposed physics-based analytical proxy generally captures the physics of the problem in low order but a very fast fashion procedure.

The application of analytical models in automated history matching and reservoir characterization was further investigated using the extended Kalman filter (EKF). For this case, Butler/Reis theory and the GIF concept were combined with the EKF for history matching the heterogeneous reservoirs with uncertainty. Using synthetic data and stochastic reservoir realizations, it was shown how analytical models are helpful in reservoir characterization.

While the analytical solution is placed at the centre of the optimization process, the second objective of this research was explored by applying the ensemble Kalman filter (EnKF) to link monitoring data to the simulator(s). For this reason, an iterative geomechanical-flow coupling code was developed and assembled with the EnKF. Through numerical simulations using synthetically generated data, the significance of considering geomechanical monitoring data in reservoir surveillance was examined. It was observed that proper coupled simulation mimics larger portion of the real physics of SAGD process, and as a result, geomechanical observations can add value to facilitate the data assimilation algorithms.

## ACKNOWLEDGMENTS

The author gratefully acknowledges the guidance and insight given by his smart supervisor Prof. Rick Chalaturnyk. His continuous support from the very beginning of the research when the topic was finalized up to my departure from Edmonton is warmly appreciated.

I would like to thank some other people at the University of Alberta who have been my support directly or indirectly during the last five years: Steve Gamble, Ann Jones, Prof. Clayton Deutsch, Dr. Oy Leuangthong, and Hope Walls. I thank my friend and colleague Nathan Deisman who generously spent his time on reviewing some of my papers. The many discussions with Sahar Movaghati helped with understanding the fundamentals of the Kalman filter theory. Thank you for your time and valuable advice.

I owe thanks to my family, my parents, sister and brother, who encouraged me so much remotely from Iran and helped me out with their positive energy and financial aids. I could have never finished my graduate studies without their support. Thank you a lot!

# TABLE OF CONTENTS

<b>CHAPTER 1:INTRODUCTION .....</b>	<b>1</b>
INTRODUCTION.....	1
DIFFERENT OPTIMIZATION LOOPS IN A SMART FIELD .....	2
RESEARCH MOTIVATION .....	3
RESEARCH OBJECTIVE .....	4
SCOPE OF RESEARCH.....	4
RESEARCH METHODOLOGY.....	4
ANALYTICAL SOLUTION STUDY .....	5
GEOTECHNICAL DATA ASSIMILATION.....	7
STRUCTURE OF DISSERTATION .....	8
<b>CHAPTER 2:A MATHEMATICAL IMPROVEMENT TO SAGD USING GEOMECHANICAL MODELING 10</b>	
ABSTRACT.....	10
INTRODUCTION.....	11
DRAINAGE MODEL .....	12
PREVIOUS WORKS BY BUTLER AND REIS .....	12
MODIFIED DRAINAGE MODEL – MODEL OF SLICES.....	14
ENERGY BALANCE TO CALCULATE STEAM INJECTION RATE .....	16
LINEAR GEOMECHANICAL SAGD (LGS) MODEL .....	17
LIMIT EQUILIBRIUM ANALYSIS TECHNIQUE.....	18
FORMULATION .....	19
AVERAGE VOLUMETRIC STRAIN .....	19
SHEAR-INDUCED DILATION.....	22
VALIDATION OF THE MODEL OF SLICES .....	24
HISTORY MATCHING BY LGS MODEL .....	27
CONCLUSION.....	33
REFERENCES .....	33
APPENDIX A: MODEL OF SLICES .....	35
<b>CHAPTER 3:AN IMPROVED SAGD ANALYTICAL SIMULATOR: CIRCULAR STEAM CHAMBER GEOMETRY .....</b>	<b>37</b>
ABSTRACT.....	37
INTRODUCTION.....	38
METHOD OF SLICES .....	41

ANALYTICAL MODEL FOR CIRCULAR GEOMETRY .....	44
DRAINAGE THEORY.....	44
MATERIAL BALANCE .....	47
ENERGY BALANCE .....	48
INITIAL CONDITIONS .....	49
MODEL VALIDATION: EXPERIMENTAL DATA.....	50
MODEL VALIDATION: NUMERICAL SIMULATION .....	51
REVIEW AND DISCUSSION ON PRACTICAL ASPECTS OF THE PROPOSED MODEL .....	55
CONCLUSIONS .....	56
ACKNOWLEDGEMENTS .....	57
REFERENCES .....	57
APPENDIX A: INITIAL CONDITION .....	58
<b>CHAPTER 4:APPLICATION OF ANALYTICAL PROXY MODELS IN FAST HISTORY</b>	
<b>MATCHING FOR SAGD PROCESS: UTF PROJECT CASE STUDY .....</b>	<b>60</b>
ABSTRACT.....	60
INTRODUCTION.....	61
PROXY MODELLING AND ANALYTICAL SOLUTIONS .....	63
SAGD ANALYTICAL MODELS.....	64
HOW ANALYTICAL MODELS PREDICT .....	66
GEOMECHANICS AND SAGD.....	68
UNDERGROUND TEST FACILITY (UTF) - DOVER PROJECT .....	71
UTF PHASE A AND B ANALYTICAL SIMULATION.....	75
HISTORY MATCHING RESULTS .....	79
STEAM CHAMBER LOCATION .....	80
SUMMARY AND CONCLUSIONS .....	81
REFERENCES .....	82
APPENDIX A .....	84
<b>CHAPTER 5:NUMERICAL STUDY OF SAGD: GEOMECHANICAL-FLOW COUPLING</b>	
<b>FOR ATHABASCA OIL SANDS RESERVOIRS .....</b>	<b>86</b>
ABSTRACT.....	86
INTRODUCTION.....	87
STEAM ASSISTED GRAVITY DRAINAGE (SAGD).....	89
GEOMECHANICAL-FLOW COUPLING .....	90
IN-SITU STRESS ARRANGEMENT IN ATHABASCA OIL SAND RESERVOIR.....	92
MODELS AND OPERATION STRATEGY .....	93
MATERIAL AND FLUID PROPERTIES.....	95

RESULTS – OIL PRODUCTION AND STEAM/OIL RATIO .....	98
RESULTS – DISPLACEMENT WITHIN THE RESERVOIR .....	103
RESULTS – STEAM CHAMBER GROWTH.....	105
RESULTS – SURFACE HEAVE HISTORY .....	106
RESULTS – GEOMECHANICAL EFFECTS WITHIN THE RESERVOIR .....	108
RESULTS – COMPUTATIONAL EFFORT .....	113
GEOMECHANICAL IMPACT FACTOR (GIF) .....	113
CONCLUSION AND DISCUSSION .....	117
ACKNOWLEDGEMENTS .....	119
REFERENCES .....	119
<b>CHAPTER 6: REAL-TIME RESERVOIR MODEL UPDATING IN THERMAL RECOVERY: APPLICATION OF ANALYTICAL PROXIES AND KALMAN FILTERING .....</b>	<b>121</b>
ABSTRACT.....	121
INTRODUCTION.....	122
SAGD – THERMAL RECOVERY PROCESS .....	123
SAGD UNIFIED DRAINAGE (FLOW) PROXY .....	125
EXPERIMENTAL LAB TEST RESULTS.....	127
RESULTS OF NUMERICAL SIMULATION.....	130
GEOMECHANICAL CONSIDERATIONS.....	131
METHODOLOGY.....	133
CASE STUDY: SHALLOW SAGD.....	136
PERMEABILITY AND POROSITY STOCHASTIC MODELLING.....	136
OBSERVATION DATA – REFERENCE NUMERICAL SIMULATION .....	138
EVALUATING UNCERTAINTY IN STOCHASTIC MODELS .....	140
RANKING THE MODELS – TRACKING THE REFERENCE MODEL.....	141
DATA ASSIMILATION – DYNAMIC MODEL UPDATING .....	144
CONCLUSION .....	147
ACKNOWLEDGEMENTS .....	148
REFERENCES .....	152
<b>CHAPTER 7: THE ROLE OF GEOMECHANICAL OBSERVATION IN CONTINUOUS UPDATING OF THERMAL RECOVERY SIMULATIONS USING THE ENSEMBLE KALMAN FILTER.....</b>	<b>155</b>
ABSTRACT.....	155
INTRODUCTION.....	156
ITERATIVE FLOW-GEOMECHANICAL SIMULATION IN THERMAL RECOVERY .....	158
HISTORY MATCHING AND DATA ASSIMILATION USING THE ENKF.....	159

CASE STUDY I: SHALLOW TRIPLE SAGD.....	161
STOCHASTIC REALIZATIONS FOR PERMEABILITY AND MODULUS OF ELASTICITY .....	162
GEOMECHANICAL FLOW SIMULATION OF THE TRUTH MODEL .....	164
SOLUTION WORKFLOW AND SETTINGS .....	169
HISTORY MATCHING RESULTS .....	170
DATA REPRODUCTION RESULTS.....	174
CASE STUDY II: SINGLE SHALLOW SAGD .....	177
PROBLEM FRAMEWORK AND SETTINGS.....	178
HISTORY MATCHING RESULTS .....	179
DATA REPRODUCTION RESULTS.....	181
SUMMARY AND CONCLUSIONS .....	183
SUGGESTIONS AND FURTHER STUDIES .....	184
REFERENCE .....	185
<b>CHAPTER 8: CONCLUSION AND RECOMMENDATIONS FOR FURTHER STUDIES .....</b>	<b>188</b>
SUMMARY AND CONCLUSIONS .....	188
PROPOSED PROCEDURE FOR COMBINING MODELS .....	190

# LIST OF TABLES

## CHAPTER 1

## CHAPTER 2

TABLE 1: EXPERIMENTAL PARAMETERS, CHUNG AND BUTLER, 1988. ....	25
TABLE 2: PARAMETERS OF THE LGS MODEL. ....	28

## CHAPTER 3

TABLE 1: EXPERIMENTAL PARAMETERS, CHUNG AND BUTLER (1988). ....	51
TABLE 2: PARAMETERS OF THE NUMERICAL MODEL. ....	52

## CHAPTER 4

TABLE 1: SOME OF THE ANALYTICAL MODELS PROPOSED FOR SAGD. ....	65
TABLE 2: PROPERTIES OF THE MODEL REQUIRED FOR ANALYTICAL MODELS. ....	66
TABLE 3: GEOLOGICAL STRATA ARRANGEMENT AT UTF SITE (SUMMARIZED FROM CHALATURNYK, 1996). ....	73
TABLE 4: MATERIAL PROPERTIES AND SAGD OPERATIONAL SPECIFICATIONS FOR UTF PHASES A AND B. ....	77

## CHAPTER 5

TABLE 1: GEOMETRY AND APPLIED STRESS/PRESSURE. ....	95
TABLE 2: TWO CASES FOR HORIZONTAL STRESS ARRANGEMENT. ....	96
TABLE 3: HYDRAULIC PROPERTIES OF THE RESERVOIR. ....	96

## CHAPTER 6

TABLE 1: LIST OF SAGD ANALYTICAL PROXIES USED IN THIS STUDY FOR OIL PRODUCTION, STEAM INJECTION AND GEOMECHANICAL CONSIDERATION. ....	129
TABLE 2: MATERIAL PROPERTIES OF THE EXPERIMENTAL SAGD TEST (CHUNG AND BUTLER, 1988) ..	129
TABLE 3: PROPERTIES OF THE RESERVOIR ROCK USED IN NUMERICAL SIMULATION AND HISTORY MATCHING BY THE SAGD PROXIES. ....	130
TABLE 4: LIST OF PARAMETERS AND THEIR FINAL VALUES. ....	139

## CHAPTER 7

TABLE 1: PHYSICAL PROPERTIES OF GEOLOGICAL LAYERS. ....	166
TABLE 2: ROCK PROPERTIES FOR RESERVOIR SIMULATION. ....	168
TABLE 3: MEASUREMENT ERRORS FOR EACH MONITORING DATA. ....	170

# LIST OF FIGURES

## CHAPTER 1

FIGURE 1: MANAGEMENT OPTIMIZATION LOOP IN A SMART FIELD. ....	2
FIGURE 2: LOCATION OF ANALYTICAL SOLUTIONS IN A SMART FIELD SIMULATION PATH (PARTIALLY ADAPTED FROM BP'S TOP DOWN RESERVOIR MODELING). ....	5
FIGURE 3: OPTIMIZATION LOOP AND ITS COMPONENTS IN A CLOSED LOOP.....	6

## CHAPTER 2

FIGURE 1: BUTLER (LEFT) AND REIS (RIGHT) MODELS: STEAM CHAMBER SHAPES AND METHODOLOGIES. .....	13
FIGURE 2: MODEL OF SLICES: A MODIFIED VERSION OF REIS MODEL (1992) AND LIANG (2005).....	14
FIGURE 3: EFFECTIVE FORCES ON THE FAILURE WEDGE. ....	20
FIGURE 4: TRIAXIAL TEST RESULTS REPORTED ON ATHABASCA OIL SAND BY SAMIEH (1995): DEVIATORIC STRESS VS. AXIAL STRAIN (LEFT) AND VOLUMETRIC STRAIN VS. AXIAL STRAIN (RIGHT). ....	23
FIGURE 5: FLOWCHART OF THE COUPLED SOLVER. ....	24
FIGURE 6: OIL SATURATION IN FRONT OF THE STEAM CHAMBER. ....	26
FIGURE 7: RESULTS OF LAB DATA COMPARED TO RESULTS OF THE MODEL OF SLICES AND REIS MODEL (1992).....	27
FIGURE 8: GEOMETRY OF THE NUMERICAL MODEL BY LI (2006) ON LEFT AND LGS MODEL ON RIGHT..	29
FIGURE 9: OIL PRODUCTION AND STEAM INJECTION PREDICTED BY THE MODEL OF SLICES. ....	30
FIGURE 10: OIL PRODUCTION AND STEAM INJECTION PREDICTED BY THE LGS MODEL. ....	31
FIGURE 11: RESULTS OF THIS STUDY COMPARED TO NUMERICAL MODELING: CUMULATIVE SOR FOR UNCOUPLED SIMULATION (TOP), CUMULATIVE SOR FOR COUPLED SIMULATION (BOTTOM). ...	32
FIGURE 12: RESULTS OF LGS MODEL: (A) GROWTH OF SHEAR ZONE VS. GROWTH OF STEAM CHAMBER, (B) GROWTH OF SHEAR ZONE VS. TIME, (C) GROWTH OF THE STEAM CHAMBER IN COUPLED AND UNCOUPLED ANALYSIS.....	32

## CHAPTER 3

FIGURE 1: BASIC ELEMENTS OF A SAGD PROJECT. ....	39
FIGURE 2: MODEL OF SLICES, FROM AZAD AND CHALATURNYK (2010). ONE SLICE HAS BEEN PLOTTED ON ONE SIDE OF THE STEAM CHAMBER AS AN EXAMPLE.....	42
FIGURE 3: GROWTH OF STEAM CHAMBER OBSERVED DURING PHASE A OF UTF PROJECT (ADOPTED FROM ITO AND SUZUKI, 1996). ....	43
FIGURE 4: COMPARISON BETWEEN LINEAR AND CIRCULAR GEOMETRY OF THE STEAM CHAMBER.....	43
FIGURE 5: POSSIBLE POSITIONS FOR A CIRCULAR STEAM CHAMBER. ....	44

FIGURE 6: MODEL OF SLICES FOR CIRCULAR GEOMETRY OF STEAM CHAMBER.....	45
FIGURE 7: STEAM CHAMBER PARAMETERS FOR CASES B (LEFT) AND C (RIGHT). .....	46
FIGURE 8: DEFINITION OF LOCAL VELOCITY AT DIFFERENT POSITION OF STEAM CHAMBER (SC) AND THE LOCATION AT WHICH FLOW RATE IS CALCULATED. ....	47
FIGURE 9: COMPARISON BETWEEN THE EXPERIMENTAL DATA REPORTED BY CHUNG AND BUTLER (1988).....	50
FIGURE 10: RELATIVE PERMEABILITY CURVES RESULTED FROM HISTORY MATCHING. ....	53
FIGURE 11: HISTORY MATCHING OF OIL PRODUCTION AND STEAM INJECTION RATE BY THE CURRENT ANALYTICAL MODEL.....	53
FIGURE 12: CUMULATIVE OIL PRODUCTION AND STEAM INJECTION PREDICTED BY THE CURRENT NUMERICAL MODEL COMPARED TO THE NUMERICAL ANALYSIS RESULTS. ....	54
FIGURE 13: STEAM/OIL RATIO PREDICTED DURING HISTORY MATCHING COMPARED TO THE RESULTS OF A NUMERICAL SIMULATOR. ....	54
FIGURE 14: OIL SATURATION DISTRIBUTION AT THREE MOMENTS OF THE ANALYSIS. ....	55

#### **CHAPTER 4**

FIGURE 1: LOCATION OF DIFFERENT MODELS ALONG A SIMULATION PATH (PARTIALLY ADAPTED FROM BP'S TOP-DOWN RESERVOIR MODELLING, WILLIAMS ET AL., 2004). ....	62
FIGURE 2: UNCERTAINTY ANALYSIS FLOWCHART OF SAGD PERFORMANCE USING BUTLER THEORY (PARTIALLY ADAPTED FROM VANEGAS PRADA ET AL., 2009).....	64
FIGURE 3: STEAM CHAMBER GEOMETRY: (A) BUTLER MODEL, (B) LINEAR GEOMETRY, AND (C) CIRCULAR GEOMETRY.....	65
FIGURE 4: OIL PRODUCTION RATE SIMULATED BY THE ANALYTICAL MODELS. ....	67
FIGURE 5: CUMULATIVE OIL PRODUCTION PREDICTED BY THE ANALYTICAL MODELS.....	68
FIGURE 6: THERMAL STRESS DISTRIBUTION INSIDE THE RESERVOIR CAUSES RESERVOIR DEFORMATION AND HEAVE.....	69
FIGURE 7: STRESS DISTRIBUTION IN ADVANCE OF THE STEAM CHAMBER (AFTER CHALATURNYK, 1996). .....	70
FIGURE 8: LOCATION OF UNDERGROUND TEST FACILITY (UTF) SITE IN ALBERTA, CANADA (ADAPTED FROM CHALATURNYK, 1996).....	72
FIGURE 9: OVERALL LAYOUT OF UNDERGROUND TEST FACILITY / PHASE A (FROM CHALATURNYK, 1996).....	72
FIGURE 10: PLAN VIEW OF UTF PHASES A AND B, AND BOREHOLE ARRANGEMENTS. ....	74
FIGURE 11: TIMELINE AND OPERATIONAL STRATEGIES OF UTF/PHASE A (GENERATED FROM EDMUNDS ET AL., 1994). ....	74
FIGURE 12: TIMELINE AND OPERATIONAL STRATEGIES OF UTF/PHASE B (GENERATED FROM O'ROURKE ET AL., 1997). ....	75

FIGURE 13: CROSS SECTION A-A' (SEE FIGURE 10) OF UTF / PHASE A.....	75
FIGURE 14: CROSS SECTION B-B' (SEE FIGURE 10) OF UTF / PHASE B. ....	76
FIGURE 15: RELATIVE PERMEABILITY CURVES FOR UTF SIMULATION (FROM CHALATURNYK, 1996). ..	76
FIGURE 16: HISTORY MATCHING RESULTS ON CUMULATIVE PRODUCTION AND INJECTION FOR UTF / PHASES A AND B. ....	78
FIGURE 17: STEAM/OIL RATIO (SOR) RESULTING FROM HISTORY MATCHING FOR UTF / PHASES A AND B. ....	79
FIGURE 18: STEAM CHAMBER PREDICTED BY THE CIRCULAR MODEL COMPARED TO THE FIELD DATA FOR UTF/PHASE A. ....	81

## CHAPTER 5

FIGURE 1: SAGD PROCESS AND STEAM CHAMBER GROWTH IN THE RESERVOIR.....	89
FIGURE 2: COUPLING CYCLES AND THE INTERACTIVE LINUX CODE.....	91
FIGURE 3: DISTRIBUTION OF HORIZONTAL AND VERTICAL STRESSES IN ATHABASCA OIL SAND RESERVOIRS, AFTER COLLINS (2007). ....	92
FIGURE 4: GEOMETRY OF MODELS FOR COUPLING RUNS. ....	94
FIGURE 5: TWO CASES FOR HORIZONTAL STRESS ARRANGEMENT. ....	94
FIGURE 6: RELATIVE PERMEABILITY (TOP) AND VARIATION OF VISCOSITY BY TEMPERATURE (BOTTOM), AFTER CHALATURNYK (1996). ....	97
FIGURE 7: CUMULATIVE OIL PRODUCTION FOR MODEL 1. ....	100
FIGURE 8: CUMULATIVE OIL PRODUCTION FOR MODEL 2. ....	100
FIGURE 9: CUMULATIVE OIL PRODUCTION FOR MODEL 3. ....	101
FIGURE 10: CUMULATIVE STEAM/OIL RATIO (SOR) FOR MODEL 1.....	101
FIGURE 11: CUMULATIVE STEAM/OIL RATIO (SOR) FOR MODEL 2.....	102
FIGURE 12: CUMULATIVE STEAM/OIL RATIO (SOR) FOR MODEL 3.....	102
FIGURE 13: TYPICAL RESERVOIR DEFORMATION DURING A SAGD PROCESS. ....	104
FIGURE 14: TEMPERATURE DISTRIBUTION WITHIN HALF OF THE RESERVOIR AFTER 200 DAYS (LEFT) AND 700 DAYS (RIGHT). FROM TOP TO BOTTOM: UNCOUPLED, COUPLED WITH THE FIRST STRESS ARRANGEMENT, COUPLED WITH THE SECOND STRESS ARRANGEMENT. (3000 KPA INJECTION PRESSURE) ....	105
FIGURE 15: MAXIMUM HEAVE HISTORY FOR MODEL 1. ....	106
FIGURE 16: MAXIMUM HEAVE HISTORY FOR MODEL 2. ....	107
FIGURE 17: MAXIMUM HEAVE HISTORY FOR MODEL 3. ....	108
FIGURE 18: GEOMECHANICAL CHANGES IN MODEL 1 AND THE 1ST STRESS ARRANGEMENT AT 3000 KPA INJECTION PRESSURE.....	110

FIGURE 19: GEOMECHANICAL CHANGES IN MODEL 1 AND THE 2ND STRESS ARRANGEMENT AT 3000 kPA INJECTION PRESSURE.....	110
FIGURE 20: GEOMECHANICAL CHANGES IN MODEL 2 AND THE 1ST STRESS ARRANGEMENT AT 6000 kPA INJECTION PRESSURE.....	111
FIGURE 21: GEOMECHANICAL CHANGES IN MODEL 2 AND THE 2ND STRESS ARRANGEMENT AT 6000 kPA INJECTION PRESSURE.....	111
FIGURE 22: GEOMECHANICAL CHANGES IN MODEL 3 AND THE 1ST STRESS ARRANGEMENT AT 9000 kPA INJECTION PRESSURE.....	112
FIGURE 23: GEOMECHANICAL CHANGES IN MODEL 3 AND THE 2ND STRESS ARRANGEMENT AT 9000 kPA INJECTION PRESSURE.....	112
FIGURE 24: COMPARISON OF COMPUTATIONAL EFFORT BETWEEN COUPLED AND UNCOUPLED MODELS. ....	113
FIGURE 25: KF LINE IN P'-Q' PLOT.....	115
FIGURE 26: EFFECTS OF GEOMECHANICAL MODELING ON OIL PRODUCTION.....	116
FIGURE 27: EFFECTS OF GEOMECHANICAL MODELING ON CSOR.....	116
FIGURE 28: ROCK PROPERTY IMPROVEMENT VS. GEOMECHANICAL IMPACT FACTOR (GIF). ....	117

## CHAPTER 6

FIGURE 1: STEAM ASSISTED GRAVITY DRAINAGE (SAGD) PROCESS. HORIZONTAL BOREHOLES ARE LOCATED WITHIN THE CLASSICAL STEAM CHAMBER AT THE STEAM TEMPERATURE MARKED AS ZONE 1. ALSO, THE TRANSITION ZONE BETWEEN THE STEAM CHAMBER AT THE STEAM TEMPERATURE AND THE RESERVOIR AT THE ORIGINAL TEMPERATURE HAS BEEN MARKED AS ZONE 2. ....	124
FIGURE 2: INTERLOCKED STRUCTURE OF OIL SAND (LEFT) [AFTER DUSSEAULT AND MORGENSTERN, 1978] AND DILATIVE BEHAVIOUR OF OIL SAND (RIGHT). DILATIVE BEHAVIOR OF OIL SAND WHICH IS TYPICAL BETWEEN DENSE SANDS CAN BE DEPICTED FROM THE TWO GRAPHS. UNDER A TRIAXIAL TEST, AN OIL SAND SAMPLE EXPERIENCES MAXIMUM SHEAR RESISTANCE AT 'P' AND RETURNS TO A CONSTANT STRENGTH AT 'R' .....	125
FIGURE 3: SHAPE AND LOCATION OF THE CLASSICAL STEAM CHAMBER AT DIFFERENT STAGES OF THE SAGD PROCESS. THIS FIGURE SHOWS THE GROWTH OF THE STEAM CHAMBER AT DIFFERENT STAGES OF THE PROCESS BASED ON LINEAR GEOMETRY OF THE STEAM CHAMBER PROPOSED BY REIS (1992). ....	126
FIGURE 4: GROWTH OF THE STEAM CHAMBER IN A 15 BY 20 CM LABORATORY CELL AT TIMES 20, 60 AND 90 MINUTES (FROM LEFT TO RIGHT). (AFTER CHUNG AND BUTLER, 1988). EACH SINGLE FIGURE PLOTS ONLY RIGHT HALF OF THE CELL.....	128
FIGURE 5: COMPARISON BETWEEN THE RESULTS OF AN EXPERIMENTAL SAGD PROCESS BY CHUNG AND BUTLER (1988) AND THE RESULTS OF ANALYTICAL PROXIES FOR OIL PRODUCTION RATE, STEAM	

CHAMBER HEIGHT AND STEAM CHAMBER WIDTH (FROM TO BOTTOM). THE ARROW ON EACH CHART SHOWS THE TIME OF SWITCHING BETWEEN PROXIES AFTER THE STEAM CHAMBER REACHES THE CEILING. ....	128
FIGURE 6: OIL RATE (LEFT) AND CUMULATIVE STEAM RATE (RIGHT): COMPARISON BETWEEN NUMERICAL SIMULATION AND SAGD PROXY MODELS. THE ARROW ON EACH CHART SHOWS APPROXIMATE TIME THAT THE STEAM CHAMBER TOUCHES THE TOP OF THE MODEL AND PROXIES ARE CHANGED. ....	131
FIGURE 7: GEOMECHANICAL CALCULATION; THE RESERVOIR IS REPRESENTED BY A SINGLE ELEMENT: (A) THE NUMERICAL ELEMENT FOR SIMULATION AND ITS BOUNDARY CONDITIONS (B) IN SITU STRESSES ACTING ON THE ELEMENT BEFORE THE SAGD OPERATION AND (C) THE RESULTANT STRESS INCREASE AFTER THE SAGD PROCESS.....	132
FIGURE 8: FUNDAMENTALS OF BUTLER MODEL. (A) INCREMENTAL FLOW RATE (DQ) IN A CHANNEL IN FRONT OF THE STEAM CHAMBER, (B) TEMPERATURE DISTRIBUTION IN ADVANCE OF THE MOVING STEAM CHAMBER FRONT.....	134
FIGURE 9: WORKFLOW OF THE PROPOSED ALGORITHM FOR RANKING STATIC MODELS. ....	136
FIGURE 10: HISTOGRAMS OF WELL DATA: PERMEABILITY (LEFT) AND POROSITY (RIGHT).....	137
FIGURE 11: E-TYPE MEAN (LEFT) AND CONDITIONAL VARIANCE (RIGHT) OF PERMEABILITY IN NORMAL SCORE SPACE FOR 100 STOCHASTIC REALIZATIONS. WELL LOCATIONS HAVE BEEN MARKED AT THE TOP SURFACE BY AN ARROW ABOVE EACH WELL. ....	137
FIGURE 12: E-TYPE MEAN (LEFT) AND CONDITIONAL VARIANCE (RIGHT) OF POROSITY IN NORMAL SCORE SPACE FOR 100 STOCHASTIC REALIZATIONS. WELL LOCATIONS HAVE BEEN MARKED AT THE TOP SURFACE BY AN ARROW ABOVE EACH WELL. ....	138
FIGURE 13: GEOMECHANICAL-RESERVOIR MODEL AND BOUNDARY CONDITIONS FOR COUPLED SIMULATION. ....	139
FIGURE 14: TEMPERATURE (°C) PROFILE IN THE RESERVOIR 450 DAYS AFTER THE SAGD PROCESS (SIMULATION RESULT FOR THE REFERENCE MODEL). ....	140
FIGURE 15: OIL PRODUCTION RATE AND SOR HISTORIES FOR THE REFERENCE MODEL AND THE OTHER 99 MODELS. ....	141
FIGURE 16: COMPARISON OF CALCULATED AVERAGE PERMEABILITY AND POROSITY BASED ON THE AVERAGING ASSUMPTION OVER REFERENCE MODELS (A) IN ZONE 1 FOR POROSITY, AND (C) IN ZONE 2 FOR PERMEABILITY. COMPARISON BETWEEN THE TOTAL ERROR AND THE PROXY ERROR (B) FOR POROSITY, AND (D) FOR PERMEABILITY. ....	142
FIGURE 17: (A) RANKING HISTORY OF REFERENCE MODELS, AND (B) PROBABILITY OF BEING THE TRUTH MODEL FOR REFERENCE MODELS. ....	143
FIGURE 18: DATA ASSIMILATION ANALYSIS FOR PERMEABILITY MODELS (LEFT COLUMN IN MD) AND POROSITY MODELS (RIGHT COLUMN IN %). FROM TOP TO BOTTOM: REFERENCE MODELS, E-TYPE	

MEAN OF INITIAL MODELS, E-TYPE MEAN OF UPDATED MODELS AFTER 300 DAYS, AND E-TYPE MEAN OF UPDATED MODELS AFTER 700 DAYS. ....	144
FIGURE 19: AVERAGE STANDARD DEVIATION OF E-TYPE MODEL FOR PERMEABILITY (LEFT) AND POROSITY (RIGHT). ....	145
FIGURE 20: (A) AVERAGE PERMEABILITY AND (B) AVERAGE POROSITY OF THE TRUTH MODEL AMONG OTHER 99 MODELS. (C) AVERAGE ESTIMATED PERMEABILITY AND (D) AVERAGE ESTIMATED POROSITY BY ENKF AMONG OTHER 99 MODELS ASSIMILATED USING ENKF. ....	146
 <b>CHAPTER 7</b>	
FIGURE 1: (A) ITERATIVE RESERVOIR-GEOMECHANICAL SIMULATION LOOP, (B) POSITION OF RESERVOIR GRIDS SURROUNDED BY GEOMECHANICAL GRIDS. ....	159
FIGURE 2: HISTOGRAMS OF THE SYNTHETIC DATA SETS: MODULUS OF ELASTICITY (LEFT) AND PERMEABILITY (RIGHT). ....	162
FIGURE 3: SEMIVARIOGRAMS FOR EACH DATA SET IN THREE PRINCIPAL CONTINUITY DIRECTIONS. ....	163
FIGURE 4: E-TYPE MEAN AND VARIANCE OF THE 100 STOCHASTIC REALIZATIONS FOR PERMEABILITY. ....	163
FIGURE 5: E-TYPE MEAN AND VARIANCE OF THE 100 STOCHASTIC REALIZATIONS FOR MODULUS OF ELASTICITY. ....	164
FIGURE 6: TRUTH FLOW-GEOMECHANICAL COUPLED MODEL: DIMENSIONS AND BOUNDARY CONDITIONS. ....	165
FIGURE 7: OIL PRODUCTION (LEFT) AND STEAM/OIL RATIO (RIGHT) FOR THE TRIPLE SHALLOW SAGD CASE STUDY: COUPLED AND UNCOUPLED RESULTS. ....	167
FIGURE 8: STEAM CHAMBER GROWTH AFTER 300 DAYS, TEMPERATURE PROFILE (°C): UNCOUPLED SIMULATION (TOP) AND COUPLED SIMULATION (BOTTOM). ....	168
FIGURE 9: COUPLED FLOW-GEOMECHANICAL SIMULATION RESULTS USING INITIAL ENSEMBLES. ....	171
FIGURE 10: HISTORY MATCHING RESULTS FOR THE FIRST STRATEGY: FLOW MONITORING DATA AND ASSIMILATION OF DYNAMIC PERMEABILITY USING ONLY FLOW SIMULATION. ....	172
FIGURE 11: HISTORY MATCHING RESULTS FOR THE SECOND STRATEGY: FLOW MONITORING DATA AND STATIC ASSIMILATION OF PERMEABILITY AND MODULUS OF ELASTICITY USING FLOW-GEOMECHANICAL COUPLED SIMULATION. ....	172
FIGURE 12: HISTORY MATCHING RESULTS FOR THE THIRD STRATEGY: FLOW AND GEOMECHANICAL MONITORING DATA AND STATIC ASSIMILATION OF PERMEABILITY AND MODULUS OF ELASTICITY USING FLOW-GEOMECHANICAL COUPLED SIMULATION. ....	173
FIGURE 13: HISTORY MATCHING RESULTS: OVERALL CUMULATIVE SOR (LEFT) AND VERTICAL DISPLACEMENT PROFILE (RIGHT) AT GROUND SURFACE AT 700 DAYS BEFORE (TOP) AND AFTER (BOTTOM) APPLYING THE ENKF ALGORITHM IN THE THIRD STRATEGY. ....	173
FIGURE 14: VARIATION OF MEAN (TOP) AND STANDARD DEVIATION (BOTTOM) OF ASSIMILATION ERROR: MODULUS OF ELASTICITY (LEFT) AND PERMEABILITY (RIGHT). ....	175

FIGURE 15: REFERENCE POPULATION (TOP) AND E-TYPE MEAN OF THE INITIAL 100 STOCHASTIC REALIZATIONS. ....	176
FIGURE 16: ASSIMILATED STATIC DATA AFTER 300 AND 700 DAYS IN THE THIRD STRATEGY: PERMEABILITY (LEFT) AND MODULUS OF ELASTICITY (RIGHT).....	176
FIGURE 17: COMPARISON BETWEEN THE TRUTH AND THE ASSIMILATED DYNAMIC DATA IN MD AFTER 300 AND 700 DAYS IN THE FIRST STRATEGY. ....	177
FIGURE 18: DISPLACEMENT MONITORING AT THREE LOCATIONS: VERTICAL DISPLACEMENT ON THE GROUND SURFACE AS WELL AS THE RESERVOIR TOP AND HORIZONTAL DISPLACEMENT AT THE CENTRE LINE OF THE MODEL. ....	178
FIGURE 19: COMPARING THE SIMULATION RESULTS OF THE 25 STOCHASTIC REALIZATIONS BEFORE HISTORY MATCHING. ....	179
FIGURE 20: RESULTS OF HISTORY MATCHING USING THE ENKF. FROM LEFT TO RIGHT: WITH (1) VERTICAL DISPLACEMENT DATA ON THE GROUND SURFACE, (2) VERTICAL DISPLACEMENT DATA AT THE RESERVOIR TOP, AND (3) HORIZONTAL DISPLACEMENT AT THE CENTRE LINE. ....	180
FIGURE 21: DISPLACEMENT HISTORIES BEFORE (TOP) AND AFTER (BOTTOM) APPLYING THE ENKF ALGORITHM. FROM LEFT TO RIGHT: VERTICAL DISPLACEMENT ON THE GROUND SURFACE, VERTICAL DISPLACEMENT AT RESERVOIR TOP, AND HORIZONTAL DISPLACEMENT AFTER 700 DAYS. ....	181
FIGURE 22: DATA ASSIMILATION RESULTS AFTER 700 DAYS OF HISTORY MATCHING; FROM TOP TO BOTTOM: REFERENCE MODEL, E-TYPE MEAN OF THE 25 STOCHASTIC MODELS, DATA ASSIMILATION RESULTS USING VERTICAL DISPLACEMENT AT GROUND SURFACE, VERTICAL DISPLACEMENT AT RESERVOIR TOP, AND HORIZONTAL DISPLACEMENT. ....	182

## CHAPTER 8

FIGURE 1: ARRANGEMENT OF MODELS WITH DIFFERENT RESOLUTIONS IN THE SIMULATION UNIT.....	190
--	-----

## CHAPTER 1: INTRODUCTION

### INTRODUCTION

Production optimization, cost minimization, and reservoir recovery improvement are the three major purposes of a smart field. For almost a decade, many oil and gas companies have been installing smart technologies inside wells, downstream, and in engineers' offices. Much has been researched and written on successful implementing intelligent wells, generating real-time and reliable data, and employing powerful computing capabilities. Moreover, some studies have been carried out on optimization, monitoring, and controlling intelligent assets. However, intelligent field workflow between technology and the two other elements- process and people- is still under discussion, as is the functioning of fast closed-loop workflow in both oil and gas fields. Such a workflow could define optimization objectives locally and globally. Establishing controllable parameters for modeling and decision making is the key to a coherent system.

In Canada, the Steam Assisted Gravity Drainage (SAGD) process, a thermal recovery technique, has been widely practiced for nearly 25 years in unconventional oil-sand reservoirs. It is estimated that 82% of ultimately recoverable oil must be extracted using in-situ techniques. SAGD would be the framework for Canada's future oil fields, and hence, an intelligent SAGD field should be drawn by all affected disciplines. The required technologies are almost in place. Current SAGD operations show that the first challenging issue is real-time monitoring/forecasting commonly called history matching. Since the nature of the SAGD process is almost fully understood, it is necessary to exploit a link between monitoring and prediction.

The SAGD process has been investigated and theorized by many researchers, starting with Butler in early 1980s. Two main mechanisms dominate in the thermal SAGD process: three phase fluid flow and geomechanical behaviour of the porous media—the latter being less studied. Recommended geomechanical coupling methods are numerical, and history matching is time consuming. Therefore, smart fields require the development of a fast simulation methodology which considers the essential elements of physics and is capable of working with/in an optimization loop.

### DIFFERENT OPTIMIZATION LOOPS IN A SMART FIELD

Optimization in a smart field may be meaningful in different categories. In an engineering project, cost, time, and recovery ratio are the main objectives of optimization. Operational strategies, development, and future challenges can also be optimized. The first closed loop, therefore, is the ‘management loop’ as a whole. Figure 1 clearly shows the optimization cycle in this category. Fast, intelligent communication between the involved disciplines guarantees the most effective workflow in the system. In this category, optimization refers to the efficient management of smart field assets. People, process, and monitoring technology are the elements of the first optimization loop. The first loop determines the most effective way to communicate each element and assign duties to them.

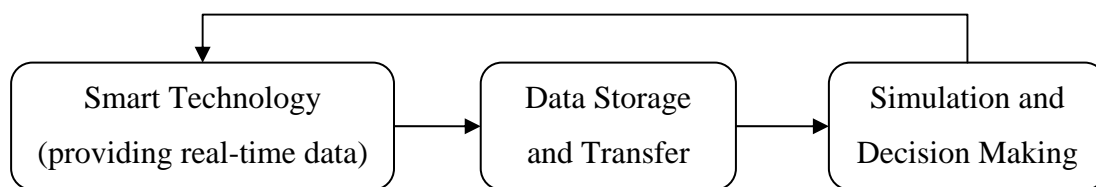


**Figure 1: Management optimization loop in a smart field.**

Each subdivision in a smart field has its own optimization loop. Optimization is meant to ease the design, installation, and operation of smart technologies in field. Optimization is also intended to transfer high quality data to engineering offices.

Data is then transferred digitally. The transfer and safe storage of high resolution data for usage in web-connected computers are the roles of optimization in this loop.

In the “simulation and decision making” box in Figure 1, optimization has different meanings. Optimization methodologies are used at the beginning of the project to achieve the best primary design. The goal of such optimization is to select the method of oil/gas recovery that will maximize production. Fundamental elements of the recovery method are also designed based on an optimized production strategy. Needless to say, financial considerations are always an effective parameter in any optimization loop.

The optimization loop that is addressed in this research is in numerical simulation. Simulation and history matching is the heart of field development. In this segment of the management loop, the operation process is simulated. In each cycle of the loop, the volume of actual data rises while uncertainties are reduced. In history matching, optimization is the connection between monitoring and control units where data integration happens in the system. In this internal loop, optimization tries to consolidate the data and decrease uncertainties. Data comes from different sources and merges at simulation units for the next cycle realization. The ultimate goal of this loop is production optimization.

## **RESEARCH MOTIVATION**

A quick review of the industry’s latest challenges reveals that both intelligent technology and high demand for oil and gas will soon change the face of this industry, increasing automated and closed loop engineering and management. To achieve this goal, each discipline will have to redefine its location in this closed circle to prevent bottlenecks in the system and refine its flow rule to act as a member of the scenario.

The role of geomechanics cannot be ignored in reservoir engineering of the SAGD process. However, considering every detail of induced thermal stress analysis dramatically increases computational time and cost. Integrated reservoir modeling, therefore, will be the challenge in SAGD fields. Thus, research on how to implement geomechanical theories into future fields would be timely. Such fields must take into account all influencing mechanisms, and should be compatible with fast, automated management systems.

## **RESEARCH OBJECTIVE**

The objective of this research is to develop a fast analytical/mathematical simulator that can capture essential features of physics, including geomechanics, in a SAGD process. The research also proposes a methodology to combine the developed model with other low order proxies and high order numerical simulators in a closed loop fashion for fast history matching.

## **SCOPE OF RESEARCH**

The proposed research does not include any laboratory tests or field analysis. However, the results of past lab-scale and field-scale experiments will be compared to verify the model. For simulation purposes, the developed model will be coded, and commercial simulators will be used to cover numerical analysis.

## **RESEARCH METHODOLOGY**

The first objective of the proposed study is to develop a fast model, which would become one of the several simulators needed in the decision-making path. An analytical solution, which would be the foundation of this model, lies between a full field model and other coarse scale models. Therefore, the model should be a robust solution to cover the essential elements of physics. Indeed, geomechanical effects must be included in the methodology for the SAGD process. The solution run time is also a promising goal. Figure 2 determines the levels of complexity and uncertainty of the input data for such a model compared to other available simulation methods. Proposing a geomechanical coupled analytical solution for SAGD will close the gap in the simulation path for smart field purposes.

The other objective of this research falls into the optimization phase. While a fast simulator is important for modeling and forecasting, input data is essential to run any simulator. For this reason, data assimilation algorithms will be utilized for data integration. Reservoir surveillance and monitoring sensors provide real time data from two sources: flow and geomechanical fields. This process does work interactively with a simulator and will improve the system towards production optimization.

## Analytical Solution Study

Simulation is the core of future forecasting and decision making in an oil field. Choosing a proper simulator that promises the goals of a smart field under the proper time intervals of a SAGD project is challenging. There are currently three major categories of methods available to tackle this problem. The first is that of numerical simulators that can solve complex reservoirs and have been developed for many years. Geomechanical models can also be coupled implicitly or explicitly to flow simulators for modeling purposes. Though they are powerful design tools, simulators in this category require a huge amount of input data for a single run, which is not always available due to uncertainties. Furthermore, they require many hours for computation. These caveats make numerical simulators suitable only for decision making or history matching that is not time sensitive.

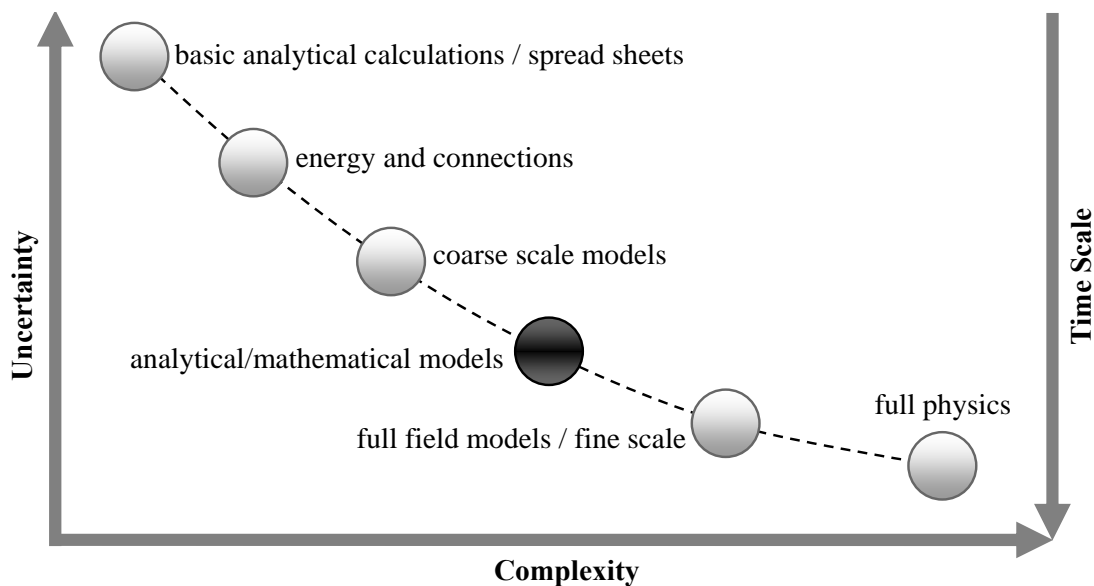


**Figure 2: Location of analytical solutions in a smart field simulation path (partially adapted from BP's top down reservoir modeling).**

The second category is that of intelligent algorithms such as genetic algorithms do history matching and forecasting quickly and well. They work as a function between input and output data and make forecasting possible. These methods can be used in some stages for perfect history matching, but have their own limitations. Learning steps conducted at the early stages need lots of reliable data. The algorithms in this category suffer, as they do not support the physics. Because of a lack of physical

meaning, the produced models are difficult to judge. The third category is that of analytical solutions. This modeling approach is not as accurate as that of numerical simulators. The advantage, however, is that it partially considers the physics of a problem. The closed form and mathematical nature of solutions in this category provides a fast and accurate tool for modeling. The third category seems to be a proper option, and will be investigated in this study.

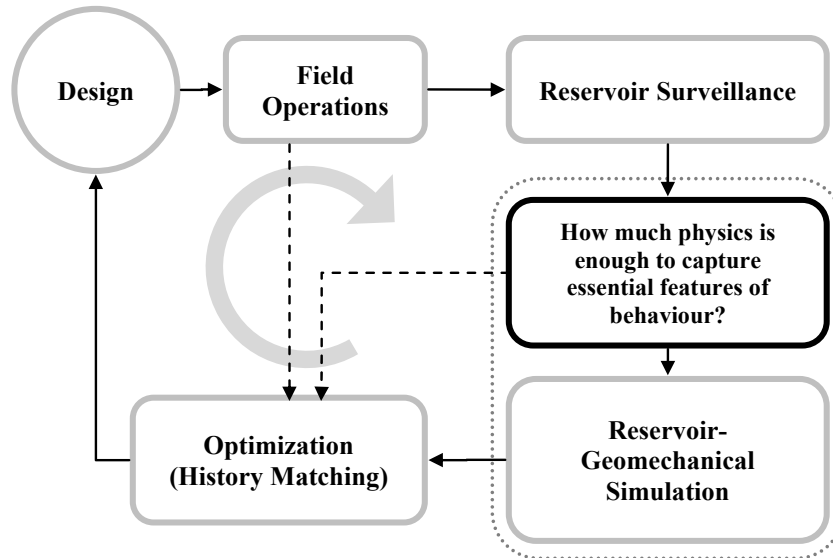


**Figure 3: Optimization loop and its components in a closed loop.**

Some past studies on analytical modeling of SAGD are helpful for developing a new geomechanical coupled simulator. However, they must be revised and upgraded. For the most part, past models have been proposed for evaluating SAGD process. For this reason, the following ideas apply to the Butler/Reis model to perform the first stage of this research:

- To avoid complexity in the form of the solution, past studies consider many simplifying assumptions. For simulation, however, using a single term and simple equation is not the goal. Some basic assumptions, such as anisotropy in reservoir properties and variation of steam chamber movement velocity can be introduced in the theory.
- The steam chamber has been modeled for rising and lateral growth in separate theories and both are combined to cover the process. A new circular geometry can be proposed to model the process from beginning to end.

- Geomechanics is the concern of this study. A geomechanical model must be developed to work beside the flow simulator. This should be the same as the flow simulator in terms of complexity and accuracy. The limit equilibrium method of analysis is the recommended geomechanical solver of the model. It is the most effective and fastest method and has been practiced for a long time in civil and geotechnical engineering.
- Permeability significantly varies with changes in saturation (relative permeability concept). Ignoring this fact and replacing it with average values has reduced the accuracy of the past models. This assumption can be improved.
- The method of slices is a technique to solve the integrals with no closed form solution. It will be applied in this study to remove the assumptions that have simplified past theories.
- All above hypotheses will certainly change the one-equation format of past studies into a series of mathematical equation sets. A computer program is needed to mathematically solve the problem. Microsoft Visual Basic will be used.

### **Geotechnical Data Assimilation**

In thermal recovery processes, dynamic data such as oil production and steam injection rates are monitored to update multi-phase flow reservoir models. Geomechanical observations are also recorded dynamically in the field. Surface heave, displacement, pore pressure, and strains are data commonly available from geomechanical sensors in the field. These two sources of data should be used to constrain the models to estimate the current reservoir properties, and later for future forecasting. The updated model is also used for production optimization and field development. Geomechanics should be considered in the whole process, from data integration to history matching (an optimization problem). It helps the uncertainty assessment to be done wisely, as it constrains the results. On the other hand, it makes calculations more complex due to the strong nonlinear coupling between reservoir flow and geomechanics. To deal with this part of the problem, this study proposes to develop a methodology for data assimilation, uncertainty assessment, and fast history

matching. As a result, simulators are replaced by simple proxies to avoid complexity in the structure of the problem.

Statistical methods, intelligent systems, and ensemble filters are among the techniques to be investigated. The best tool will be chosen and proposed to work with a geomechanical coupled SAGD process. Since such a geomechanical process has not been studied, this research field is in the primary stages of maturity. Therefore, proposing a full approach is not a goal of this research. In this step, feasibility and the technique will be assessed, and a methodology proposed.

## **STRUCTURE OF DISSERTATION**

This dissertation has been completed in paper format and selected manuscripts have been submitted for peer review in journals or conferences. However, the introduction and the conclusion chapters are included separately from papers. Below is a quick review on the content of each chapter.

### Chapter 1: Introduction

The chapter contains brief background, and the structure of the research.

### Chapter 2: A Mathematical Improvement to SAGD Using Geomechanical Modeling

The linear geometry model of SAGD considering the effect of geomechanics on production and injection is provided in this chapter.

### Chapter 3: An Improved SAGD Analytical Simulator: Circular Steam Chamber Geometry

The circular geometry drainage model that is an improved version of the linear geometry model presented in Chapter 2, is included in this chapter.

### Chapter 4: Application of Analytical Models in Fast History Matching of SAGD Process: UTF Project Case Study

In this chapter the application of the proposed drainage model proposed in the previous chapter for history matching purposes is presented. Two case studies are appended to explain the procedure.

### Chapter 5: Numerical Study of SAGD: Geomechanical-Flow Coupling for Athabasca Oil Sand Reservoirs

This chapter explains the methodology of developing an iterative coupling simulation. A brief summary about computer coding to combine two software packages is included. Some numerical examples have been solved to investigate the effect of reservoir depth and the in situ stress regime on SAGD process.

### Chapter 6: Reservoir Characterization: Application of Extended Kalman Filter and Analytical Physics-Based Proxy Models in Thermal Recovery

Application of analytical models in reservoir characterization is further discussed in this chapter. The methodology uses the EKF for rock property characterization of heterogeneous reservoirs under SAGD process.

### Chapter 7: The Role of Geomechanical Observation in Continuous Updating of Thermal Recovery Simulations using the Ensemble Kalman Filter

Chapter 7 explains the importance of geomechanical monitoring in history matching and reservoir characterization. Combined with the EnKF and coupled simulation, the methodology shows how geomechanical effectively improves data assimilation process and which source of data has the greatest impact.

### Chapter 8: Conclusion

References and conclusions of each research paper are not repeated in this chapter. Instead, the results of individual papers are summarized to show the coherency of the research. At the end of the chapter, a philosophy of merging all the techniques presented in the research is proposed in a single hierarchical methodology. Recommendations for further studies wrap up the dissertation.

## CHAPTER 2: A MATHEMATICAL IMPROVEMENT TO SAGD USING GEOMECHANICAL MODELING\*

### ABSTRACT

Steam Assisted Gravity Drainage (SAGD) is a thermal oil recovery technique which has been used mostly for Alberta's unconventional oil sand reservoirs. Dr. Roger Butler- known as the father of SAGD- was the first one to establish a theory and an analytical model for SAGD. His model is a rigorous solution and is widely referred to as a SAGD fast flow simulator. However, geomechanics which has been shown to be a relevant part of SAGD's physics has not been included in the model. When rock properties are influenced by geomechanical behavior, Butler theory is not able to capture the complete physics of the SAGD process. In such cases, the model must adopt unrealistic or high values for rock properties.

In this study, a classical theory in the field of geotechnical engineering (limit equilibrium) is employed to act as the geomechanical module for SAGD's mathematical coupled simulation. Butler/Reis model has been also improved using model of slices for flow simulation. Methodology of combining these two models in a single coupled mathematical simulator has been presented in this paper. The solver is a fast and realistic proxy and can be used as a low-order tool for history matching. The results of coupled simulations show that the model is able to predict permeability and porosity of the reservoir closer to real values than uncoupled (flow only) modeling.

---

\* This paper was presented at the Canadian International Petroleum Conference, 16-18 June 2009, Calgary. The paper was then peer reviewed and published in the Journal of Canadian Petroleum and Technology, vol. 49(10), SPE-141303-PA, pp. 53-64.

## INTRODUCTION

Analytical solutions are widely used, for practical approaches in engineering calculations. Since the majority of closed form or mathematical solutions are constructed based on simple assumptions, minimum inputs are required to run the models. Due to the lack of exact data, analytical models are mostly used as rapid simulators for primary evaluation purposes. They are also employed as low-order proxies in multi-layer optimization cycles for real-time history matching. Therefore, a reliable analytical/mathematical model that captures essential features of the process physics can be very helpful.

For SAGD, Butler and his colleagues (e.g., Butler and Stephens, 1981) proposed the first analytical solution that is able to predict oil production rate. The theory has been assembled using fundamental theories of flow and heat transfer. The model, which is usually known as the ‘Butler theory’, was firstly used as a tool to evaluate SAGD’s concept and to check the capability of such a technique in thermal oil recovery. Based on simple assumptions, Butler’s model is a rigorous solution to SAGD and is widely used in industry. The original theory has been gradually improved by Butler and his team. However, they never included geomechanics which can potentially be a significant part of SAGD’s physics (Chalaturnyk, 1996).

In addition to Butler, more researchers such as Reis (1992 and 1993), Akin (2005), Liang (2005), and Nukhaev et al. (2006) have worked on analytical solutions of SAGD. All have added more aspects of the process to a model which is very similar to Butler’s theory. This means that while the foundation of their models is grounded in Butler’s theory, they differ in the complexity of their assumptions. Similar to Butler’s model, their models do not contain a geomechanical component.

In the following sections, a mathematical methodology is proposed to improve the current drainage models and to make geomechanical coupling analysis possible. A new drainage model called ‘model of slices’ is presented based on the models of Butler and Reis. To consider geomechanics, the limit equilibrium analysis method is adopted from geotechnical engineering to work with the flow simulator. The nascent

geomechanical model is not mature enough to be extended to all areas in petroleum geomechanics. This simple model would be a converter to explain the changes in permeability and porosity only. Together with a coupling technique, these two models can offer solutions to SAGD problems that are fast, reasonably robust, and physics-based. The proposed models are then validated with laboratory data and numerical simulator results.

## **DRAINAGE MODEL**

In a SAGD process, two different mechanisms are dominant: multi-phase flow in porous media and the heat transfer mechanism. These work interactively and must be included in a drainage model. In such a model, thermal conduction theory can describe the basis of changes in viscosity and then, Darcy's law would define the relationship between the fluid flow and the potential function. In the following sections, two of the models that have been used to develop the drainage model of this study are summarized. The details of the modified drainage model (using the model of slices) are then explained. Energy balance is also derived to calculate the steam injection rate.

### **Previous Works by Butler and Reis**

There are some analytical models in the literature that can be used as a core of an analytical simulator. However, they are all similar in terms of methodology and for the most part, have been developed based on Butler's theory. Butler and his colleagues proposed a theory that was able to estimate the rate of oil production in a SAGD process. Their first goal, however, was to study the feasibility of SAGD and to provide a mathematical proof for SAGD. After his original theory, Butler occasionally tried to modify the theory to overcome some shortcomings such as (a) steam chamber not touching the production borehole, and (b) overestimation of production. Although the modified versions were better able to predict the lab data, the basis of the theory was not changed, and the theory was modified based on experimental findings. The original Butler theory is expressed in Equation (1):

$$q = 2L \sqrt{\frac{2kg\alpha\rho_o\phi\Delta S_o H}{m\mu_{os}}} \dots\dots\dots(1)$$

In 1992, Reis originated his model, which had basically the same formulation and methodology as Butler’s model. The difference was in the shape of the steam chamber. Reis considered a linear geometry (triangular form) for the steam chamber, while in Butler’s theory, the shape was not predefined, and an s-curve shape was calculated out of the formulation. Reis also used an experimental multiplier, *a*, to simplify the analytical integration over the depth of the reservoir.

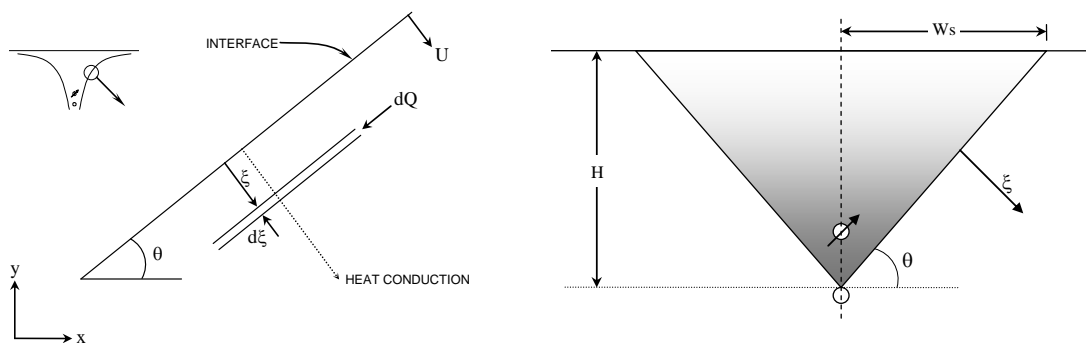


**Figure 1: Butler (left) and Reis (right) models: steam chamber shapes and methodologies.**

Fig. 1 shows the difference between the two models in predicting the shape of the steam chamber. Equation (2) calculates the oil rate proposed by Reis:

$$q = 2L \sqrt{\frac{kg\alpha\rho_o\phi\Delta S_o H}{2am\mu_{os}}} \dots\dots\dots(2)$$

in Equations (1) and (2):

- q* oil production rate
- L* boreholes’ length
- k* permeability
- α* reservoir thermal diffusivity
- ρ<sub>o</sub>* oil density
- φ* porosity
- ΔS<sub>o</sub>* (initial – residual) oil saturation
- H* height of reservoir from producer to the caprock
- a* dimensionless velocity constant - experimental
- m* dimensionless viscosity constant - experimental
- μ<sub>os</sub>* viscosity of oil at steam temperature

It should be noted that Reis recommends using oil relative permeability, while Butler's theory uses absolute permeability in the formulation. Other than a in the nominator of Equation (2), both equations are similar. Reis' model predicts oil production as low as 80 to 90% of Butler's model.

### Modified Drainage Model – Model of Slices

Although Butler's and Reis' models are successful in matching lab data, they are still unable to capture the variations and fluctuations of oil production that occur in the field. Both models predict a constant rate of production from the beginning of the process to the end.

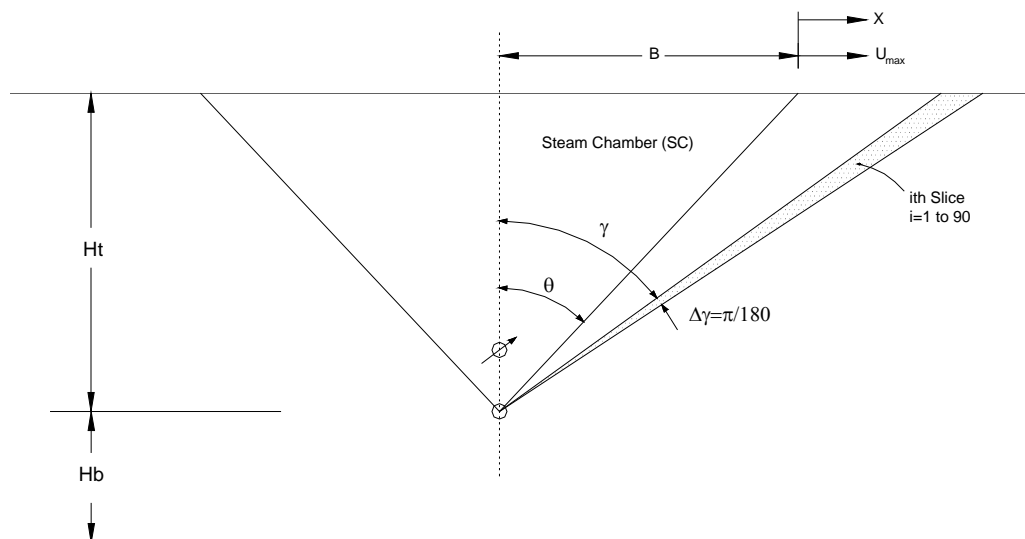


**Figure 2: Model of Slices: a modified version of Reis model (1992) and Liang (2005).**

The model of slices has two objectives. The first is to calculate material balance in the zones in front of the steam chamber instead of in the whole reservoir. This helps the model to predict the variation of oil saturation in the reservoir and allows for changing those properties that vary with oil saturation (e.g., relative permeability). The second objective is to consider anisotropy of permeability in the reservoir. The model of slices is a version of Reis' model that has the same methodology as Butler's theory. It is similar to Reis' model because the geometry and format of derivation are the same. However, the approach to the problem is the same as that in the theories of both Reis and Butler. Assuming symmetry about the well pairs, the model of slices,

divides one half of the reservoir into slices. While the number of slices is optional, choosing a high number increases computational time with no increase in accuracy. For simplicity, in this study, the number of slices is assumed to be 90. Fig. 2 shows the location of the steam chamber and the shape of one slice.

The general idea in this model is that at each time step (or at each position of the steam chamber), all the slices in front of the steam chamber can produce oil, and oil saturation changes in each slice. From a mathematical point of view, this is a simple numerical method of integration; the lower band of the integral is the steam chamber, and the upper band is the reservoir. Each slice is one segment of the integral. However, at each step of integration, additional information is collected at each slice to update the oil saturation in the subsequent step. The principle of this approach is to allow the multiple slices in front of the steam chamber to be active (have the potential to produce oil). All the slices, however, will not produce oil and by setting a minimum value of oil production as a criterion for setting a slice 'inactive', integration can be stopped once the first inactive slice is reached.

Unlike other models that consider only material balance inside the steam chamber, in the current proposed model, material balance is calculated in each slice. This approach gives a more realistic solution to predict the volume of oil produced from the production well. Therefore, at each time step, oil saturation is updated and permeability can be picked based on any available chart that relates relative permeability to oil saturation.

Reservoir anisotropy can also be applied to the model. The relationship between horizontal and vertical permeability is expressed as:

$$K_{\gamma}^2 = \frac{K_o^2}{(\sin \gamma)^2 + (n \cos \gamma)^2} \dots\dots\dots(3)$$

where:

- $K_{\gamma}$  permeability in the slice with angle  $\gamma$
- $K_o$  horizontal oil permeability
- $N$  horizontal/vertical permeability ( $K_o / K_v$ )

If Darcy’s law and the theory of heat transfer (to calculate the value of viscosity at each reservoir location) are combined, oil rate at time  $t$  (or steam chamber at angle  $\theta$ ) can be calculated by Equation (4). Equation (4) has been derived using the same method that Reis3 used for SAGD and that Liang6 used for CSS (Cyclic Steam Stimulation). A complete derivation is listed in Appendix A.

$$q_{t,i} = \frac{2K_o \rho_o g H_t}{\mu_{os}} \int_{\theta}^{\frac{\pi}{2}} \frac{\exp\left[\frac{-amU_{\max} H_t (\tan \gamma - \tan \theta)}{\alpha}\right]}{\left[(\sin \gamma)^2 + (n \cos \gamma)^2\right]^{1.5}} d\gamma \dots\dots\dots(4)$$

It is assumed that the steam chamber moves from one slice to the other when it sweeps the first front slice. Therefore, time steps ( $\Delta t$ ) are calculated based on this approach from one location to the next, and at each time step, oil saturation is updated in each slice. Equation (5) calculates the time that it takes to get from slice  $i$  to the next slice. Using Equation (6), the oil saturation for each active slice is updated.

$$\Delta t = \frac{H_t^2 \phi \left[ \tan\left(\theta + \frac{\pi}{180}\right) - \tan \theta \right] (S_{o,i} - S_{o,R})}{q_{t,i}} \dots\dots\dots(5)$$

$$S_{o,i} = S_{o,i} - \frac{q_{t,i} \Delta t}{H_t^2 \phi \left[ \tan(\gamma_i) - \tan(\gamma_{i-1}) \right]} \dots\dots\dots(6)$$

In equations (4) to (6):

- $q_{t,i}$  oil production rate at slice  $i$  and time  $t$
- $U_{\max}$  maximum horizontal velocity of the steam chamber at overburden (see Fig. 2)
- $\rho_o$  oil density
- $H_t$  height of reservoir from producer to the caprock
- $\gamma$  angle (see Fig. 2)
- $\theta$  angle (see Fig. 2)
- $S_{o,i}$  current oil saturation in slice  $i$
- $S_{o,R}$  residual oil saturation
- $\Delta t$  time difference

**Energy Balance to Calculate Steam Injection Rate**

To determine the required steam injection rate, Reis3 used the law of conservation of energy. Heat loss was calculated in three zones: heat loss inside the steam chamber, heat loss from double sides of the triangular steam chamber, and heat loss to the

overburden from the top of the steam chamber. With the same approach but a different drainage model, the steam injection rate can be estimated using Equation (7).

$$M(L_s + c_w \Delta T) = (q_s \cdot \rho_w)(L_s + c_w \Delta T) = \frac{d}{dt}(Q_{in} + 2Q_{side} + Q_{top}) \dots\dots\dots (7)$$

where:

$M$	steam mass
$L_s$	specific latent heat of steam
$c_w$	specific heat of hot water
$\Delta T$	(steam – reservoir) temperature
$q_s$	steam injection rate (in volume of water)
$\rho_w$	water density
$Q_{in}$	heat loss in the steam chamber
$Q_{side}$	heat loss from one side of the steam chamber
$Q_{top}$	heat loss from the top of the steam chamber

## LINEAR GEOMECHANICAL SAGD (LGS) MODEL

In addition to the drainage model, a geomechanical model is also needed for a reservoir simulator. Stress-induced strain occurring in a SAGD process usually affects rock properties, especially permeability and porosity. Also, reservoir deformation (e.g., heave on the surface) is the result of geomechanical processes. In SAGD, two groups of stresses are active. The first is the stress caused by gravity that acts downward (vertically) on any mass. This produces a high level of stress in deep reservoirs, which behave differently than shallow reservoirs. The second group of stresses is generated by the thermal process. In SAGD, the injection of high-temperature steam will create a complex interaction between pore pressure and temperature within the reservoir as the steam chamber evolves. Temperature variations induce thermal stress in the reservoir, sequentially redistributing stress in the local and global stress field.

There are both simple and complex constitutive theories that can model the behavior of geo-materials. However, these are not easy to apply analytically and may require many parameters. Such parameters are not always available, or may themselves require extensive lab testing. These caveats aside, the equations that should be solved are mostly nonlinear and take time even for a simple plastic model.

For the purposes of this study, a simple model is adopted because: (a) the geomechanical model should be of a similar complexity to the drainage model in order to show its full capability, and (b) the model must be fast enough to be a reasonable replacement for numerical methods. Hence, in this study, a very popular method of analysis in classic geotechnical engineering, called limit equilibrium analysis, has been employed for geomechanical modeling. Limit equilibrium analysis assesses whether a mass of soil is at a state of shear failure and does not include the capacity to analyze deformations. Consequently, limit equilibrium approaches are adopted in this study, to detect shear failure and convert porosity/permeability to new values as a result of shear failure. In this sense, it only acts as a permeability/porosity converter and cannot predict any other geomechanical behavior such as heave, pore pressure, stress-strain, etc.

### **Limit Equilibrium Analysis Technique**

Limit equilibrium analysis is based on the principal of statics. Static equilibrium is achieved when the net force (and moment) on every mass body of a system is zero. However, limit equilibrium analysis looks for the body on which some known (and unknown) forces are at equilibrium. Limit equilibrium analysis theory is used in geotechnical engineering to determine the force acting on retaining walls or to determine the location of a potential failure surface in a slope. As an example, consider a concrete wall that has been backfilled with compacted soil. To find the load acting on the wall from the backfill soil, limit equilibrium analysis searches for the limit at which failure occurs. If the wall moves off the backfill, a sheared surface will initiate from the footing of the wall to the surface. But the position of the failure surface is unknown. However, on the failure surface, shear and normal forces are related based on plastic theories. Now, the problem is finding a surface on which the relation is satisfied and on which net force on the failed body is zero. Once the surface is defined, the force on the wall can be determined. More details of this technique and a comparison between limit equilibrium analysis and numerical methods have been summarized by Duncan (1996).

## Formulation

Previous research and observations (e.g. Tortike, 1993, Chalaturnyk, 1996, Li & Chalaturnyk, 2003 and 2009, Collins, 2007) confirm that changes in volumetric strain cause changes in permeability and porosity. This means that calculating volumetric strain is the first goal.

### *Average volumetric strain*

Average volumetric strain in a reservoir is defined as in Equation (8).

$$\bar{\varepsilon}_v = \left( \frac{\Delta V}{V_0} \right) \dots\dots\dots (8)$$

where:

- $\bar{\varepsilon}_v$       Average volumetric strain
- $\Delta V$       differential reservoir volume change
- $V_0$       initial reservoir volume (affected area)

Differential reservoir expansion can be determined by modifying the equations proposed by Wong and Lau (2006). The total expansion of a reservoir is the combined effect of heating the reservoir and fluid injection (see Equation 13). The first term is the volume of steam that is converted to equivalent water ( $V_S$ ). The second and third terms are expansions of material due to the release of heat from steam phase to water phase (latent heat) and from boiling temperature to the reservoir equilibrium temperature ( $V_{LH}$  and  $V_H$ ). The addition of the fourth term is to consider the volume of oil production coming out of the reservoir ( $V_P$ ).

$$V_s = q_s \Delta t \dots\dots\dots (9)$$

$$V_{LH} = (q_s \Delta t) L_s \left[ \frac{(1-\phi)\alpha_s + \phi S_w \alpha_w + \phi S_o \alpha_o}{(1-\phi)c_s + \phi S_w c_w + \phi S_o c_o} \right] \dots\dots\dots (10)$$

$$V_H = (q_s \Delta t) \Delta T' \left\{ \left[ \frac{(1-\phi)\alpha_s + \phi S_w \alpha_w + \phi S_o \alpha_o}{(1-\phi)c_s + \phi S_w c_w + \phi S_o c_o} \right] c_w - \alpha_w \right\} \dots\dots\dots (11)$$

$$V_p = q_t \Delta t \dots\dots\dots (12)$$

$$V_{total,\Delta t} = V_s + V_{LH} + V_H - V_P \dots\dots\dots(13)$$

In Equations (9) to (13):

- $V_s$  volume of steam converted to equivalent water
- $V_{LH}$  expansion of materials due to latent heat
- $V_H$  expansion of material due to differential temperature
- $V_P$  volume of oil production
- $V_{total,\Delta t}$  incremental volume changes
- $q_s$  rate of the injected steam
- $\Delta T'$  (current – equilibrium) temperature, equilibrium temperature of water
- $\Delta t$  time increment
- $\alpha_s$  thermal expansion coefficient of sand
- $\alpha_o$  thermal expansion coefficient of oil
- $\alpha_w$  thermal expansion coefficient of water
- $c_s$  heat capacity of solid grains
- $c_o$  heat capacity of oil
- $c_w$  heat capacity of water

Although the differential volume changes can be calculated by Equation (13), these equations do not provide the effective area on which deformation occurs. The limit equilibrium analysis method is adopted to compute the area or zone of shear induced deformation.

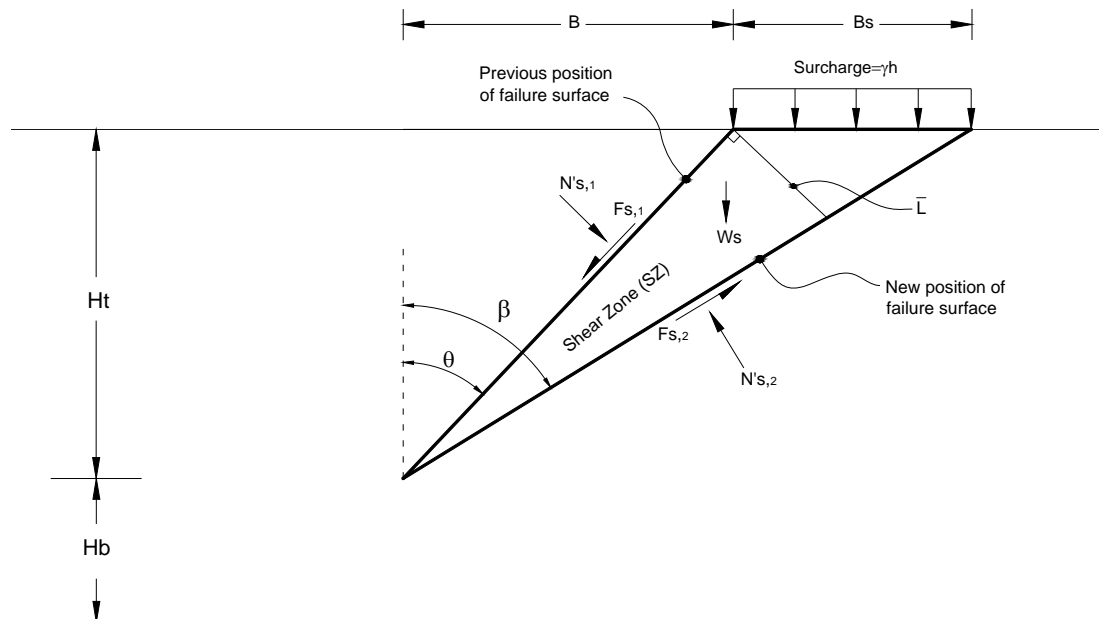


**Figure 3: Effective forces on the failure wedge.**

For the current model, it is assumed that a zone of shear failure (due to pore pressure and temperature changes) will exist at the outer edges of the advancing steam

chamber. Consider a failure surface moving in front of the steam chamber that makes a shear zone (SZ in Fig. 3). This shear zone exists in front of the steam chamber bounded by two failure surfaces. The first surface is the edge of the steam chamber that has experienced failure previously and is at residual strength. The second surface forms the right side of the shear zone and the stress state along this surface is assumed to be at the state of limit equilibrium – a state of incipient failure. The geometry of the triangular shear zone is defined by the angle  $\beta$ , which is unknown and can be determined from limit equilibrium analysis.

Using statics equations in the horizontal and vertical directions and assuming that geo-materials obey the Mohr-Coulomb criteria, Equations (14) and (15), the normal force on the left side can be calculated as reflected in Equation (16). Equation (14) shows a general form of Mohr-Coulomb criteria on the left side of the shear zone which is assumed to have reached residual strength and Equation (15) is for the right side is assumed to be at peak strength.

$$N_{s,1} = F_{s,1} \cdot \tan \phi'_r \dots\dots\dots (14)$$

$$N_{s,2} = F_{s,2} \cdot \tan \phi'_p \dots\dots\dots (15)$$

$$N'_{s,1} = \frac{\left( \frac{P_{thermal,x}}{\cos \beta - \sin \beta \tan \phi'_p} \right) - \left( \frac{P_{thermal,y} - W_s - P_{surcharge}}{\sin \beta + \cos \beta \tan \phi'_p} \right)}{\left( \frac{\cos \theta - \sin \theta \tan \phi'_r}{\cos \beta - \sin \beta \tan \phi'_p} - \frac{\sin \theta + \cos \theta \tan \phi'_r}{\sin \beta + \cos \beta \tan \phi'_p} \right)} \dots\dots\dots (16)$$

In Equations (14) to (16):

$N$	normal force
$N'$	effective normal force
$F$	shear force
$\phi'_p$	friction angle of oil sand at peak
$\phi'_r$	friction angle of oil sand at residual
$P_{thermal}$	thermal force
$W_s$	body force
$P_{surcharge}$	surcharge pressure on top of the wedge

The geometry and configuration of the forces acting on a shear zone are illustrated in Fig. 3. Both body force and surcharge pressure are calculated by multiplying the unit weight of the material by the effective area. However, calculation of the thermal force

is slightly more complex. This study proposes to determine the temperature difference between endpoints of the line shown by  $\bar{L}$  in Fig. 3, and to use the theory of elasticity to calculate the thermal force:

$$P_{thermal} = \frac{1}{2}(\bar{\alpha}\Delta T_{\bar{L}})EH_t / \cos \beta \dots\dots\dots(17)$$

where:

- $\Delta T$  temperature difference at both ends of  $\bar{L}$  in Fig. 3
- $E$  module of elasticity of oil sand
- $\bar{\alpha}$  coefficient of linear thermal expansion

Once all forces on an arbitrary wedge (for each steam chamber shape) are defined, a search phase begins to locate the position of a new failure surface on the right side of the shear zone illustrated in Fig. 3. The position of this new surface is determined by searching for the value of  $\beta$  where  $N'_{s,1}$  (Equation 16) reaches an extremum. This value of  $\beta$  provides the bounds of the affected shear zone at a time step and is used to calculate the average volumetric strain in the steam chamber and the shear zone.

### ***Shear-Induced Dilation***

Volume changes in a reservoir are comprised of both elastic and plastic components. Average volumetric strain calculated in the previous section (Equation 8) averages both categories. For the shear zone in the LGS model, it is assumed that the elastic component of strain is small and it does not contribute to the volume change and only shear strain induced plastic strains produce volume changes that influence porosity and permeability. Variation in shear stress and occurrence of shear failure in dense sands such as oil sand result in dilation. To calculate the value of volumetric shear strain due to dilation, Vaziri (1990) used Equation (18), which was originally proposed by Hansen (1985). The equation assumes that the significant portion of volumetric strain is due to dilation in oil sands compared to the small value of elastic strain.

$$\Delta\varepsilon_v = -\sin \psi' \Delta\gamma_{max} \dots\dots\dots(18)$$

In this equation:

- $\Delta\varepsilon_v$  differential volumetric strain due to dilation
- $\psi'$  dilatancy angle
- $\Delta\gamma_{\max}$  change of maximum shear strain ( $= \Delta\varepsilon_1 - \Delta\varepsilon_3$ )

As noted earlier, limit equilibrium analysis methods do not have the capability to compute deformations or strains. To apply Equation (18), however, an estimate of  $\Delta\gamma_{\max}$  and  $\psi'$  is required within the shear zone. These values can be estimated using experimental lab results due to the boundary conditions of residual shear on the left side and peak shear on the right side of the shear zone.

To determine the volumetric strain, the experimental lab results on Athabasca oil sand samples by Samieh (1995) are chosen for this study. Results of six triaxial drained tests have been plotted in Fig. 4. The shaded region in Fig. 4 is the range of axial strain between the peak strength and the residual strength. In this study, it is assumed that dilation occurring within the shear zone varies from residual strength bound to the peak strength bound. Therefore, 4.2% and 3.6% can be chosen for average axial strain and average volumetric strain, respectively.

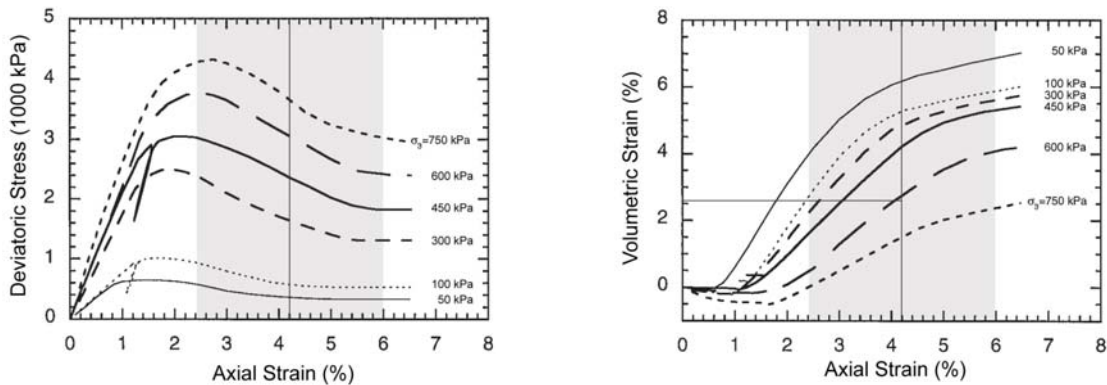


**Figure 4: Triaxial test results reported on Athabasca oil sand by Samieh (1995): deviatoric stress vs. axial strain (left) and volumetric strain vs. axial strain (right).**

In addition to Samieh’s work, Li and Chalaturnyk (2005) validated a numerical model using Samieh’s data and proposed Equation (19) to calculate the dilatancy angle where  $\gamma_p$  is the plastic shear strain.

$$\psi' = 27.348 - 1.5302\gamma_p \dots\dots\dots(19)$$



reproduced by mixing crude oil and glass beads. The range of grain sizes was chosen to satisfy Reynolds' number between the prototype and a typical oil sands reservoir. This means that only the hydraulic characteristics of the model were reconstructed, and no more consideration was made for geomechanical properties. In the study by Chung and Butler (1988), no apparent rock/soil structure can be expected in between the glass beads. Other than interaction between the glass beads, no surcharge load was applied to simulate the overburden pressure. Also, the rate of loading (thermal loading in SAGD) was uncontrolled to mimic the stress field. Therefore, the results of this lab test can be used for validation of the drainage model (the model of slices) only. The lab data is provided in Table 1.

**Table 1: Experimental parameters, Chung and Butler, 1988.**

Properties	Value	Unit
porosity	39	%
initial oil saturation	100	%
residual oil saturation	5	%
absolute permeability	2930	Darcy
relative permeability	0.48	-
oil density	0.98	gm/cc
model height	0.21	m
thermal diffusivity	0.0507	m <sup>2</sup> /day
constant 'a'	0.4	-
constant 'm'	3.6	-
oil viscosity	9	m <sup>2</sup> /day
model thickness	0.03	m

Utilizing the data in Table 1, LGS simulations without geomechanics were run to match the lab test. Fig. 6 plots the variation of oil saturation at any point in front of the steam chamber. Although the exact value of oil saturation was not included in the paper by Chung and Butler (1988), the location of the steam chamber is comparable to the result of this study. This graph shows a new ability of theoretical models to determine oil saturation in the reservoir at each specific time.

Simulated results of oil production rate, steam chamber angle, and cumulative oil production are compared with lab data and also with the results of Reis' model in Fig. 7. While Reis' model predicts a constant value of oil production, the model of slices (this study) is reasonably capable of tracking the variation of oil rate. The difference also shows up in the nonlinearity of cumulative oil production. Although on a laboratory scale these differences appear minor, these differences are magnified for a

full scale reservoir. It is expected that the nonlinear capability embedded in the model of slices will provide improved history matches to field performance.

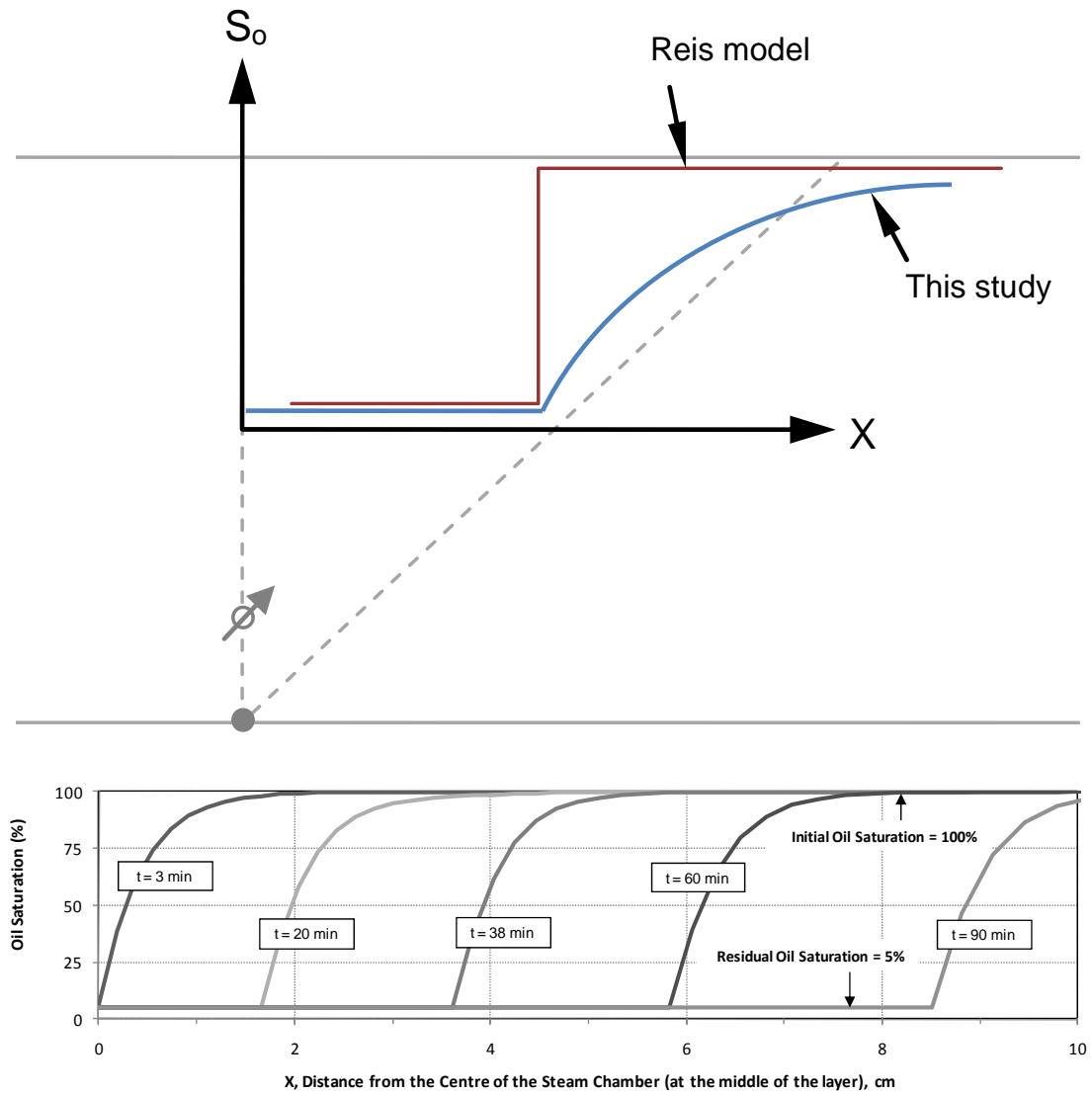


**Figure 6: Oil saturation in front of the steam chamber.**

Fig. 6 and 7 validates the accuracy of the model of slices and shows that the model can be a useful tool for drainage simulation purposes in a SAGD process. The fluctuation of oil rate predicted by the model of slices at the very beginning of the process shares the same limitation as other similar models (e.g. Reis' and Butler's models) where it is assumed that the steam chamber grows only laterally in the model and the upward growth of the steam chamber is not included in the formulation.

## HISTORY MATCHING BY LGS MODEL

History matching is a technique in which the results of a simulator are fitted to observed performance data by adjusting some effective parameters like permeability or porosity. This process is time consuming when the simulator has a numerical-based solver and each run takes between a couple of hours and a couple of days.

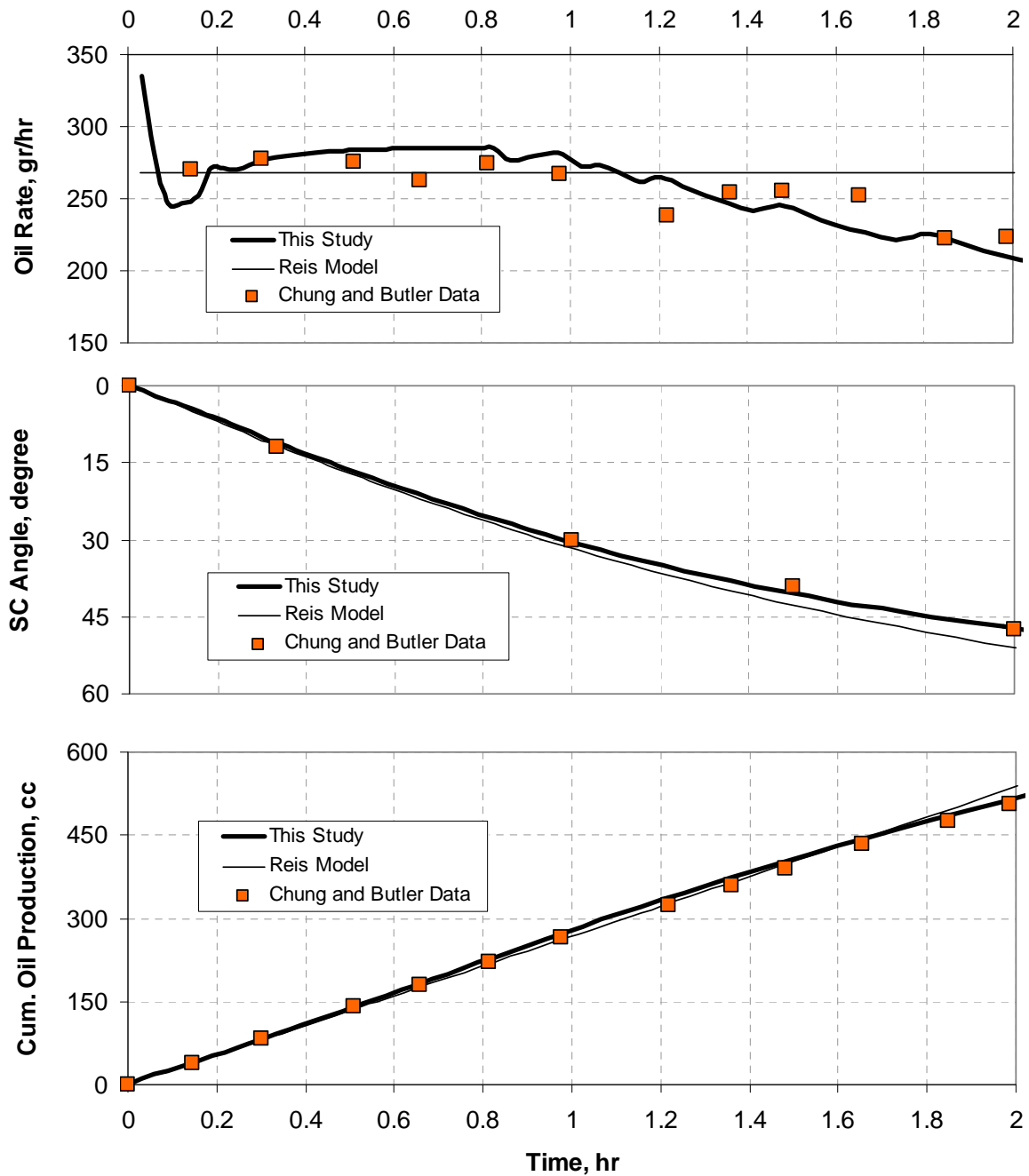


Figure 7: Results of lab data compared to results of the model of slices and Reis model (1992).

The difficulty of history matching is increased when another solver is added to perform a geomechanical coupled analysis. In this section, the result of a sample coupled numerical modeling reported by Li (2006) has been adapted as truth data, and history matching is applied to the data using the proposed LGS model. Li (2006) proposed his methodology by coupling a flow and a geomechanical simulator, and validated it using field monitoring results from the UTF phase A project. Therefore, the sample model employed from Li's work is assumed to be rather realistic.

**Table 2: Parameters of the LGS model.**

Property	Value	Unit
horizontal/vertical permeability	2	-
horizontal permeability	1100	mD
average relative oil permeability	0.48	-
Oil density	1008	kg/m <sup>3</sup>
gravity acceleration	9.81	m/s <sup>2</sup>
reservoir thickness	50	m
surcharge height	317	m
dynamic viscosity at steam temperature	0.007	Pa.s
porosity	34	%
oil saturation difference	68	%
reservoir thermal diffusivity	0.0000006	m <sup>2</sup> /s
reservoir temperature	11	°C
steam temperature	240	°C
equilibrium temperature	100	°C
formation heat capacity	2100000	J/ (m <sup>3</sup> °C)
latent heat of steam	1740000	J/Kg
steam quality	98	%
water density	1000	kg/ m <sup>3</sup>
formation density	21950	N/ m <sup>3</sup>
linear thermal expansion coefficient	0.000001	1/°C
Young's modulus	756000000	Pa
oil-sand friction angle, peak	45°	-
oil-sand friction angle, residual	20°	-
sand thermal expansion	0.00005	1/°C
water thermal expansion	0.00045	1/°C
oil thermal expansion	0.00062	1/°C
specific heat capacity of water	4200	J/(kg °C)
specific heat capacity of oil	1658	J/(kg °C)
specific heat capacity of sand	735	J/(kg °C)
coefficient of viscosity change, m	3.9	-
coefficient of average velocity, a	0.4	-
initial oil saturation	85	%
initial water saturation	15	%
injector/collector length	700	m

Reservoir and geomechanical properties of the model are listed in Table 2 to the extent they are needed for the LGS model. Since the width of Li's model was not

infinity, LGS simulations are run until the steam chamber nears the boundaries. Fig. 8 compares the geometry of the two models. In the first step, the data is compared to the results of the flow model (model of slices). Fig. 9 shows the history matching results of oil production and steam injection without geomechanical coupling. The history matching results for both oil and steam is done well, with close agreement.

There are two regions in which the data and the predicted model do not match perfectly. At the beginning of the process, the shape of the simulated curve is not close enough to the data. Since the model of slices simulates the process only when the steam chamber reaches the caprock, and the process is unrealistic at the beginning, turbulence is expected. After this sudden change, the simulation correctly follows the data. The other disagreement between data and simulation results occurs at the end of simulation. This is also acceptable and can be attributed to the effects of side boundaries.

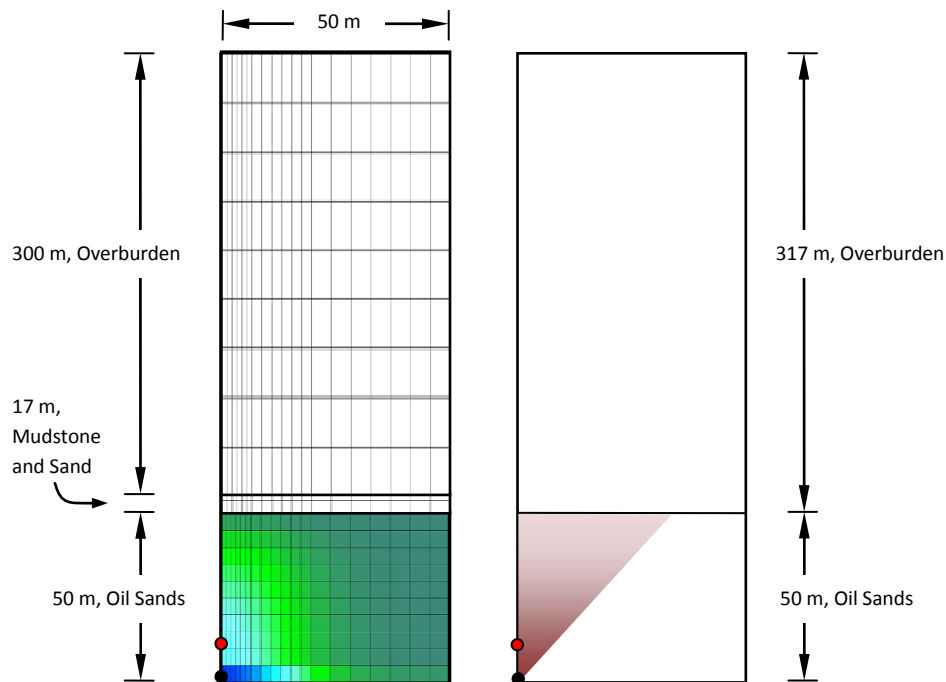


**Figure 8: Geometry of the numerical model by Li (2006) on left and LGS model on right.**

Coupled history matching is illustrated in Fig. 10. The two graphs in this figure also agree strongly with the data. However, the beginning and end of the simulation do have the same divergence, for the reason discussed above. Steam/Oil Ratio (SOR) is

sometimes referred to as the financial chart of SAGD. Cumulative SOR for both coupled and uncoupled cases is plotted in Fig. 11. Three major elements may affect SOR in the two charts: the model of slices, the LGS model, and the theory that interprets the required steam injection. Fig. 11 shows that for both cases, there is a slight difference between prediction and the results of the numerical simulator (Li's data). The error in prediction comes mostly from the poor prediction of steam injection, and has the same effect in both coupled and uncoupled simulations. This reveals that the geomechanical model is at the same level of accuracy as the drainage model, and does not inject higher divergence into the mathematical simulation. It is also showing that the calculated SOR is higher in the case of uncoupled modeling than in coupled simulations when geomechanical effects are considered.

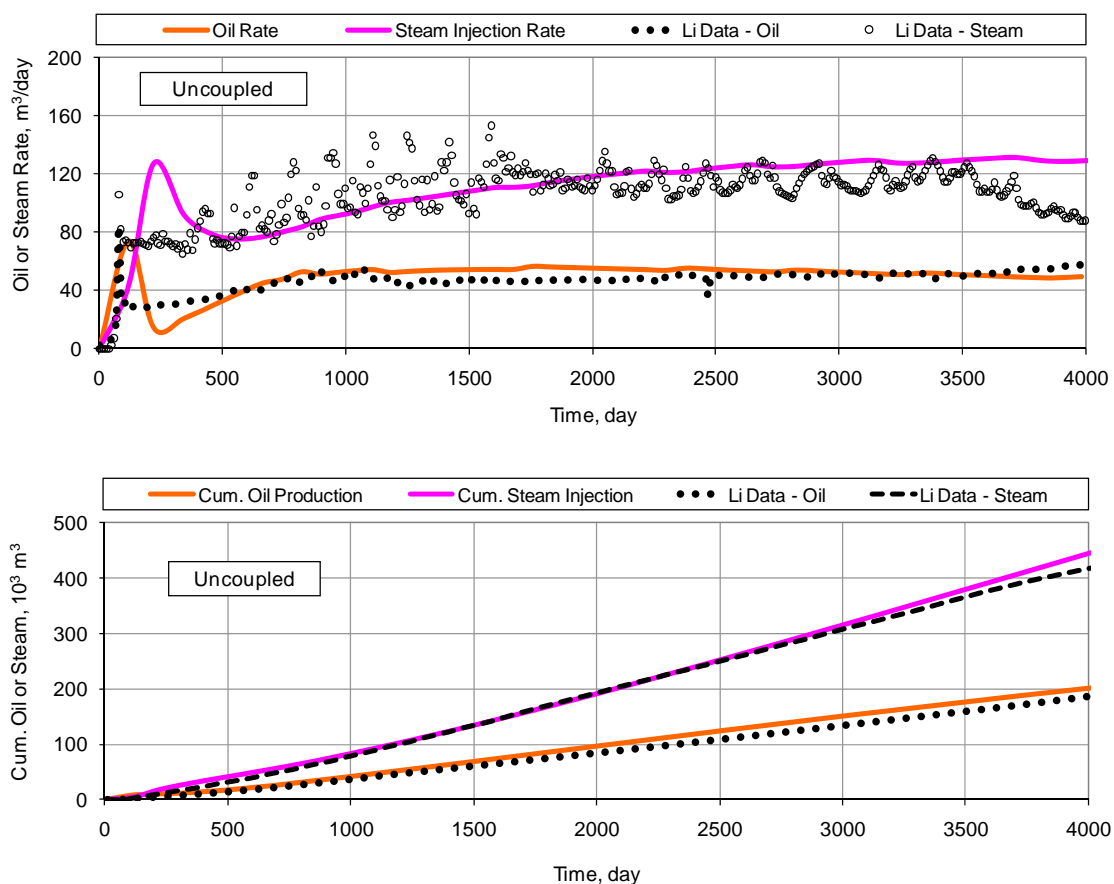


**Figure 9: Oil production and steam injection predicted by the model of slices.**

Additional results from the LGS model are shown in Fig. 12(a) to 12(c). Each sub-graph in Fig. 12 reflects the contribution of the geomechanical process in SAGD and

is discussed below. Fig. 12(a) shows the growth of the shear zone vs. the growth of the steam chamber. The jump of the shear zone from zero to 20 degrees is analogous to passive shear failure in retaining walls where the failure surface appears at  $\pi/4 - \phi'/2$  ( $=22.5^\circ$  in our case). Passive loading condition for the SAGD case arises from thermal expansion induced stress. This means that the supporting idea of geomechanics in LGS is working well. This would not happen outside the lab, as the steam chamber does not start growing after touching the cap rock. The figure also shows that after the steam chamber gets close to 50 degrees, no shear zone appears in front of the chamber, and expansion is limited to the steam chamber.

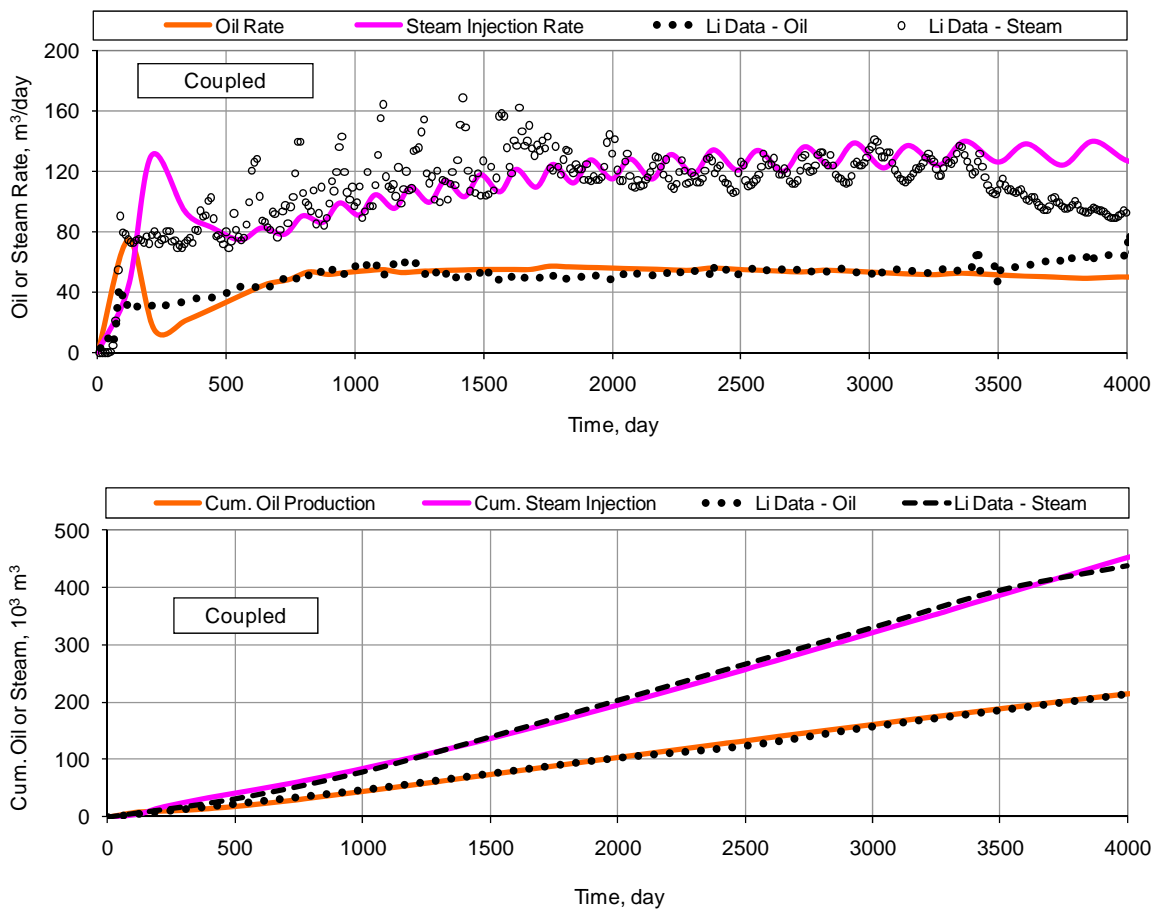


**Figure 10: Oil production and steam injection predicted by the LGS model.**

It should not be forgotten that in this case (50 degrees), a very large part of the reservoir is recovered by the steam chamber. Growth of shear zone vs. time is also shown in Fig. 12(b). The figure says that geomechanical effects appear mostly at the

early stages of the SAGD process. Histories of the position of the steam chamber in coupled and uncoupled simulation have been compared in Fig. 12(c). This plot shows that the position of steam chamber does change significantly in coupled analysis.

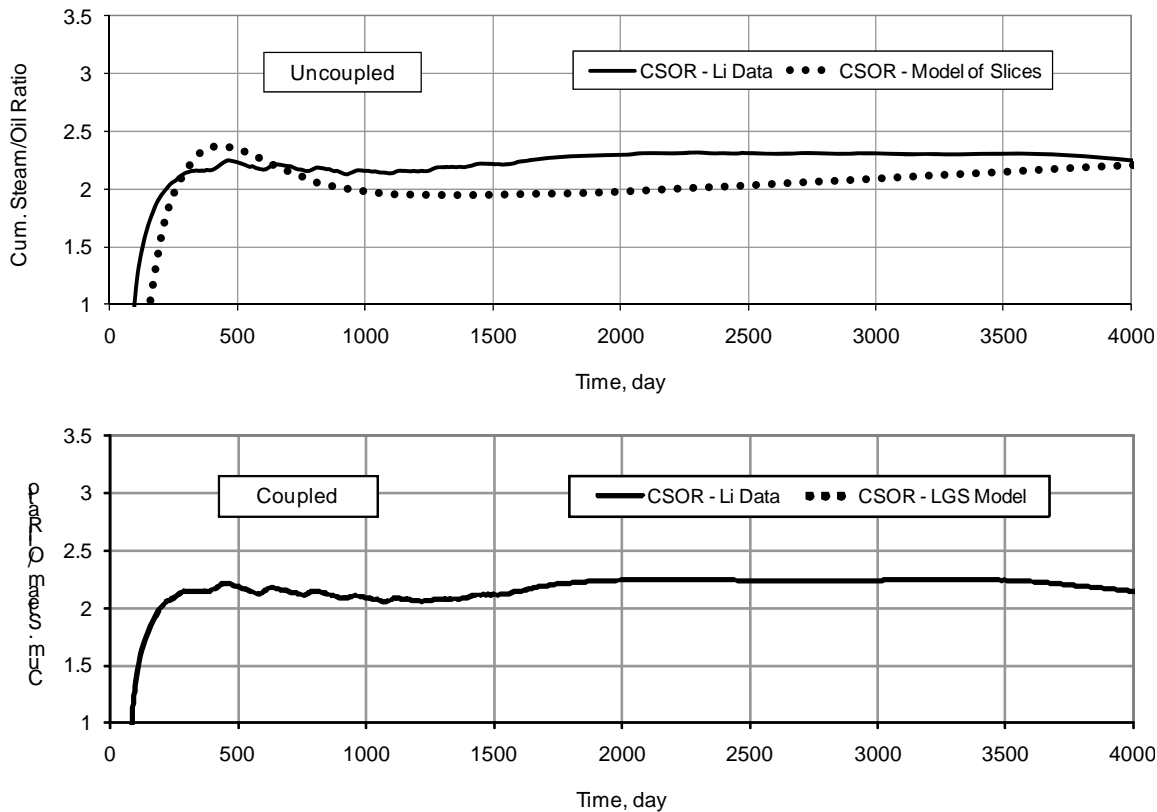


Figure 11: Results of this study compared to numerical modeling: cumulative SOR for uncoupled simulation (top), cumulative SOR for coupled simulation (bottom).

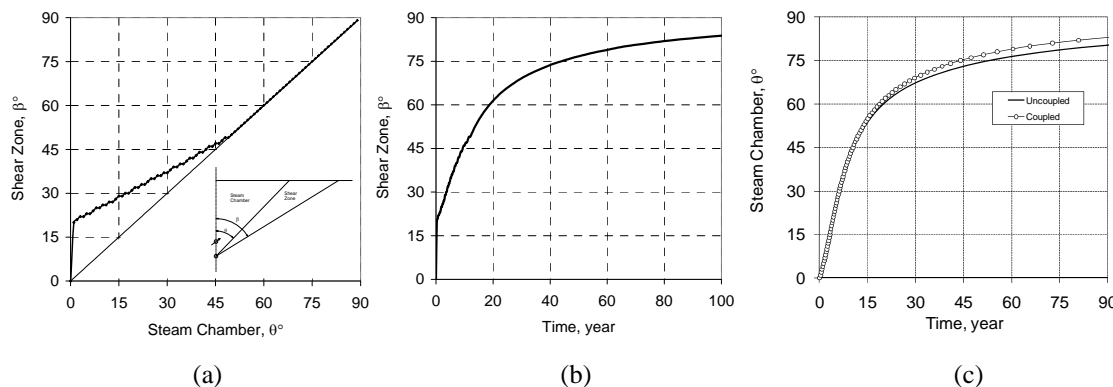


Figure 12: Results of LGS model: (a) growth of shear zone vs. growth of steam chamber, (b) growth of shear zone vs. time, (c) growth of the steam chamber in coupled and uncoupled analysis.

## CONCLUSION

Current geomechanical coupling practice for modeling a SAGD process suggests combining a numerical multi-phase flow and a (geo)mechanical simulator. This technique, though reasonably correct and inclusive of full physics, is very time consuming for history matching purposes. When real time monitoring data is available, it is almost impossible to update numerical models in real time. Therefore, low-order analytical models that can capture essential parts of physics with certain levels of divergence would be acceptable for fast history matching. Numerical models would work as a proxy in a multi-layer optimization loop.

In this paper, the idea of replacing numerical coupling methods with an analytical coupling model was developed for SAGD. The model has two elements: (a) a drainage model which is founded on the Butler/Reis theory and benefits from the model of slices to calculate oil saturation in front of the steam chamber as it grows, and (b) a geomechanical solver called the LGS model, with limit equilibrium analysis method within the model to update permeability and porosity.

The model of slices and the LGS model were validated by data available in the literature. The model can reasonably predict the SAGD process and honors the realistic values of permeability and porosity.

The comparison of simulations using the proposed models in this study with lab testing results and reservoir-geomechanical simulation results has shown that the models can be deployed as a proxy model for real time history matching. Additional work is continuing at enhancing the capability of the model to incorporate improved treatment of the steam chamber geometry, including components of the vertical growth of the steam chamber. As this is the first time that this method is applied in SAGD simulations, it is recommended to be used with caution, however.

## REFERENCES

Akin, S. 2005. Mathematical modelling of steam-assisted gravity drainage. *SPE Reservoir Evaluation and Engineering*. 8(5): 372-376.

- Butler, R.M., and Stephens, D.J. 1981. The gravity drainage of steam-heated heavy oil to parallel horizontal wells. *Journal of Canadian Petroleum Technology*. 20(2): 90-96.
- Chalaturnyk, R.J. 1996. Geomechanics of the Steam-Assisted Gravity Drainage Process in Heavy Oil Reservoirs. *PhD Dissertation*, University of Alberta, Edmonton, Canada.
- Chung, K.H. and Butler, R.M. 1988. Geometrical effect of steam injection on the formation of emulsions in the steam-assisted gravity drainage process. *Journal of Canadian Petroleum Technology*. 27(1): 36-42.
- Collins, P.M. 2007. Geomechanical effects on the SAGD process. *SPE Reservoir Evaluation & Engineering*. 10(4): 367-375.
- Duncan, J.M. 1996. State of the art: limit equilibrium and finite element analysis of slopes. *Journal of Geotechnical Engineering*. 122(7): 577-596.
- Hansen, B. 1985. Line ruptures regarded as narrow rupture zones, basic equation based on kinematics considerations. *Proc., the Brussels Conference on Earth Pressure Problems*, 39-48.
- Li, P. 2006. Numerical simulation of the SAGD process coupled with geomechanical behaviour. *PhD Dissertation*, University of Alberta, Edmonton, Canada.
- Li, P., and Chalaturnyk, R.J. 2003. Discussion of SAGD and geomechanics. *The Journal of Canadian Petroleum Technology*. 42(9): 37-39.
- Li, P. and Chalaturnyk, R.J. 2005. Geomechanical model of oil sands. *Proc., SPE International Thermal Operations and Heavy Oil Symposium*, 1-3 November, Calgary, Canada.
- Li, P. and Chalaturnyk, R.J. 2009. History match of the UTF Phase A project with coupled reservoir geomechanical simulation. *The Journal of Canadian Petroleum Technology*. 48(1): 29-35.
- Liang, L. 2005. An Analytical Model for Cyclic Steaming of Horizontal Wells. *MSc Thesis*. Stanford University, USA.
- Nukhaev, M., Pimenov, V., Shandrygin, A. and Tertychnyi, V. 2006, A New Analytical Model for the SAGD Production Phase. *Proc., SPE Annual Technical Conference and Exhibition*, 24-27 September, San Antonio, Texas, USA.
- Reis, J.C. 1992. A steam-assisted gravity drainage model for tar sands linear geometry. *Journal of Canadian Petroleum Technology*. 31(10): 14-20.
- Reis, J.C. 1993. A steam-assisted gravity drainage model for tar sands radial geometry. *Journal of Canadian Petroleum Technology*. 32(8): 43-48.

Samieh, A.M. 1995. Behavioral characteristics and constitutive modeling of Athabasca tar sand at low effective stresses. *PhD Dissertation*, University of Calgary, Calgary, Canada.

Tortike, W.S. 1991. Numerical simulation of thermal multiphase fluid flow in an elasto-plastic deforming oil reservoir. *PhD Dissertation*, University of Alberta, Edmonton, Canada.

Tortike, W.S. and Farouq-Ali, S.M. 1993. Reservoir simulation integrated with geomechanics. *Journal of Canadian Petroleum Technology*. 32(5): 28-37.

Vaziri, H.H. 1990. Numerically-derived stress, strain and thermodynamic properties of Athabasca oil sand. *Proc., the Annual Technical Meeting, CIM-SPE*, Calgary.

Wong, R.C.K. and Lau, J. 2006. Surface heave induced by steam stimulation in oil sand reservoirs. *Proc., the 7<sup>th</sup> Canadian Int. Petroleum Conference*, Calgary, Canada.

## APPENDIX A: MODEL OF SLICES

General form of Darcy's law for a slice (refer to Fig. 2) at time t (or steam chamber angle of  $\theta$ ) can be written as:

$$dq_t = \frac{K_\gamma \rho_o}{\mu(X)} \nabla \Phi dA \dots\dots\dots (A-1)$$

where:

- $K_\gamma$  relative permeability of oil along the centre of the slice
- $\rho_o$  oil density
- $\mu(X)$  oil viscosity at distance 'X' from the top of the steam chamber
- $\nabla \Phi$  flow potential function
- $dA$  differential effective area

Equations (A-2) and (A-3) express the viscosity of oil at distance X from a moving front with a constant velocity. It should be noted that the parameter a is dimensionless and has been used here to justify the maximum velocity.

$$\mu(X) = \frac{\mu_{os}}{(T^*)^m} \dots\dots\dots (A-2)$$

$$(T^*)^m = \exp\left(\frac{-amU_{\max}X}{\alpha}\right) \dots\dots\dots (A-3)$$

$$\nabla \Phi = \frac{gH_t}{r} = \frac{gH_t}{H_t/\cos \gamma} = g \cos \gamma \dots\dots\dots (A-4)$$

$$dA = rd\gamma = \frac{H_t}{\cos \gamma} d\gamma \dots\dots\dots (A-5)$$

Combining equations (A-1) to (A-5) gives (A-6):

$$dq_t = \frac{K_\gamma \rho_o g H_t}{\mu_{os}} \exp\left[\frac{-amU_{\max} H_t (\tan \gamma - \tan \theta)}{\alpha}\right] d\gamma \dots\dots\dots (A-6)$$

Plugging the relation between horizontal and vertical permeability from Equation (A-7), multiplying it by 2 and integrating from zero to 90 degrees yields to Equation (A-9). This equation determines oil flow rate at each position of the steam chamber (or at a specific time,  $t$ ).

$$K_\gamma^2 = \frac{K_o^2}{(\sin \gamma)^2 + (n \cos \gamma)^2} \dots\dots\dots (A-7)$$

$$dq_t = \frac{K_o \rho_o g H_t}{\mu_{os}} \times \frac{\exp\left[\frac{-amU_{\max} H_t (\tan \gamma - \tan \theta)}{\alpha}\right]}{[(\sin \gamma)^2 + (n \cos \gamma)^2]^{0.5}} d\gamma \dots\dots\dots (A-8)$$

$$q_t = \frac{2K_o \rho_o g H_t}{\mu_{os}} \int_{\theta}^{\frac{\pi}{2}} \frac{\exp\left[\frac{-amU_{\max} H_t (\tan \gamma - \tan \theta)}{\alpha}\right]}{[(\sin \gamma)^2 + (n \cos \gamma)^2]^{0.5}} d\gamma \dots\dots\dots (A-9)$$

# CHAPTER 3: AN IMPROVED SAGD ANALYTICAL SIMULATOR: CIRCULAR STEAM CHAMBER GEOMETRY\*

## **ABSTRACT**

An elegant analytical model for the Steam Assisted Gravity Drainage (SAGD) process was firstly proposed by Butler and his colleagues for oil sands reservoirs in Canada. Some years later, Reis proposed two additional analytical linear and radial geometry models that were able to mimic the SAGD process satisfactorily. Since then, other mathematical models have been developed all with similar approaches considering that steam chamber has been reached the caprock. This assumption causes the model to predict a constant oil production rate, which is not closely the case in reality.

To overcome this shortcoming for practical history matching purposes, the current study modifies the Butler/Reis model to simulate the SAGD process from the beginning of the steam chamber growth. The study offers a circular geometry formulation using a discrete method of analysis, called the method of slices, to solve the analytical equations. The proposed geometry and formulation show better capability to reproduce the SAGD process analytically.

---

\* A version of this chapter was published in Azad, A. and R.J. Chalaturnyk, 2012. An Improved SAGD Analytical Simulator: Circular Steam Chamber Geometry. J. of Petroleum Science and Engineering, Vol. 82-83, pp. 27-37.

## INTRODUCTION

Steam Assisted Gravity Drainage (SAGD) is a thermal recovery process developed in early 80's for Canadian oil sands reservoirs. The process includes a pair of horizontal boreholes drilled one on top of the other with some vertical spacing near the bottom of the reservoir. Steam is injected through the top borehole, called the injector, and the lower borehole, the producer, is responsible of collecting oil. SAGD is usually deployed in the reservoirs when the oil sand formation lies in depth and it is not minable. Configuration of a SAGD process is illustrated in Figure 1. The fundamental SAGD concept is that the injected steam transfers internal heat into the reservoir and the steam is then transformed to liquid phase. The heat loss will mobilize the bitumen locked in the oil sand structure by decreasing the viscosity, and then drains to the producer under gravity. This process generally happens in a region influenced by the injected steam around the injector at the steam temperature. The affected region is called the steam chamber and it is used to demonstrate the SAGD progress inside the reservoir. In the preheating period at the beginning of the process, steam is circulated in both wells to establish the communication between the two boreholes and to increase the injectivity. It takes several months until the injector is opened for injecting high pressure and high temperature steam into the reservoir and the bottom borehole is converted into a production well. Steam injection causes the steam chamber to grow and it gradually occupies larger regions of the reservoir. The physics of the SAGD process appears simple and the predominant production mechanism is thermal heat transfer. However, other mechanisms are also involved in SAGD process. As an example, geomechanical reactions of the reservoir system (reservoir, caprock, over and underburden) are shown to occur simultaneously (Chalaturnyk, 1996).

Butler et al. (1980, 1981) were the first team to work on SAGD. Focusing on small scale experimental tests, they investigated the development of SAGD for industrial purposes. Moreover, they proposed an analytical model, commonly called 'Butler model', that was able to generally predict the process. Butler model was founded on two simple theories: (a) one dimensional heat transfer (thermal) that solves the heat distribution for a moving front, and (b) Darcy's law (flow) to calculate the potential

and magnitude of the flow of oil. Using these two theories and a non-linear assumption for variation of viscosity in front of the steam chamber, Butler model is the most elegant drainage model for SAGD. The model however, had some shortcomings. In the original model, the steam chamber was not constrained for passing across the producer. This problem was later solved in TANDRAIN model (Butler and Stephens, 1981) by considering a reduction factor to oil production. Another concern was about the growth of the steam chamber before touching the top of the reservoir (cap rock). Butler model assumes that the production initiates when the steam chamber touches the cap rock and the lateral growth is started. Therefore, the model was regularly revised and more features of the process were appended to the model in separate theories. The rising steam chamber model and a model to consider the effect of boundaries were proposed later by Butler to capture more essential phenomena of the SAGD process (Butler, 1997).

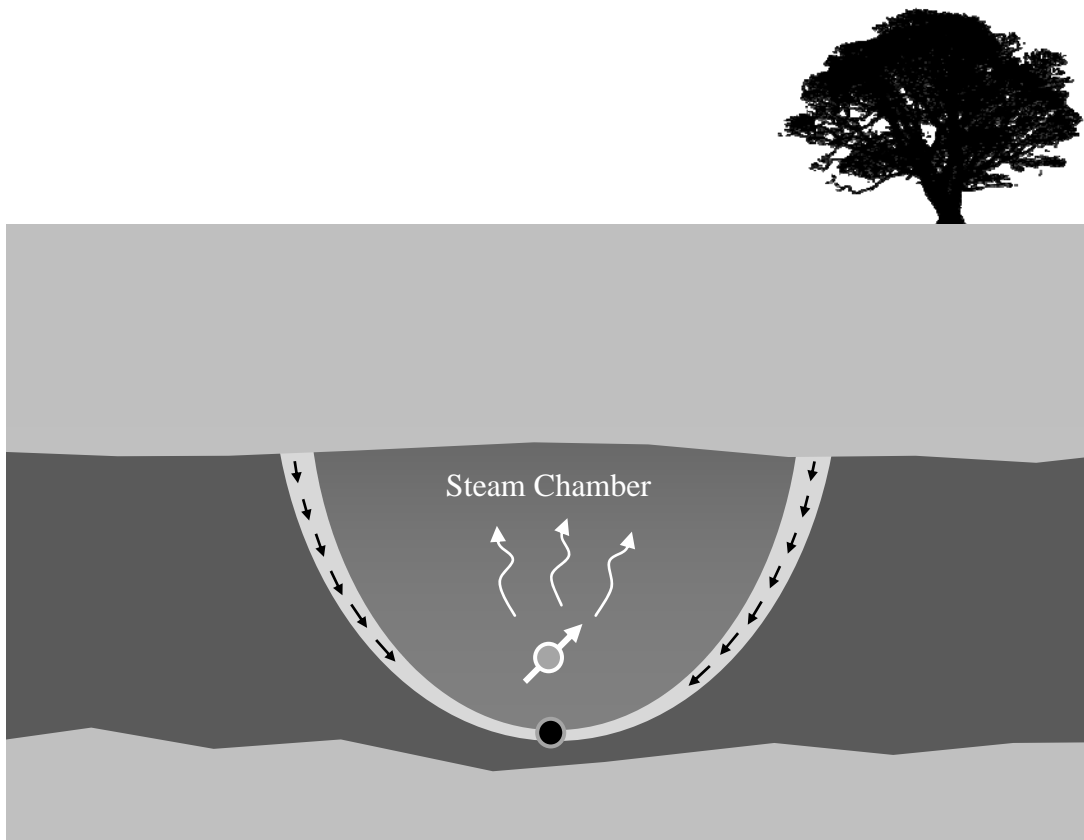


**Figure 1: Basic elements of a SAGD project.**

Experimental works by Butler et al. (1980, 1981), Chung and Butler (1988), and the results of the Underground Test Facility (UTF), Phase A (e.g., reported by Chalaturnyk, 1996 and Edmunds et al., 1994) showed that the growth of the steam chamber have different stages. When the communication between the injector and the producer is established, the steam chamber rises up to touch the reservoir caprock, and then begins to grow laterally.

Although Butler theory assumes that the steam chamber grows laterally only, it is still the foundation of all other theoretical models. Reis (1992) based on the fundamentals of Butler theory, proposed a new model to support the drainage mechanism of SAGD by constraining the shape of the steam chamber to a linear geometry and found similar results to Butler model. He indicated that his model is a function of Butler theory and they can be transformed to each other by a constant multiplier. Eq. 1 shows the mathematical form of the Butler model for oil production rate. Eq. 1 can be compared to the Reis theory in Eq. 2 to show that both models even with different steam chamber geometry but with the same approach obtain similar results. The two models predict a constant value for the oil production and additional modifications are needed to be employed to simulate the truth of the process.

$$q = 2L \sqrt{\frac{2kg\alpha\rho\phi\Delta S_o H}{m\mu_{os}}} \dots\dots\dots(1)$$

$$q = 2L \sqrt{\frac{kg\alpha\rho\phi\Delta S_o H}{2am\mu_{os}}} \dots\dots\dots(2)$$

where:

- $q$  = oil production rate
- $L$  = length of boreholes
- $k$  = absolute oil permeability
- $\alpha$  = thermal diffusivity of the reservoir
- $\rho$  = oil density
- $\phi$  = porosity
- $\Delta S_o$  = (initial – residual) oil saturation
- $\mu$  = dynamic oil viscosity at steam temperature
- $H$  = reservoir height
- $m$  = coefficient of viscosity
- $a$  = coefficient of velocity

Other researches on analytical modeling of SAGD includes Reis (1993), Akin (2005), Liang (2005), Nukhaev et al. (2006), and Azad and Chalaturnyk (2010) all of which studied different aspects of steaming the horizontal wells. However, the fundamental assumption in all cases is the concept introduced in Butler theory with one-way steam chamber growth. As an example, Azad and Chalaturnyk (2010) proposed an improved model for SAGD by considering geomechanics in the theory. They took the Reis model with linear geometry and used a numerical approach to solve the equations to count for the gradual changes of the oil saturation at the edge of the steam chamber. Although their model was successful to capture essential features of the SAGD physics, it needs to be developed to realistically mimic the different stages of the steam chamber expansion.

The work presented here improves the analytical Butler/Reis drainage solution by removing the previous geometrical assumptions. The model benefits from a discrete method of analysis, called the method of slices, for flow simulation in SAGD and uses the growing circular steam chamber geometry. The circular geometry can model the whole process since the steam chamber appears, gradually rises to touch the cap rock, and when it expands laterally to cover large parts of the reservoir.

## **METHOD OF SLICES**

When additional features of the SAGD process are combined to the Reis or Butler models, the integrals are not usually solvable in closed form. Hence, a numerical approach is required for integration. A well-established technique in mathematics for solving an integral is to divide the area under the integral function into limited slices (e.g. rectangles or trapezoids). It is of interest to define the equation variables and the integral limits so that the slices under the function get a physical meaning, too. This idea was adapted in the model proposed by Azad and Chalaturnyk (2010), called the method of slices. Figure 2 shows the framework of the method of slices proposed for linear geometry of the steam chamber. Each slice in advance of the steam chamber represents a numerical slice of its integral. It should be noted that the equations are derived in a continuum medium and is not divided into slices from the beginning.

Therefore, slices are the result of mathematical solution rather than physical separation.

Unlike past theories, this approach can consider relative permeability variation with oil saturation changes. The methodology divides the reservoir into several slices. Subsequently, the material balance is calculated for each slice in front of the steam chamber. Eventually, the oil saturation is updated due to the oil produced from each slice at each specific time (or steam chamber position).

When the steam chamber is at a specific location, for each slice in front of the separation line, oil rate is calculated. It is assumed that the steam chamber moves from one slice to the other only when the current oil saturation of the first front slice declines to residual oil saturation. Therefore, the remaining oil volume in the first slice can be used to calculate relative permeability and the time needed to produce the oil from that slice. This is also the required time for the steam chamber to move on.

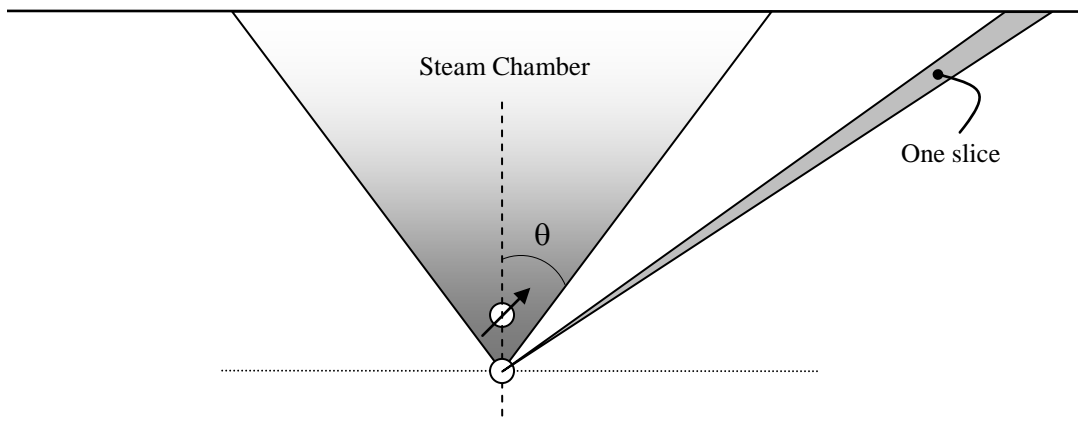


**Figure 2: Model of slices, from Azad and Chalaturnyk (2010). One slice has been plotted on one side of the steam chamber as an example.**

The model proposed by Azad and Chalaturnyk (2010) originally uses a linear geometry for steam chamber slices that grows laterally only assuming that the steam chamber has reached the caprock. They showed that this theme is inadequate to predict the first and final stages of the process. Figure 3 has plotted the growth of steam chamber observed in UTF phase A (Ito and Suzuki, 1996). From the temperature isolines illustrated in Figure 3, one might pick a circular geometry for the steam chamber rather than a straight line. It is also required that the geometry be

flexible to capture the growth of the steam chamber before and after touching the caprock.

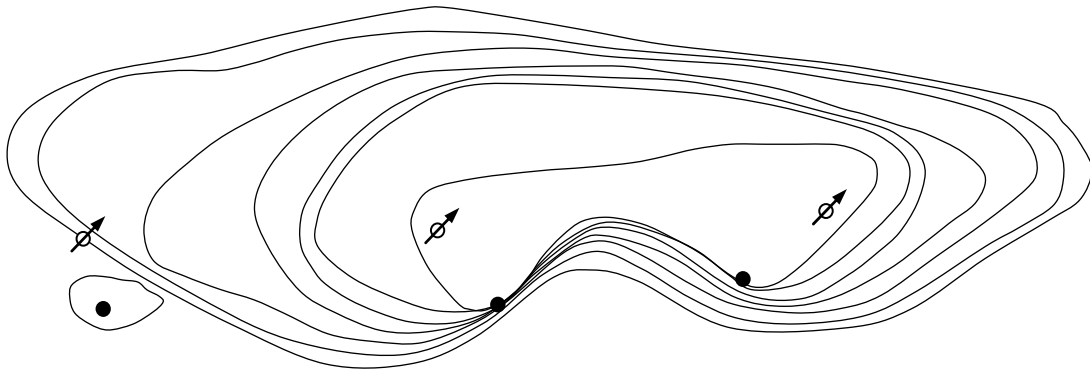


**Figure 3: Growth of steam chamber observed during phase A of UTF project (adopted from Ito and Suzuki, 1996).**

Linear geometry and circular geometry of the steam chamber in SAGD have been compared in Figure 4. The figure shows that the circular geometry can be a better option compared to the linear shape of the steam chamber because it can mimic the initial stages of the process. In addition, in long time perspective, the steam chamber does not need to get unrealistic shape to cover further reservoir regions.

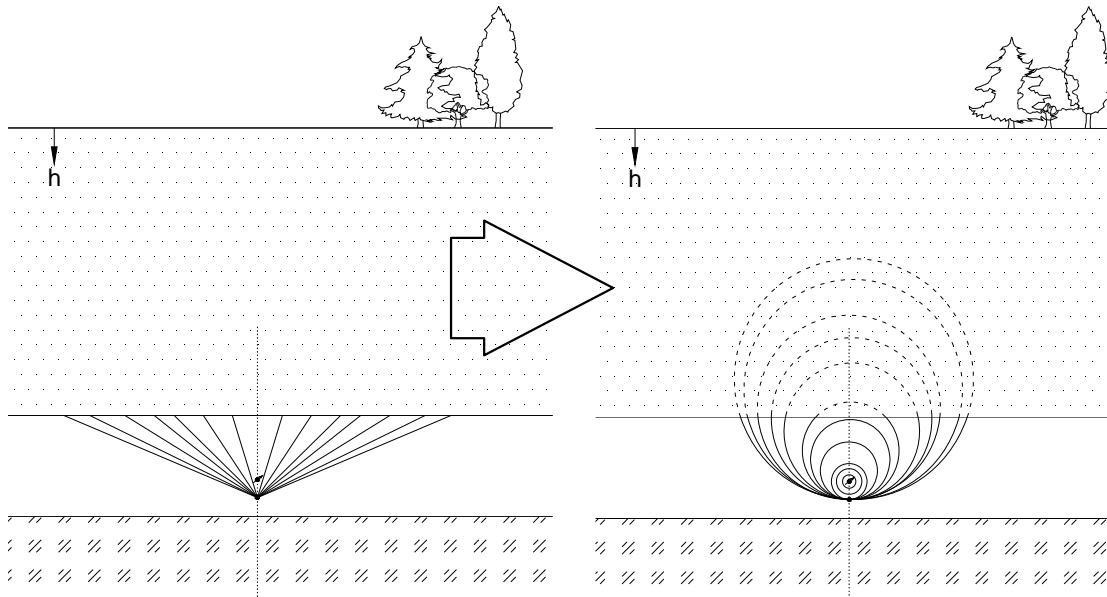


**Figure 4: Comparison between linear and circular geometry of the steam chamber.**

## ANALYTICAL MODEL FOR CIRCULAR GEOMETRY

### Drainage Theory

For a circular geometry, different possible steam chamber locations have been plotted in Figure 5. It is assumed that the SAGD process starts when the steam chamber reaches the producer borehole. This happens after the primary period of heating or ‘start up’ phase in which steam is injected through both injector and producer to establish communication in between boreholes. Therefore, the first steam chamber (‘Start’ in Figure 5) is the circle whose center is the injector borehole and its radius is the well spacing. This circle appears a short time after the ‘start up’ phase. The bottom point at which the steam chamber touches the producer borehole is now fixed and the steam chamber grows while its lower point is attached to the producer borehole. Case ‘A’ occurs when the steam chamber has not reached the cap-rock. As soon as the steam chamber touches the cap-rock the shape is not a complete circle anymore. Two possible positions of steam chamber may occur: case ‘B’ when the center of the circle is located inside the oil sand layer and case ‘C’ where the steam chamber extends to the overburden.

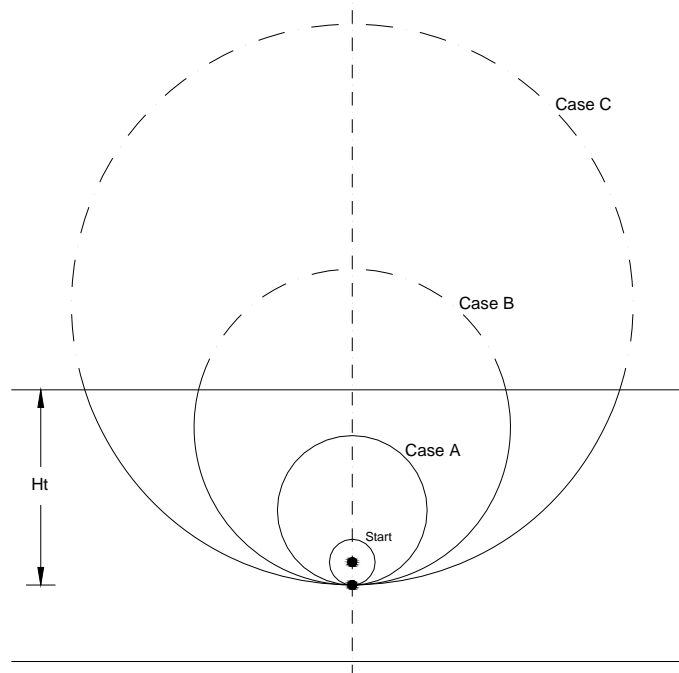


Figure 5: Possible positions for a circular steam chamber.

The foundation of the theory proposed by Butler is Darcy's law for flow of oil shown in Eq. 3. This can be applied to one slice as shown in Figure 6 to follow the model of slices, where relative permeability is estimated from current oil saturation of the slice. For SAGD process, it is common to consider two phase only, oil-water, neglecting any gas coming out of solution during the SAGD process. Therefore, relative permeability of oil is the shared factor between two phases; water and oil.

$$dq_t = \frac{K_{ro} K_o \rho_o}{\mu} \nabla \Phi dA \dots\dots\dots(3)$$

where:

- $dq_t$  = differential flow of oil at time t
- $K_{ro}$  = relative oil permeability
- $K_o$  = absolute oil permeability
- $\rho_o$  = oil density
- $\mu$  = oil viscosity
- $\nabla \Phi$  = flow potential function
- $dA$  = differential area

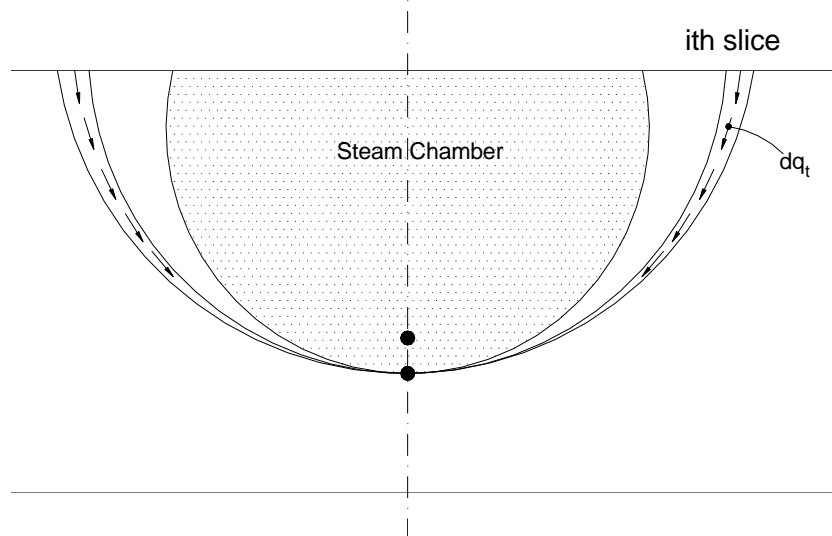


**Figure 6: Model of slices for circular geometry of steam chamber.**

All the material properties in Eq. 3 are defined for the slice on which calculation is carried out. If oil density is assumed constant, viscosity has to be calculated. To estimate viscosity at distance  $\xi$  from steam chamber that moves with velocity equal to  $U$  in a medium whose thermal diffusivity is  $\alpha$ , Butler proposed to use Eq. 4 in which

$m$  is a constant between 3 and 5 and  $\mu_{os}$  is the oil viscosity at the steam chamber temperature.

$$\mu(\xi) = \frac{\mu_{os}}{\exp(-\frac{mU\xi}{\alpha})} \dots\dots\dots(4)$$

Combining Eq. 3 and Eq. 4 yields to Eq. 5 where  $a$  is another constant. Reis (1992) recommends 0.4 for  $a$  that adjusts the maximum local velocity of the steam chamber.

$$dq_t = \frac{K_{ro}K_o\rho_o}{\mu_{os}} \exp(\frac{-amU_{local}\xi}{\alpha}) \nabla\Phi dA \dots\dots\dots(5)$$

At case A when  $D < H_t$ , the flow potential function and the effective area can be expressed using Eq. 6 and 7. In these Equations,  $D$  represents the diameter of any circle larger than the diameter of steam chamber ( $D_{SC}$ ).

$$\nabla\Phi = \frac{Dg}{0.5\pi D} = \frac{2g}{\pi} \dots\dots\dots(6)$$

$$dA = 1.0 \times d\xi = dD \dots\dots\dots(7)$$

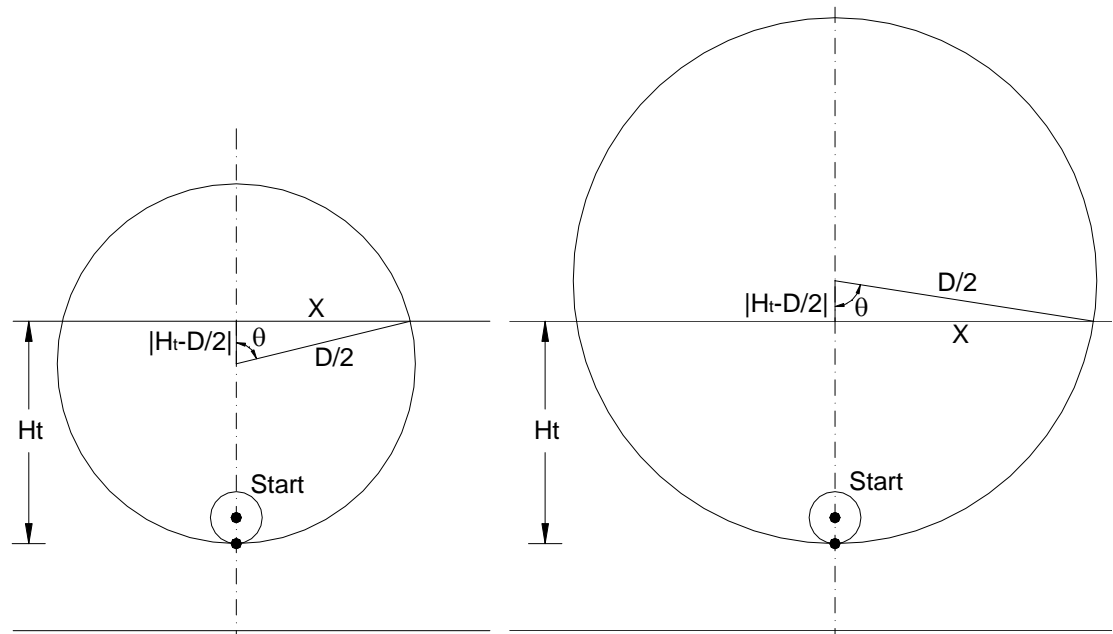


Figure 7: Steam chamber parameters for cases B (left) and C (right).

In all other cases based on the definition of  $X$  and  $D$  in Figure 7, steam chamber parameters are calculated as follows:

$$X = \left[ \left( \frac{D}{2} \right)^2 - \left( H_t - \frac{D}{2} \right)^2 \right]^{0.5} \dots\dots\dots (8)$$

$$\theta = \text{Sin}^{-1} \left( \frac{X}{D/2} \right) = \text{Sin}^{-1} \left( \frac{2X}{D} \right) \dots\dots\dots (9)$$

If  $H_t > D/2$ , then flow potential function is stated as in Eq. 10; otherwise Eq. 11 is the flow function. For both cases  $d\xi$  is the differential area and all the remaining parameters have been plotted in Figures 7 and 8.

$$\nabla\Phi = \frac{H_t g}{0.5(\pi - \theta)D} = \frac{2H_t g}{(\pi - \theta)D} \dots\dots\dots (10)$$

$$\nabla\Phi = \frac{H_t g}{0.5\theta D} = \frac{2H_t g}{\theta D} \dots\dots\dots (11)$$

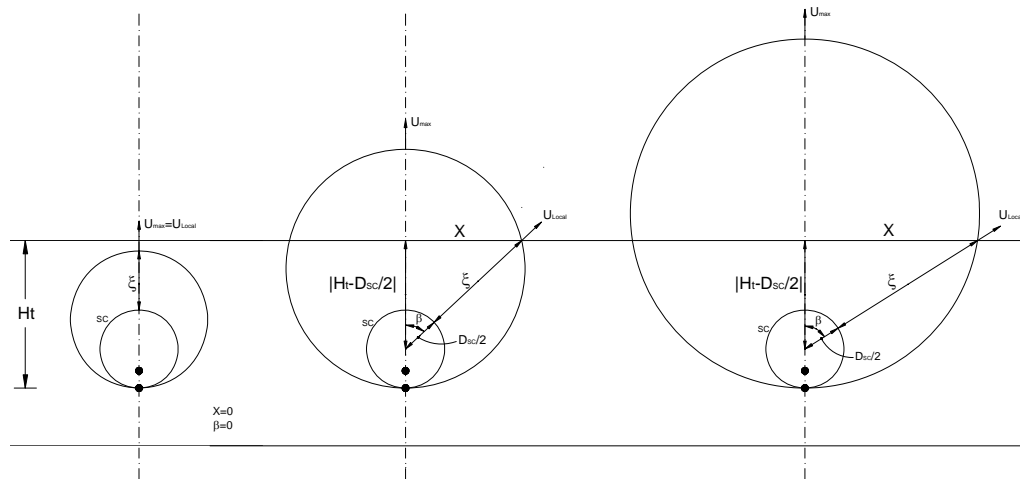


**Figure 8: Definition of local velocity at different position of steam chamber (SC) and the location at which flow rate is calculated.**

## Material Balance

Material balance is applied to each slice in front of the steam chamber. Consider that the steam chamber is at a specific location and it moves with the local velocity,  $U_{local}$ . Using Eq. 5, each slice outside of the steam chamber produces oil. It is assumed that the steam chamber jumps from its current location ( $n$ ) to the next location ( $n+1$ ) when all of the recoverable oil flows out of the current slice. Therefore, based on the material balance in the first slice, the time that takes to get the residual oil saturation value can be calculated:

$$\Delta t = \frac{(S_{o,1} - S_{o,R})}{dq_{t,1}} \dots\dots\dots(12)$$

In Eq. 12,  $S_{o,1}$  and  $dq_{t,1}$  are the current oil saturation and oil rate of the adjacent slice to the steam chamber and  $S_{o,R}$  is the residual oil saturation (maximum available recovery). Based on the time calculated in Eq. 12, oil saturation in other slices ( $i = 1, 2, 3 \dots n$ ) is updated as follows:

$$S_{o,i} = S_{o,i} - \frac{q_{t,i} \Delta t}{\Delta A} \dots\dots\dots(13)$$

The calculation process is repeated for those slices whose flow rate is not significant.

### Energy Balance

Reis (1992) utilized the law of conservation of energy to calculate the required steam injection into to the reservoir. With the same approach, the injection rate can be derived.

$$mL_s = (q_s \cdot \rho_w)L_s = \frac{d}{dt}(Q_{in} + Q_{out}) \dots\dots\dots(14)$$

where:

- $L_s$  = specific latent heat of steam
- $q_s$  = steam injection rate (in volume of water)
- $\rho_w$  = density of water
- $Q_{in}$  = the heat energy inside the steam chamber
- $Q_{out}$  = the heat loss around the steam chamber

Eq. 14 has two main terms; the left side is the rate of injection of energy into the reservoir, and the right side determines the energy distribution rate through the steam chamber into the reservoir. For energy balance, slices are not considered in calculation. The energy inside the steam chamber is calculated using Eq. 15 where  $\rho$  is the density of the formation,  $c$  is the specific heat of the formation,  $T_s$  is the steam temperature and  $T_r$  is the reservoir temperature. Each movement from one slice ( $n$ ) to the next ( $n+1$ ) would be used to determine the last term,  $dA/dt$ .

$$\frac{dQ_{in}}{dt} = \rho c (T_s - T_r) \frac{dA}{dt} \dots\dots\dots(15)$$

In each case from A to C (see Figure 5), energy loss from the body of the steam chamber is calculated as follows:

$$Q_{side} = \int_0^\theta \int_0^\infty \rho c \Delta T d\xi (rd\theta) \dots\dots\dots(16)$$

$$Q_{side} = \rho c (T_s - T_r) \int_0^\theta \int_0^\infty \exp\left(-\frac{U_{local}\xi}{\alpha}\right) d\xi (rd\theta) \dots\dots\dots(17)$$

$$Q_{side} = \rho c \alpha (T_s - T_r) \left(\frac{r}{U_{local}}\right) \int_0^\theta d\theta \dots\dots\dots(18)$$

$$Q_{side} = \frac{\rho c \alpha (T_s - T_r) r \theta}{U_{local}} \dots\dots\dots(19)$$

$$\frac{dQ_{side}}{dt} = \frac{d}{dt} \left( \frac{\rho c \alpha (T_s - T_r) D \theta}{a U_{max} (1 - \cos \theta)} \right) \dots\dots\dots(20)$$

At cases B and C that steam chamber is not a full circle, and energy loss occurs through the overburden at the separation line between oil sand formation and other layers as derived by Reis (1992):

$$\frac{dQ_{top}}{dt} = 2 \sqrt{\frac{\alpha}{\pi}} \rho c (T_s - T_r) U_H \sqrt{t} \dots\dots\dots(21)$$

where:

$U_H$  = horizontal velocity of the steam chamber at separation line

$t$  = cumulative time after touching the cap rock

### Initial Conditions

When a clear communication between injector and producer boreholes is identified, the steam chamber shape appears in the reservoir around the injector. The maximum velocity of the steam chamber growth is determined by Eq. 22 (See Appendix A).

$$U_{max,initial}^2 = \frac{8K_o \rho_o \alpha g}{\mu_{os} a m \phi \Delta S_o \pi^2 D_{Start}} \dots\dots\dots(22)$$

## MODEL VALIDATION: EXPERIMENTAL DATA

Chung and Butler (1988) conducted laboratory tests and compared the data to the results of their analytical model. The small scale laboratory model was 35 cm wide, 22 cm high and 3 cm thick. They designed two injection strategies: scheme ‘A’ and ‘B’. In scheme ‘A’ the injector was horizontal and slightly above the producer. In scheme ‘B’, single multiple vertical circulating steam injectors were installed. Scheme ‘B’ was considered to mimic the condition in which the steam chamber grows laterally only and was very similar to the geometry of the Butler model. They found that Butler model is able to reproduce the results of the test with scheme ‘A’ configuration. Only TANDRAIN, a modified version could predict the scheme ‘A’ configuration test. Reis (1992) and Akin (2005) also used the results of scheme ‘B’ to validate their models.

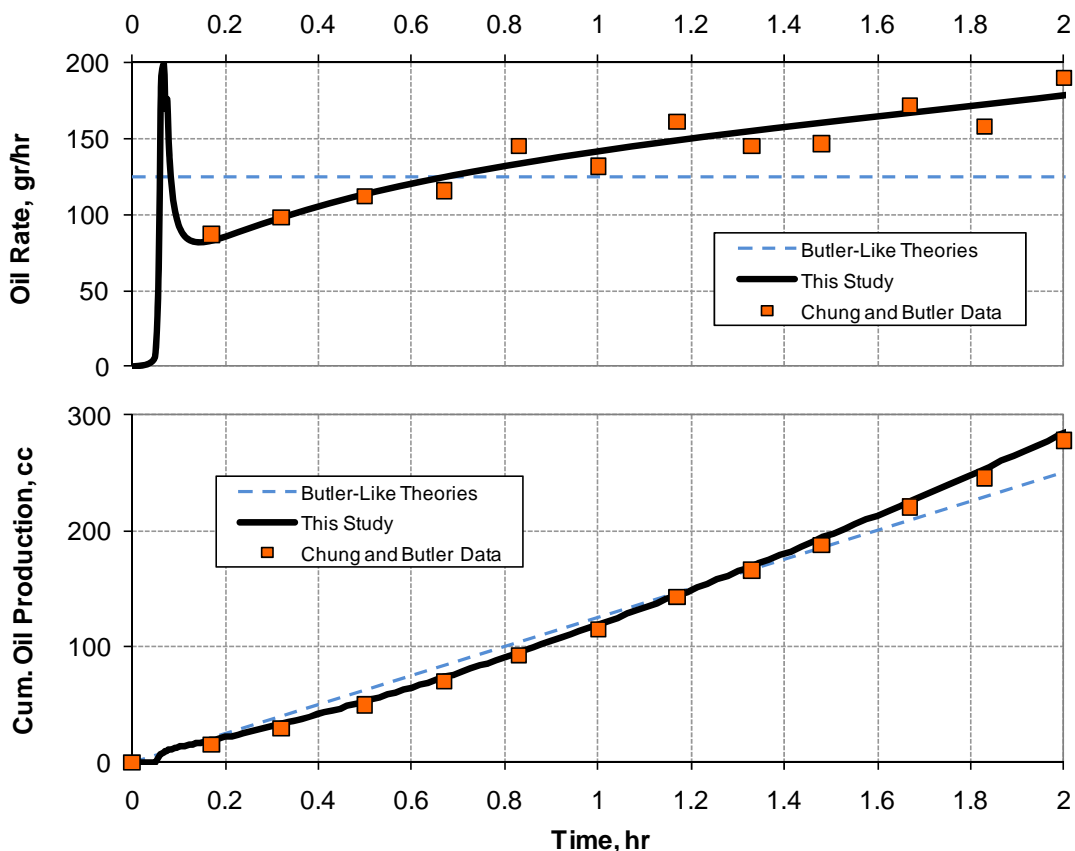


Figure 9: Comparison between the experimental data reported by Chung and Butler (1988).

Figure 9 shows the results of the model presented in this study compared to the scheme 'A' data. The parameters that have been used to run the model are listed in Table 1. Close agreement between the laboratory test data and the proposed model, reveals two new aspects of this model; (a) Unlike the past theories, the current model does not predict a constant value of oil rate and it is able to follow the variation of the oil production. (b) Circular geometry model, unlike one-directional models, is able to predict the results of a real SAGD geometry test.

**Table 1: Experimental parameters, Chung and Butler (1988).**

Properties	Value	Unit
Porosity	39	%
Initial Oil Saturation	100	%
Residual Oil Saturation	5	%
Absolute Permeability	2930	Darcy
Relative Permeability	0.48	-
Oil Density	0.98	gm/cc
Model Height	0.21	m
Thermal Diffusivity	0.0507	m <sup>2</sup> /day
Constant 'a'	0.4	-
Constant 'm'	3.6	-
Oil Viscosity	9	m <sup>2</sup> /day
Model Thickness	0.03	m

## MODEL VALIDATION: NUMERICAL SIMULATION

Experimental validation in the last section confirmed that running the proposed model with the exact values reported from laboratory is able to match the experimental model. This means that the model is capable of working as a flow simulator for history matching purposes while other models may not be powerful enough. To showing how this model can be utilized as a flow simulator to match the history, numerical analysis results have been compared to the current model.

A numerical simulation has been run to produce synthetic data for comparison. Material properties and other required data are listed in Table 2. It is important that the information in the table is a small portion of the whole data needed to run a numerical simulator. In addition, Table 2 shows the number of parameters that is required for simulation by the current analytical model.

For history matching, relative permeability curves were selected as the unknown parameter. The history matching was then trained on the history of oil production. For the first run, a common for oil sands relative permeability curve shown in Figure 10 was selected. After each run, oil production history was compared to the results of the numerical model and a multiplier between 0 and 1 was selected to modify the relative permeability. The trial and error process was continued until close agreement was found. Since each run takes five seconds only, the whole history matching process was done in 5 minutes. Although the final relative permeability curve was not quite the same as the curve used in the numerical analysis, the average value was the same. This feature may explain why Butler chose the average permeability to be the effective parameter in his theory.

**Table 2: Parameters of the numerical model.**

Property	Value	Unit
permeability	2500	mD
average relative oil permeability	0.48	-
oil density	1008	kg/m <sup>3</sup>
gravity acceleration	9.81	m/s <sup>2</sup>
H <sub>t</sub>	20	m
dynamic viscosity at steam temperature	0.007	Pa.s
porosity	32	%
reservoir thermal diffusivity	0.0000006	m <sup>2</sup> /s
reservoir temperature	10	°C
steam temperature	240	°C
formation heat capacity	2100000	J/ (m <sup>3</sup> °C)
latent heat of steam	1740000	J/Kg
steam quality	95	%
water density	1000	kg/ m <sup>3</sup>
coefficient of viscosity change, m	3.9	-
coefficient of average velocity, a	0.4	-
initial oil saturation	85	%
initial water saturation	15	%

Figure 11 and 12 illustrate the history matching process. A close look at Figure 10 clarifies that the analytical model has been successful in predicting the trend of oil production from the very beginning of the process where there is quick jump to the time when the oil rate is decreasing. Comparing this ability in the current model to the constant oil rate prediction by Butler-like theories confirms that this new model can be a good tool for fast history matching.

The nonlinear oil production curve in Figure 11 has been captured by the analytical simulator while Butler-like theories are incapable of predicting a nonlinear trend. Steam injection, however, has not been predicted well. The problem is more likely due to the simplicity of the theory used for energy balance or the complexity of the heat propagation in the numerical simulator.

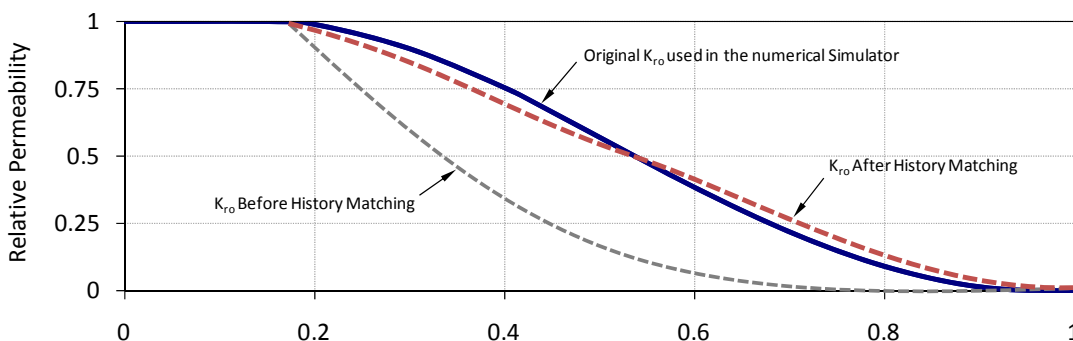


Figure 10: Relative permeability curves resulted from history matching.

The dashed horizontal line in Figure 11 and the dashed straight line in Figure 12 have been included to be a representative of Butler-like models. Any parallel line to the dashed line in Figure 11 and any line that passes through the coordinate of the chart can be matched by changing permeability. It means that regardless of the value of permeability, the nature of these models is not flexible enough to be used as a practical simulator. These two lines show the inadequate capability of Butler or Reis model for history matching.

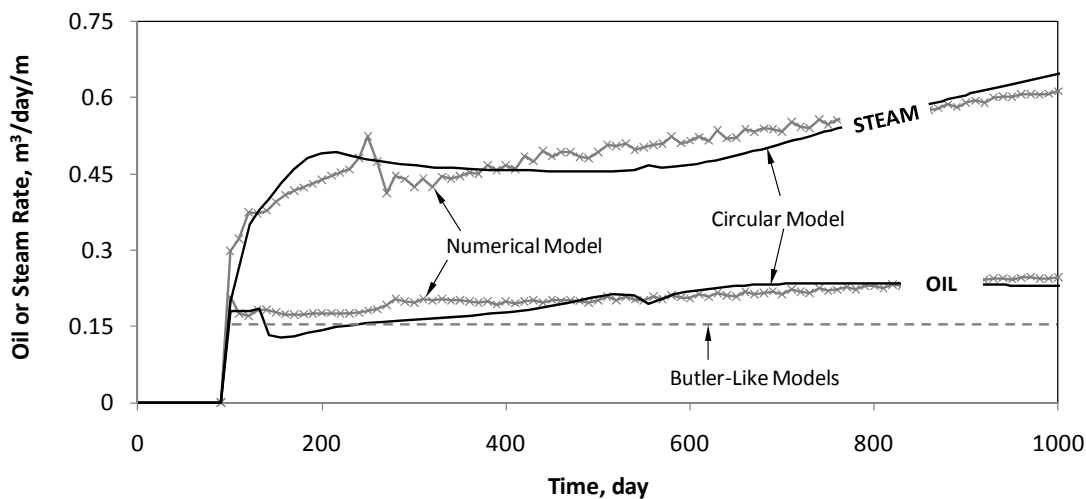


Figure 11: History matching of oil production and steam injection rate by the current analytical model.

Other than the mismatch between the reported data and predicted results for steam injection, steam/oil ratio (SOR) plotted in Figure 13 is in good agreement. The difference between SORs at the zone that has the most divergence (from 200 to 500 days) is only 0.25 in average. This difference when original Reis model is employed to predict the steam injection rate can vary from 1 to 10 (dashed line in Figure 13). This means that the circular geometry and the model of slices have improved the analytical approach to SAGD.

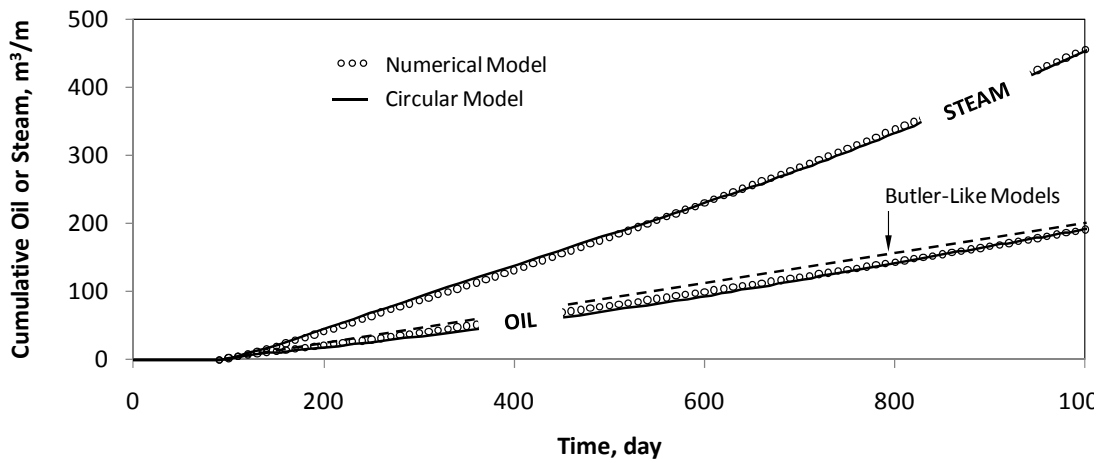


Figure 12: Cumulative oil production and steam injection predicted by the current numerical model compared to the numerical analysis results.

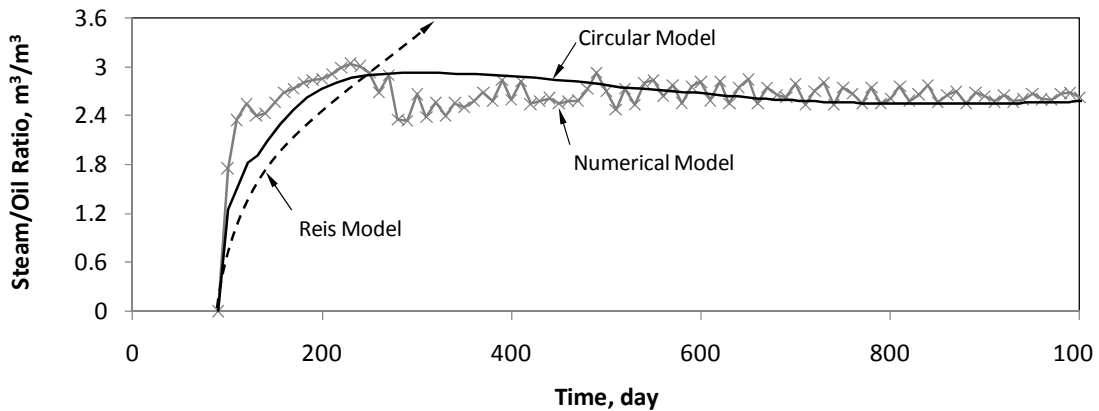


Figure 13: Steam/Oil Ratio predicted during history matching compared to the results of a numerical simulator.

The transition zone of temperature has been shown for three moments of recovery process in Figure 14. Similar to Butler theory, this model also considers a sharp separation between the steam chamber and other parts of the reservoir as is shown in

Figure 14 by dashed curves. However, the location of the steam chamber is fairly predicted.

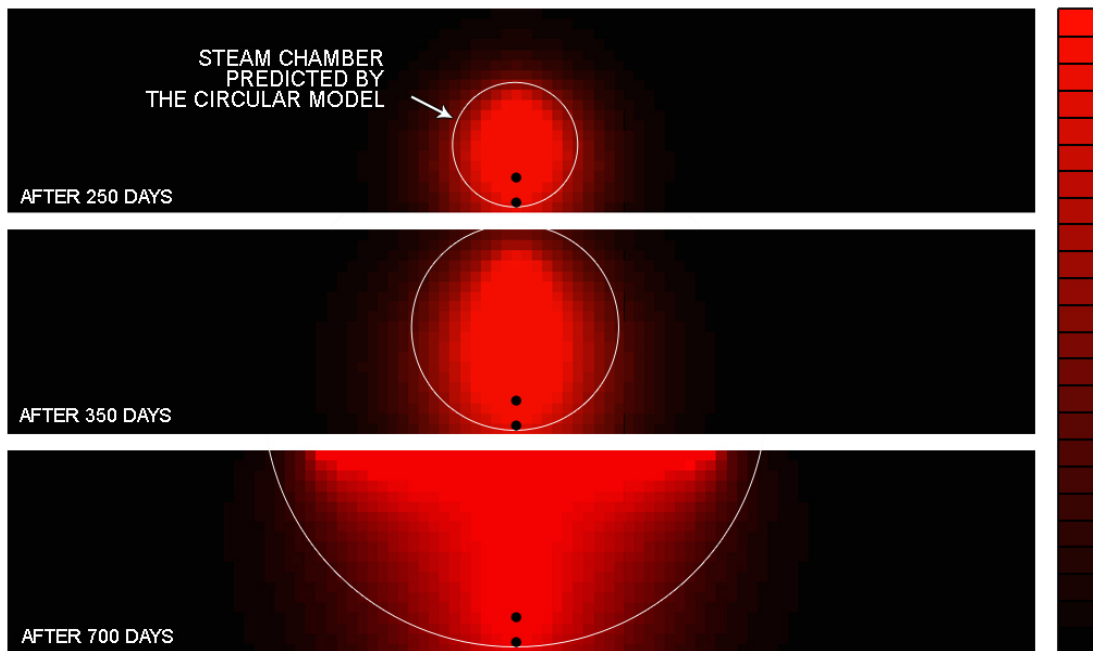


Figure 14: Oil saturation distribution at three moments of the analysis.

## REVIEW AND DISCUSSION ON PRACTICAL ASPECTS OF THE PROPOSED MODEL

Reservoir simulation is one of the most important tools in an engineering design work. Simulation of a field is necessary at two steps; firstly at the very beginning of a project when engineers need to evaluate the total cost/benefit of the project and design the proper recovery method and secondly while a project is working. Using a simulator, an engineer can estimate the effective parameters and predict the production for future decision making. As it is obvious, a reliable simulator that is capable of catching the physics of the problem is very essential. Other than reliability, a simulator should be fast enough to be used at the assigned design time. While technology is growing and data gathering is close to real time, such a simulator is of the highest priority of a project. The main goal of this study is to develop a tool with all above functionalities and it seems that the proposed analytical model has the potential to be utilized as the core simulator for SAGD projects.

In this paper, a numerical-based theory was developed with fundamentals that are simple and straightforward, but include enough physics to be useful. The model is based on the methodology presented by Butler and Reis theory. Flow simulation uses Darcy's law and material balance (the law of conservation of mass) to calculate the rate of oil production. Required steam injection rate is calculated by applying the law of conservation of energy. These two concepts are used beside the two new major features of this model. In the proposed model, the steam chamber is circular and has two degrees of freedom. Using a circular geometry, steam chamber growth will be simulated more closely to the reality. Such a steam chamber shape is able to cover all the stages of the SAGD process from when a clear communication between injector and collector appears to the time when production decreases rapidly. The second benefit of this model is considering the variation of relative permeability regards to the changes in oil saturation.

To apply these aspects, the method of slices that was previously applied successfully by the authors to a linear geometry model has been employed. Method of slices attempts to explain the fact that different zones in a reservoir, based on how much they are saturated, produces at different oil rates.

The proposed model was validated using the laboratory data reported by Chung and Butler (1988). The comparison shows that the proposed model is able to mimic the small scale tests while other models can model the test that is calibrated to their assumptions only. Also, unlike past studies that propose a constant rate for oil production, the current study can predict the natural nonlinear form of the production curve. Validation was then followed by another comparison with the result of a numerical simulator. The comparison gave more details of the capability of the model on history matching. In the numerical model comparison, the analytical model predicted the large scale oil production trends fluctuating trends. Results of the steam injection were, however, not as close to the data as the oil rate was.

## **CONCLUSIONS**

In conclusion it can be said that the proposed model which benefits from a circular geometry of steam chamber and method of slices, can be a very helpful method to be

used as a fast simulator in SAGD projects. The advantage of the model is that the fast speed run time is served by a physics-based theory, not a ‘black-box’ algorithm. This long term goal of this simulator is to join with an optimization methodology, providing a powerful tool for fast on-line decision making stages in an ongoing project.

## ACKNOWLEDGEMENTS

Authors would like to acknowledge Nathan Deisman for his contribution on reviewing this paper. His technical support and helpful comments are highly appreciated.

## REFERENCES

- Azad, A., and Chalaturnyk, R.J. 2010. A mathematical improvement to SAGD using geomechanical modelling. *Journal of Canadian Petroleum Technology*. 49(10): 53-64.
- Akin, S. 2005. Mathematical modeling of steam-assisted gravity drainage. *SPE Reservoir Evaluation & Engineering*. 8(5): 372-376.
- Butler, R.M., 1997. GravDrain's Blackbook: Thermal Recovery of Oil and Bitumen. GravDrain Inc., Calgary Alberta, Canada. 528 p.
- Butler, R.M. and Stephens, D.J. 1981. The gravity drainage of steam-heated heavy oil to parallel horizontal wells. *Journal of Canadian Petroleum Technology*. 20(2): 90-96.
- Butler, R.M., Stephens, D.J., and Weiss, M. 1980. The vertical growth of steam chambers in the in-situ thermal recovery of heavy oils. *Proc., 30th Canadian Chemical Engineering Conference*, Vol. 4: 1152-1160.
- Butler, R.M., McNab, G. S., and Lo, H.Y. 1981. Theoretical studies on the gravity drainage of heavy oil during Steam Heating. *Canadian Journal of Chemical Engineering*. 59: 455-460.
- Chalaturnyk, R.J. 1996. Geomechanics of the Steam-Assisted Gravity Drainage Process in Heavy Oil Reservoirs. *PhD Dissertation*. University of Alberta, Edmonton, Canada.
- Chung, K.H., and Butler, R.M. 1988. Geometrical effect of steam injection on the formation of emulsions in the steam-assisted gravity drainage process. *Journal of Canadian Petroleum Technology*. 27(1): 36-42.

Edmunds, N.R., Kovalsky, J.A., Gittins, S.D., and Pennacchioli, E.D. 1994. Review of phase A steam-assisted gravity-drainage test. *SPE Reservoir Engineering*. 9(2): 119-124.

Ito, Y., and Suzuki, S. 1996. Numerical simulation of the SAGD process in the Hangingstone Oil Sands Reservoir. *Proc., the 47th Annual Technical Meeting of the Petroleum Society of CIM*, Calgary, Alberta, Canada.

Liang, L. 2005. An Analytical Model for Cyclic Steaming of Horizontal Wells. *MSc Thesis*. Stanford University.

Nukhaev, M., Pimenov, V., Shandrygin, A., and Tertychnyi, V. 2006. A new analytical model for the SAGD production phase. *Proc., SPE Annual Technical Conference and Exhibition*, San Antonio, Texas, SPE No. 102084.

Reis, J.C. 1992. A steam-assisted gravity drainage model for tar sands linear geometry. *Journal of Canadian Petroleum Technology*. 31(10): 14-20.

Reis, J.C. 1993. A steam-assisted gravity drainage model for tar sands radial geometry. *Journal of Canadian Petroleum Technology*. 32(8):43-48.

## APPENDIX A: INITIAL CONDITION

When steam chamber's diameter is less than  $D_{Start}$ , Eq. 5 can be rewritten for any size of steam chamber ( $D$ ) as follows. The shape of the steam chamber is none of the cases 'A' to 'C' (see Figure 5). In this case, the centre of the circle is on the injector and it grows before touching the producer.

$$dq_t = \frac{K_o \rho_o}{\mu_{os}} \exp\left(\frac{-amU_{\max} \xi}{\alpha}\right) \left( \frac{g \left[ \frac{D_{Start}}{2} + \frac{D}{2} \right]}{\left[ \frac{D_{Start}}{2} - \frac{D}{2} \right] + \frac{\pi}{2} D} \right) d\xi \dots\dots\dots(A-1)$$

$$dq_t = \frac{K_o \rho_o}{\mu_{os}} \exp\left(\frac{-amU_{\max} \xi}{\alpha}\right) \left( \frac{g [D_{Start} + D]}{[D_{Start} - D] + \pi D} \right) d\xi \dots\dots\dots(A-2)$$

$$q_t = \int_0^{\infty} \frac{K_o \rho_o}{\mu_{os}} \exp\left(\frac{-amU_{\max} \xi}{\alpha}\right) \left( \frac{g [D_{Start} + D]}{[D_{Start} - D] + \pi D} \right) d\xi \dots\dots\dots(A-3)$$

$$q_t = \left( \frac{K_o \rho_o}{\mu_{os}} \right) \left( \frac{\alpha}{amU_{\max}} \right) \left( \frac{g [D_{Start} + D]}{[D_{Start} - D] + \pi D} \right) \dots\dots\dots(A-4)$$

Material balance for the same case would be:

$$q_t = \frac{d}{dt} \left[ (\phi \Delta S_o) \left( \frac{1}{8} \pi D^2 \right) \right] = \frac{1}{8} (\phi \Delta S_o) (2\pi D) \frac{dD}{dt} = \frac{1}{4} (\phi \Delta S_o) (\pi D U_{\max}) \dots\dots\dots (A-5)$$

Therefore, the maximum velocity at the beginning of the production is formulated:

$$q_t = \left( \frac{K_o \rho_o}{\mu_{os}} \right) \left( \frac{\alpha}{am U_{\max}} \right) \left( \frac{g [D_{Start} + D]}{[D_{Start} - D] + \pi D} \right) = \frac{1}{4} (\phi \Delta S_o) (\pi D U_{\max}) \dots\dots\dots (A-6)$$

$$U_{\max, initial}^2 = \left( \frac{K_o \rho_o}{\mu_{os}} \right) \left( \frac{\alpha}{am} \right) \left( \frac{g [D_{Start} + D]}{[D_{Start} - D] + \pi D} \right) \left( \frac{4}{\phi \Delta S_o \pi D} \right) \dots\dots\dots (A-7)$$

$$U_{\max, initial}^2 = \frac{8 K_o \rho_o \alpha g}{\mu_{os} am \phi \Delta S_o \pi^2 D_{Start}} \dots\dots\dots (A-8)$$

# CHAPTER 4: APPLICATION OF ANALYTICAL PROXY MODELS IN FAST HISTORY MATCHING FOR SAGD PROCESS: UTF PROJECT CASE STUDY\*

## **ABSTRACT**

Steam Assisted Gravity Drainage (SAGD) has been successfully employed in the last 25 years in Canada. SAGD is a thermal recovery process that was invented to extract highly viscous bitumen from deep Canadian oil sands reservoirs. To date, the original idea of SAGD has not changed greatly since the first pilot test in 1987. However, field operation and reservoir management have been influenced by recent developments in technology. High-tech drilling techniques, automated production control, and real-time data monitoring are gradually transforming SAGD process into Smart fields. As such, improving current history matching techniques would significantly support fast decision making requirements in closed loop reservoir management.

This paper recommends analytical solutions for simulations with medium to high levels of uncertainty. It shows how an analytical simulator can be effectively improved to mimic the essential features of a SAGD field for fast history matching. Combined with the analytical model recently proposed by the authors, this paper investigates the methodology to apply uncomplicated analytical/mathematical solutions to practical cases. The two UTF pilot test case studies covered in this paper provide a better understanding of the proposed methodology. History matching results show that the current analytical models are suitable to act as proxy models for optimization purposes.

---

\* This paper has been submitted to the Journal of Canadian Petroleum Technology, July 2011.

## **Introduction**

Steam Assisted Gravity Drainage (SAGD) is a thermal recovery process introduced in the early 1980s for highly viscous oil sand reservoirs in Canada (Butler, 1997). Since then, SAGD has been well studied and the physics of the process is generally understood. In SAGD, two horizontal wells are drilled, one on top of the other, at the bottom of the reservoir formation. Steam is injected through the top borehole, called the injector. Under high pressure, the high temperature steam gradually establishes an affected zone around the injector, called the steam chamber. The thermal energy of the injection reduces the viscosity of the oil inside the steam chamber, and gravity causes the oil to flow towards the bottom borehole. This process has shown that the geomechanical behaviour of oil sands is also active and dynamically changes rock properties (e.g., Chalaturnyk, 1996). Reservoir simulators are now able to mimic a SAGD process in 3D, considering many complexities in geology, flow/rock properties, and operational strategies. Fully geomechanical coupled solutions are also available (e.g., Settari and Walters, 2001) which honour the geomechanical behaviour of the oil sands formation.

To date, the original idea of SAGD has not changed greatly since the first pilot test in 1987. However, field operation and reservoir management have been influenced by recent technological developments. High-tech drilling techniques, automated production control, and real-time data monitoring are gradually transforming SAGD process into Smart fields. Although recent developments in computational modelling and the progress in providing optimized solution algorithms have effectively improved the potential of numerical simulators, long computation time remains an issue for high resolution models and, in particular, reservoir-geomechanical simulations. In addition, in some stages of project planning and operation, levels of uncertainty in the geological model or material properties need to be initially quantified by simple models to provide reliable data for numerical simulators. To overcome this problem, proxy models are usually recommended for their efficient response time and successful practices in petroleum engineering. Any mathematical or statistical function capable of representing the reservoir or the process for selected

input parameters can act as a proxy. Figure 1 graphically shows models of varying complexity that can be employed at different stages of a project. The uncertainty axis compares the uncertainty embedded within each model. The project timing axis suggests the project stages at which each model can be employed. For instance, it is suggested that simple spreadsheets (far less certain than the full physics model) be used at the initial stages of a project, mainly for planning purposes.

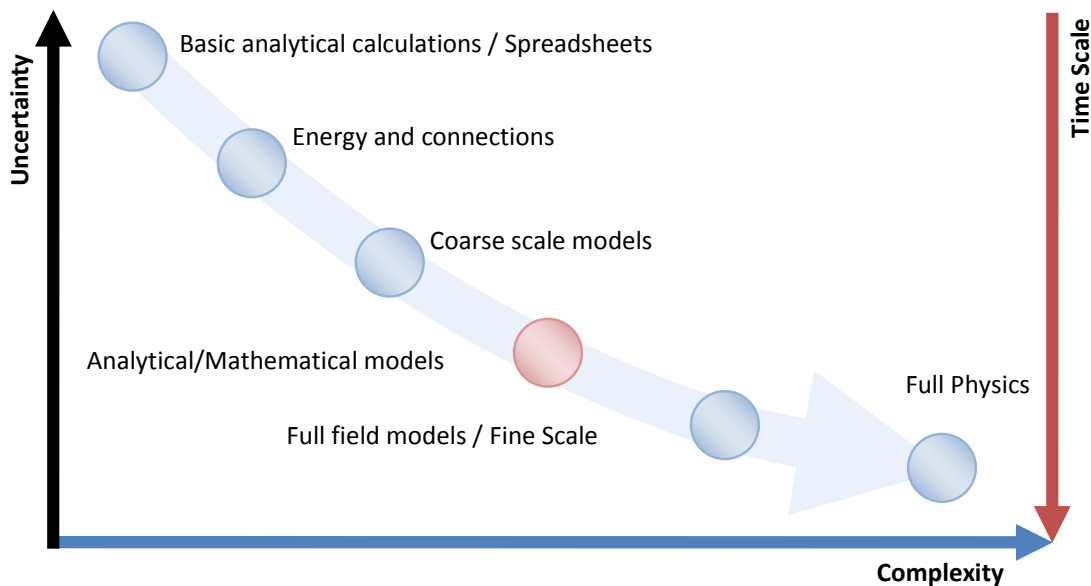


**Figure 1: Location of different models along a simulation path (partially adapted from BP's top-down reservoir modelling, Williams et al., 2004).**

The first analytical theory for SAGD, proposed by Butler and his colleagues (Butler et al., 1981), is generally known as the Butler model, and all other models studied since are fundamentally similar to it. However, recent models are able to consider different aspects of SAGD, and despite their respective limitations, each can be a proxy model in SAGD simulations. Since such models can generally mimic essential features of SAGD physics, they gain a lot of attention.

This paper compares current analytical/mathematical models of SAGD. Thereafter, the circular model recently proposed by the authors is used to show the capability of physics-based models in history matching. Two case studies are used to provide a better understanding of the methodology. The project (Dover Project, UTF Phase A and B) is located 60 kilometres north of Fort McMurray, Alberta, Canada and has

been working for more than two decades. It should be noted that the numbers in the production and steam/oil ratio curves in the result section have been intentionally removed to protect the confidentiality of the data.

## **PROXY MODELLING AND ANALYTICAL SOLUTIONS**

In statistics, proxy modelling is used to evaluate uncertain variables in complex systems. It is the variable probability, and not the proxy itself, that is of interest. For this reason, the proxy variable should have a close correlation with the inferred value. As long as the correlation between the truth model and the estimated model is acceptable, the proxy works well in a statistical problem. In engineering, this methodology is used to evaluate the probability of uncertain variables.

In petroleum engineering, reservoir systems are highly nonlinear, and fully detailed simulations are very expensive and time consuming. When uncertainty in material properties makes such systems even more complex, adequate high quality data sets are needed for uncertainty analysis. Lacking these or a full reservoir simulation, proxy models are adopted to work alongside or in place of a simulator. They are employed in wide range of workflows in petroleum engineering such as history matching, sensitivity analysis, risk analysis, field development planning, reservoir characterization, and process optimization. Several models are well studied for oil and gas industry application. Polynomial regression-based models (Sarma and Xie, 2011), Artificial Neural Network algorithm (Silva et. al, 2008), Genetic algorithm (Sun and Mohanty, 2005), response surface models (Fetel and Caumon, 2008), and surrogate models (Queipo et. al, 2001) are among the proxy models in this category. Although these are shown to be successful substitutes for full reservoir simulations (Zubarev, 2009), they have some intrinsic disadvantages. Awashti et al. (2007) identified some practical difficulties in applying existing proxy model-based methods, emphasizing that they are purely data driven and do not usually consider the relevant underlying physics. Put simply, proxy models act as black boxes, and the process under which prediction and optimization occurs does not have a related physical meaning. It seems that if a proxy model honours the minimum features of the physics

of the reservoir at an acceptable scale, it performs beyond the original purposes of using proxy models.

There is some SAGD work that benefits from using physics-based proxy models. Vanegas Prada et al. (2008) used the Butler model to assess the uncertainty of the performance of SAGD, mimicking a SAGD reservoir in which rock properties are heterogeneously populated. Figure 2 shows a generic application of analytical models to analyze uncertainty in SAGD processes.

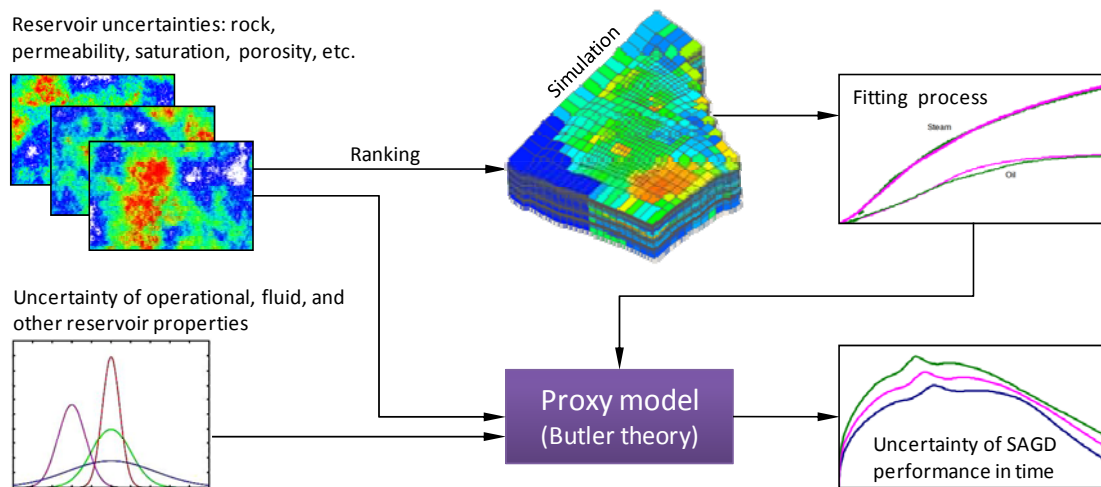


**Figure 2: Uncertainty analysis flowchart of SAGD performance using Butler theory (partially adapted from Vanegas Prada et al., 2009).**

## SAGD ANALYTICAL MODELS

There are several analytical models proposed for SAGD process. Some are briefly summarized in Table 1, along with their general capabilities in forecasting and history matching.

The theory that is generally known as the Butler model was first introduced by Butler et al. (1981). Since then, some aspects have been redefined or added to the original theory. Butler and Stephens (1981) adjusted the production rate by fixing the steam chamber passing the injector borehole (TANDRAIN model). In their study, they also proposed a methodology to allow for the confining effects of adjacent wells. Figure 3a has plotted the shape of the steam chamber expected from the Butler model. Butler (1997) stated that the initial stage of steam chamber development, before it touches the overburden and grows laterally, is predicted by the rising steam chamber theory,

and that this is to be used beside the drainage model. In this paper, the combination of the TANDRAIN model, the rising steam chamber theory, and the confining effects of adjacent wells is called the modified Butler model.

**Table 1: Some of the analytical models proposed for SAGD.**

Model	Reference	Specifications
Circular Model	Azad & Chalaturnyk (2011a)	anisotropy, circular geometry of steam chamber, relative permeability, rising and lateral growth of steam chamber
Linear Geomechanical SAGD (LGS) Model	Azad & Chalaturnyk (2010)	anisotropy, geomechanics, linear geometry of steam chamber, relative permeability, lateral growth of steam chamber
TANDRAIN Model, Eq. A1	Butler & Stephens (1981)	allows for the confining effect of adjacent wells, lateral growth of steam chamber, average relative permeability
Rising Steam Chamber, Eq. A2	Butler (1997)	rising process of steam chamber, average relative permeability
Linear Geometry, Eq. A3	Reis (1992)	Linear geometry of steam chamber, average relative permeability, lateral growth of steam chamber
Synthetic Model, Eq. A4	Ito & Suzuki (1998)	Fitted equation on several runs using numerical simulators, anisotropy, average relative permeability

The Butler model has been the origin of several newer models in the last thirty years. Reis (1992) applied the fundamentals of the Butler theory to propose his model for a linear geometry steam chamber. Reis' theory was improved by Azad and Chalaturnyk (2010) to account for the geomechanical behaviour of oil sands. They also developed a model (Azad and Chalaturnyk, 2011a) with circular steam chamber geometry that can model all stages of steam chamber growth in SAGD. Figure 3 compares the geometry of the steam chamber in different models.

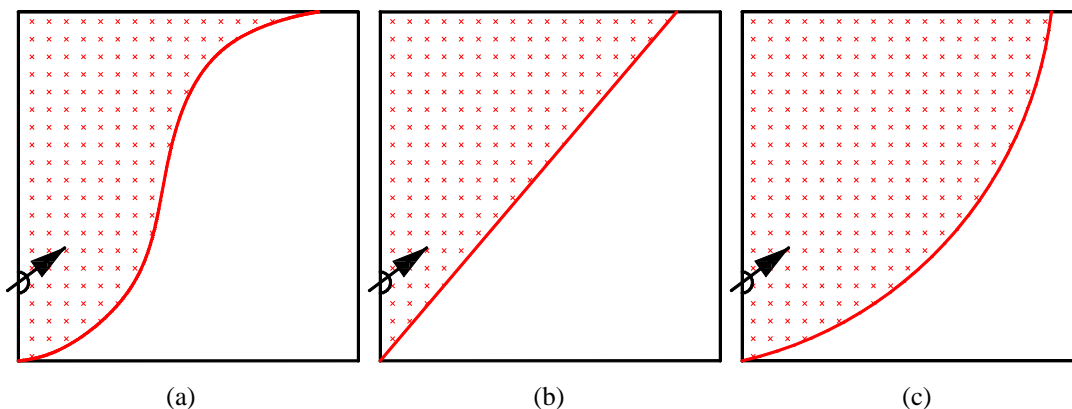


**Figure 3: Steam chamber geometry: (a) Butler model, (b) linear geometry, and (c) circular geometry.**

## HOW ANALYTICAL MODELS PREDICT

To show how various analytical models would predict a process, the modified Butler model, the Reis model, and the circular model were used to solve a sample SAGD. In addition, the mathematical function provided by Ito and Suzuki (1998), which is the product of curve fitting on synthetic numerical simulations, was chosen to consider anisotropy of permeability. All of the specifications of the example have been listed in Table 2. It should be noted that each model needs a part of the information provided in Table 2. For example, the permeability ratio is used by the circular and the synthetic model only, while reservoir height is embedded in all of the theories. The height and properties of the reservoir were chosen to resemble a practical SAGD project in Alberta, Canada.

**Table 2: Properties of the model required for analytical models.**

Parameter	Value	Unit
reservoir height	30	M
absolute permeability	10,000	mD
average relative permeability	0.4	-
initial oil saturation	0.85	%
residual oil saturation	0.4	%
reservoir porosity	0.3	%
dynamic viscosity at steam temperature	0.007	Pa-s
dynamic oil viscosity at 60° lower than steam	50	Cp
oil density	1,008	kg/m <sup>3</sup>
reservoir thermal diffusivity	6×10 <sup>-7</sup>	m <sup>2</sup> /s
$k_v/k_h$	0.5	-
m	3.6	-
A	0.4	-
w (boundary effect)	30	M
c	0.07065	m <sup>2</sup> .cp <sup>0.33</sup> /day.md <sup>0.75</sup>
borehole length	55	M

The Reis model and the Ito-Suzuki equation predict a constant oil production rate. These two values have been plotted in Figure 4 with dashed and dotted lines. The considerable difference between them is due to anisotropy of permeability. The Reis model cannot estimate the effect of anisotropy, and higher oil rate is calculated based on horizontal permeability. The disadvantage of these two or similar models is that they can only be used to predict the maximum rate. The variation of oil production in

different stages of steam chamber growth is predictable using either the modified Butler model or the circular geometry model.

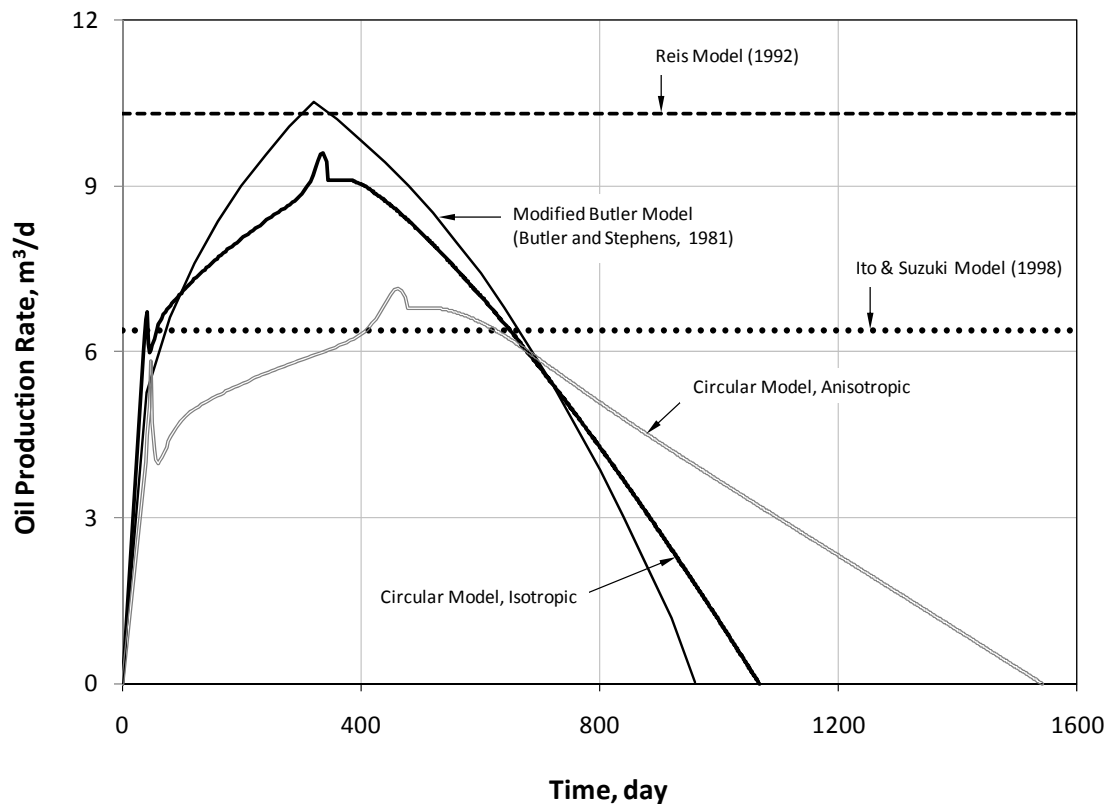


**Figure 4: Oil production rate simulated by the analytical models.**

Figure 4 shows the oil production rate calculated by the four analytical simulators. The maximum oil production rate values for the isotropic and anisotropic models are quite similar. The circular model and the modified Butler model show similar trends in oil production. Figure 4 reflects that the circular model can simulate the rising chamber, lateral growth, and depletion of the steam chamber all in one theory. That model is also shown to be capable of considering anisotropy in permeability. The peak oil rate predicted by the circular model at the beginning of the process is due to the high initial rate of growth of the steam chamber before the producer is opened, which is quite similar to reality.

Figure 5 plots cumulative oil production curves. Those models that consider a non-flow boundary (confining effects) merge at the level of the maximum recoverable oil. However, other models that calculate a constant rate of oil production continuously generate oil to cover all of the spaces in the reservoir. Based on this simple

comparison, it can be concluded that each model has its advantages and can be used depending on the subject of the study. For the case studies in this paper, the circular model has been chosen to act as an analytical simulator for the following reasons: (a) the model combines all of the separate theories to consider the growth of the steam chamber from the beginning to the end of the process, (b) the model considers the variation in oil saturation in advance of the steam chamber, and (c) anisotropy of permeability is to be applied optionally in the circular model. It should be noted that the modified Butler model can also be modified for this study.

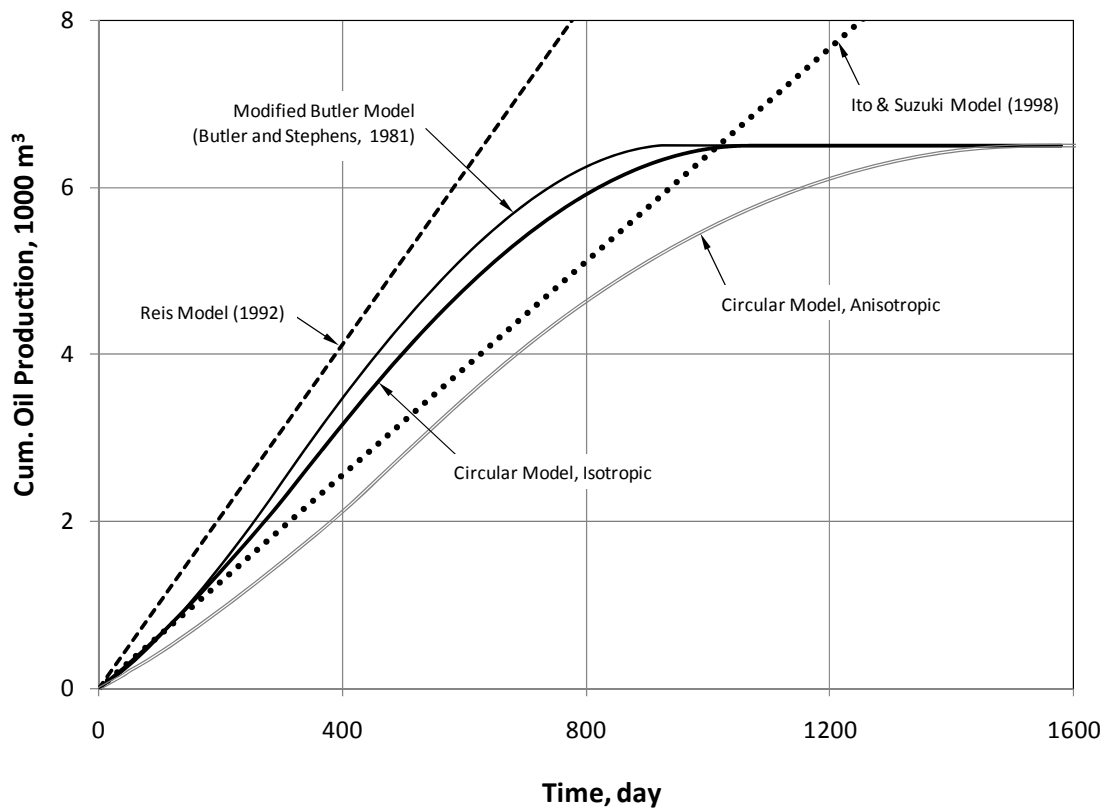
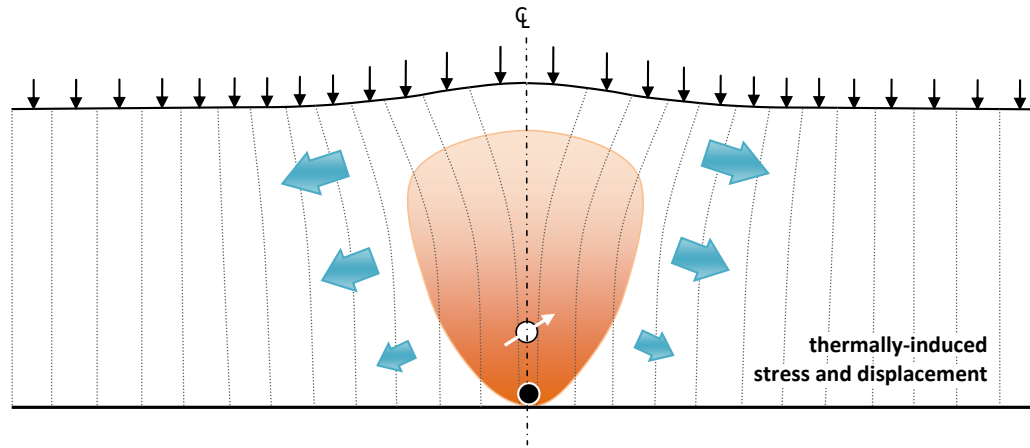


Figure 5: Cumulative oil production predicted by the analytical models.

## GEOMECHANICS AND SAGD

When steam is injected into the reservoir, oil viscosity is not the only targeted parameter that changes. The high-temperature, high-pressure steam applies thermally-induced stress in the reservoir that redistributes the stress and strain fields around the steam chamber. The geomechanical reaction of the material is not limited to reservoir formation, and affects a large portion of underburden and overburden.

It is widely accepted that steam chamber evolution is partially related to the interaction between the flow process and geomechanical behaviour (Chalaturnyk, 1996). At certain levels of shear stress, oil sands tend to dilate. This deforms the reservoir and changes the permeability and porosity of the oil sand. (e.g., Scott et al., 1994). Figure 6 schematically shows the deformation inside the reservoir and the heave on top that results from the thermally-induced stress of SAGD.



**Figure 6: Thermal stress distribution inside the reservoir causes reservoir deformation and heave.**

Based on observations in UTF pilot tests and experimental-simulation studies, Chalaturnyk (1996) explained the geomechanical response of a reservoir under SAGD. He argued that the increase in horizontal stress in advance of the steam chamber and the elevated pore pressure causes a decrease in effective stress that leads the material to experience high shear stresses or shear failure. This process is schematically reproduced in Figure 7. Geomechanical behaviour continuously contributes to production and improves the process through changes in permeability and porosity.

The geomechanics of SAGD is very complex and are not easily implemented in analytical models. Although recent research on the analytical modelling of SAGD considers geomechanics (e.g., Azad and Chalaturnyk, 2010 or Cokar et al., 2011), the models are not yet mature enough to be used in all cases. For this reason, the simple theory recommended by Azad and Chalaturnyk (2011b) for Athabasca oil sands reservoirs is used for the case studies in this paper. Based on geomechanical coupling simulation results, it was observed that the stress ratio  $q'/p'$  (Geomechanical Impact

Factor, GIF) is a relatively good indicator of stress levels in a reservoir. This factor indirectly considers the effect of *in situ* stresses and injection pressure in calculating the permeability and porosity of oil sands. Equations 1 to 6 define the steps of calculating the GIF.

$$q' = \frac{\sigma'_1 - \sigma'_3}{2} \dots\dots\dots (1)$$

$$p' = \frac{\sigma'_1 + \sigma'_3}{2} \dots\dots\dots (2)$$

$$\sigma'_h = \sigma_h - p_{inj} - \sigma_T \dots\dots\dots (3)$$

$$\sigma'_H = \sigma_H - p_{inj} - \sigma_T \dots\dots\dots (4)$$

$$\sigma'_V = \sigma_V - p_{inj} \dots\dots\dots (5)$$

$$\sigma_T = (1 + \nu)\alpha E \Delta T \dots\dots\dots (6)$$

In these equations:

$\sigma'_1$  and  $\sigma'_3$  are the maximum and the minimum effective stresses.  $\sigma'_H$  and  $\sigma'_h$  are the maximum and the minimum horizontal effective stresses.  $\sigma'_V$  is the vertical effective stress.  $p_{inj}$  is the injection pressure.  $\sigma_T$  is the thermal stress.  $\alpha$  is the linear coefficient of thermal expansion.  $\Delta T$  is the temperature difference between reservoir and injected steam.  $E$  and  $\nu$  are modulus of elasticity for reservoir and Poisson's ratio, respectively.

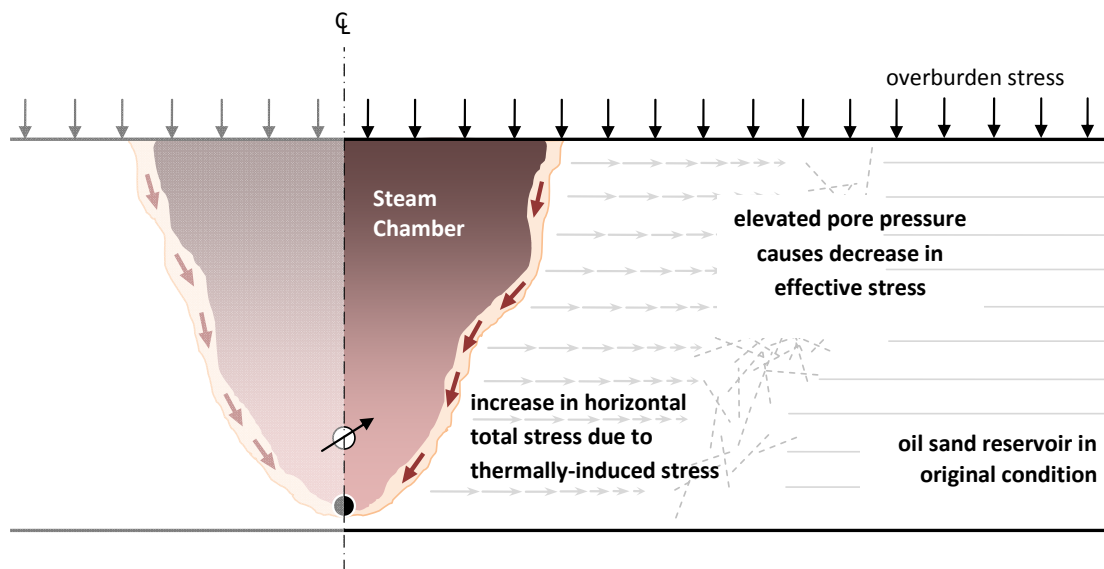


Figure 7: Stress distribution in advance of the steam chamber (after Chalaturnyk, 1996).

## **UNDERGROUND TEST FACILITY (UTF) - DOVER PROJECT**

The Underground Test Facility (UTF) was initiated in 1984 by AOSTRA and is located 60 kilometres northwest of Fort McMurray, Alberta, Canada (Figure 8). The main purpose of the UTF is to develop and test promising *in situ* methods to efficiently recover the deeper bitumen from the Athabasca oil sands deposits (O'Rourke et al., 1994). A general stratigraphy of the UTF is included in Table 3. Heavy oil bitumen is located within the McMurray Formation, which contains bitumen of grades ranging from very low to almost 70%. The reservoir consists of approximately 20 metres of rich oil sand interrupted by several horizontally-stretched shaley zones at the bottom few metres of the formation. The reservoir rests on Devonian limestone, with well-defined contact between the two formations. The 15 metres of the McMurray Formation on top of the reservoir contains a combination of shale and oil sand, up to the sandy shale at the top of the formation. This is generally believed to contribute least to SAGD recovery. The McMurray Formation is overlain by 2 metres of sand of the Clearwater formation. The 120 metre overburden to the surface contains shale, sandy shale, and gravel (Chalaturnyk, 1996).

UTF was planned to have different phases. A detailed design of the UTF/Phase A was completed in 1982. However, the Steam Assisted Gravity Drainage (SAGD) thermal process was chosen as the recovery technique in 1985. UTF/Phase A consists of two vertical shafts drilled from the surface to 15 metres within the limestone formation below the reservoir. A horseshoe-shaped horizontal tunnel was then excavated in the limestone to increase access to the reservoir. Three pairs of 55-metre boreholes were then drilled through the limestone at the bottom of the McMurray Formation. Figure 9 schematically shows the configuration of UTF/Phase A.

UTF/Phase A confirmed the feasibility of SAGD as a thermal recovery technique for Canadian oil sand formations in Athabasca, with more than 60% recovery and a steam/oil ratio (SOR) of close to 2.5. Phase B aimed to check the commercial potential of SAGD.

The Phase B wells were drilled from 1990 to 1991. In this case, the horizontal tunnels of Phase A were extended and prepared for the drilling of longer horizontal

boreholes. Three 500-metre borehole pairs were drilled perpendicular to the direction of the boreholes in Phase A. Figure 10 plots the layout of the three wellbore pairs for both phases.

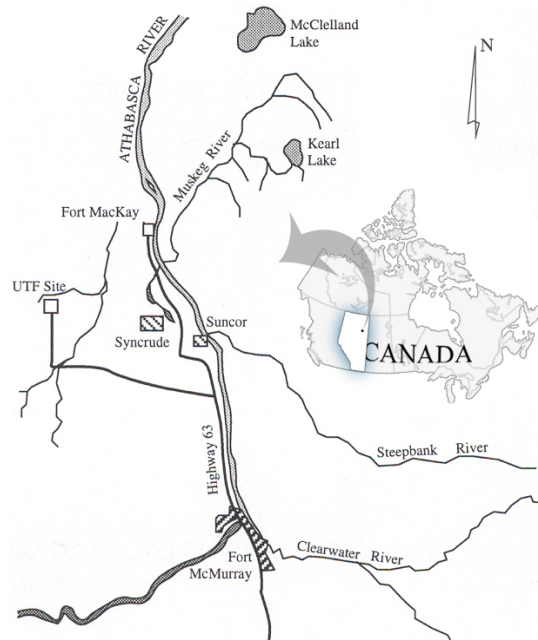


**Figure 8: Location of Underground Test Facility (UTF) site in Alberta, Canada (adapted from Chalaturnyk, 1996).**

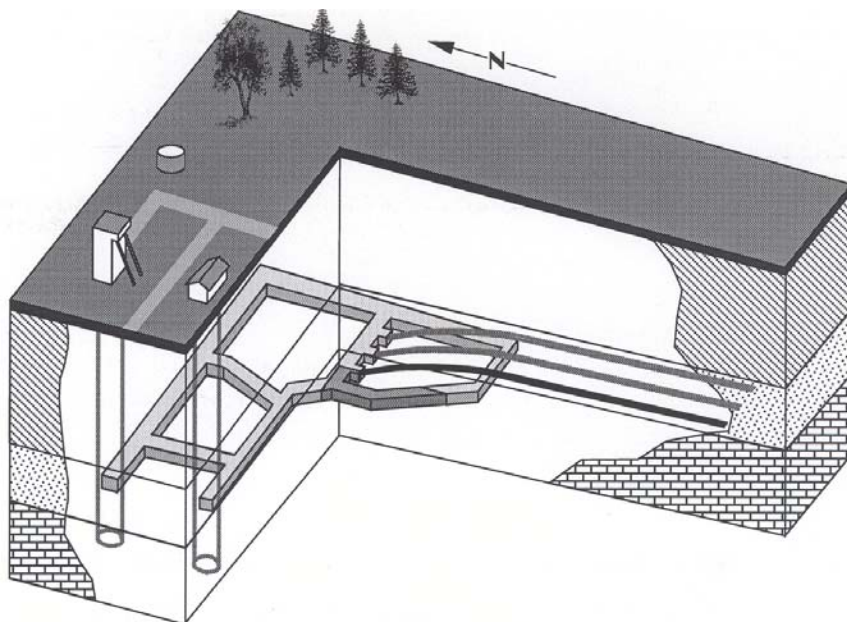


**Figure 9: Overall layout of Underground Test Facility / Phase A (from Chalaturnyk, 1996).**

After the successful completion of Phase B in 1996, the next phases of the UTF project were planned. Phases D and E were designed and implemented from 1996 to

2002, with longer borehole lengths. In later phases, however, the horizontal boreholes were drilled directly from the surface using high-tech drilling techniques, and the shaft/tunnel concept was no longer employed.

**Table 3: Geological strata arrangement at UTF site (summarized from Chalaturnyk, 1996).**

Unit Name Reservoir	Formation	General Description	Average Thickness (m)	Average Porosity (%)	Water Saturation (%)
A	Wabiskaw Member, Clearwater	Wabiskaw sand, medium- to coarse-grained, light grey, friable, salt and pepper sand, permeability: high, no bitumen.	2.4	33.1	50.0
B		Light to dark grey soft shales mixed with sand (65% shale and 35% sand), permeability: low, no bitumen.	7.4	31.8	77.0
C	•	Fine- to medium-grained, dark brown, oil sand interbedded with light brown shale, 70% oil sand and 30% shale.	5.2	32.4	12.5-35.0
D	• McMurray	Rich oil sand, dark brown, bitumen saturated oil sands, 80% oil sand and 20% shale, permeability: moderate to low.	8.8	33.0	28.0
E	•	Richest unit, dark brown sand, bitumen saturated, 90% oil and 10% shale, permeability: moderate.	9.5	31.0	13.0
F	•	Dominantly shale (70% shale and 30% oil sand), permeability: low.	1.7	30.8	58.0
G	•	Black, bitumen saturated, medium- to coarse-grained sand, permeability: low to moderate.	3.3	32.8	17.6
H	Waterways	Limestone, no bitumen, non-permeable, bottom seal to steam chamber.	-	9.62	5.68

Although more than 35 years have passed since the first UTF phase, the valuable monitoring and operational data is not yet available to the public. However, general specifications of the project can be extracted from limited publications. For the purpose of this study, three types of data were collected from different sources:

- (a) the production/injection history, which is confidential and will not be reported numerically in this paper
- (b) operational strategies, which have been partially included in some papers. The timeline and operational strategies of Phase A explained by Edmunds et al. (1994) are shown in Figure 11. The same information for Phase B, extracted from the paper by O'Rourke et al. (1997), is illustrated in Figure 12.

(c) the SAGD layout and geometry, material properties, and geology of the site, which are all available from many sources with quality acceptable for this research (e.g., Chalaturnyk, 1996). However, for numerical simulation more detailed data is required.

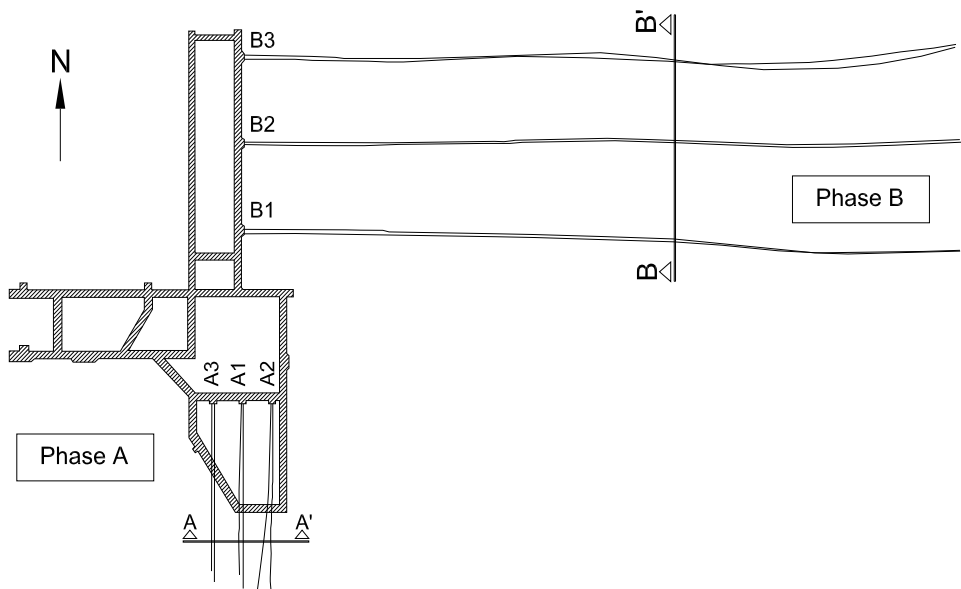


Figure 10: Plan view of UTF Phases A and B, and borehole arrangements.

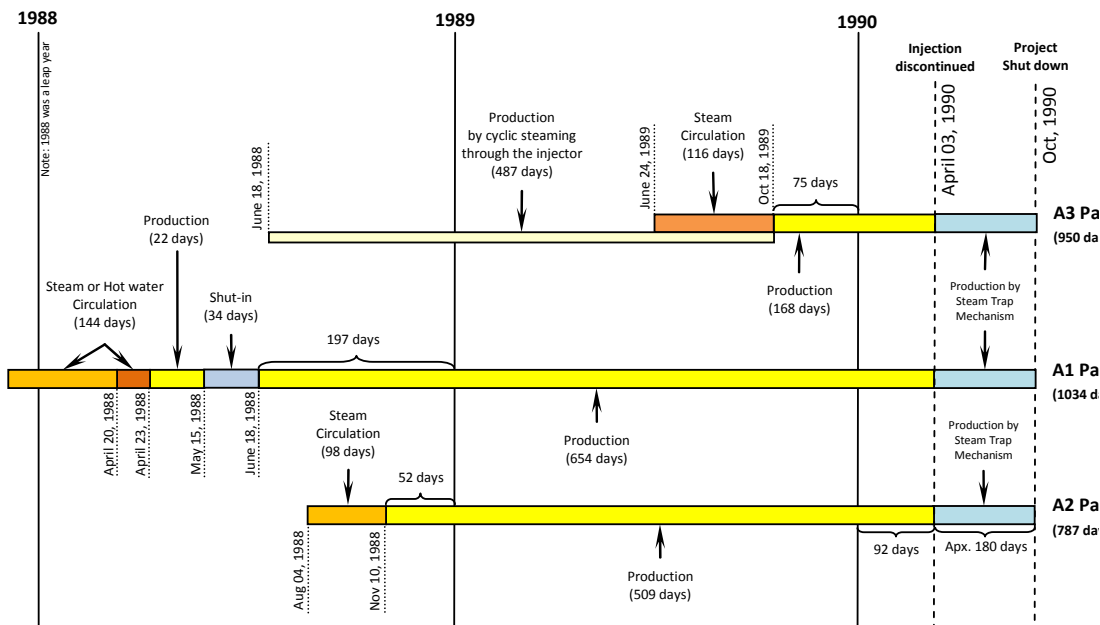


Figure 11: Timeline and operational strategies of UTF/Phase A (generated from Edmunds et al., 1994).

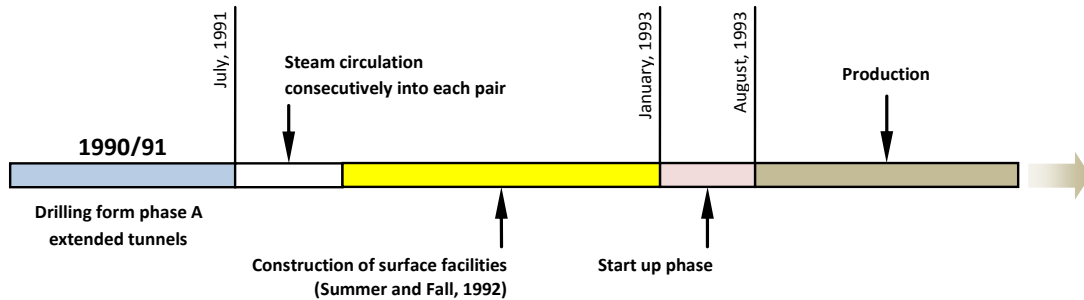


Figure 12: Timeline and operational strategies of UTF/Phase B (generated from O'Rourke et al., 1997).

## UTF PHASE A AND B ANALYTICAL SIMULATION

All the analytical models currently available are two-dimensional, and do not consider the process in the third axis. Therefore, a two-dimensional cross section was selected for each of the phases to represent the whole SAGD model. Cross sections A-A' and B-B' indicated in Figure 10 are plotted in Figures 13 and 14, respectively. The reservoir is located between the two bold lines that separate the rich portion of oil sand in the McMurray Formation from others.

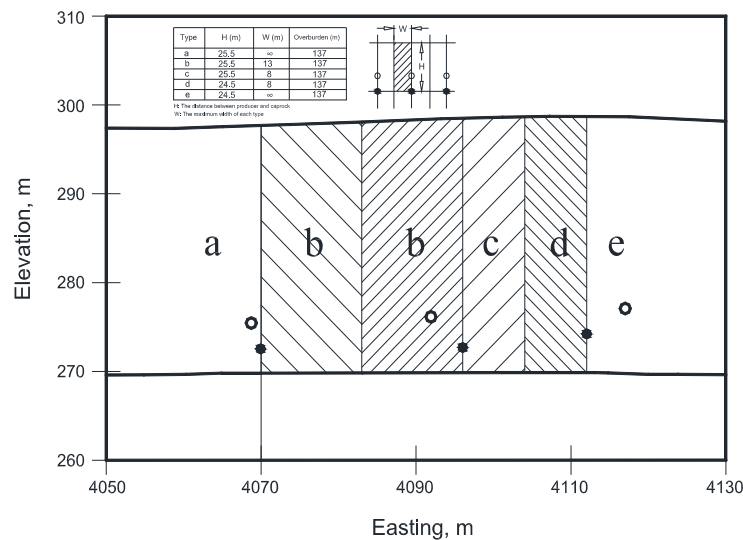


Figure 13: Cross section A-A' (see Figure 10) of UTF / Phase A.

In both cross sections, the space between each pair has been divided into two equal zones. Four zones are shaded in total. The zones at either end of the section are not shaded because a boundary effect is not applied to them. The zones have been categorized according to geometry, and the specifications are listed in a table for each cross section.

Material properties have been assumed to be generally the same for both phases. However, different values have been used in some cases reported in the literature (e.g., residual oil saturation). A complete list of oil sand hydraulic and physical properties is provided in Table 4. The table also contains information on borehole specifications, geomechanical *in situ* stress, and operational injection pressure.

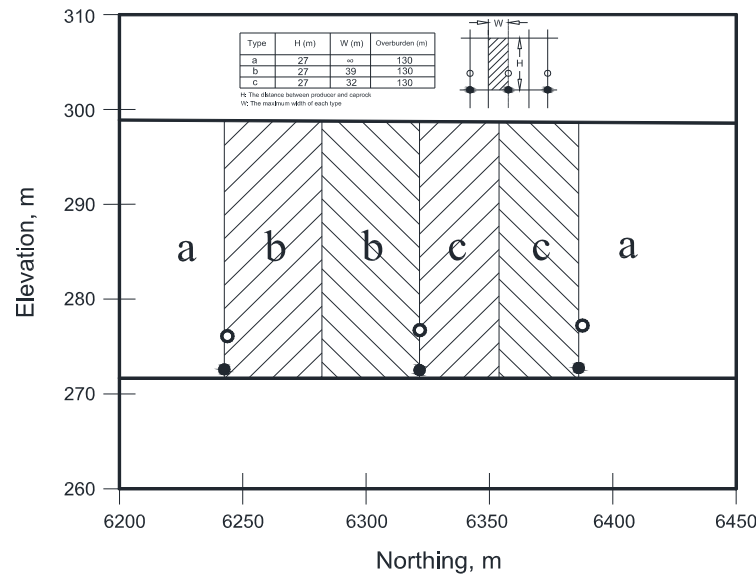


Figure 14: Cross section B-B' (see Figure 10) of UTF / Phase B.

The circular model used as a simulator in this study is capable of taking into account variations in relative oil permeability. Figure 15 illustrates the relative permeability curve that is regenerated from Chalaturnyk (1996).

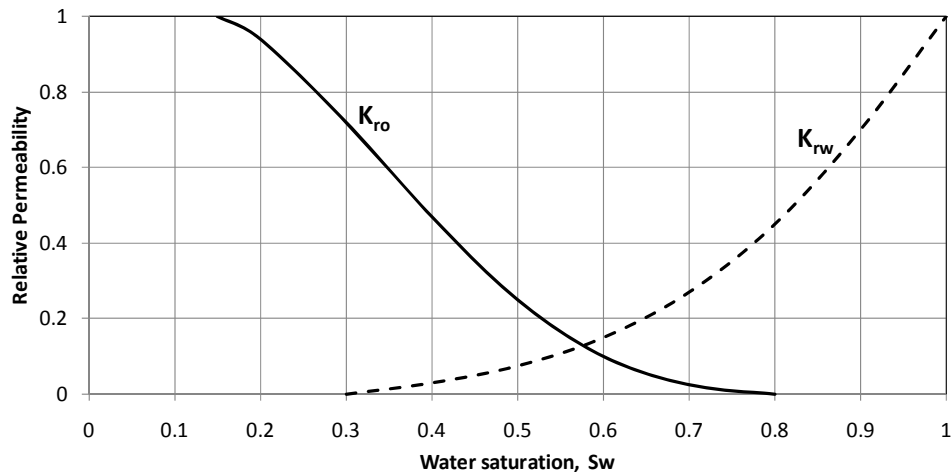


Figure 15: Relative permeability curves for UTF simulation (from Chalaturnyk, 1996).

For history matching, the cumulative production and injection curves are supposed to match the true history. For production, horizontal permeability is chosen as a variable parameter, and its adjustment is attempted. This means that the permeability values in Table 4 are the result of history matching after considering the geomechanical impact factor.

**Table 4: Material properties and SAGD operational specifications for UTF Phases A and B.**

	Parameters	Phase A	Phase B	Unit
Borehole Specifications	borehole length	55	500	m
	injector-producer spacing	5	5	m
Flow Simulator Parameters	horizontal absolute permeability	5820	6145	mD
	vertical/horizontal absolute permeability	0.5	0.5	-
	oil density	1008	1008	Kg/m <sup>3</sup>
	dynamic viscosity at steam temperature	0.007	0.007	Pa·s
	porosity	0.32	0.32	%
	initial oil saturation	0.85	0.85	%
	residual oil saturation	0.4	0.3	%
	reservoir thermal diffusivity	0.0000006	0.0000006	m <sup>2</sup> /s
	coefficient of average velocity, $a_0$	0.4	0.4	-
	coefficient of viscosity, $m$	3.6	3.6	-
Parameters for Steam Calculation	formation heat capacity	1865000	1955000	J/(m <sup>3</sup> ·°C)
	specific heat of steam condensation	2000000	2000000	J/Kg
	reservoir temperature	7	7	°C
	steam temperature	230	220	°C
	steam quality	0.95	0.95	%
Parameters for Geomechanical Analysis	formation density	2200	2200	Kg/m <sup>3</sup>
	horizontal stress ratio, min	1.2	1.2	-
	horizontal stress ratio, max	2	2	-
	reservoir pressure	550	550	kPa
	injection pressure	2800	2600	kPa
	GIF (Geotechnical Impact Factor)	0.88	0.8	-
	permeability increase ratio	35	25	%

The cumulative steam injection history is matched with the calculated permeability. The only variable parameter for injection, formation heat capacity, has a very narrow range of variation. These two steps show that the history matching focuses more on production than injection. The reason is that the drainage models are more realistic than steam injection theories (energy balance) due to the complexity of thermal heat transfer theories. Almost none of the theories proposed for calculating the steam injection rate consider thermal energy propagation similar to what happens in a SAGD reservoir because they avoid complexity in the analytical model.

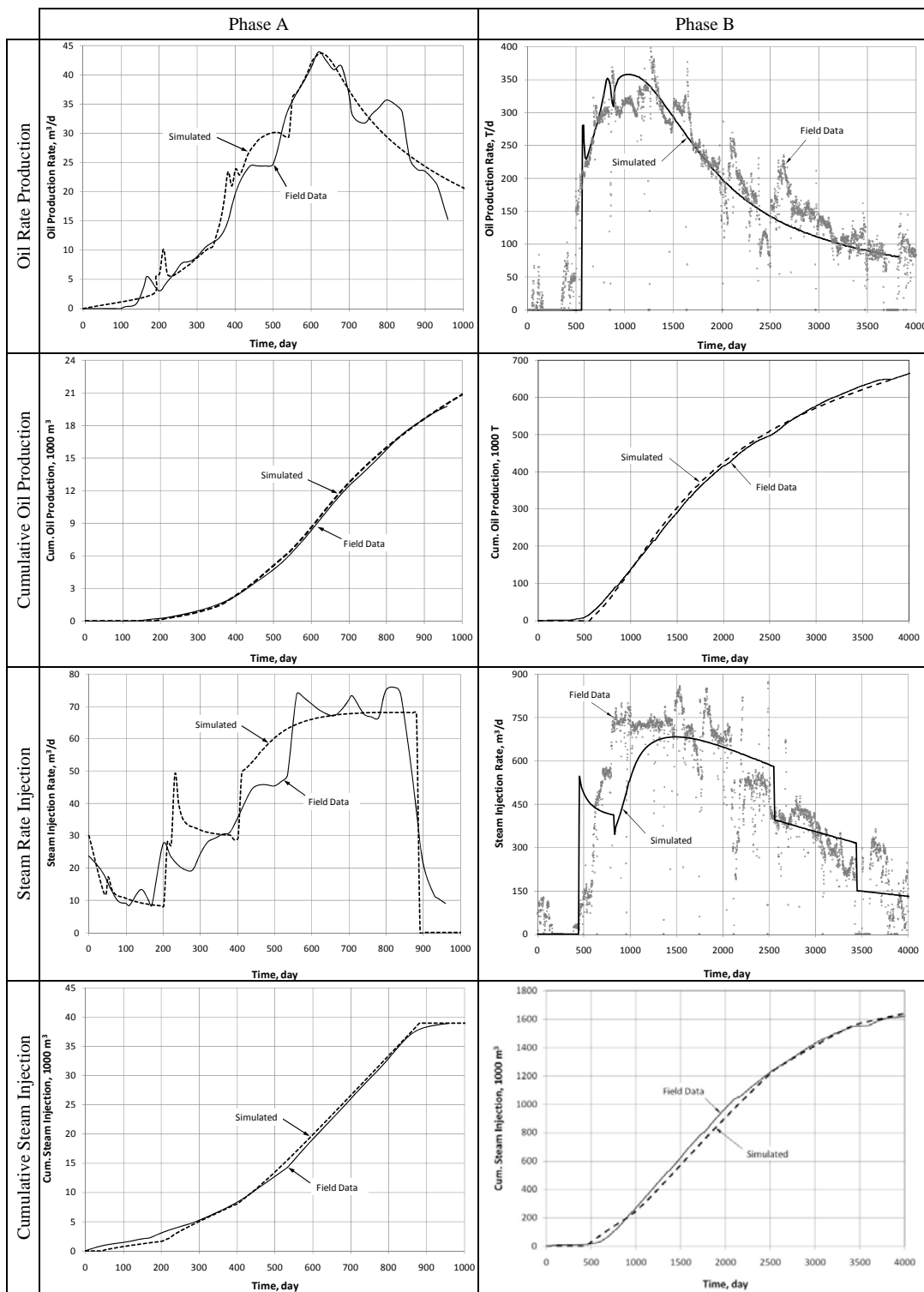


**Figure 16: History matching results on cumulative production and injection for UTF / Phases A and B.**

## HISTORY MATCHING RESULTS

In general, history matching is a minimization process of an error objective function. Because only one parameter is adjusted for the case studies in this research, the simple Newton-Raphson algorithm was employed. However, for simultaneous adjustment of more than one variable, more efficient algorithms should be used. The error function that is minimized in this study is the Root Mean Square (RMS) of the cumulative production/injection curves. Figure 16 demonstrates the result of the history matching process of oil production and steam injection. The results show a generally good match between the field data and the simulation data predicted by the circular model.

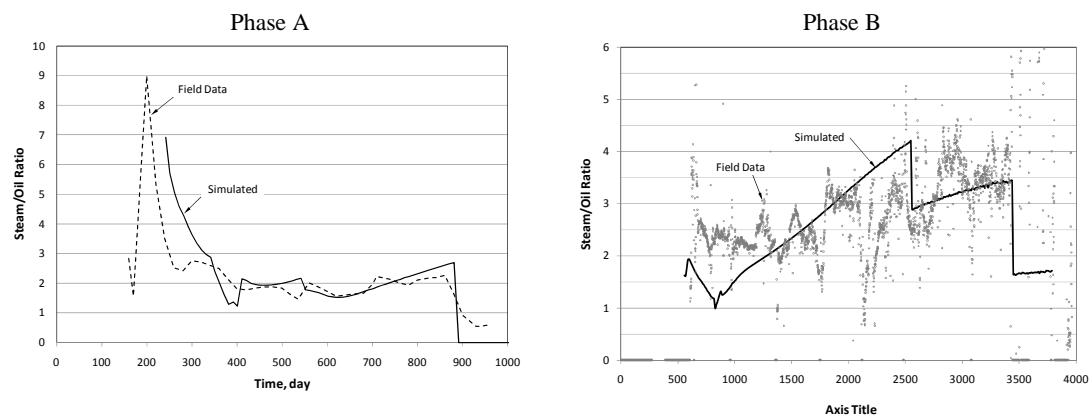


**Figure 17: Steam/oil ratio (SOR) resulting from history matching for UTF / Phases A and B.**

As expected, the production histories of both phases match fairly well. The consistency between the simulated curve and the history of oil rate proves that the simulation results followed the SAGD process. In addition, the steam injection prediction does not have significant levels of agreement compared to the results of the drainage model. Although the injection history perfectly matches in some intervals, steam injection does not show successful history matching. This deficiency is magnified when instantaneous steam/oil ratio (ISOR) is plotted against time. Figure 17 plots ISOR for both phases. Figure 17 shows better history matching in Phase A than in Phase B. The simulated SOR in Phase A has the same general shape as the history, while it is still unable to simulate the first noisy stage.

Quality of history matching is not the only result that should be discussed. More attention should be paid to predict values for permeability, which here is an average value for the reservoir. In many references, horizontal permeability ranges between 5000 and 12000 mD (e.g., Edmunds et al., 1994, or Komery et al., 1995). However, based on UTF/A geomechanical-reservoir history matching, Li (2006) predicted horizontal permeability of 5000 mD. He showed that this value would be larger when geomechanical effects are not considered. The horizontal permeability values listed in Table 4 show an average predicted value of 6000 mD. If the geotechnical increase ratio is applied, the average value changes to 7200 mD. It seems that the value predicted in this study is approximately 1000 mD more than what predicted in numerical modelling by Chalaturnyk (1996) or Li (2006), but is still in an acceptable range. Since no past studies have modelled the heterogeneity of the reservoir, the variation of permeability cannot be strictly limited to a short range. Therefore, as long as there is not a significant difference between the values, the prediction of this study is reasonably in range and close to reality. If the results of the numerical models reported by Li (2006) or Chalaturnyk (1996) are assumed to be true, it can be concluded that the analytical model in this study has predicted the permeability with approximately 20% uncertainty. This is not a certain value, but generally demonstrates the level of uncertainty when analytical models are used.

## **STEAM CHAMBER LOCATION**

The zone categories that were suggested before starting the history matching process (Figures 13 and 14) are not quite the same as those applied throughout the analyses. During the history matching process, it appeared that the zones should not be equally divided between the well pairs. Due to the time lag between steam injections, the steam chamber can occupy a larger (or smaller) area before the other injector begins. For instance, in Phase A, where the injectors do not begin working simultaneously, one of them is shut in and does not come back to the system.

None of these injection scenarios are predicted in a simple analytical model. However, altering available tools (such as shifting the effective boundary width) can be helpful, as shown in Figure 18 for Phase A. If the width of Zone b is kept the same

as what was selected in Figure 13, the steam chamber would not grow beyond its size at 700 days.

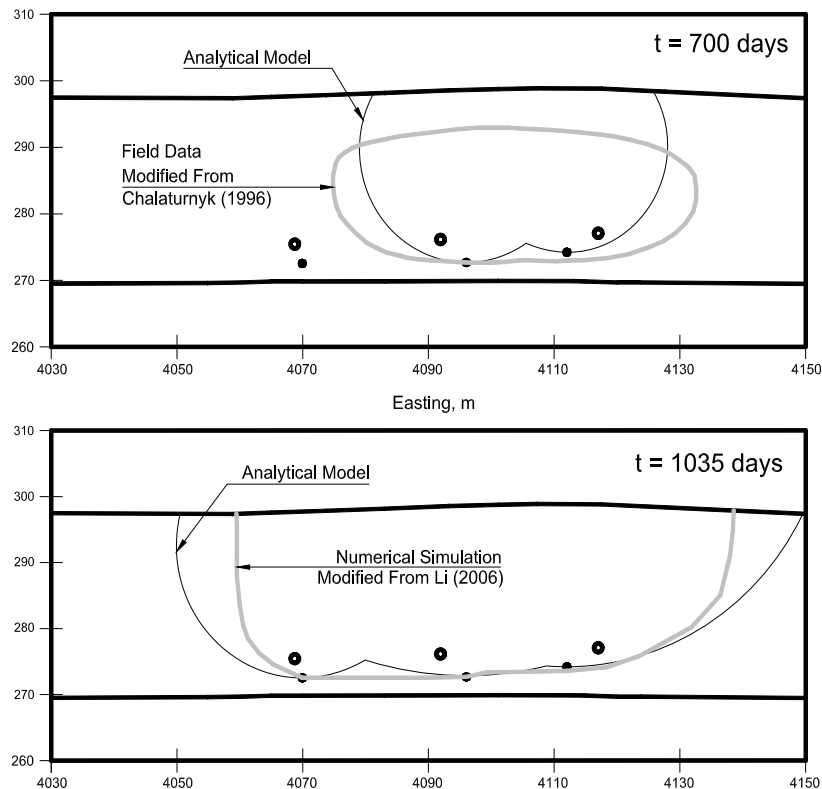


**Figure 18: Steam chamber predicted by the circular model compared to the field data for UTF/Phase A.**

## SUMMARY AND CONCLUSIONS

In this study, the application of SAGD analytical physics-based models for history matching purposes was assessed through comparing current analytical models. A mathematical procedure that takes geomechanical considerations into account was proposed for history matching SAGD processes. Two case studies of the UTF pilot test (Phase A and B) were also covered to check the reliability and level of uncertainty of such models. The following observations are derived from this study:

Drainage models performed well in history matching. While there are some limitations in analytical models when employed in real SAGD with complex geometry and operation strategies, they are flexible enough to be modified without losing the physical meaning of the process.

It is difficult to be conclusive about the level of uncertainty in the predictions of analytical models, but those for the case studies presented in this paper were more than 80% reliable.

Steam injection theories demonstrated lower functionality in history matching. Due to the complexity of steam injection mechanisms and heat transfer theory, current theories need to be modified or altered.

Generally, history matching results showed that analytical physics-based models can be used as an alternative to numerical simulators. Since all of the variables have their own physical meaning, uncertainty analysis within the system or within the prediction is much more promising than other proxies. The required resolution and uncertainty of the results determines the application of the model in different stages of a SAGD project.

## REFERENCES

Awasthi, A., Sankaran, S., Nikolaou, M., Saputelli, L., and Mijares, G. 2007. Closing the gap between reservoir modeling and production optimization. *Proc., the Digital Energy Conference and Exhibition*, 11-12 April 2007, Houston, Texas, U.S.A.

Azad, A., and Chalaturnyk, R.J. 2010. A mathematical improvement to SAGD using geomechanical modelling. *Journal of Canadian Petroleum Technology*. 49(10): 53-64.

Azad, A., and Chalaturnyk, R.J. 2011a. An improved SAGD analytical simulator: circular steam chamber geometry. Submitted to the *Journal of Petroleum Science and Engineering*.

Azad, A., and Chalaturnyk, R.J. 2011b. Numerical study of SAGD: geomechanical-flow coupling for Athabasca oil sand reservoirs. *Proc., the 45th US Rock Mechanics/Geomechanics Symposium*, June 26-29, San Francisco.

Butler, R.M., and Stephens, D.J. 1981. The gravity drainage of steam-heated heavy oil to parallel horizontal wells. *Journal of Canadian Petroleum Technology*. 20(2): 90-96.

Butler, R.M. 1997. *Thermal Recovery of Oil and Bitumen*. Calgary, Alberta, Canada.

Butler, R.M., McNab, G. S., and Lo, H.Y. 1981. Theoretical studies on the gravity drainage of heavy oil during Steam Heating. *Canadian Journal of Chemical Engineering*. 59: 455-460.

- Chalaturnyk, R.J. 1996. Geomechanics of the Steam-Assisted Gravity Drainage Process in Heavy Oil Reservoirs. *PhD Dissertation*. University of Alberta, Edmonton, Canada.
- Cokar, M., Kallos, M.S., and Gates, I.D. 2011. A new thermogeomechanical theory for gravity drainage in SAGD. *Proc., the World Heavy Oil Congress 2011*, Edmonton, Canada.
- Edmunds, N.R., Kovalsky, J.A., Gittins, S.D., and Pennacchioli, E.D. 1994. Review of phase A steam-assisted gravity-drainage test. *SPE Reservoir Engineering*. 9(2): 119-124.
- Fetel, E., and Caumon, G. 2008. Reservoir flow uncertainty assessment using response surface constrained by secondary information. *Journal of Petroleum Science and Engineering*. 60: 170–182.
- Ito, Y., and Suzuki, S., 1998. Effect of reservoir parameter on Oil rates and steam Oil ratios in SAGD projects. *Proc., the 7<sup>th</sup> UNITAR International Conference on Heavy Crude and Tar Sands*, Beijing, China, 27-30.
- Komery, D.P., Luhning, R.W., Pearce, J.V., and Good, W.K. 1998. Pilot testing of post-steam bitumen recovery from mature SAGD wells in Canada. *Proc., the 7<sup>th</sup> UNITAR International Conference on Heavy Crude and Tar Sands*, Beijing, China.
- Li, P. 2006. Numerical Simulation of the SAGD Process Coupled with Geomechanical Behaviour. *PhD Dissertation*. University of Alberta, Edmonton, Canada.
- O'Rourke, J.C., Chambers, J.I., Suggett, J.C., and W.K. Good. 1994. UTF project status and commercial potential. *Proc., the 48th Annual Technical Meeting of the Petroleum Society of CIM*, June 12–15, Calgary. Paper No. 94-40.
- Queipo, N.V., Goicochea P., J.V., Pintos, S. 2001. Surrogate modeling-based optimization of SAGD processes. *Proc., SPE International Thermal Operations and Heavy Oil Symposium*, 12-14 March 2001, Porlamar, Margarita Island, Venezuela, 9 p.
- Reis, J.C. 1992. A steam-assisted gravity drainage model for tar sands linear geometry. *Journal of Canadian Petroleum Technology*. 31(10): 14-20.
- Sarma, P., and Xie, L. 2011. Efficient and robust uncertainty quantification in reservoir simulation with polynomial chaos expansions and non-intrusive spectral projection. *Proc., SPE Reservoir Simulation Symposium*. 21–23 February 2011, The Woodlands, Texas, USA.

Scott, D., Proskin, S.A., and D.P. Adhikary. 1994. Volume and permeability changes associated with steam stimulation in an oil sands reservoir. *Journal of Canadian Petroleum Technology*. 33(7): 44-52.

Settari, A., and Walters, D.A. 2001. Advances in Coupled Geomechanical and Reservoir Modeling With Applications to Reservoir Compaction. *SPE Journal*. 6(3): 334-342.

Silva, P.C., Maschio, C., and Schiozer, D.J. 2008. Application of neural network and global optimization in history matching. *Journal of Canadian Petroleum Technology*. 47(11): 22-25.

Sun, X., and Mohanty, K.K. 2005. Estimation of flow functions during drainage using genetic algorithm. *SPE Journal*. 10(4): 449-457.

Vanegas P, J.W., Deutsch, C.V., and Cunha, L.B. 2008. Uncertainty assessment of SAGD performance using a proxy model based on Butler's theory. *Proc., SPE Annual Technical Conference and Exhibition*. 21-24 September 2008, Denver, Colorado, USA.

Williams, G.J.J., Mansfield, M., MacDonald, D.G., and Bush, M.D. 2004. Top-down reservoir modeling. *Proc., SPE Annual Technical Conference and Exhibition*. 26-29 September 2004, Houston, Texas.

Zubarev, D.I. 2009. Pros and cons of applying proxy-models as a substitute for full reservoir simulations. *Proc., SPE Annual Technical Conference and Exhibition*, 4-7 October 2009, New Orleans, Louisiana.

## APPENDIX A

The oil production formulations used in this paper are as follows:

$$\begin{aligned} \frac{q_{TD}}{L} &= 2 \left( \sqrt{\frac{3}{2}} - \left(\frac{t}{w}\right)^2 \frac{kg\alpha}{\phi\Delta S_o m v_s h} \sqrt{\frac{2}{3}} \right) \sqrt{\frac{kg\alpha\phi\Delta S_o h}{m v_s}} \\ &= \left( \frac{6kg\alpha\phi\Delta S_o h}{m v_s} \right)^{\frac{1}{2}} - \left(\frac{t}{w}\right)^2 \sqrt{\frac{8}{3}} \left( \frac{kg\alpha}{m v_s} \right)^{\frac{3}{2}} (\phi\Delta S_o h)^{-\frac{1}{2}} \dots\dots\dots(A-1) \end{aligned}$$

$$\frac{q_{RS}}{L} = 3 \left( \frac{kg\alpha}{m v_s} \right)^{\frac{2}{3}} (\phi\Delta S_o h)^{\frac{1}{3}} t^{\frac{1}{3}} \dots\dots\dots(A-2)$$

$$\frac{q_{LG}}{L} = 2 \left( \frac{kg\alpha\phi\Delta S_o h}{2am v_s} \right)^{\frac{1}{2}} \dots\dots\dots(A-3)$$

$$\frac{q_{SM}}{L} = \frac{2ch k_h^{0.75} \left( \frac{k_v}{k_h} \right)^{0.4} \Delta S_o \phi^{0.45}}{\mu_{os,60}^{0.33}} \dots\dots\dots (A-4)$$

where:

- $q_{TD}$  = oil production rate, TANDRAIN model
- $q_{RS}$  = oil production rate, rising steam model
- $q_{LG}$  = oil production rate, linear geometry model
- $q_{SM}$  = oil production rate, synthetic model

$L$  = length of boreholes

$t$  = time

$w$  = half of the horizontal distance to the adjacent injector

$k$  = Effective permeability

$g$  = gravity

$\alpha$  = thermal diffusivity of the reservoir

$\phi$  = porosity

$\Delta S_o$  = (initial – residual) oil saturation

$h$  = reservoir height

$m$  = coefficient of viscosity

$\nu_s$  = kinematic oil viscosity at steam temperature

$a$  = experimental dimensionless temperature coefficient

$k_v$  = vertical effective permeability

$k_h$  = horizontal effective permeability

$c$  = constant

$\mu_{os, 60^\circ}$  = dynamic oil viscosity at 60°C lower than steam saturation temperature

# CHAPTER 5: NUMERICAL STUDY OF SAGD: GEOMECHANICAL-FLOW COUPLING FOR ATHABASCA OIL SANDS RESERVOIRS\*

## **ABSTRACT**

Steam Assisted Gravity Drainage (SAGD) process has been successfully employed for unconventional oil sand reservoirs in Canada. In this process, two horizontal boreholes are drilled one on top of the other at the bottom of a reservoir. Steam is injected through the top borehole and oil is produced from the bottom borehole. Beside the flow process, geomechanical processes are also active and can play a role in SAGD. It has been shown that porosity and permeability are the two major rock properties that are highly influenced by geomechanical behavior of oil sand during a thermal recovery process. This paper investigates the SAGD process numerically when geomechanics is considered. For this reason, a code was developed to couple a flow simulator and a geomechanical module based on iterative coupling approach for different 2D models. Results confirm that oil production is improved when geomechanics is involved in simulation and the impact of geomechanics on each case is explored. The results have been also compared to the analytical models and a geomechanical impact factor (GIF) is introduced for uncoupled simulations.

---

\* This paper was presented at the 45<sup>th</sup> US Rock Mechanics/Geomechanics Symposium held in San Francisco, CA, June 26–29, 2011. The paper was selected for presentation at the symposium by an ARMA Technical Program Committee based on a technical and critical review of the paper by a minimum of two technical reviewers.

## INTRODUCTION

Canadian oil is mostly recovered from oil sand pay zone that is deposited at different depths of the ground. In those reservoirs that are closer to the ground surface, oil sand is mined and the extracted material is washed by warm water and chemicals to remove oil out of the rock pores. Physical properties of the rock and understanding the chemical reactions between materials are important factors in this recovery method. This method is applicable only to 20% of the recoverable oil in Canada. However, other 80% is not minable and has to be recovered in site.

Steam Assisted Gravity Drainage (SAGD) is an in-situ thermal oil recovery process developed in Alberta in early 80's (Butler, 1994). This technique has been successfully employed in the last three decades and it is still the first option among in-situ recovery methods. In a SAGD process, high pressure and temperature steam is injected into the reservoir to decrease the oil viscosity. Low viscous oil then flows downward due to gravity. The complex physics of this process is generally understood. Unlike oil recovery by surface mining, geomechanics and thermodynamics both actively affect the SAGD process. It has been shown that geomechanical behavior of oil sand can alter the hydraulic characteristics of the reservoir. Permeability and porosity are the two major properties that are dynamically changing by any changes in geomechanical behavior and deformation of the reservoir. In-situ stresses and injected steam pressure redistribute the stress field within the reservoir that can dictate different strain fields and result in different permeability and porosity distributions. This phenomenon has been well studied in the last twenty years (Albahlani and Babadagli, 2008).

Experimental studies on oil sand by Dusseault and Morgenstern (1978), Kosar (1989), Agar (1984), and Scott and Seto (1986) are among the first works to explain the geomechanical and thermal properties of Athabasca oil sand reservoirs. These studies revealed the high strength and dilatancy, the strain-softening behavior, and unique sand matrix structure of the oil sands formation. These studies were followed by other laboratory researches on the changes of permeability and porosity during steam stimulation and temperature changes (Oldawski, 1994, and Scott et al., 1994).

Recent experimental studies have been focused more to capture constitutive model of behavior for oil sand. The results of such studies can feed numerical codes to facilitate computer modeling (Touhidi-Baghini, 1998, Chalaturnyk, 1996, and Samieh, 1995).

Although geomechanical models of oil sand have been explored both experimentally and numerically, more attempts are needed to merge geomechanics and flow principals in a numerical model. Chalaturnyk (1996) and Li (2006) have proposed a framework to couple a flow simulator with a geomechanical code. They showed how a geomechanical coupled simulation could explain the changes in the reservoir properties while an uncoupled (flow only) model could not. The work by Settari et al. (2000) is another major reference in geomechanical coupling. Their research showed how geomechanics can be used for modeling integrated reservoir analysis.

This paper has employed a numerical model to explore a typical SAGD process in different conditions when geomechanics is considered. Athabasca, the largest oil sand reservoir in Canada, has been chosen for material reference. For this reason, a numerical code was developed to couple a flow simulator (STARS, CMG<sup>®</sup>) and a geomechanical module (FLAC, ITASCA<sup>®</sup>) based on iterative coupling approach. Initial hydraulic properties of the reservoir are assumed constant for different generated models. The initial geomechanical properties, i.e. the constitutive model of oil sand, are also kept unchanged. However, operational variables such as injection pressure and temperature- determined by the depth of the reservoir and the hydraulic fracturing stress- vary in this study. In addition, the arrangement of the in-situ stresses is another parameter that has been evaluated. This study aims to investigate firstly, the level of geomechanical impact on the process at different reservoirs and operational conditions and secondly, to define a simple factor to evaluate the level of geomechanical importance in a reservoir under SAGD process. It is important to note that the analyses in this study focus on the geomechanical effects on production. Other major issues such as caprock integrity, while very important, are not considered in this paper.

## STEAM ASSISTED GRAVITY DRAINAGE (SAGD)

SAGD, a thermal recovery process, was developed in Alberta and enabled petroleum engineers to recover heavy oil when the reservoir is deposited in depth. The first pilot test, Underground Test Facility (UTF) Phase A, was successfully deployed in Athabasca reservoir located 60 Km north of McMurray in Canada during 1990 to 1993 (Edmunds et al., 1994, and O'Rourke et al., 1994).

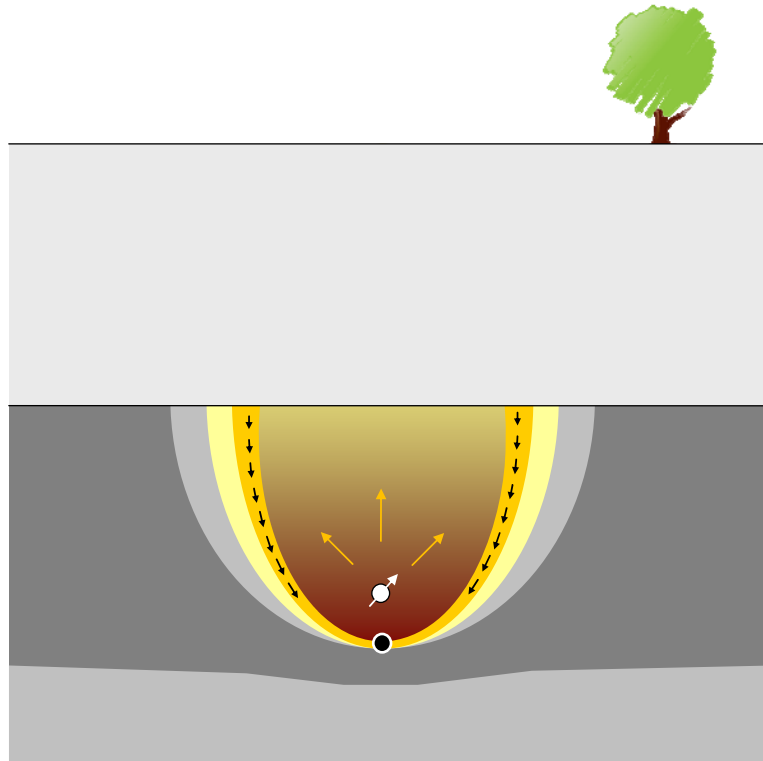


Figure 1: SAGD process and steam chamber growth in the reservoir.

For a SAGD process, two horizontal boreholes are drilled one on top of the other close to the bottom of a reservoir. The top borehole is called the injector and the other one drilled at the bottom is called the producer. The philosophy of such a process is to lower the viscosity of heavy oil by the means of heating the reservoir. Thermal energy is provided by injecting high temperature and pressure steam from bottom of the reservoir. The steam will grow up a zone around the injector borehole which is called 'steam chamber' as shown in Fig. 1. On the edge of the steam chamber, low viscosity oil has the potential to flow toward the bottom of the steam chamber and a production well is used to transfer the accumulated oil to the surface.

At the beginning of the project when the reservoir is at its original temperature, the oil viscosity is extremely high and no flow is possible between the two horizontal wells. Circulation of steam inside each borehole called reservoir preheating is considered for several months to increase the temperature in the region around the boreholes. Preheating increases the reservoir injectivity and inter-borehole communication.

After preheating, the upper well remains an injection well where steam is injected for the predicted life of the reservoir and the lower well is converted into a production well. To maximize the recovery ratio, multiple pairs of boreholes are drilled beside each other and each steam chamber is designed to recover bitumen from a part of the reservoir.

### **GEOMECHANICAL-FLOW COUPLING**

During SAGD process two major mechanisms occur at the same time;

- Flow mechanism: pressure and temperature difference in reservoir cause fluids to flow. Thermodynamics and fluid mechanics can describe and numerically solve the equation of state. Many commercial packages are available in petroleum industry to solve this part of the process. Most of these softwares have been coded using finite difference method.
- Geomechanical mechanism: changes in stress field, e.g., fluid pressure will redistribute the stress-strain field in the reservoir. This mechanism can cause reservoir deformation, ground heave, and changes in material properties such as porosity and absolute permeability.

These mechanisms can be solved at the same time in one set of equations. However, fully coupled solutions are significantly complex and might encounter many convergence problems. A technique that is usually used is known as iterative coupling where the solution is run in short time steps. At each time step, both mechanisms are solved separately and the in-common properties are shared or updated continuously. Fig. 2 shows the tasks for each time step that are done in a closed cycle.

For iterative coupling in this study, two commercial finite difference codes were utilized; (1) STARS a flow simulator by CMG and (2) FLAC-2D a geomechanical module by ITASCA. The coupling algorithm was coded in FORTRAN and it was run under a LINUX script program.

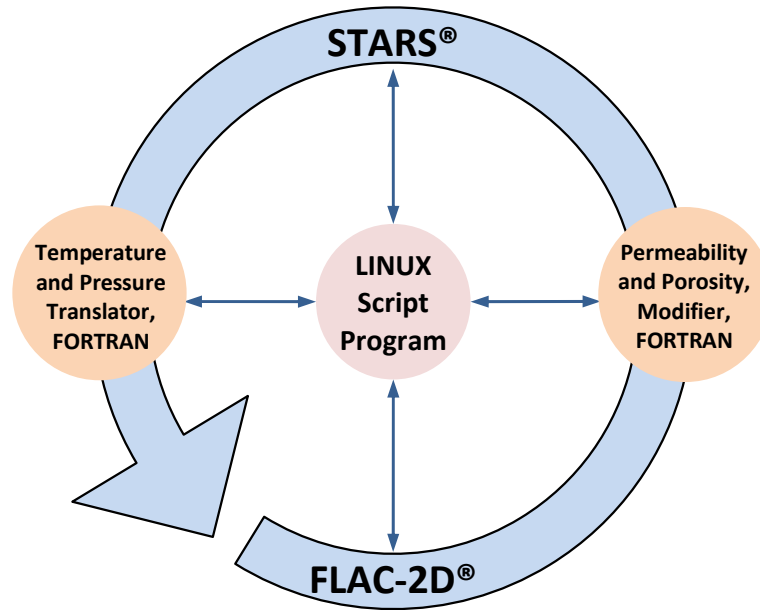


**Figure 2: Coupling cycles and the interactive LINUX code.**

At each time step, STARS is run and the calculated temperature and pressure are transferred from the results into FLAC as inputs. The solution provided by FLAC is then updated the magnitude of porosity and permeability for the next cycle. Time steps are chosen such that it could capture essential features of the process. To do this, time steps should not be too short because it dramatically amplifies the run time and it should not be too large to lose the material balance accuracy. Excellent guidance on stability, accuracy and efficiency of sequential methods for coupled flow and geomechanics is provided by Kim et al. (2009).

In each cycle, permeability and porosity are updated based on volumetric strain. This term is shown to be the only major parameter to change hydraulic conductivity and pore volumes of oil sand. For this reason, experimental equations proposed by Touhidi-Baghini (1998) are used as follows:

$$\ln\left(\frac{K}{K_0}\right) = \frac{n}{\phi_0} \varepsilon_v \dots\dots\dots(1)$$

$$\phi = \frac{\phi_0 + \varepsilon_v}{1 + \varepsilon_v} \dots\dots\dots(2)$$

In Eq. (1) and (2),  $K$  is permeability,  $\phi$  is porosity, and  $\varepsilon_v$  is the volumetric strain. Initial values of each parameter are shown using subscript ‘0’. For horizontal permeability  $n$  is 2 and for vertical permeability  $n$  is 5.

**IN-SITU STRESS ARRANGEMENT IN ATHABASCA OIL SAND RESERVOIR**

Understanding the magnitude and orientation of the three principal in-situ stresses is essential in any geomechanical modeling. Orientation of maximum and minimum stresses could change the location and layout of most underground structures.

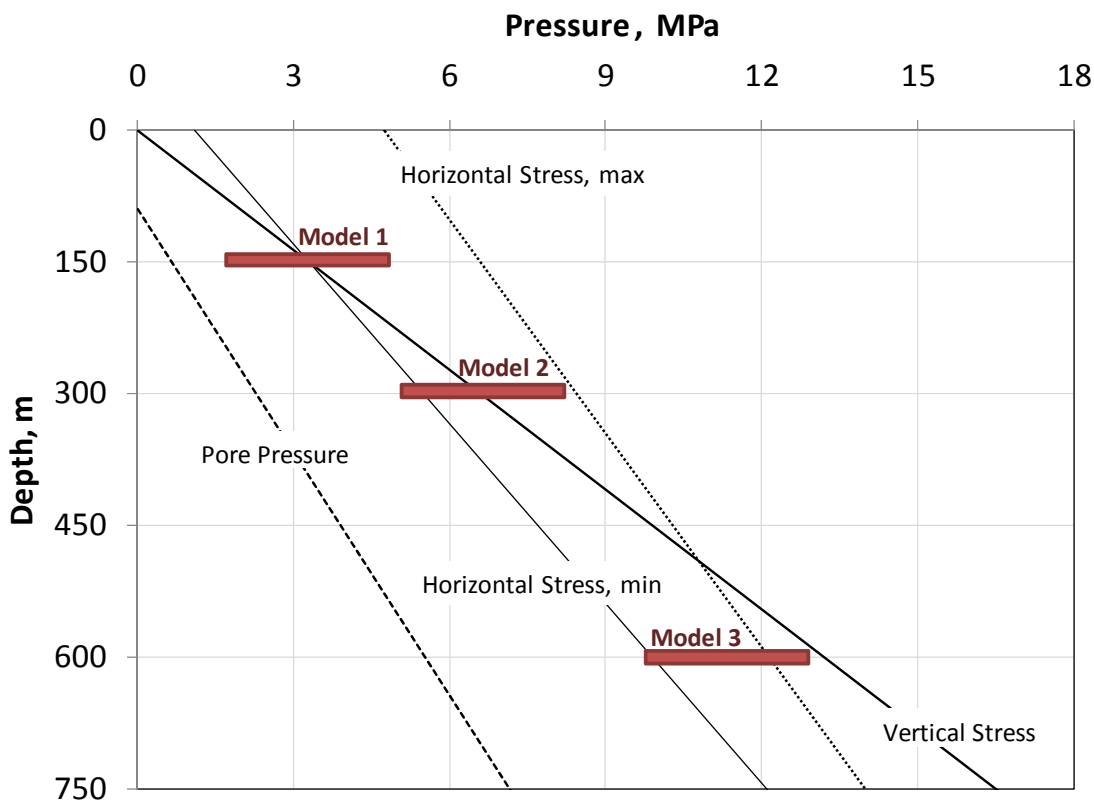


Figure 3: Distribution of horizontal and vertical stresses in Athabasca oil sand reservoirs, after Collins (2007).

The same scenario is true in reservoir geomechanics. Neglecting this fact might prevent a reservoir from producing the maximum recoverable oil or sometimes, can cause undesired problems such as caprock failure. The effect of stress orientation on SAGD has been studied by Collins (2007). For Athabasca oil sand reservoir he combined field and lab data from different sources and roughly calculated the variation of horizontal and vertical stresses and pore pressure. Fig. 3 has been generated the stress variation proposed by Collins. Although Fig. 3 is not always correct and may vary from place to place, it has been adopted in this study as the reference stress trend for our numerical modeling.

Three models are studied in this paper. (a) Model 1: is located at 150 m depth. Vertical stress and minimum horizontal stresses are the same and the maximum horizontal stress is the maximum in-situ stress. (b) Model 2: is located at 300 m depth. Vertical stress is larger than the minimum horizontal stress, but it is less than the maximum horizontal stress. (c) Model 3: is located at 600 m depth. At this depth, vertical stress is the maximum in-situ stress and both horizontal stresses are less than the vertical stress.

## **MODELS AND OPERATION STRATEGY**

In the Athabasca regions oil sand is found at varying depths underlain by the Devonian limestone. The three models described above mimic different depths of the oil sand reservoir; Model 1 is a shallow reservoir similar to UTF/A, Model 2 is a medium and Model 3 is a deep reservoir.

For geomechanical modeling three layers are considered; overburden including caprock, 20 m thick oil sand reservoir, and 50 m thick limestone at the bottom of the model. The width of the geomechanical model, however, should be chosen wide enough to prevent any boundary effects on the analysis. Table 1 has listed all the geometry parameters plotted in Fig. 4 for each model. Other than the geometry of models, initial stress ratios and initial reservoir pressure have been also calculated from Fig. 3. Three operating steam pressure levels are designed to be applied in separate models. Maximum injection pressure has been kept lower than the hydraulic fracturing pressure at each position of the reservoir.

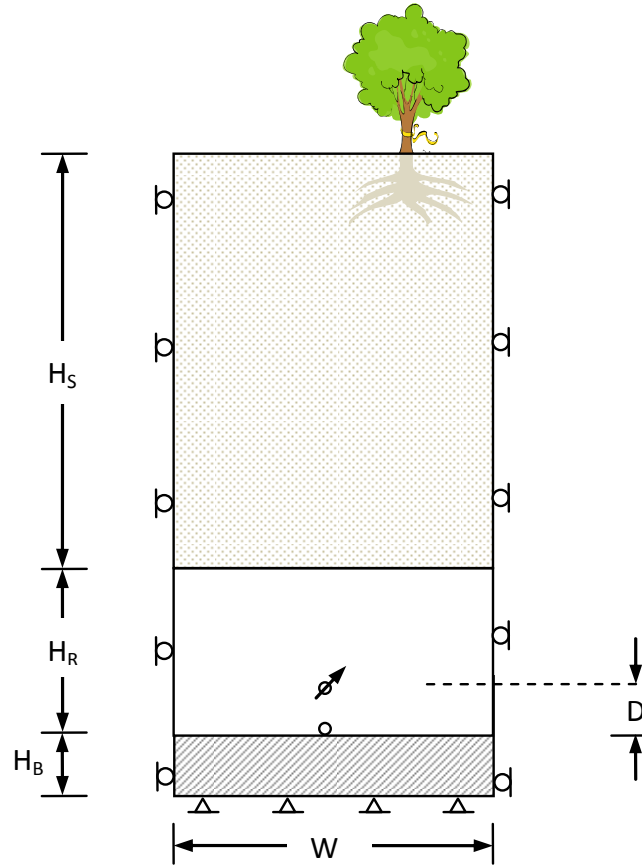


**Figure 4: Geometry of models for coupling runs.**

Boundary conditions around the model are illustrated graphically in Fig. 4. Horizontal displacement on either sides and both vertical and horizontal displacements at the bottom of the model are fixed. It should be noted that since the model is symmetric and properties are all homogeneous and isotropic, only half of the reservoir is required to be modeled. For our case, because this study is the primary stage of an extensive project, both halves have been modeled for next stages.

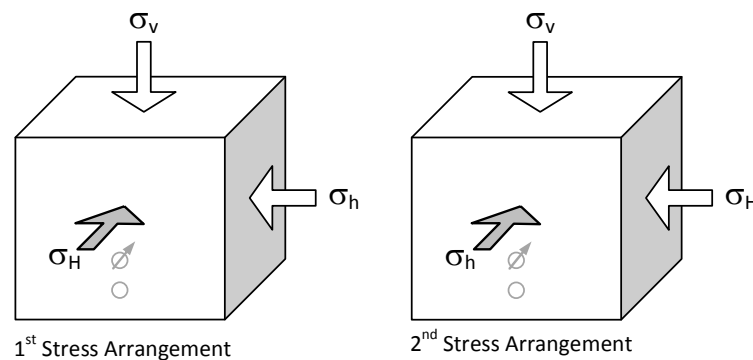


**Figure 5: Two cases for horizontal stress arrangement.**

In the flow simulator, STARS, the reservoir layer is modeled only. For this reason grid sizes are kept the same in both simulators for the reservoir.

**Table 1: Geometry and applied stress/pressure.**

Parameter	Model 1:	Model 2:	Model 3:
	Shallow Reservoir	Medium Reservoir	Deep Reservoir
$H_S$ (m)	140	290	590
$H_R$ (m)	20	20	20
$H_B$ (m)	50	50	50
W (m)	400	400	400
D (m)	4	4	4
reservoir width (m)	100	100	100
min. horizontal/vertical stress ratio	1	0.85	0.8
max. horizontal/vertical stress ratio	2	1.3	0.9
initial Reservoir pressure (kPa)	650	2300	5500
injection pressures (kPa)	1000 2000 3000	4000 5000 6000	7000 8000 9000

The width of the model is chosen somehow to minimize the flow boundary effects. It means that as soon as flow streams are getting closer to the boundary, the results are not trustable and includes error. This is a tradeoff between choosing a wide model to decrease the computational error and choosing a narrow model to decrease the computational effort. In-situ stress arrangement is another parameter that is targeted in this study to be investigated. Two different stress arrangements can be applied to the reservoir. (a) if the maximum horizontal stress ( $\sigma_H$ ) is perpendicular to the face of the reservoir (normal to page), and (b) if the minimum horizontal stress ( $\sigma_h$ ) is perpendicular to the face of the reservoir. Both cases are shown in Fig. 5. Considering these two stress arrangements, 18 models will be analyzed.

## MATERIAL AND FLUID PROPERTIES

Athabasca oil sand reservoir has been extensively studied and the material properties are generally known. However, a large portion of field data is still confidential and is not allowed to be published. The material and fluid properties for this paper have been selected from limited published papers in the literature among which, the study by Chalaturnyk (1996) is the major reference. The framework of the study by Li and Chalaturnyk (2009) on history matching of the UTF pilot test / phase A is the other reference for iterative geomechanical coupling. They have adjusted both

geomechanical and fluid properties based previous experimental and numerical works.

**Table 2: Two cases for horizontal stress arrangement.**

Zone	Parameter	Value	Ref.
Overburden	constitutive model	linear elastic	Chalaturnyk, 1996
	bulk density (kg/m <sup>3</sup> )	2200	
	module of elasticity, E (MPa)	800	
	Poisson's ratio, $\nu$	0.3	
	coefficient of linear thermal expansion (°K <sup>-1</sup> )	$2 \times 10^{-5}$	
Reservoir	constitutive model	elastic perfectly plastic	Li and Chalaturnyk, 2009
	bulk density (kg/m <sup>3</sup> )	2200	
	module of elasticity, E	$950P_a \left( \frac{\sigma'_3}{P_a} \right)^{0.5}$	
	Poisson's ratio, $\nu$	0.3	
	cohesion (MPa)	0	
	friction angle (°)	60	
	dilation angle (°)	15	
coefficient of linear thermal expansion (°K <sup>-1</sup> )	$2 \times 10^{-5}$		
Underburden	constitutive model	linear elastic	Chalaturnyk, 1996
	bulk density (kg/m <sup>3</sup> )	2200	
	module of elasticity, E (MPa)	5000	
	Poisson's ratio, $\nu$	0.3	
	coefficient of linear thermal expansion (°K <sup>-1</sup> )	$2 \times 10^{-5}$	

**Table 3: Hydraulic properties of the reservoir**

Parameter	Unit	Reservoir	Ref.
Porosity	%	32	Chalaturnyk, 1996
Horizontal Permeability	mD	5000	-
Vertical Permeability	mD	2500	-
Initial Oil Saturation	%	85	-
Initial Water Saturation	%	15	-
Initial Gas Saturation	%	0	-
Initial Temperature	°C	10	-
Rock Compressibility	1/kPa	$5 \times 10^{-6}$	Chalaturnyk, 1996
Rock Expansion Coefficient	°C <sup>-1</sup>	$3.84 \times 10^{-5}$	Chalaturnyk, 1996
Rock Heat Capacity	kJ/kg°K	1865	Li, 2006
Rock Thermal Conductivity	W/m°K	1.736	Chalaturnyk, 1996
Well radius	m	0.1	-
Preheating Period	Days	90	-
Steam Quality	%	95	-
Steam Trap difference	°C	10	-

As argued earlier, the selection of injection pressure is such that it prevents the caprock (a thin layer of impermeable rock on top of the reservoir) from any failure and large deformation. Hence, all the geological rock layers over the reservoir are

assumed to behave elastic in a unit layer called overburden. At the bottom, the material is very stiff and small deformation is expected to occur at the pressure level that is applied to the model. Underburden is also kept elastic to prevent complexity in modeling.

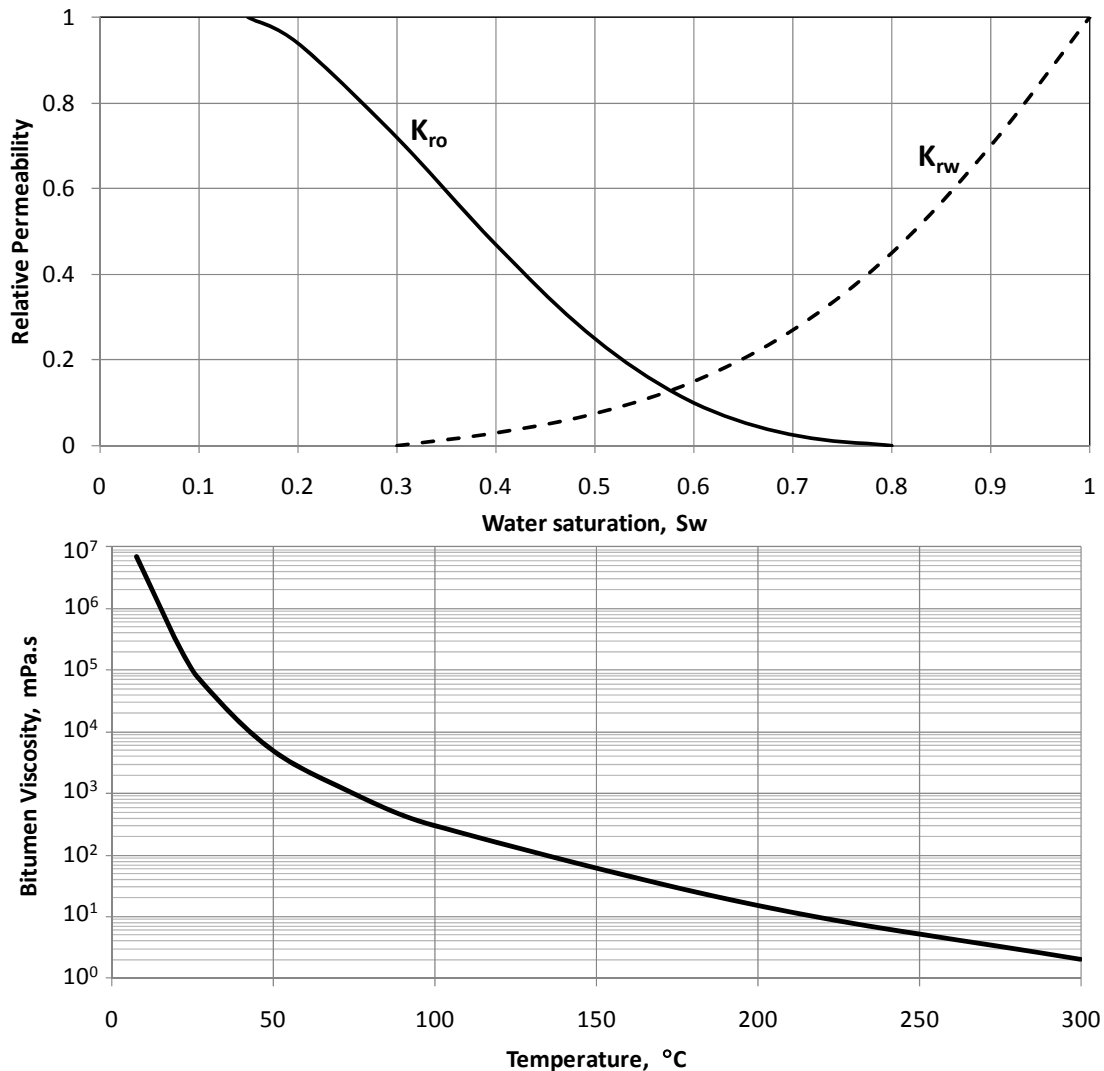


**Figure 6: Relative permeability (top) and variation of viscosity by temperature (bottom), after Chalaturnyk (1996).**

The oil sand behaves as a strain softening material in post plastic region. However, for this study an elastic perfectly plastic behavior was selected for the reservoir layer with dilation. The modulus of elasticity is varying with the changes in confining stress suggested by Chalaturnyk (2006). Table 2 has listed all the geomechanical properties of the three layers. For flow simulation two sorts of input data are

essential; (a) rock properties, and (b) fluid properties. Table 3 shows hydraulic and thermal properties of the oil sand reservoir. The table also includes some operational information for preheating and steam trap production control.

Another major rock property is relative permeability when more than one phase contributes to the flow. Relative permeability defines the portion of permeability allocated to each fluid. Relative permeability is plotted in Fig. 6. The plot has also shows the variation of heavy oil viscosity by temperature changes. It is very clear from the chart that the viscosity will decrease 5 to 6 orders of magnitude when the temperature changes from the reservoir to the steam temperature.

## **RESULTS – OIL PRODUCTION AND STEAM/OIL RATIO**

The first set of results that are presented is the oil production. Fig. 7 to 9 show cumulative oil production for the three models. For each model, three curves are plotted for each injection pressure level: (a) coupled simulation for the 1st stress arrangement, (b) coupled simulation for the 2nd stress arrangement, and (c) uncoupled simulation.

All the curves are continuously growing. To avoid boundary effects on the results only 700 days of each run is chosen for analyzing in this section. In model 2 and 3 after this period of time, the steam chamber touches the boundary and the analysis might not be acceptable. The plateau at the end of each curve in Fig. 8 and 9 might have different curvature if the model is wider. In 100 days at the beginning of the process, oil is not produced because of the preheating period that is reflected in each graph.

Pressure levels selected for each model are appeared to apply the least variation in oil production in deep reservoirs while it has produced up to two times oil in model 1 when pressure changes from 1000 kPa to 3000 kPa in the same production duration.

Comparing oil production in the three models confirms that significant difference between oil production using coupled and uncoupled simulations is predicted in the shallow reservoirs, i.e., model 1 in Fig. 7. Although there is no remarkable

improvement when the injection pressure is as low as 1000 kPa, for the other two pressure levels coupled modeling has improved the oil production.

In general, it can be concluded that geomechanical mechanisms in SAGD that cause improvements in permeability and porosity has more effect on the oil production when the reservoirs are shallow rather than deep. Unlike the effects of geomechanics on production, simulation results show that horizontal stress arrangements do not change oil production on any of shallow to deep models in Athabasca oil sand reservoir.

The same charts as plotted for oil production are reproduced for cumulative Steam/Oil Ratio (SOR). SOR shows the rate of steam consumption in a SAGD process compared to oil production rate. High values for SOR explains that the process needs more steam than a process with low SOR. Therefore, SOR can be translated to reveal the efficiency of the process.

Figures 10 to 12 show cumulative SOR for all 18 model runs. Generally speaking, coupled models have lower SOR than the models with no geomechanics in simulation.

In models 2 and 3 almost no difference is observed between the coupled and uncoupled results. In addition, SORs coincide for the same models with different stress arrangements.

Considerable difference in SOR is distinguished in model 1 (shallow reservoir). In this model, the difference between coupled and uncoupled results get larger when higher injection pressure is applied. For the model with 3000 kPa pressure, coupled simulation shows approximately 5% lower SOR than uncoupled simulation.

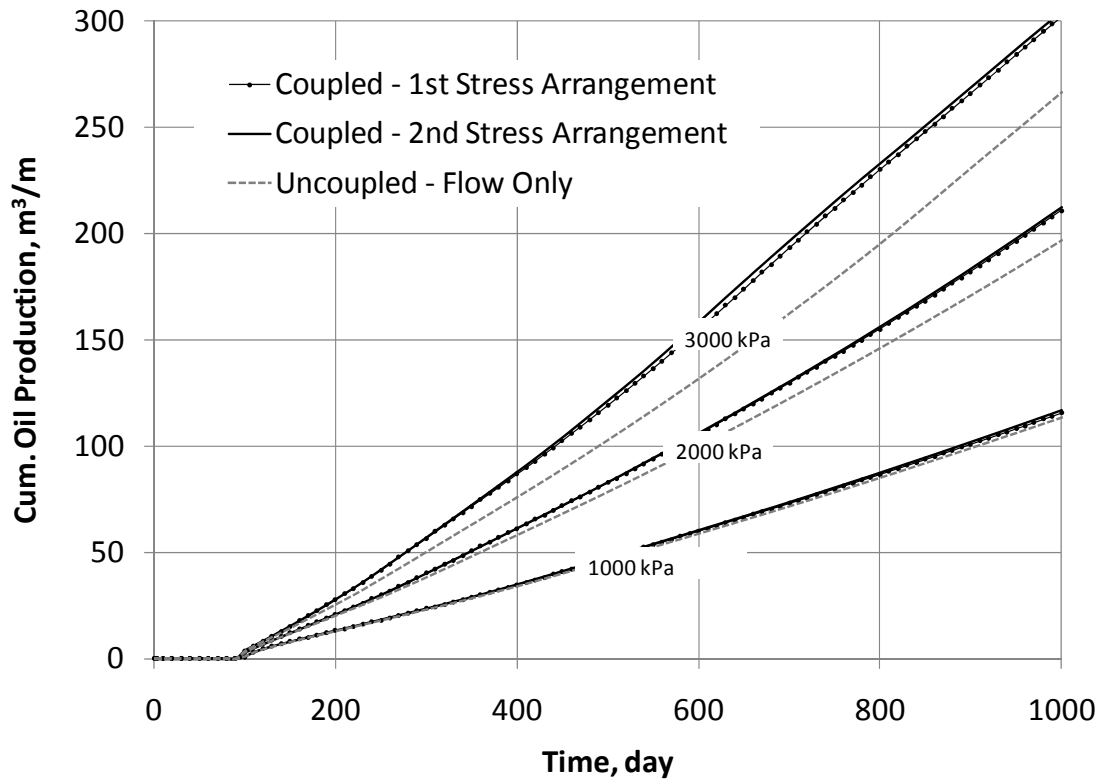


Figure 7: Cumulative oil production for model 1.

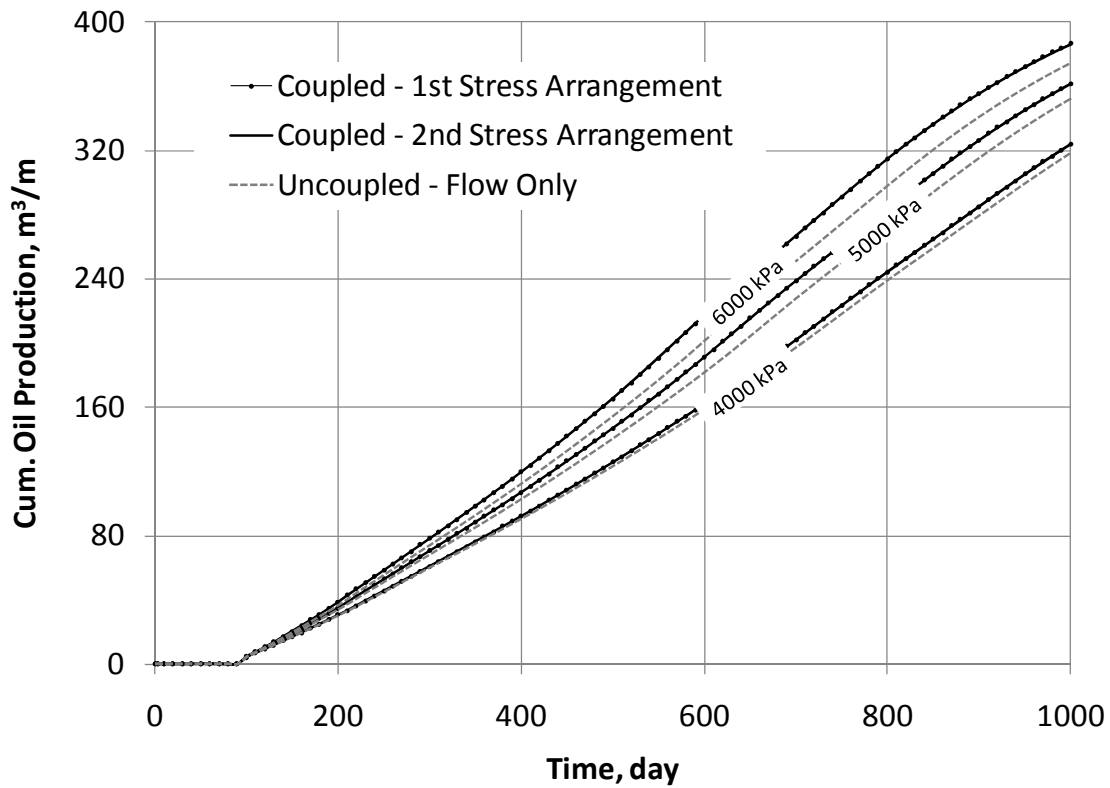


Figure 8: Cumulative oil production for model 2.

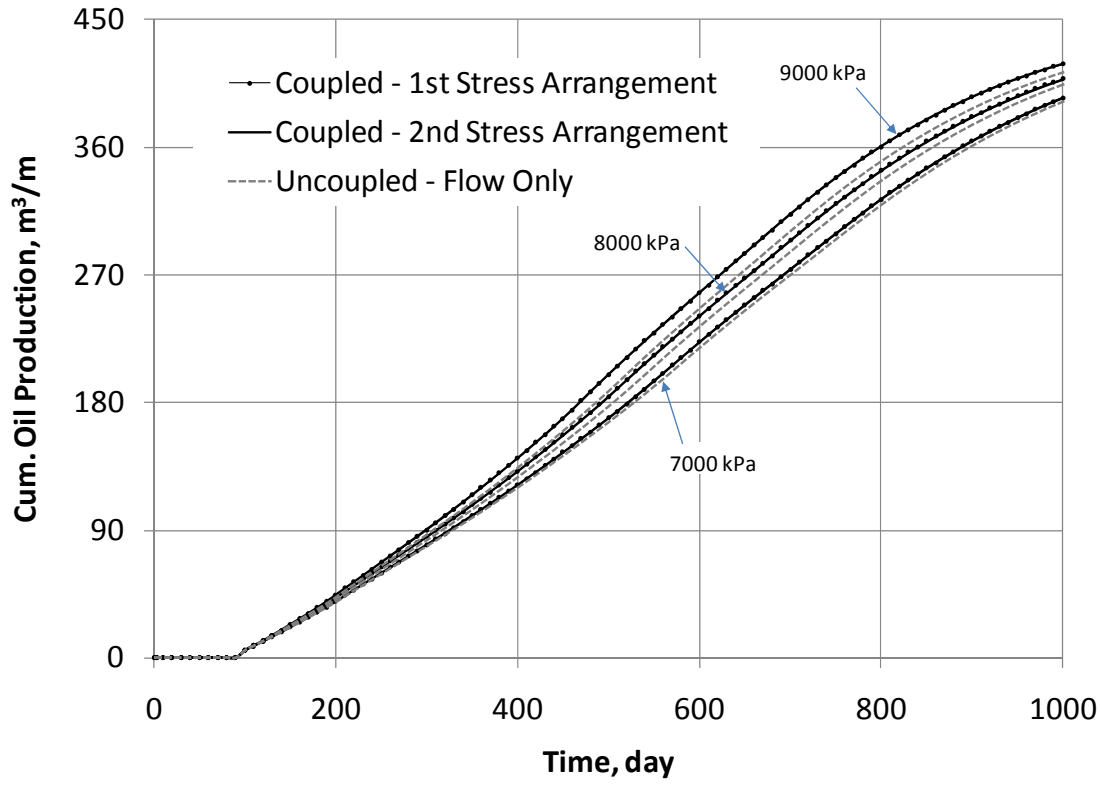


Figure 9: Cumulative oil production for model 3.

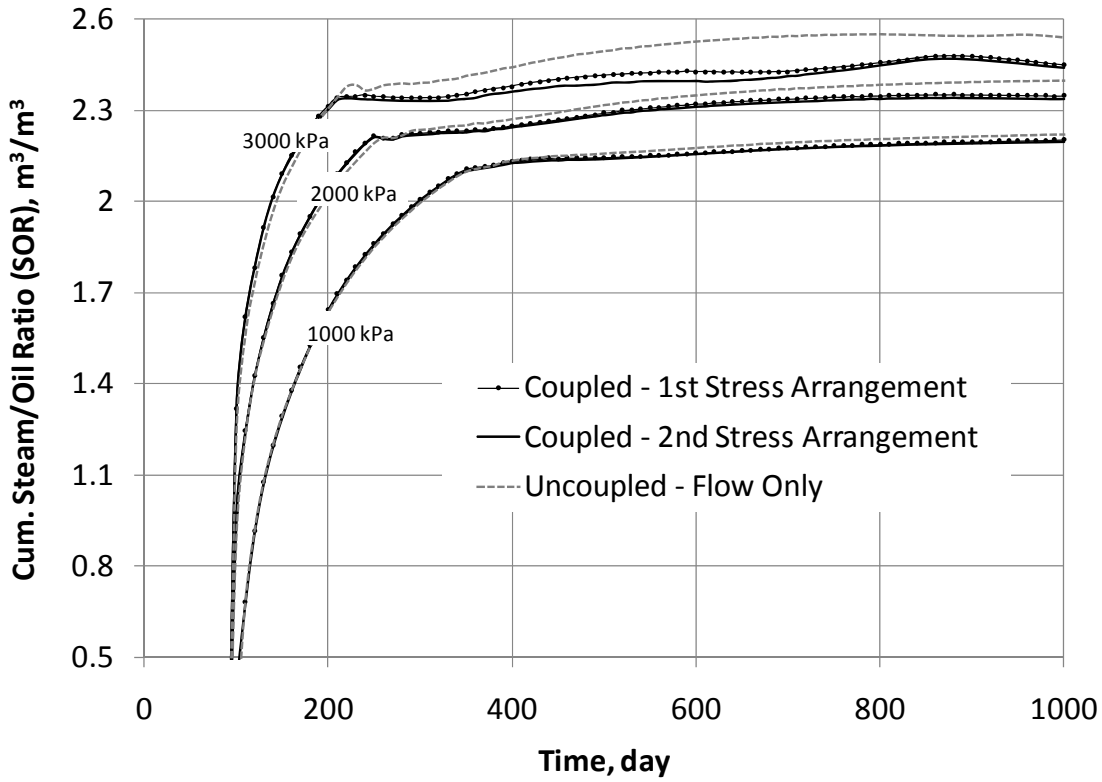


Figure 10: Cumulative Steam/Oil Ratio (SOR) for model 1.

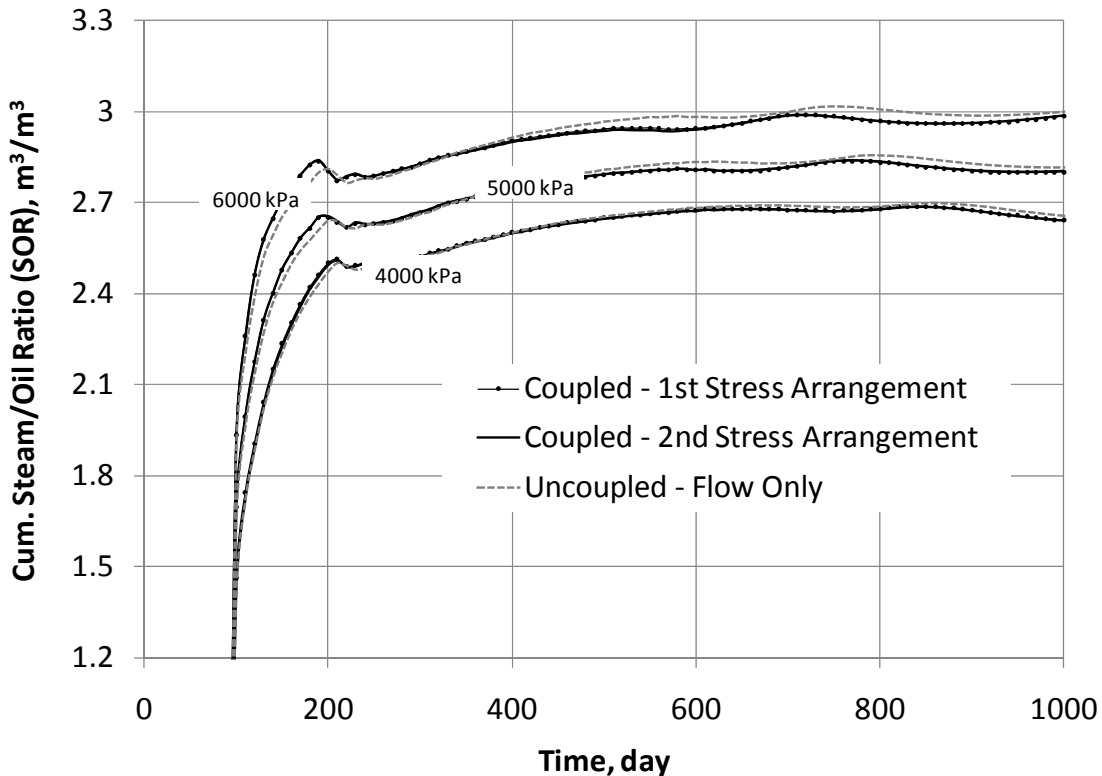


Figure 11: Cumulative Steam/Oil Ratio (SOR) for model 2.

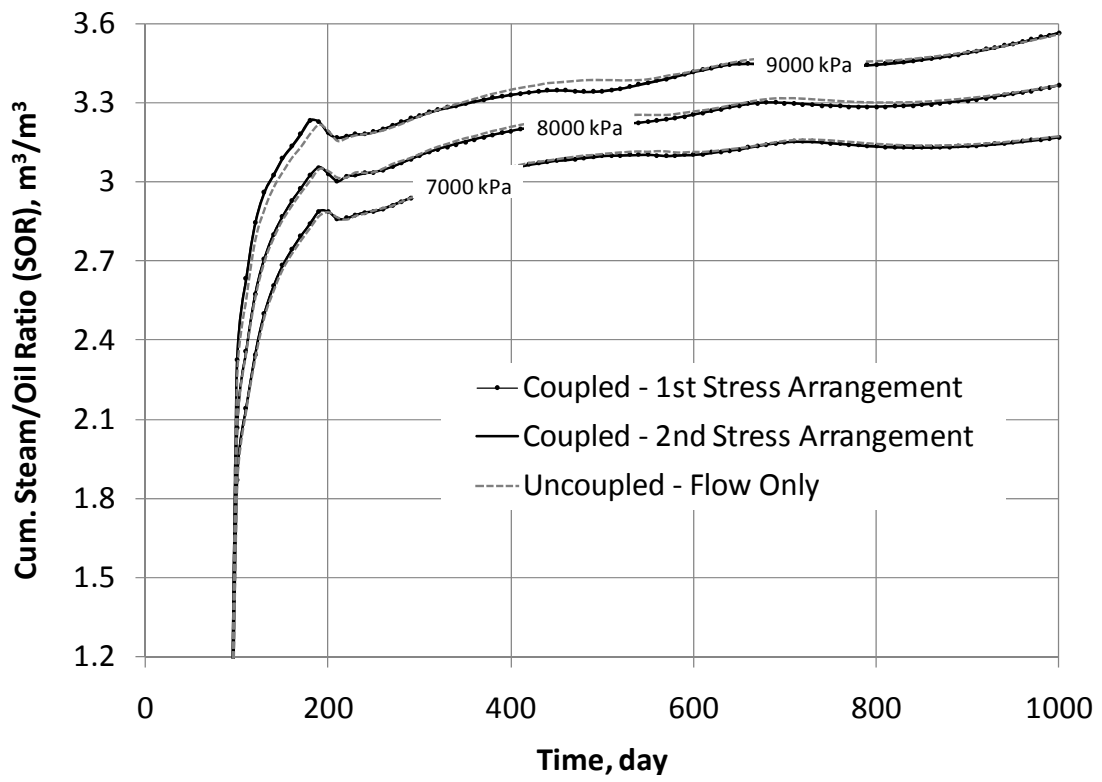


Figure 12: Cumulative Steam/Oil Ratio (SOR) for model 3.

## RESULTS – DISPLACEMENT WITHIN THE RESERVOIR

Fig. 13 illustrates the position of the reservoir simulator grid boundary inside the geomechanical grid boundary. This is a schematic graph for one of the models to show the displacement regime inside the reservoir. Displacement vectors are plotted in green. The vectors show a bell shape curve of heave on top of the reservoir for one pair of injector/producer.

The figure also includes the position of the steam chamber. The white arrows over the steam chamber have been added to show the general trend of displacement in the steam chamber area.

All around the steam chamber, displacement vectors are towards sides of the model and as it gets closer to the surface the tendency would be more upward. For the zone closer to the bottom of the reservoir, however, displacement has a different direction compared to the general trend in the model.

To better analyze the case, decompose displacement vectors into horizontal and vertical vectors. The vertical displacement starts from zero at the bottom of the reservoir to the largest value on the surface. The maximum vertical displacement occurs on the surface at the centerline. For the horizontal displacement a similar situation will happen except for the steam chamber area. Although displacement on top and inside the steam chamber is directed outwards to the sides, it has opposite direction in the middle and bottom of the reservoir.

If we want to compare displacement field with lateral pressure in retaining walls, we might say that the material on top of the reservoir is under higher stress that is similar to passive pressure. But the zone at lower levels (especially middle of the reservoir) is under lower stress that might be translated to active lateral pressure. This comparison tells us that plastic zones or critical situations in terms of failure would probably occur close to caprock or at the bottom of the reservoir. This process will be discussed more in the next sections by evaluation plastic points and volumetric strain plots within the reservoir.

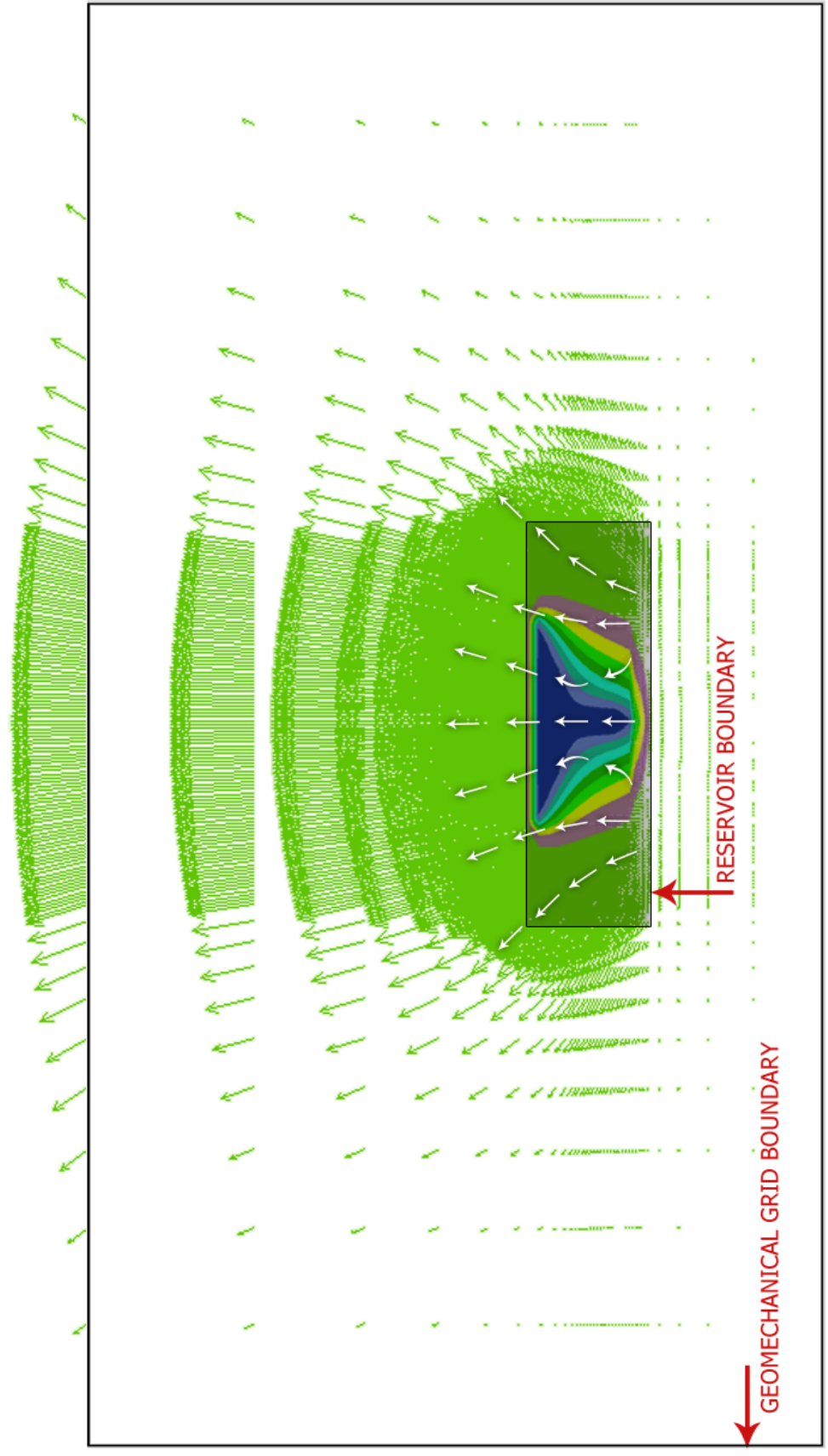
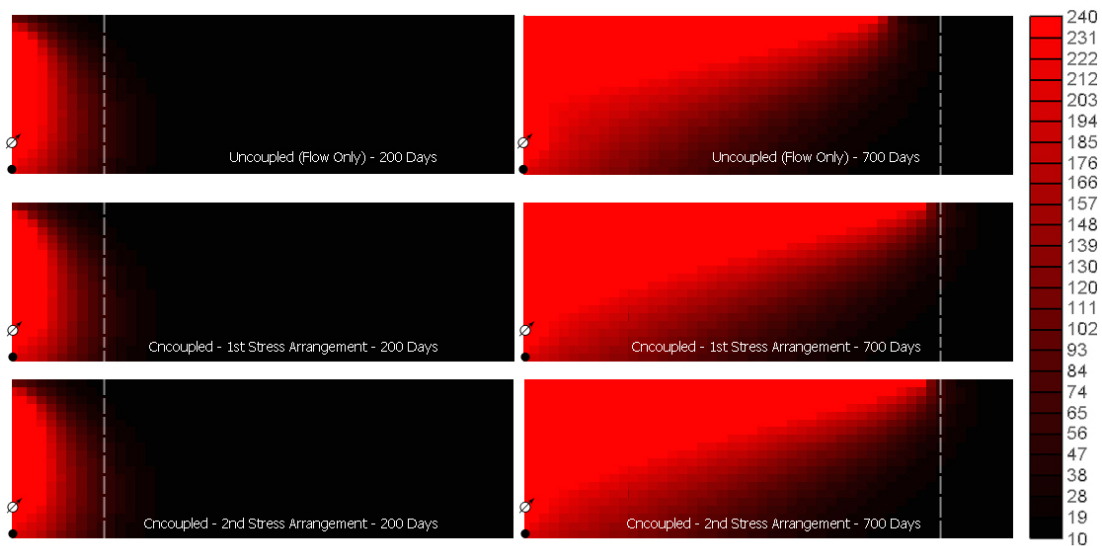


Figure 13: Typical reservoir deformation during a SAGD process.

## RESULTS – STEAM CHAMBER GROWTH

‘Steam chamber’ is a general definition for the heated zone around the injector which should be at the steam temperature. Based on this definition, a sharp edge would separate the steam chamber from the reservoir.

In the analytical theory developed by Butler et al. (1997), oil is fully recovered inside the steam chamber and for this reason oil saturation is at residual value. In contrast, all other parts of the reservoir are at initial (or reservoir) oil saturation and temperature. Unlike Butler theory, Li (2006) argued that the steam chamber could not be limited to this definition. He proposed drained, partially drained and undrained zones by defining ranges for oil viscosity. A transition zone has been also reported by Sharma and Gates (2010).



**Figure 14: Temperature distribution within half of the reservoir after 200 days (left) and 700 days (right). From top to bottom: uncoupled, coupled with the first stress arrangement, coupled with the second stress arrangement. (3000 kPa injection pressure)**

Regardless of how the edges of steam chambers are defined, temperature is the major parameter to change viscosity, stress, and energy balance in the reservoir. It is also more convenient in the field to monitor temperature than other parameters that are directly or indirectly related to temperature.

Temperature profile has been selected in this paper to monitor the steam chamber growth within geomechanical coupled and uncoupled models. Fig. 14 shows the

temperature distribution of one of the models. Results of other models also follow the same style. Left sub-plots in Fig. 14 are the progress of the steam chamber before touching the caprock. It seems that they are all the same at the beginning of the process. Sub-plots on the right side are the steam chamber after 700 days. These sub-plots confirm that the steam chamber is predicted to grow more when geomechanics is considered in modeling. However, initial horizontal stress magnitude and orientation has almost no effect on the steam chamber growth.

## RESULTS – SURFACE HEAVE HISTORY

Maximum surface heave occurs at the centre of the model. Monitoring the variation of vertical displacement at this location could be useful to find a link between the changes in the reservoir and the changes at the surface.

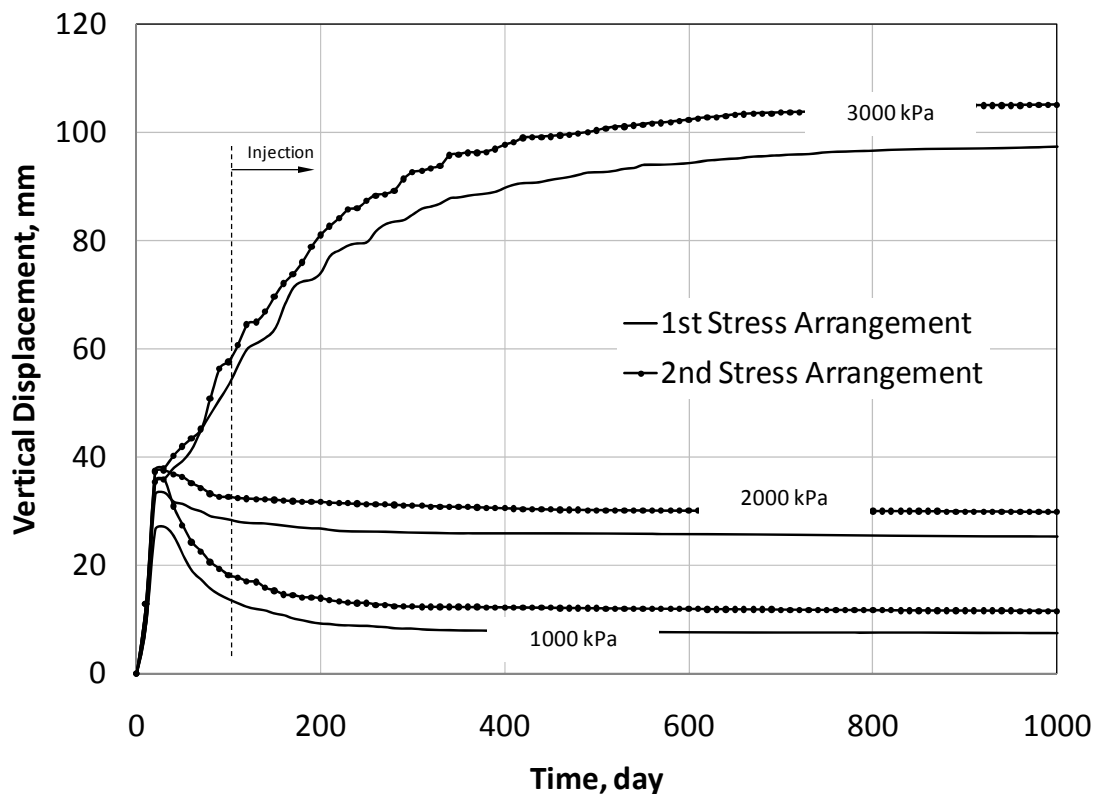


Figure 15: Maximum heave history for model 1.

Fig. 15 to 17 show the displacement history of the maximum vertical displacement for each geomechanical coupled model in 1000 days. Unlike other results, horizontal stress arrangements have come to different results. The general rule anticipated is that

the models under the 2<sup>nd</sup> stress arrangement have experienced larger heave than the models under the first stress arrangement.

The dashed line in each of the figures is located at 100 days showing the time at which steam begins to get injected. A trend that is repeated for all the models is that a large displacement is recorded at the first 50 days of preheating period. This phase gradually continues after the steam is injected into the reservoir and finally gets a constant value (plateau) up to the end of the process. This trend is not true for low injection pressures in model 1 because displacement drops after injection. It is believed that low pressures in this model mobilized less pressure/stress than preheating period in the reservoir.

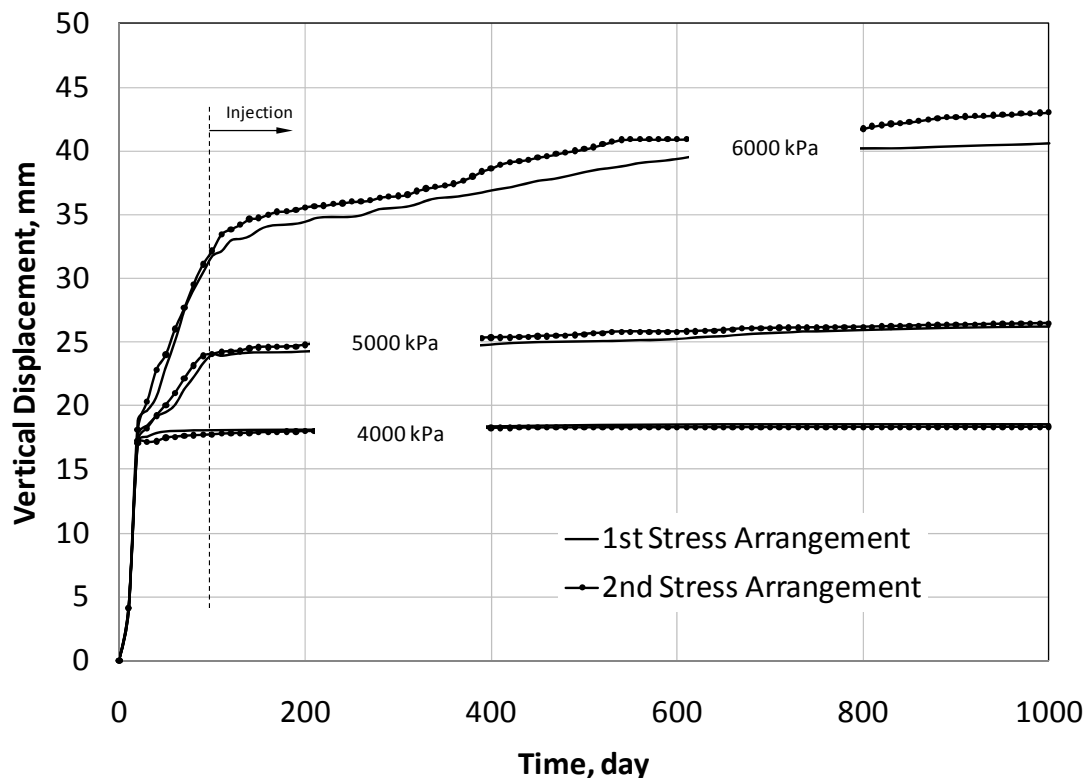


Figure 16: Maximum heave history for model 2.

According to the results, maximum surface heave occurs in shallow reservoirs and the minimum value is in the deep reservoirs. This might alert that more attention should be taken into account when high pressures are injected into shallow reservoirs. Comparing Fig. 15 with Fig. 17 shows that while the maximum injection pressure in

the shallow model is one third of the maximum pressure in the deep reservoir, vertical displacement in the shallow reservoir is 3 to 4 times more than the deep reservoir.

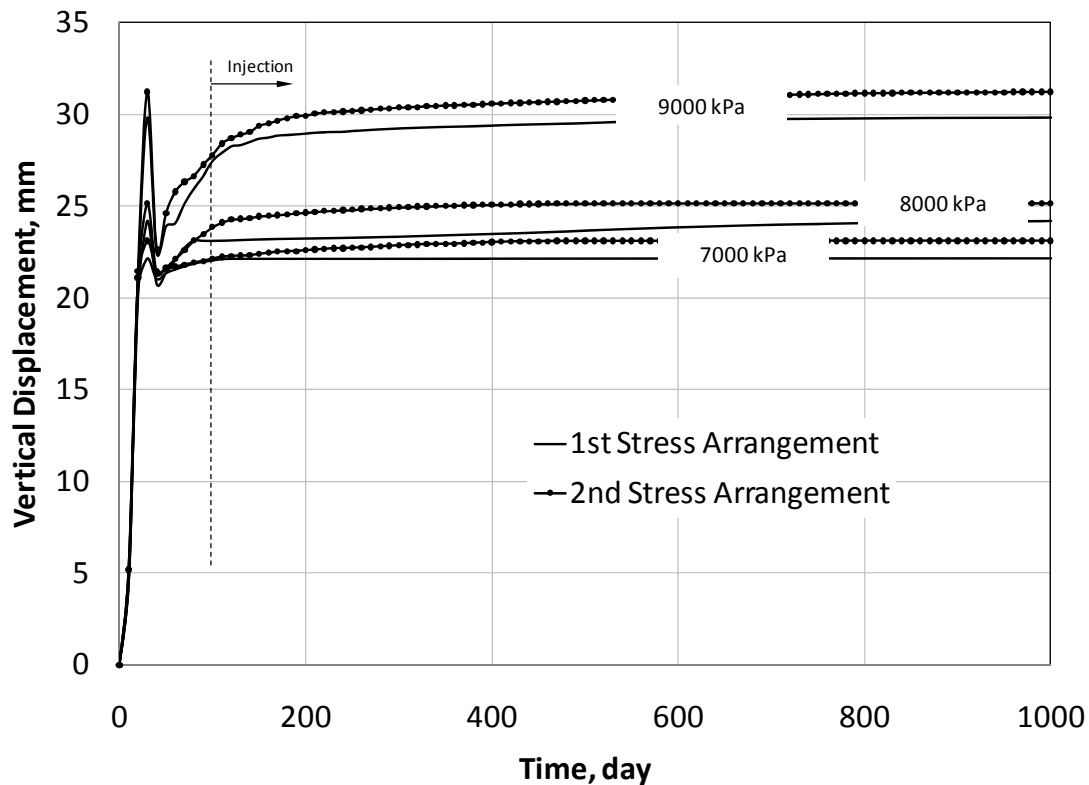


Figure 17: Maximum heave history for model 3.

The only relation that could be taken from comparing the maximum heave history is that pressure and reservoir depth are not the only parameters affecting surface displacement. In-situ stress arrangement and geomechanical properties of the reservoir are also affecting the process to generate higher or lower surface heave. Only geomechanical-coupled simulation could predict the process to establish displacement and deformation in SAGD process.

## RESULTS – GEOMECHANICAL EFFECTS WITHIN THE RESERVOIR

To further illustrate geomechanical effects, four major parameters are chosen for presentation and discussion in this section as follows:

- Temperature will show the position of the steam chamber and the progress of SAGD process. Temperature profiles could be used as a reference for analyzing other variables.

- Vertical displacement could represent the deformation inside the reservoir. If it is compared to the temperature profile, the progress of deformation in the reservoir could be investigated.
- Volumetric strain is an important variable for updating permeability and porosity. Hence, plotting this variable could highlight the areas in which permeability and porosity are improved.
- Plastic or yield locations would show the places where large deformation and property changes occur.

Due to the huge amount of data, only a part of it will be presented for two specific times: 200 days (that is 100 days after injection) and 700 days. Also, the models with maximum injection pressure are chosen to represent each model.

The four parameters are plotted in Fig. 18 to 23. Figures are made up of 6 sub-plots each for half of the reservoir. The sub-plots on the left show the reservoir at 200 days and the sub-plots on the right is the reservoir at 700 days. Comparing left side and right side subplots would show the history of changes for the same property. From top to bottom, three sub-plots are inserted in each figure. The first one is the temperature profile, the second one is the vertical displacement, and the last one illustrates the volumetric strain. Plastic points are also included in the last subplot. A positive sign ('+') would indicate these points.

Comparing all the 6 figures (Fig. 18 to 23) show that main geomechanical effects including large vertical deformation, reaching plastic limit, and large amount of changes in permeability and porosity are occurred in the shallow reservoir (model 1). These effects in the medium depth reservoir are meaningfully lower than the shallow reservoir. In the deep model, almost no major geomechanical changes are observed other than the small vertical displacement.

Similar to the discussion on the heave history, the models under the 2nd horizontal stress arrangement are more geomechanically influenced by the SAGD process. In addition, as predicted from the displacement plot in Fig. 13, volume changes are located more at the top and bottom where the plastic or yield limit is exceeded.

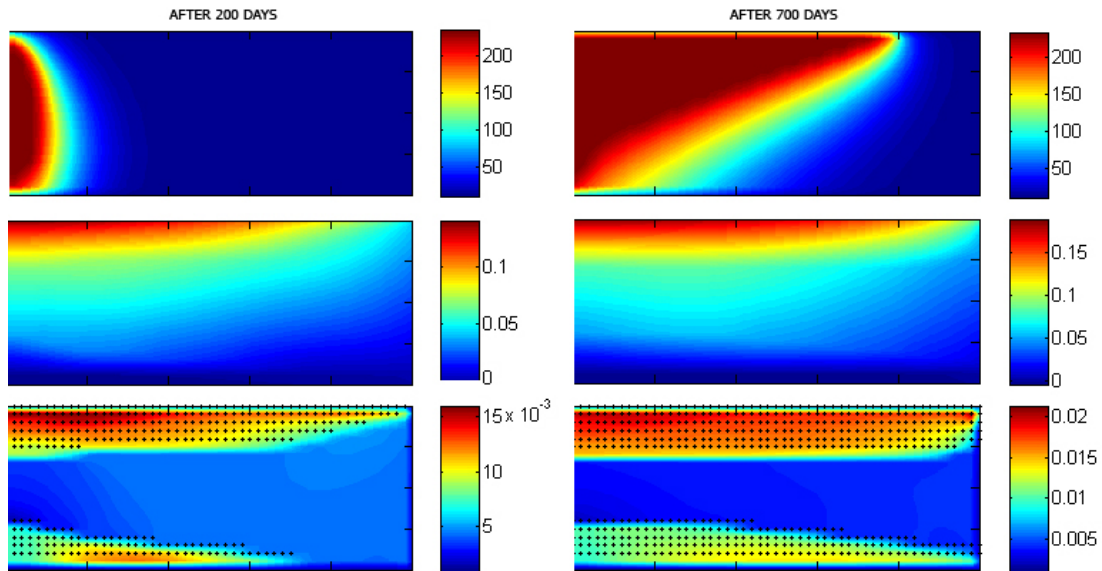


Figure 18: Geomechanical changes in model 1 and the 1<sup>st</sup> stress arrangement at 3000 kPa injection pressure.

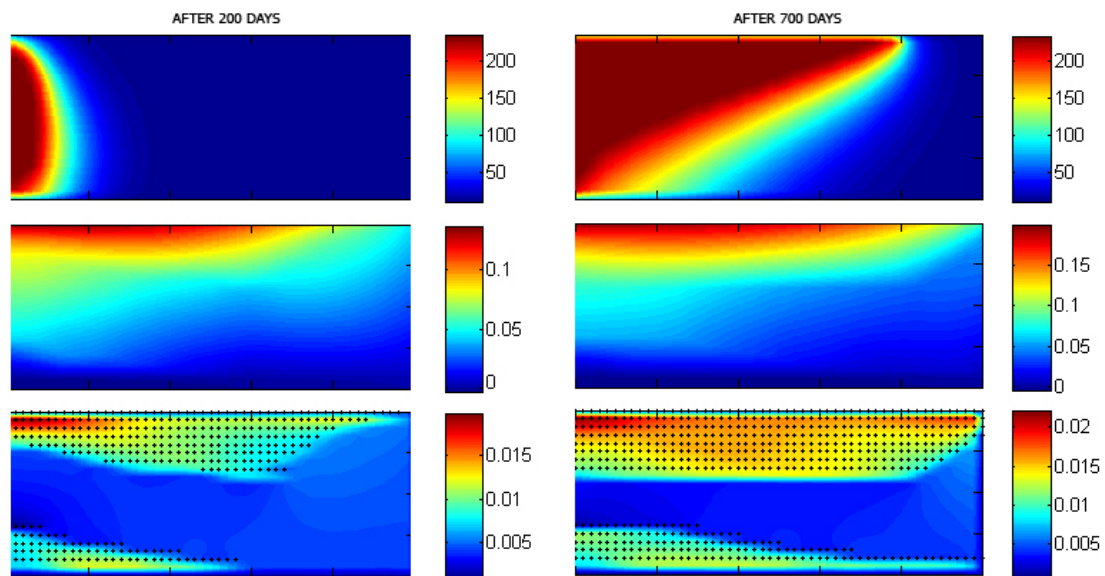
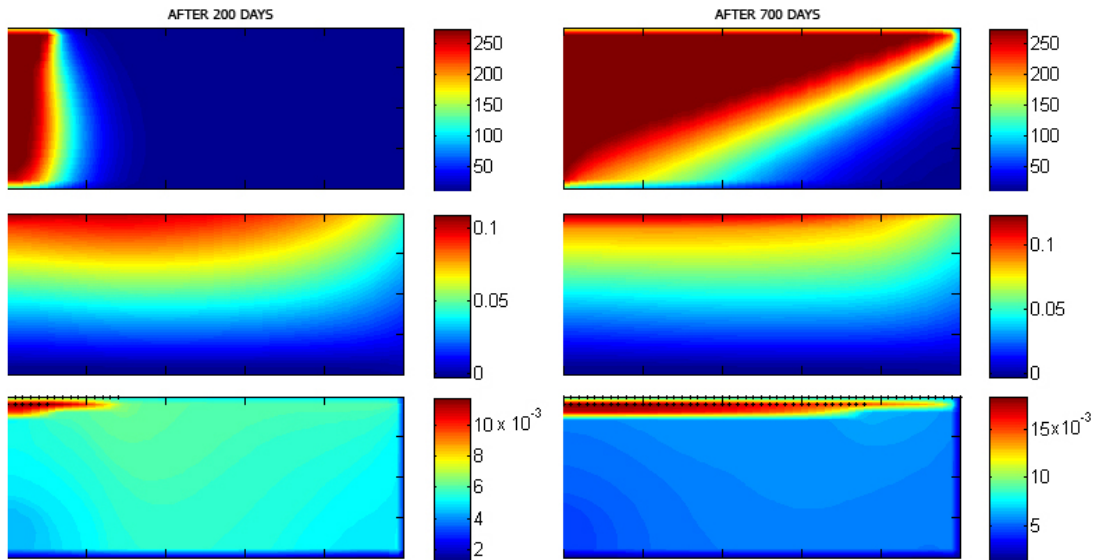
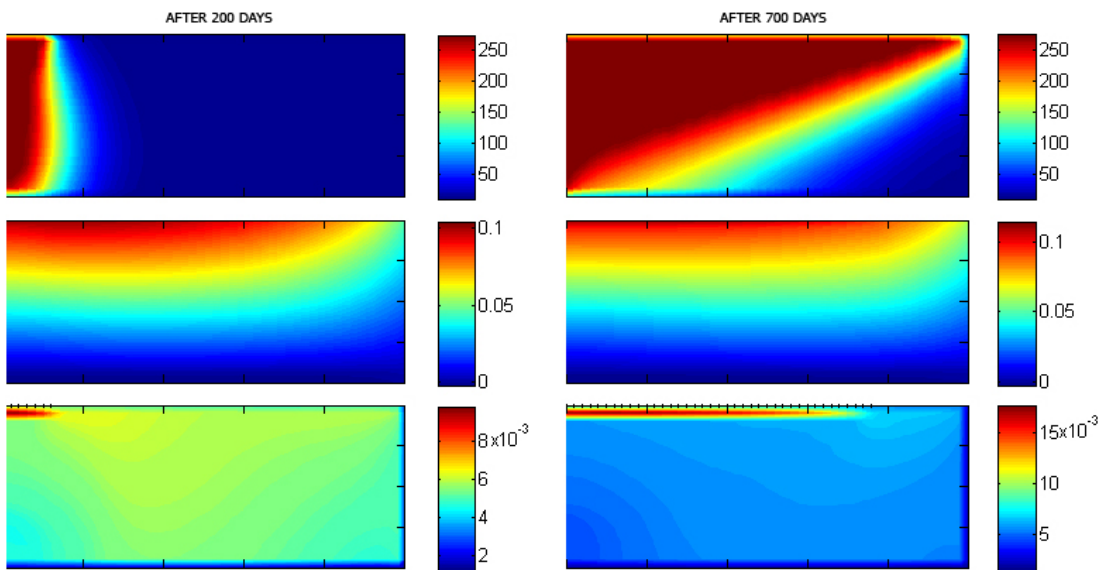


Figure 19: Geomechanical changes in model 1 and the 2<sup>nd</sup> stress arrangement at 3000 kPa injection pressure.



**Figure 20: Geomechanical changes in model 2 and the 1<sup>st</sup> stress arrangement at 6000 kPa injection pressure.**



**Figure 21: Geomechanical changes in model 2 and the 2<sup>nd</sup> stress arrangement at 6000 kPa injection pressure.**

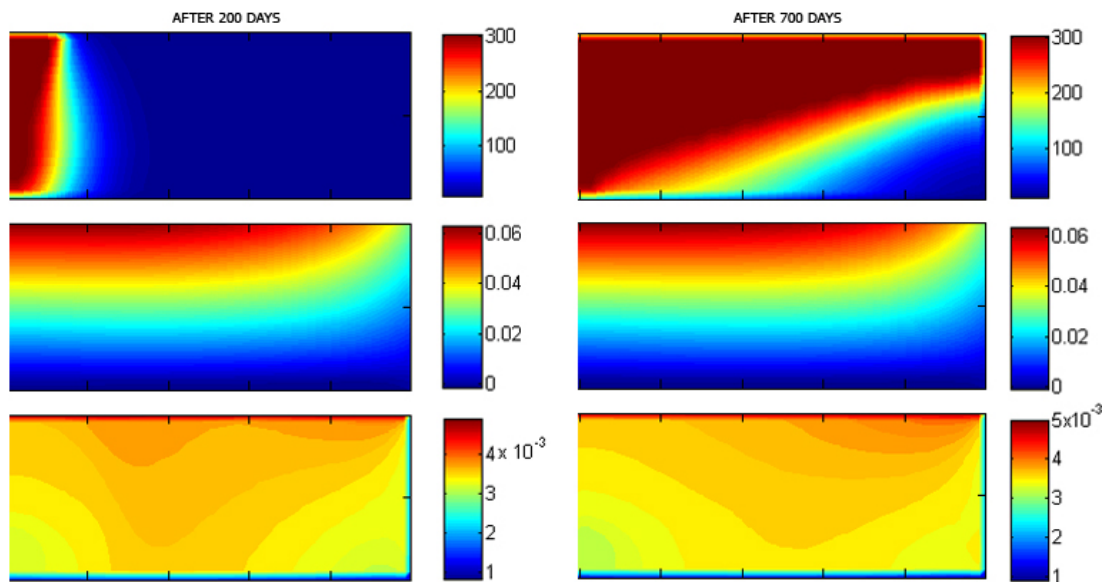


Figure 22: Geomechanical changes in model 3 and the 1<sup>st</sup> stress arrangement at 9000 kPa injection pressure.

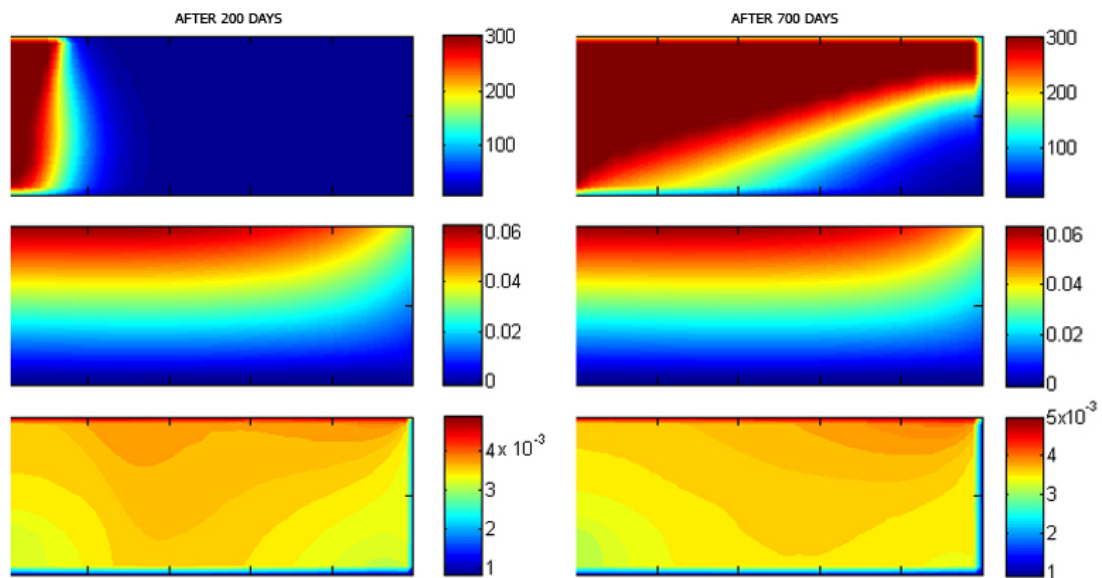
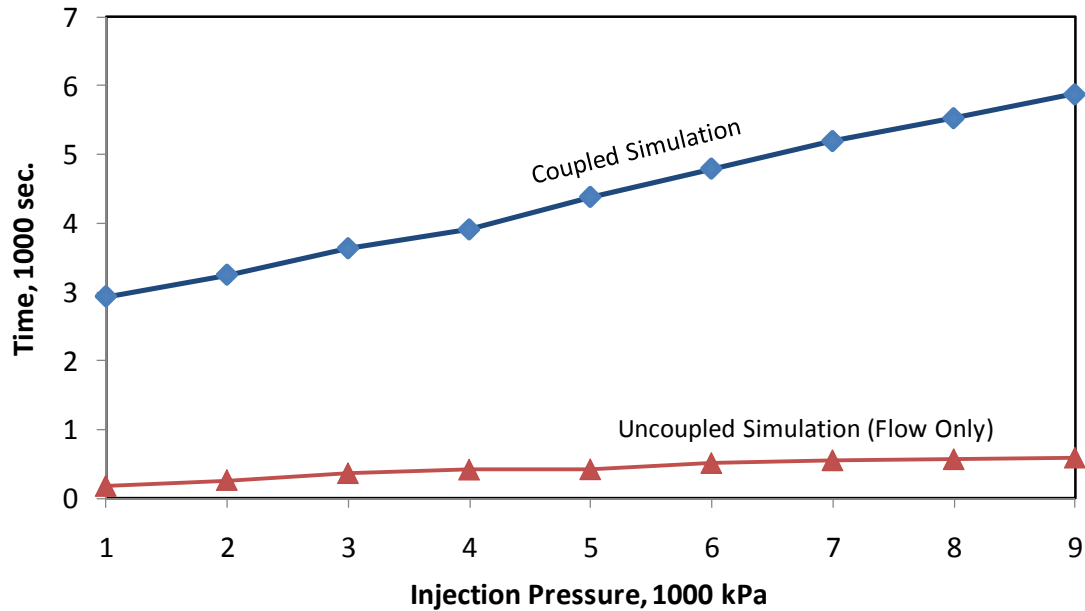


Figure 23: Geomechanical changes in model 3 and the 2<sup>nd</sup> stress arrangement at 9000 kPa injection pressure.

## RESULTS – COMPUTATIONAL EFFORT

Computational effort is an important factor that prevents an engineering team from making complex and time consuming simulations. The comparison of the time required for running each model of this study shows that the adopted coupling solution takes approximately 3 to 5 times more computational effort than conventional reservoir simulation.



**Figure 24: Comparison of computational effort between coupled and uncoupled models.**

Fig. 24 illustrated the variation of the required run time for each model while the injection pressure is changing. Higher pressure overloads the solution with higher changes in the system and takes more computational time to adjust the solution. Higher injection pressure also indirectly shows the depth of the reservoir and the need for a larger geomechanical grid that means larger matrices and more numerical computation.

## GEOMECHANICAL IMPACT FACTOR (GIF)

Geomechanical coupled simulations and their results in the previous sections confirm the geomechanical effects on the reservoir and production during SAGD process. This effect is different from model to model according to the level of injection pressure and other geomechanical parameters. On the other side, it was shown that

geomechanical coupling is expensive and needs more rock properties that are not always available. Therefore, geomechanical simulations are warranted if one can a priori know when geomechanics is an issue. Any improvement in the process by applying optimized geomechanical pressure level or any concern about the geomechanical failure in caprock could be an issue in SAGD.

Chalaturnyk and Li (2004) performed decoupled (separate flow and geomechanical analysis with no interaction) simulations on three models from shallow to deep to show the importance of geomechanics in SAGD. However, they “recommended that more realistically coupled reservoir geomechanical simulations be applied in the SAGD process, such as the sequentially coupled or fully coupled simulations.”

Drawing a line of importance for geomechanical impact, even with the results from a coupled simulation is not simple. In SAGD process many effective parameters are involved and each has its own importance. However, general understanding from geomechanical process could be reachable through defining a geomechanical ratio for SAGD.

Unlike what it is believed in petroleum engineering that the flow pressure establishes all the geomechanical impacts, the results of this study are used to suggest an alternative approach. A sensitivity analysis among some recommended factors in the literature or observed through this study show that the stress ratio  $q'/p'$  can be adopted for SAGD to show the geomechanical level of importance. Eq. (3) to (8) derive some equations that are selected to be used for SAGD.

$$q' = \frac{\sigma'_1 - \sigma'_3}{2} \dots\dots\dots(3)$$

$$p' = \frac{\sigma'_1 + \sigma'_3}{2} \dots\dots\dots(4)$$

$$\sigma'_H = \sigma_H - p_{inj} - \sigma_T \dots\dots\dots(5)$$

$$\sigma'_H = \sigma_H - p_{inj} - \sigma_T \dots\dots\dots(6)$$

$$\sigma'_V = \sigma_V - p_{inj} \dots\dots\dots(7)$$

$$\sigma_T = (1 + \nu)\alpha E \Delta T \dots\dots\dots(8)$$

In these equations:  $\sigma'_1$  and  $\sigma'_3$  are the minimum and maximum effective stresses that are selected among the maximum horizontal effective stress,  $\sigma'_H$ , minimum horizontal effective stress,  $\sigma'_h$ , the vertical effective stress,  $\sigma'_V$ . Vertical stress is defined as the total surcharge at the centre of the reservoir and horizontal stresses are calculated using the in-situ stress ratios. Other stress items that have been added to this ratio are the pore pressure,  $p_{inj}$ , and the effect of thermal stress,  $\sigma_T$  that can be calculated using Eq. (8). In Eq. (8)  $\alpha$  is the linear coefficient of thermal expansion,  $E$  is the modulus of elasticity for the reservoir, and  $\Delta T$  is the temperature difference between reservoir and the injected steam.

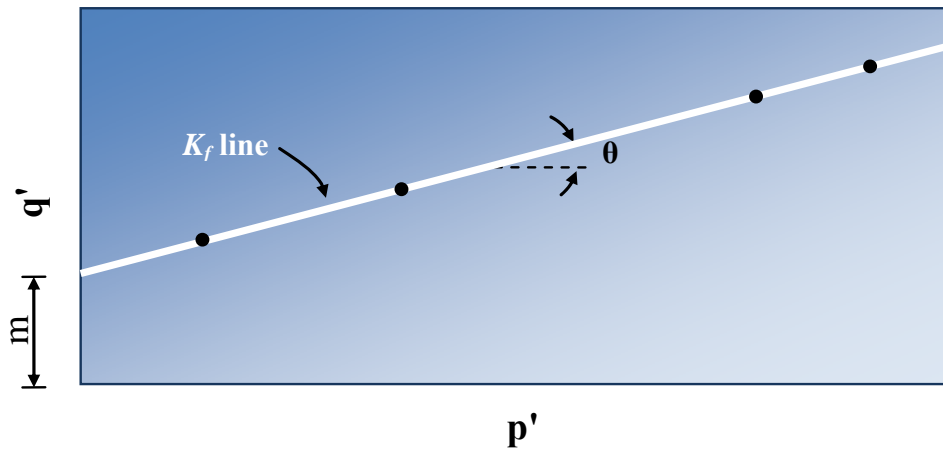


Figure 25:  $K_f$  line in  $p'$ - $q'$  plot.

$p'$ - $q'$  plots are used to illustrate the stress path of an element before it touches the failure line ( $K_f$  line in Fig. 25). If same curve is plotted for many samples of soil/rock,  $K_f$  line is defined and the strength variables ( $c$  and  $\phi$ ) can be calculated. Eq. (9) and Eq. (10) are the relation between the parameters shown in Fig. 25 and plastic variables.

$$\theta = \tan^{-1}(\sin \phi) \dots \dots \dots (9)$$

$$m = c \cos \phi \dots \dots \dots (10)$$

For this study ( $c=0$  and  $\phi=60^\circ$ ), so that at failure  $q'/p'$  ratio is calculated as  $\sqrt{3}/2$ , approximately 0.86. The adopted  $q'/p'$  ratio for SAGD can be used to show the geomechanical impact on production and CSOR. We call it the 'Geomechanical Impact Factor' or simply GIF. If the graphs of oil production and SOR are plotted

against GIF, it is seen that the curvature changes rapidly around 0.85 location on the  $q'/p'$  axis. This phenomenon is illustrated in Fig. 26 and Fig. 27.

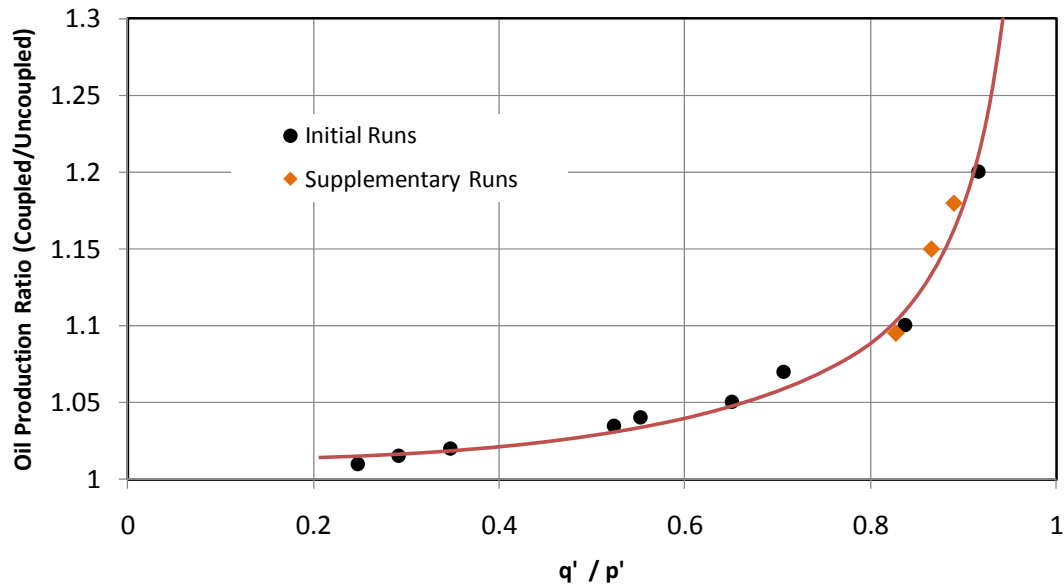


Figure 26: Effects of geomechanical modeling on oil production.

As it was discussed, due to geomechanical behavior permeability and porosity are updated. This means that permeability and porosity might get new values during the process. Using the Butler theory (1997) in Eq. (11), the changes in permeability and porosity can be calculated.

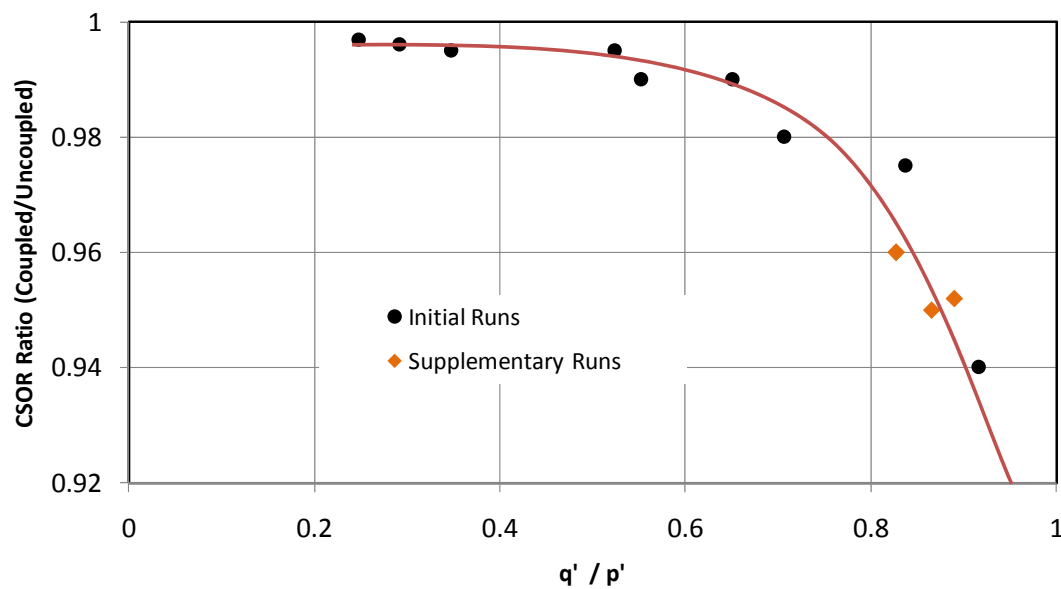


Figure 27: Effects of geomechanical modeling on CSOR.

Fig. 28 describes that the porosity-permeability changes from almost 0% at low values of GIF to 50% when GIF exceeds the failure limit.

$$\frac{q_{o,coupled}}{q_{o,uncoupled}} = \sqrt{\frac{k\phi}{k_0\phi_0}} \dots\dots\dots(11)$$

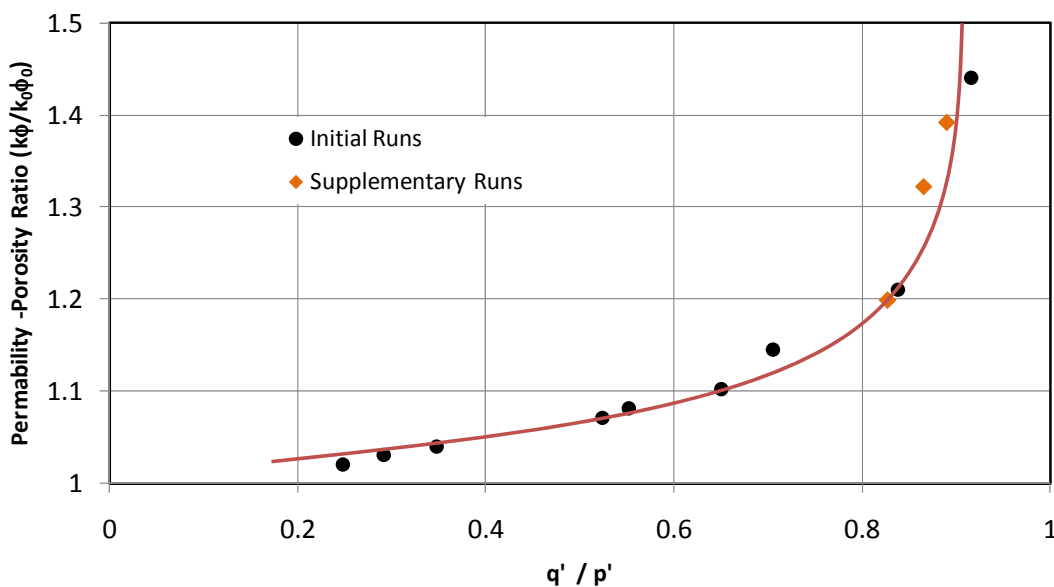


Figure 28: Rock property improvement vs. Geomechanical Impact Factor (GIF).

## CONCLUSION AND DISCUSSION

The results presented above were obtained from reservoir geomechanical coupled analyses on typical oil sand reservoirs. The numerical models were designed in different depths each with the corresponding in-situ stresses. Two different stress arrangements were also considered to evaluate the effect of horizontal stress on SAGD production. Because the study was focused on the effect of geomechanics on SAGD, injection pressures were adjusted to be under hydraulic fracturing stress to avoid any failure in the caprock. General observations and conclusions derived from this study are:

- SAGD process improvement due to geomechanical effects is observed in shallow reservoirs than deeper ones. Major process improvements are higher oil production and lower steam/oil ratio. This means that the steam chamber occupies larger area within the reservoir in shorter time.

- Horizontal stress arrangements showed almost no influence on oil production and steam injection. However, reservoir deformation and surface heave were meaningfully dependent on the orientation of the maximum horizontal stress. When the maximum horizontal stress was normal to the borehole pair, surface heave and the mobilized shear stress (and plastic points) were more than the case in which the maximum stress was parallel to the boreholes.
- Stress analysis and displacement observations within the reservoir confirmed that the zones closer to the bottom and to the ceiling of the reservoir are most likely to reach the plastic or yield limit. These zones are developed by the growth of the steam chamber. This means that for the cases that geomechanics has the most influence (e.g., shallow reservoir with high injection pressure) the operation should be designed and monitored at these critical zones. The zone at the bottom might affect the borehole design and the zone close to the top of the reservoir has to be checked for cap rock integrity.
- Depending on the grid size of the geomechanical model, an iterative geomechanical coupled modeling was proven to take 3 to 5 times more than conventional reservoir simulation.
- Sensitivity analyses showed that the Geomechanical Impact Factor (GIF) could be used to generally evaluate the importance of geomechanical modeling in SAGD. GIF has been adopted from geotechnical engineering to work for a thermal recovery process, SAGD.

Some important issues in SAGD such as cap rock integrity, reservoir steam injectivity at the preheating period, and multi-stage pressure control have been avoided in this study. It is recommended that 3D analyses be done to clearly investigate the effect of these issues and stress orientation on SAGD for shallow reservoirs. Also, more realistic constitutive models could be employed for better understanding the geomechanical behavior of reservoirs under SAGD process.

This paper studied the effects of geomechanical mechanism coupled to conventional flow simulation on a single borehole pair. In reality, multiple SAGD borehole pairs are drilled beside each other operated at the same time. Applied version of this study

should consider multiple SAGD operation to investigate geomechanical interaction of steam chambers.

## ACKNOWLEDGEMENTS

The authors gratefully acknowledge the funding provided for this research by Foundation CMG. This research was conducted as part of ongoing reservoir geomechanics research associated with the second authors Foundation CMG Chair in Reservoir Geomechanics at the University of Alberta.

## REFERENCES

- Agar, J.R. 1984. Geotechnical behavior of oil sands at elevated temperatures and pressures. *Ph.D. dissertation*. Department of Civil Engineering, University of Alberta, Canada.
- Albahlani, A.M., and T. Babadagli. 2008. A critical review of the status of SAGD: where are we and what is next? *Proc., SPE Western Regional and Pacific Section AAPG Joint Meeting, 29 March-2 April, Bakersfield, California, USA*.
- Butler, R.M. 1994. Steam-assisted gravity drainage: concept, development, performance and future. *Journal of Canadian Petroleum Technology*. 33(2): 44-50.
- Butler, R.M. 1997. Thermal Recovery of Oil and Bitumen. Calgary, Alberta, Canada.
- Chalaturnyk, R.J. 1996. Geomechanics of the Steam-Assisted Gravity Drainage Process in Heavy Oil Reservoirs. *PhD dissertation*. Department of Civil Engineering, University of Alberta, Canada.
- Chalaturnyk, R.J., and Li, P. 2004. When is it important to consider geomechanics in SAGD operations? *Journal of Canadian Petroleum Technology*. 43(4): 53-61.
- Collins, P.M. 2007. Geomechanical effects on the SAGD process. *SPE Reservoir Evaluation & Engineering*. 10(4): 367-375.
- Dusseault, M., and N. Morgenstern. 1978. Shear strength of Atabasca oil sand. *Canadian Geotechnical Journal*. 15: 216-238.
- Edmunds, N.R., Kovalsky, J.A., Gittins, S.D., and E.D. Pennacchioli. 1994. Review of phase A steam-assisted gravity-drainage test. *SPE Reservoir Engineering*. 9(2): 119-124.
- Kim, J., Tchelepi, H.A. and Juanes, R. 2009. Stability, accuracy and efficiency of sequential methods for coupled flow and geomechanics. *Proc., SPE Reservoir Simulation Symposium, 2-4 February 2009, Texas, USA*.

- Kosar, K.M. 1989. Geotechnical properties of oil sands and related strata. *PhD dissertation*. Department of Civil Engineering, University of Alberta, Canada.
- Li, P. 2006. Numerical simulation of the SAGD process coupled with geomechanical behaviour. *PhD dissertation*. Department of Civil Engineering, University of Alberta, Canada.
- Li, P., and Chalaturnyk, R.J. 2009. History match of the UTF Phase A project with coupled reservoir geomechanical simulation. *Journal of Canadian Petroleum Technology*. 48(1): 29-35.
- Oldakowski, K. 1994. Absolute Permeability of Oil Sands. *MSc Thesis*. Department of Civil Engineering, University of Alberta, Canada.
- O'Rourke, J.C., Chambers, J.I., Suggett, J.C., and W.K. Good. 1994. UTF project status and commercial potential. *Proc., the 48th Annual Technical Meeting of the Petroleum Society of CIM*. June 12 – 15, Calgary. Paper No. 94-40, 23 p.
- Scott, D., and A.C. Seto. 1986. Thermal property measurements on oil sands. *Journal of Canadian Petroleum Technology*. 25(6): 70-77.
- Scott, D., Proskin, S.A., and D.P. Adhikary. 1994. Volume and permeability changes associated with steam stimulation in an oil sands reservoir. *Journal of Canadian Petroleum Technology*. 33(7): 44-52.
- Samieh, A.M. 1995. Behavioral characteristics and constitutive modeling of Athabasca tar sand at low effective stresses. *PhD dissertation*. Department of Civil Engineering, University of Calgary, Canada.
- Settari, A., Walters, D.A., and Behie, G.A. 2000. Use of coupled reservoir and geomechanical modelling for integrated reservoir analysis and management. *Proc., the Canadian International Petroleum Conference*, June 4 - 8, Calgary, Canada.
- Sharma, J., and I.D. Gates. 2010. Multiphase flow at the edge of a steam chamber. *Canadian Journal of Chemical Engineering*. 88(3): 312-321.
- Touhidi-Baghini, A. 1998. Absolute permeability of McMurray formation oil sands at low confining stresses. *PhD dissertation*. Department of Civil Engineering, University of Alberta, Canada.

CHAPTER 6: REAL-TIME RESERVOIR MODEL  
UPDATING IN THERMAL RECOVERY:  
APPLICATION OF ANALYTICAL PROXIES AND  
KALMAN FILTERING\*

**ABSTRACT**

The Kalman filtering has many applications in engineering and technology development and has been widely employed in applied geosciences. As an estimator, it is used to predict system behaviour for forecasting analyses. It considers observations obtained over time with uncertainties and other inaccuracies to simulate system behaviour. This study customizes a physics based analytical proxy with the extended Kalman filter for nonlinear systems to characterize reservoir rock properties including porosity and permeability under the thermal recovery process. The analytical proxy represents a reservoir simulator for thermally enhanced oil recovery, and accounts for flow and geomechanical processes for unconventional heavy oil reservoirs. This paper also shows how inverse theories can be utilized to rank and update reservoir models.

---

\* This paper has been presented at IAMG 2011- the Annual Conference of the International Association for Mathematical Geosciences, 5-9 September 2011, Salzburg, Austria. The paper has been peer reviewed and published in the conference proceedings.

## INTRODUCTION

Reservoir rocks are generally do not consist of homogeneous properties; porosity, fluid saturation, bed thickness, and rock types show very little uniformity, and permeability is strongly anisotropic throughout reservoirs (Chilingarian et al., 1996). Heterogeneity and spatial variation in rock properties, particularly in unconventional resources, makes reservoir characterization a difficult task. In practice, oil and gas reservoirs are characterized and evaluated using data observed from different sources and processes such as geological structure evaluation, physical rock sampling, engineering process estimation, and numerical simulation. Informed decisions on investments, data acquisition, and reservoir management are possible if model uncertainty is adequately characterized (Oliver et al., 2008).

At the primary stage of reservoir simulation, geostatistical tools are used to generate stochastic static models constrained to well data (or any data provided). Although the models are still uncertain, they honour statistical characteristics of the original data. More importantly, these stochastic models offer estimates of spatially distributed rock properties that enable simulators to build fine reservoir models. During a recovery processes where reservoir behaviour is monitored, static models can be updated using inverse theories (known in petroleum engineering as history matching techniques). The Kalman filter (Kalman, 1960), an inverse theory, is an optimal solution to estimate the state vector  $x \in \mathcal{R}^n$  of a discrete-time process which is usually utilized in engineering problems. The extended Kalman filter (Welch and Bishop, 1995) that was proposed for nonlinear systems is hardly applicable in petroleum engineering. The work by Zhai et al. (2009) on forecasting inter-wall connectivity in waterflooding, or the work by Gravdal et al. (2010) for tuning computer models in drilling are among the limited examples. The ensemble Kalman filter (EKF) (Evenson 1994 and 2009) is another version of Kalman family which is suitable for nonlinear systems with large number of variables.

For unconventional heavy oil reservoirs, steam-assisted gravity drainage (SAGD), a thermal recovery process, is often the first option among enhanced oil recovery (EOR) strategies. Although high performance computer codes increase the accuracy

and automation of SAGD numerical modelling, long computational time remains an issue for high resolution models, especially during coupled reservoir geomechanical simulations. With a greater number of highly instrumented wells providing real-time monitoring data, slow numerical modelling environments become ineffective. To overcome this, long simulations are broken down into parallel jobs to take advantage of faster low-order simulators. A hierarchical closed-loop reservoir optimization framework is usually suggested (e.g., Williams et al., 2004) using proxies as well as full-physics numerical simulation to handle real-time data, having proxies and semi-analytical solutions characterize uncertainty for short-term decisions while numerical simulators deal with long-term management.

This research investigates the following objectives for the thermal recovery process: (1) how the current low-order analytical proxies can be customized for history matching purposes, (2) how real-time monitoring data and thermo-geomechanical proxies can be exploited within estimation algorithms for ranking stochastic models, and (3) how reservoir models can be dynamically updated.

The following definitions are used throughout this paper: (a) “Proxy” is a set of equations that can simulate the behaviour of a system (SAGD process). (b) “Model” is the distribution of rock properties inside a reservoir. Stochastic realizations are models under this definition. (c) “Reference model” is the model presumed to be the truth model or the reality. (d) “Ranking” is the activity of assigning a relevant value to a model to evaluate its resemblance to the truth model, and (e) “model updating” is the activity of replacing the latest model with a more realistic one (data assimilation).

## **SAGD – THERMAL RECOVERY PROCESS**

In the SAGD process, two parallel boreholes are drilled horizontally at the bottom of a heavy oil formation, one on top of the other. The upper borehole, called the injector, injects high temperature steam at high pressure. As shown in Figure 1, the injected steam develops a chamber surrounding both boreholes called the steam chamber. The viscosity of heavy oil inside and near the chamber gradually decreases and oil flows downwards due to gravity (Edmunds et al., 1994). The crude oil and condensate water

are then collected and driven out of the reservoir through the lower borehole, called the producer.

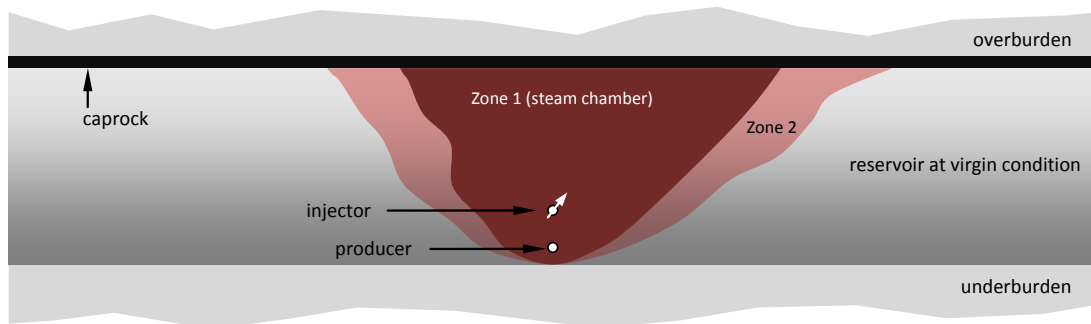


**Figure 1: Steam Assisted Gravity Drainage (SAGD) process. Horizontal boreholes are located within the classical steam chamber at the steam temperature marked as Zone 1. Also, the transition zone between the steam chamber at the steam temperature and the reservoir at the original temperature has been marked as Zone 2.**

At the beginning of the process, the steam chamber rises upward and its width does not change much before it touches the caprock. When the height of the chamber equals the thickness of the reservoir, the steam chamber tends to grow laterally, producing recoverable oil from adjacent regions. When applied to suitable formations, SAGD can recover 50-70% of the in place oil (Edmunds and Chhina, 2001). The concept of a ‘steam chamber’ is not clearly defined in the literature. Researchers developing analytical SAGD models define it as the zone around the boreholes that is heated to steam temperature and contains residual oil saturation (e.g., Butler et al., 1981). They assume a sharp edge between the steam chamber and surrounding regions heated by the steam.

Figure 1 shows a vertical cross section of a SAGD process in a heavy oil reservoir which distinguishes two zones. Zone 1 satisfies the classical steam chamber definition. However, there is a second location in advance of the classical steam chamber (see Figure 1, Zone 2) in which a gradual thermal transition occurs from the steam temperature to the virgin reservoir temperature.

The geomechanical behaviour of the reservoir rock also influences SAGD production and operation (Collins, 2007). Chalaturnyk (1996) explained that excessive pore fluid pressure and thermal stress generated within a geomechanically affected area lead to stress-strain field redistribution in a reservoir, which can change rock properties and

deform the reservoir. Geomechanical changes in reservoir rock generally accelerate the SAGD process, such as when reservoir rock dilation significantly improves permeability and porosity (Dusseault and Morgenstern, 1978), and therefore reservoir performance and oil production (Li, 2006). Reservoir deformation such as heave at the ground surface, borehole displacement, and well deformation all originate through geomechanical reactions (Collins, 2007), impacting heavy oil reservoirs under thermal processes. Figure 2 shows the interlocked structure of oil sand reported by Dusseault and Morgenstern (1978). The same figure illustrates the strain softening behaviour of oil sand under shear stress. Shear strength and volumetric strain at peak ('P') and at residual condition ('R') are also marked accordingly.

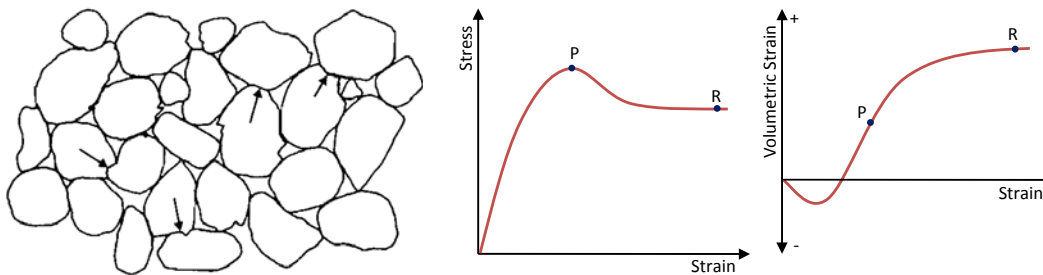


**Figure 2: Interlocked structure of oil sand (left) [after Dusseault and Morgenstern, 1978] and dilative behaviour of oil sand (right). Dilative behavior of oil sand which is typical between dense sands can be depicted from the two graphs. Under a triaxial test, an oil sand sample experiences maximum shear resistance at 'P' and returns to a constant strength at 'R'.**

### **SAGD UNIFIED DRAINAGE (FLOW) PROXY**

Proxies approximate a system and are usually statistical or mathematical. They replace complex numerical models (if they exist) to facilitate simulation, and are built using estimation algorithms to process the response of a system. Polynomial regression and artificial neural networks are two popular examples of these algorithms. Zubarev (2009) provides guidance on the advantages and disadvantages of using proxy modelling in reservoir engineering.

Beside common proxy modeling algorithms, several analytical solutions proposed based on simplified physics satisfactorily predict the SAGD process. These are validated by experimental and numerical data and are generally approved as low-order SAGD proxies. Every variable in these analytical proxies is physically meaningful, and offers a certain range of variation. Therefore, they are usually less

flexible than the proxies generated using other algorithms. Especially in history matching that variables are adjusted to provide the best match with the historical data, analytical physics-based proxies have limited degree of freedom. However, this feature enables analytical proxies to benefit from physical judgments on the adjusted variables as it is shown later in this paper. Moreover, it prevents proxies from reacting out of physical order.

Butler et al. (1981) proposed the first SAGD analytical proxy to predict production rate, commonly known as the Butler model. They developed their model based on the one-dimensional conduction heat transfer theory ahead of an advancing front and a nonlinear assumption for the viscosity gradient relationship. Although the model does not consider geomechanics as part of the physics, it adequately mimics the process when geomechanics is negligible. Other researchers such as Reis (1992) and Akin (2005) have worked in this field and added value to the Butler model. Since the SAGD analytical models are founded on the fundamentals of the Butler theory, they can work together in a unified set of proxies to predict oil production, steam chamber geometry and injection rate.

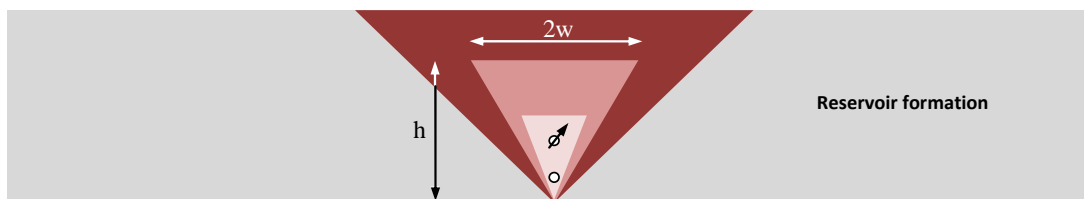


**Figure 3: Shape and location of the classical steam chamber at different stages of the SAGD process. This figure shows the growth of the steam chamber at different stages of the process based on linear geometry of the steam chamber proposed by Reis (1992).**

Table 1 lists the proxies that are used in this study in three categories. The first set of proxies (row A in Table 1, drainage proxies) predict oil production rate and steam chamber geometry before and after the steam chamber touches the caprock. Steam injection rate is predicted by the energy balance solution in row B (injection proxy) derived by Reis (1992) in the format of steam/oil ratio (SOR). Geomechanical behaviour is also considered using the proxies in row C which is discussed later. The steam chamber shape is assumed to follow the linear geometry proposed by Reis (1992) illustrated in Figure 3. Reis's model characterizes the steam chamber by two

parameters: height ( $h$ ) and width ( $w$ ). It should be noted that in Reis's original theory, the height of the steam chamber is always equal to the thickness of the reservoir. Since the equations in this study are solved sequentially in time-wise steps, the height of the steam chamber is considered to vary by time.

In Table 1, only validated and verified proxies have been selected for this study. Readers are referred to the original references for more details. However, a unique experimental SAGD lab test and the results of a numerical simulation are briefly reviewed here to validate the proxies and show proxy interaction.

### **EXPERIMENTAL LAB TEST RESULTS**

Chung and Butler (1988) carried out several small scale lab tests to study the SAGD process. Their lab model was a 21 cm by 35 cm cell with a thickness of 3 cm. The oil sand was synthetically reproduced by mixing crude oil and glass beads. Since no apparent grain structure is expected in between the glass beads, geomechanics is more likely negligible. Material properties used for this test are listed in Table 2. Figure 4 shows the growth of the steam chamber at three stages of the process; before and after touching the caprock and when the steam chamber touches the sides of the model where proxies are no longer valid.

Oil production and steam chamber geometry were history matched using the proxies from row A in Table 1 (drainage proxies). Depending on whether the steam chamber has touched the caprock, appropriate set of equations are chosen. Switching between proxies enables history matching process to capture different trends as the steam chamber grows. Figure 5 compares the experimental data against the results predicted by the proxies. An arrow in each subplot in Figure 5 shows the time when the steam chamber touches the caprock. Successful history matching for low-order proxies in a complex process such as SAGD is achieved when proxies can mimic the general trend of production using reasonable estimated variables. The history matching in Figure 5 has reproduced the essential features of the production data (i.e., production rise at the beginning and the stable period with a gentle increase) using the exact values of rock properties listed in Table 2. This validates the accuracy of drainage proxies for the purpose of this study.

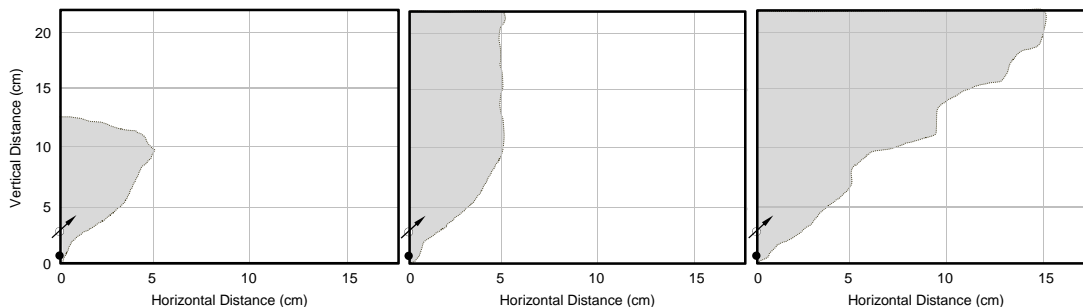


**Figure 4: Growth of the steam chamber in a 15 by 20 cm laboratory cell at times 20, 60 and 90 minutes (from left to right). (after Chung and Butler, 1988). Each single figure plots only right half of the cell.**

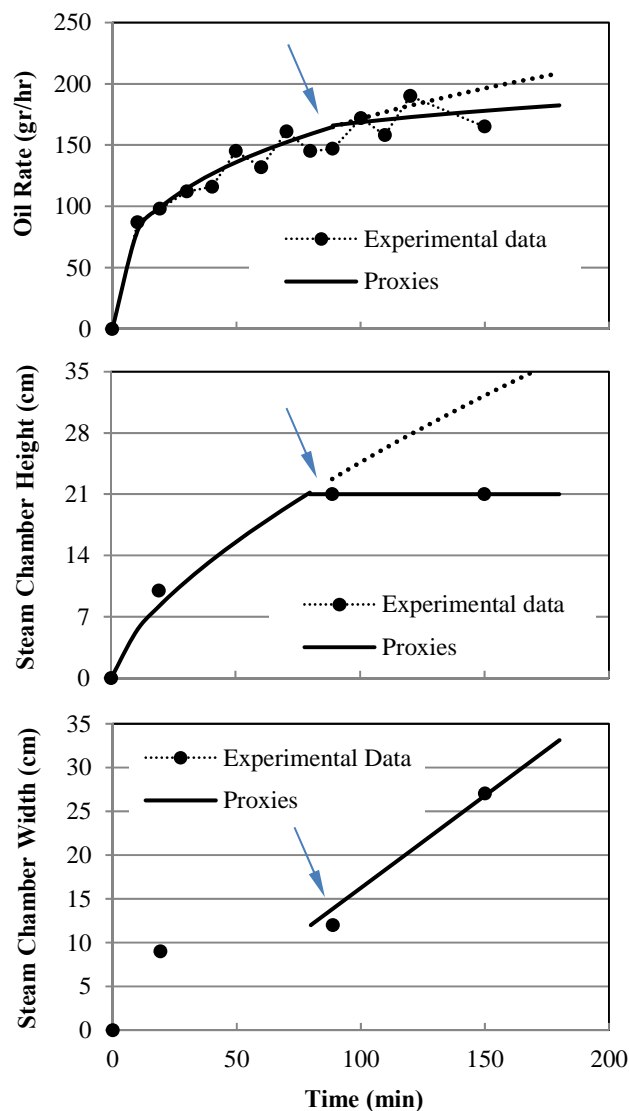


**Figure 5: Comparison between the results of an experimental SAGD process by Chung and Butler (1988) and the results of analytical proxies for oil production rate, steam chamber height and steam chamber width (from top to bottom). The arrow on each chart shows the time of switching between proxies after the steam chamber reaches the ceiling.**

**Table 1: List of SAGD analytical proxies used in this study for oil production, steam injection and geomechanical consideration.**

	MEASUREMENT	EQUATION	REFERENCE
A	oil rate	$q = 2L \sqrt{\frac{1.5kg\alpha\phi\Delta S_o h}{m v_s}}$	Butler (1997)
	before touching the caprock		
	dimension: height of the steam chamber	$h = 2 \left( \frac{kg\alpha}{m v_s \phi \Delta S_o} \right)^{\frac{1}{3}} t^{\frac{2}{3}}$	
	oil rate	$q = 2L \sqrt{\frac{kg\alpha\phi\Delta S_o h}{2am v_s}}$	Reis (1992)
after touching the caprock			
	dimension: width of the steam chamber	$w = \sqrt{\frac{2kg\alpha}{\phi\Delta S_o h a m v_s}} t$	
B	steam/oil ratio	$SOR = \frac{M_R \Delta T}{\rho_w L_s x \phi \Delta S_o} \left[ 1 + \frac{4\alpha t}{h^2 a} + \frac{4}{h} \right]$	
C	permeability improvement	$\frac{k}{k_0} = \frac{\left( 1 + \frac{\varepsilon_v}{\phi_0} \right)^3}{1 + \varepsilon_v}$	Tortike and Ali (1993)
	porosity improvement	$\phi = \frac{\phi_0 + \varepsilon_v}{1 + \varepsilon_v}$	

**Table 2: Material properties of the experimental SAGD test (Chung and Butler, 1988) .**

PROPERTIES	VALUE	UNIT
porosity	39	%
initial oil saturation	100	%
residual oil saturation	5	%
absolute permeability	2930	D
relative permeability	0.48	-
oil density	0.98	gm/cc
thermal diffusivity	0.0507	m <sup>2</sup> /day
oil viscosity	9	m <sup>2</sup> /day
a	0.4	-
m	3.6	-

## RESULTS OF NUMERICAL SIMULATION

The results of a numerical simulation are adapted as truth data in this section to compare with SAGD analytical proxies. A 20 m thick oil sand reservoir was modeled using CMG's STARS, a commercial finite difference reservoir simulator. The reservoir was assumed homogeneous in its rock properties. The simulator was then run to predict oil production and steam injection rates for 1000 days. Table 3 lists the model properties of the simulated reservoir. It should be noted that the rock properties in Table 1 are not the total input data that the numerical simulator uses to run the model. These are the only inputs that the proxies require for prediction.

**Table 3: Properties of the reservoir rock used in numerical simulation and history matching by the SAGD proxies.**

PROPERTIES	VALUE	UNIT
porosity	32	%
initial oil saturation	85	%
residual oil saturation	15	%
absolute permeability	4000	mD
relative permeability	0.48	-
oil density	0.98	gm/cc
thermal diffusivity	0.0507	m <sup>2</sup> /day
oil viscosity	12	mPas
a	0.4	-
m	3.6	-
steam quality	95	%
rock heat capacity	1865	kJ/kg°K
rock thermal conductivity	1.736	W/m°K
temperature difference	210	°K

Figure 6 plots oil production and cumulative injection rates predicted by the numerical simulator and the proxies. Similar to Figure 5, an arrow in each subplot in Figure 6 shows the time at which the steam chamber touches the caprock. These two plots confirm that the proxies have been successful in predicting the process except for the two short periods that fail in reproducing histories. At the beginning of the process steam is circulated inside the wellbore to warm up the reservoir for three months. During this period oil accumulates behind the well and rapidly flows into the well when the well is opened for the first time. Since such an operating mechanism has not considered in deriving the proxies, they are unable to simulate this peak. Other than that, proxies have not been adequately regenerating the process at the time when switching between equations.

Although history matching using the SAGD analytical proxies offers some limitations, they are reasonable low-order simulators because of two major reasons: (1) Compared to numerical simulators that require numerous amounts of data which are usually uncertain, the SAGD proxies are convenient fast tools with limited input that can be carefully applied. (2) The behavior of the proxies is heavily constrained to physics. This simplifies the diagnostic processes where any unusual estimation and mismatch can be easily determined.

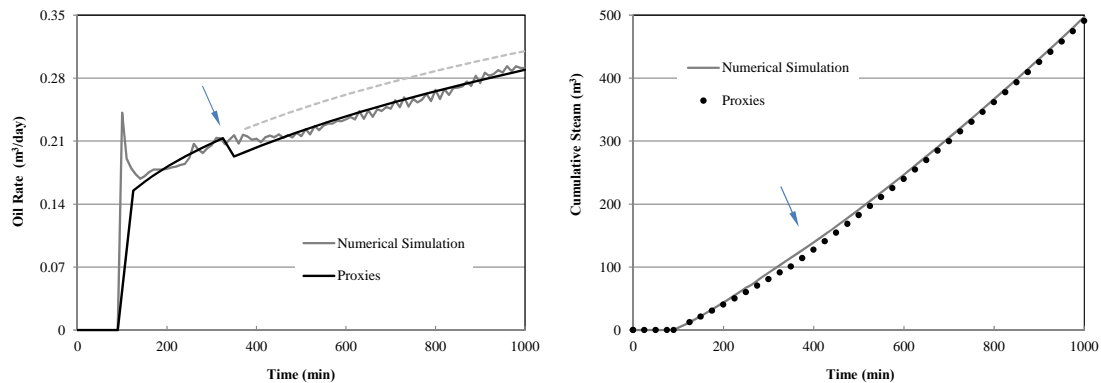


**Figure 6: Oil rate (left) and cumulative steam rate (right): comparison between numerical simulation and SAGD proxy models. The arrow on each chart shows approximate time that the steam chamber touches the top of the model and proxies are changed.**

## GEOMECHANICAL CONSIDERATIONS

There are a few modifications to the drainage proxy that consider geomechanical effects in calculating flow. For example, Azad and Chalaturnyk (2010) adopted a classical geotechnical analysis method to calculate average volumetric strain in a reservoir under the SAGD process. Although the results of their work were promising for limited experimental and numerical case studies, their model is in the primary stages of development. Most recently, Cokar et al. (2011) proposed employing the linear theory of thermal expansion instead of the plastic theory to account for geomechanics.

For the purposes of this paper, geomechanical effects are limited to updating permeability and porosity. Tortike and Ali's (1993) experimental equations to calculate the changes in rock properties used volumetric strain ( $e_v$ ), which has been shown to be the key factor in the variation of rock properties (e.g., Tohidi-Baghini, 1998, and Chalaturnyk, 1996). These equations are listed in Table 1.

While dynamic variation in volumetric strain in a reservoir cannot easily be calculated analytically, this study proposes an average value for volumetric strain. Using the fundamental theory of elasticity and plasticity, volumetric strain can be approximated for a typical two-dimensional plane strain element representing the reservoir as a whole (Figure 7).

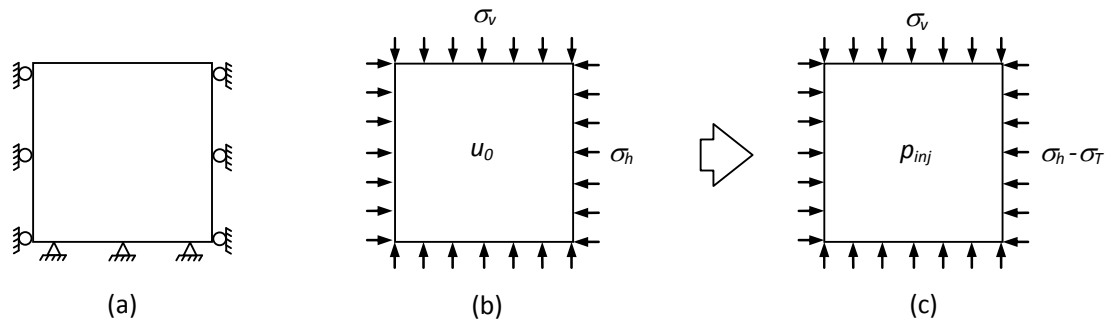


**Figure 7: Geomechanical calculation; the reservoir is represented by a single element: (a) the numerical element for simulation and its boundary conditions (b) in situ stresses acting on the element before the SAGD operation and (c) the resultant stress increase after the SAGD process.**

Figure 7a shows the element and its boundary conditions. Reservoir deformation is assumed to be mostly vertical, with negligible horizontal displacement. At the beginning of the process (Figure 7b) in situ stresses act on the element at reservoir pressure ( $u_0$ ). Steam injection then changes the stress field by applying thermal stress ( $\sigma_T$ ) and increasing initial pore pressure to the injection pressure ( $p_{inj}$ ). Though this simple model does not reflect the stress changes in different locations inside the reservoir, it can effectively determine an average value for volumetric strain. For cases of two-dimensional plane strain, thermal stress is determined using Equation 1 (derived by Hetnarski and Eslami, 2008):

$$\sigma_T = (1 + \nu_g) \alpha_T E \Delta T \dots\dots\dots(1)$$

where  $\sigma_T$  is thermally induced stress,  $\nu_g$  is the Poisson’s ratio of rock,  $\alpha T$  is the linear thermal coefficient of rock,  $E$  is the modulus of elasticity of rock and  $\Delta T$  is the temperature difference.

The geomechanical model shown in Figure 7 can be solved mathematically using mechanical plastic analysis. Davis and Selvadurai (2002) provide a step-by-step geomechanical solution of such a model. However, numerical methods embedded in

commercial software packages can solve the model very quickly. This analysis is required once at the beginning of the process.

## METHODOLOGY

The next sections explore the application of the EKF in reservoir characterization using the analytical proxies in a 2D synthetic case study with porosity and permeability being the two estimate rock properties. Although porosity and permeability are usually correlated, no correlation is assumed between the two variables, enabling demonstration of estimating uncorrelated variables.

At each time step, the SAGD analytical proxies listed in Table 1 can only predict a single bulk value for porosity and a single value for permeability, not reservoir heterogeneity. Therefore, a link must be defined between these. This is plausible through reviewing the theory behind deriving the proxies. Figure 8a shows fundamentals of the Butler theory. Incremental flow ( $dq$ ) is integrated in the channels in front of the steam chamber where flow initiates. Permeability ( $k$ ) appears in the Darcy's law equation as:

$$dq = \frac{k\rho_o}{\mu} (g \sin \theta) d\xi \dots\dots\dots(2)$$

where  $dq$  is differential flow,  $k$  is permeability,  $\rho_o$  is oil density,  $\mu$  is oil viscosity,  $g$  is gravity,  $\theta$  is steam chamber angle and  $d\xi$  is differential distance. To estimate oil viscosity, Butler used Eq. 3 which is based on temperature difference in advance of the steam chamber:

$$\frac{T - T_R}{T_S - T_R} = \exp\left(-\frac{U\xi}{\alpha}\right) \dots\dots\dots(3)$$

where  $T_R$  = virgin reservoir temperature,  $T_S$  = steam temperature,  $U$  = steam chamber interface velocity,  $\alpha$  = thermal diffusivity of the reservoir and  $T$  = the temperature at distance  $\xi$  in advance of the steam chamber perpendicular to the flow velocity vector. Figure 8b shows that the temperature decreases rapidly on the  $\xi$ -axis. This means that differential oil is produced within a certain distance from the steam chamber edge, marked as Zone 2 in Figure 1. This is the area in advance of the steam chamber inside

which permeability is active and should be calculated. On the other side, porosity comes into play to solve the conservation of mass, which is integrated inside the steam chamber. Therefore, Zone 1 (see Figure 1) is the area inside which porosity is effective.

When Zone 1 is mapped on the porosity models and Zone 2 is mapped on the permeability models, they essentially return those cells located inside the mapped zones. These cells are part of a heterogeneous model whose values are not the same. A reasonable method that can be proposed to compare the cells of different values with a single value is averaging. According to this assumption, the average of the returned cells of each model is taken and compared to the single value estimated by the proxies. Another averaging technique has previously been adapted for uncertainty assessment of SAGD performance by Vanegas et al. (2008). They proposed averaging the values on the steam chamber edge. Although the averaging technique proposed here accompanies the Butler theory more appropriately than the edge averaging, it still must be verified against real data.

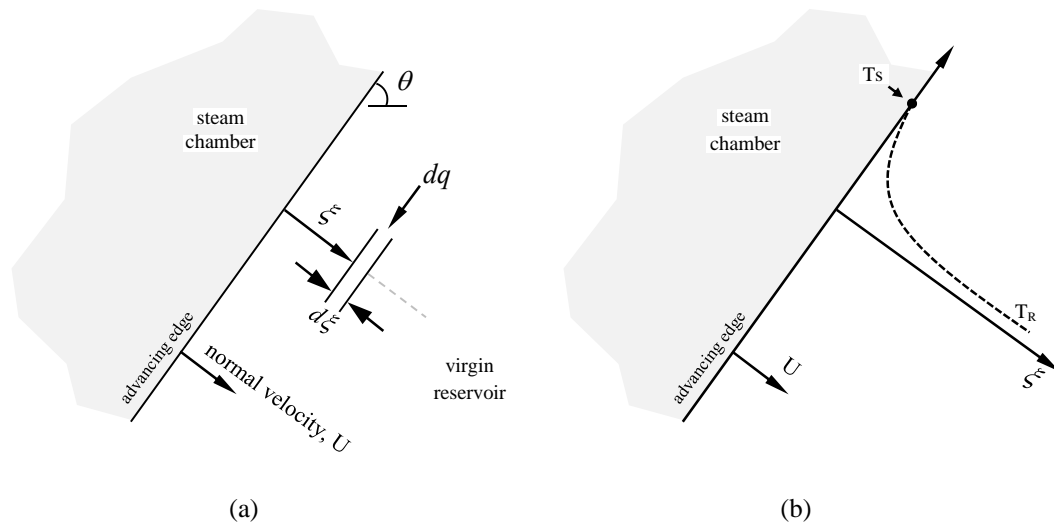


**Figure 8: Fundamentals of Butler model. (a) Incremental flow rate ( $dq$ ) in a channel in front of the steam chamber, (b) temperature distribution in advance of the moving steam chamber front.**

Therefore, the state vector of the process has two components: permeability ( $k$ ) and porosity ( $\phi$ ). Since rock properties are heterogeneous and the steam chamber occupies various zones every time step, the state vector is a function of time:

$$x_t = [k \quad \phi]_t^T \dots\dots\dots(4)$$

The observation vector  $d_{\text{obs}}$  is three dimensional. The first two elements of the vector are related to production and injection histories,  $q$  and Steam/oil Ratio ( $SOR$ ). The third element is a dimension of the steam chamber that varies before and after reaching the.  $D$  represents the height of the steam chamber before it touches the caprock and the width of the steam chamber after it touches it.

$$d_{\text{obs},t} = [q \quad SOR \quad D]_t^T \dots\dots\dots(5)$$

Figure 9 illustrates the overall workflow of the solution. It shows that at each time step, the EKF algorithm reads the three monitoring variables from three sources and estimates single values of permeability and porosity. Zone 1 is mapped on the porosity models and an average value of porosity of the cells inside Zone 1 is returned for each model. Similarly, Zone 2 is mapped on the permeability models and averages are returned. An error function then calculates porosity or permeability mismatches for every model. The porosity and permeability models are then sorted separately based on the calculated mismatches. If  $n$  models are contributed in a pool of models, they are ranked from 1 to  $n$ . The model with the least mismatch receives the 1<sup>st</sup> rank and the model with the maximum mismatch receives the  $n$ th.

Ranking the models would gradually filter out the inaccurate ones. The lower ranked models are can be removed from the pool at every time step. However, in this study, all of the models are kept to track the ranking trend. The ranking algorithm is a static process, meaning that the models are kept unchanged but repeatedly sorted.

Although the ranking process may partially reduce uncertainty by eliminating low ranked models, it is not capable of diffusing high ranked models into a more reliable ones. The truth model does not necessarily appear in stochastic modelling. It is always motivating to diffuse the data towards updating the models. In this regard, the mismatch values calculated for each model become valuable for dynamic model updating. This means that the assigned mismatch values of each model at every time step can play as an observation variable. For updating, all of the models as well as the observation vector (mismatches) are combined to construct an ensemble matrix.

Using ensemble based Kalman filtering, the models are updated to minimize the global mismatch of the observation vector. Readers are referred to the report by Mandel (2006) on efficient implementation of the ensemble Kalman filter for further details.

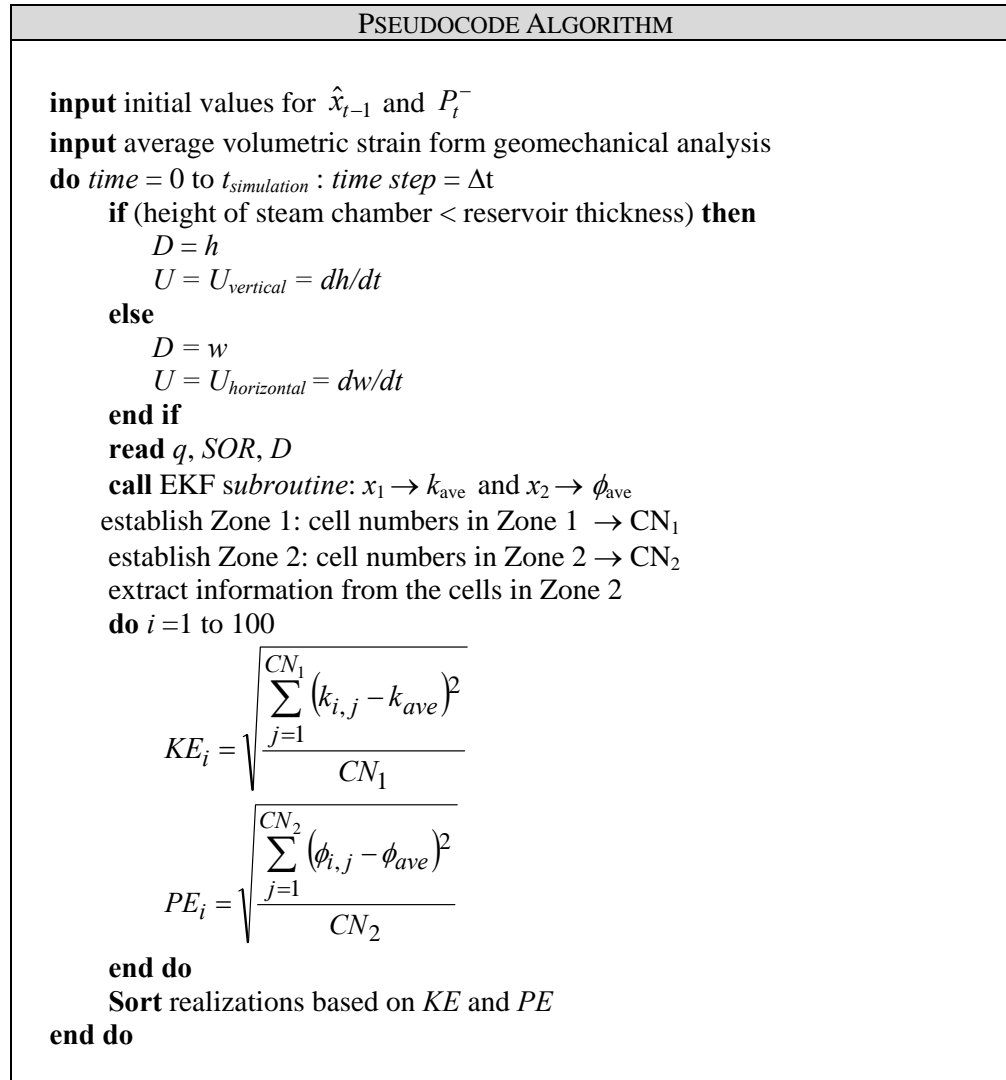


Figure 9: Workflow of the proposed algorithm for ranking static models.

## CASE STUDY: SHALLOW SAGD

### Permeability and Porosity Stochastic Modelling

To generate the initial models as well as the reference model for porosity and permeability, GSLIB (Deutsch and Journel, 1997) was used for Gaussian sequential

simulation. The reservoir model is a 20 metre ree thick oil sand reservoir located 150 metres below the ground surface. Data from nine wells in a 100 m by 30 m plan area is constrained to generate the stochastic models. Figure 10 shows the histograms of all data from the nine wells. The data set is synthetically produced. However, real field data is used to reproduce realistic well data. The two histograms in Figure 10 provide statistical information for each data set. The mean and standard deviation of permeability are approximately 4500 mD and 2607.68, respectively, and those for porosity are 26.8% and 6.4%, respectively.

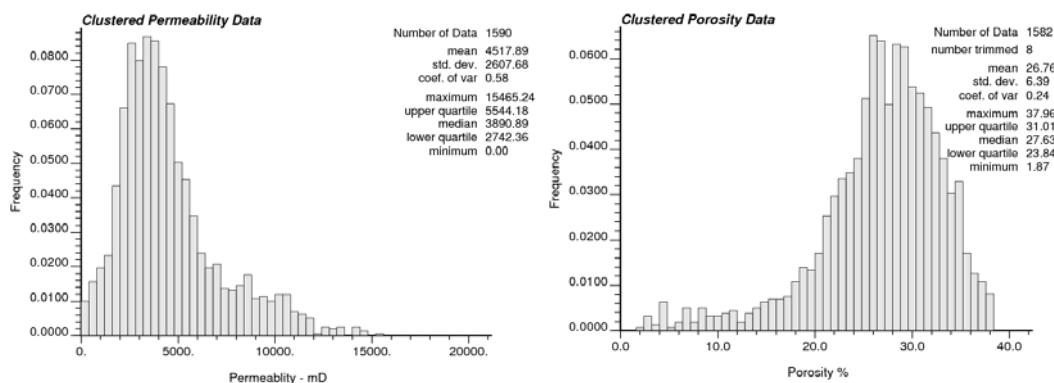


**Figure 10: Histograms of well data: permeability (left) and porosity (right).**

The well data was employed to generate 100 models for each rock property. The model contains 60,000 cells. The 100 realizations are taken as the stochastic models for uncertainty analysis. However, the seventieth realization from both sets was randomly picked to perform as the reference rock model within the reservoir.

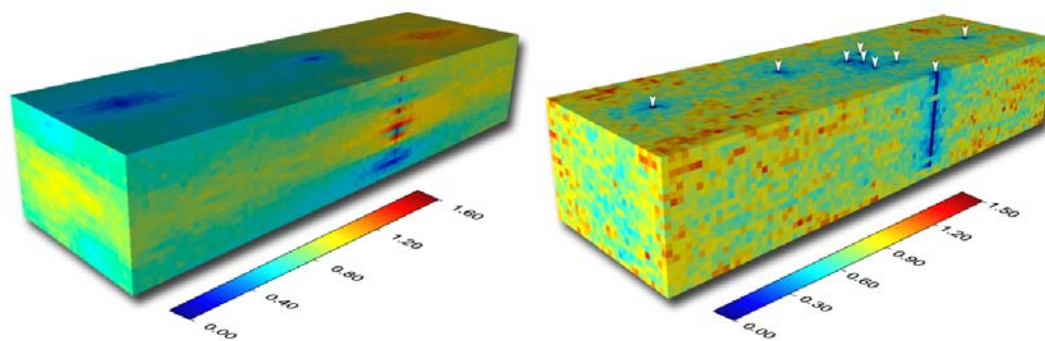


**Figure 11: E-type mean (left) and conditional variance (right) of permeability in normal score space for 100 stochastic realizations. Well locations have been marked at the top surface by an arrow above each well.**

To visualize the result of geostatistical simulations, the E-type mean (i.e. the cell-based average of the 100 realizations) and conditional variance of the 100 realizations are plotted separately for permeability (in Figure 11) and porosity (in Figure 12). These clearly show that the variance of data at the well locations is almost zero while varying in other locations.

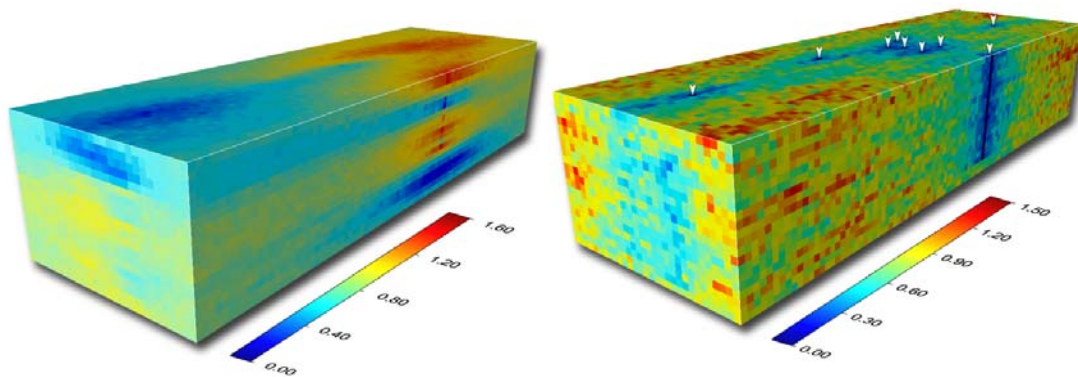


**Figure 12: E-type mean (left) and conditional variance (right) of porosity in normal score space for 100 stochastic realizations. Well locations have been marked at the top surface by an arrow above each well.**

### Observation Data – Reference Numerical Simulation

To generate the reference response (observation data), a 2D vertical section from the reference porosity and permeability models are chosen and embedded at the reservoir location shown in Figure 13. No uncertainty was considered in rock properties in all other locations for both flow and geomechanical analysis. To perform iterative coupled geomechanical flow simulation, the approach previously developed by the authors is adopted for this study (Azad and Chalaturnyk (2011)). A commercial flow simulator (STARS) and a geomechanical modeling package (FLAC2D) were linked using an interactive code that transfers data in between the simulators. Every time step, the code runs the flow simulator and transfers the predicted pressure and temperature into the geomechanical software. The code then reads the calculated volumetric strain from the geomechanical analysis and updates permeability and porosity for the next step. These two simulations are sequentially run to the end of the reservoir life. The parameters required for coupled analysis and history matching are addressed in Table 4.

**Table 4: List of parameters and their final values**

	PARAMETERS	VALUE	UNIT
FLOW SIMULATOR	oil density	1008	$Kg/m^3$
	dynamic viscosity at steam temperature	0.007	$Pa \cdot s$
	initial oil saturation	0.85	%
	residual oil saturation	0.15	%
	reservoir thermal diffusivity	$6 \times 10^{-6}$	$m^2/s$
	coefficient of average velocity, $a$	0.4	-
	coefficient of viscosity, $m$	4	-
STEAM CALCULATION	formation heat capacity	$1.865 \times 10^6$	$J/(m^3 \cdot ^\circ C)$
	specific heat of steam condensation	$2 \times 10^6$	$J/Kg$
	reservoir temperature	10	$^\circ C$
	steam temperature	240	$^\circ C$
	steam quality	0.95	%
GEOMECHANICAL ANALYSIS	formation density	2200	$Kg/m^3$
	horizontal stress ratio, $min$	1	-
	horizontal stress ratio, $max$	2	$Pa$
	reservoir pressure, $u_0$	650	$kPa$
	injection pressure, $p_{inj}$	3000	$kPa$
	modulus of elasticity	545	$MPa$
	Poisson's ratio	0.3	-
	friction angle	60	$^\circ$
	dilatancy angle	15	$^\circ$
	volumetric strain	7.8	%
	permeability improvement	185	%
porosity improvement	117	%	

In Figure 13, the geomechanical model consists of three geological layers: overburden and underburden that behave elastically, and the reservoir formation that is located between them. Only the central part of the reservoir formation highlighted in Figure 13 is modelled in the flow simulator. The simulation is stopped before the steam chamber nears the reservoir grid boundary to avoid errors in calculation.

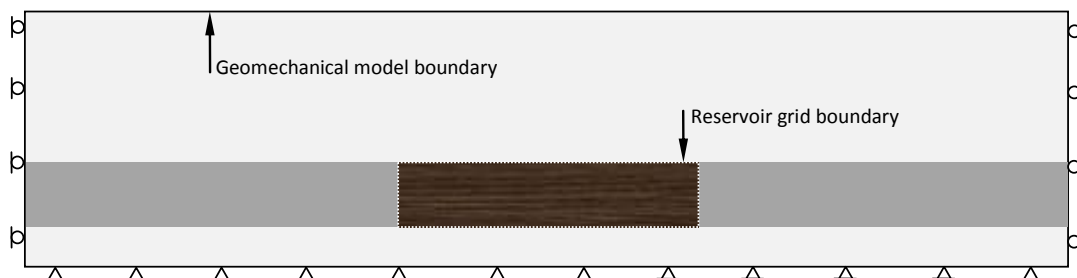
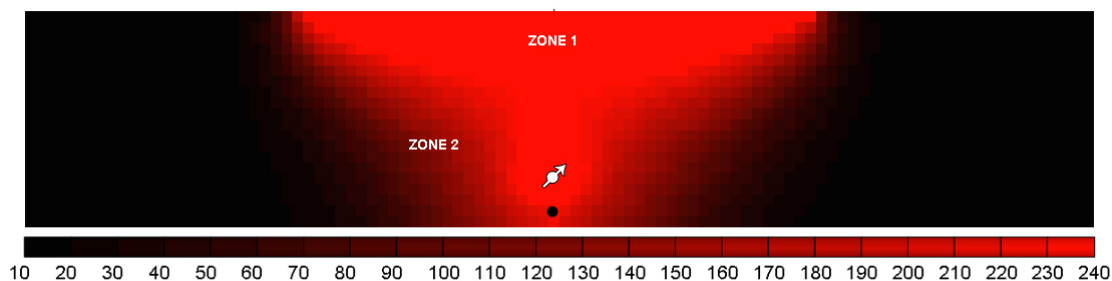
**Figure 13: Geomechanical-Reservoir model and boundary conditions for coupled simulation.**

Figure 14 shows a sample temperature profile inside the reservoir 450 days after the beginning of the SAGD process showing that the steam chamber has reached the caprock at this stage. Although more details about the location of Zones 1 and 2 are extractable, it is assumed that thermocouples that monitor the geometry of the steam chamber cannot detect such detailed data. From the reference simulation, oil production and steam injection rates are also recorded every 30 days. These are presented in the next section.



**Figure 14: Temperature ( $^{\circ}\text{C}$ ) profile in the reservoir 450 days after the SAGD process (simulation result for the reference model).**

### Evaluating Uncertainty in Stochastic Models

With the methodology explained for the reference simulation, the other 99 realizations were mounted in the simulator and the SAGD process was modelled for each of the rock property realization sets. Uncertainty can be estimated if the histories of production and injection rates are plotted coincidentally in one graph for all 100 realizations. Because the models are synthetic, uncertainty evaluation ensures that the initial (input) models have been properly generated to provide a problem with high level of uncertainty.

Figure 15 shows oil rates as well as steam injection rates for all 99 realizations and the reference model. Oil is produced 100 days after the startup period. During the first 100 days, the steam is circulated inside each well to warm up the surrounding area. Therefore, no injection or production is generated. Figure 15 shows that uncertainty of production increases by time while that of injection is almost constant. It should be noted that this figure only shows the results of 1% of the possible simulations, since 100,000 combinations of the permeability and porosity models can be simulated.

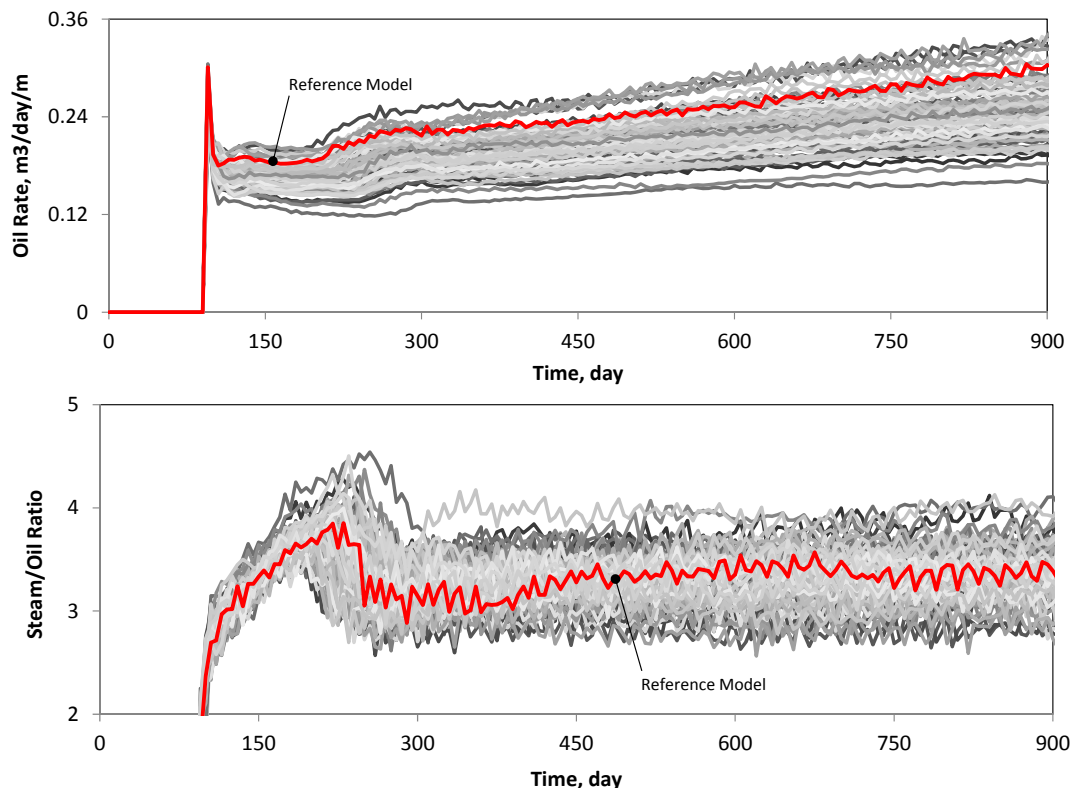


**Figure 15: Oil production rate and SOR histories for the reference model and the other 99 models.**

### **Ranking the Models – Tracking the Reference Model**

The results must confirm two major aspects of the proposed methodology. Firstly, the assumption of averaging rock properties in two zones for heterogeneous models must be examined. Regardless of the accuracy of the proxies, the EKF algorithm can predict single permeability and porosity at every time step by matching oil production, steam injection and steam chamber dimensions. As long as the Kalman gain matrix is calculated with no difficulty in matrix inversion, the algorithm provides the best fit. However, it was assumed based on the Butler theory that the predicted permeability and porosity are the average of each property in its associated zone (either Zone 1 or Zone 2). These predicted values should be tested to ensure that they are (a) in a realistic range, and (b) in agreement with the assumption. If these two criteria are not satisfied, the predicted average permeability and porosity are not valid.

Figure 16a and 16c compares the predicted average permeability and porosity with the actual average properties in the associated zones of the reference models. Both

plots highlight close agreement between the predicted average and the average calculated over the reference model. In both cases, the predicted values do not closely follow the calculated trend at the beginning of the process, but the mismatch is improved over time. Though it is difficult to be conclusive about the causes of this mismatch, the error is believed to come from two sources: the proxy itself and the assumption linking the average values to heterogeneous models. Butler's rising chamber theory and Reis' steam injection model are not precise and have been derived based on simplified hypotheses. On the other hand, there are some approximations in calculating the associated zone. Both of these sources inject noise into the system and affect the dissimilarity between the results and prediction.

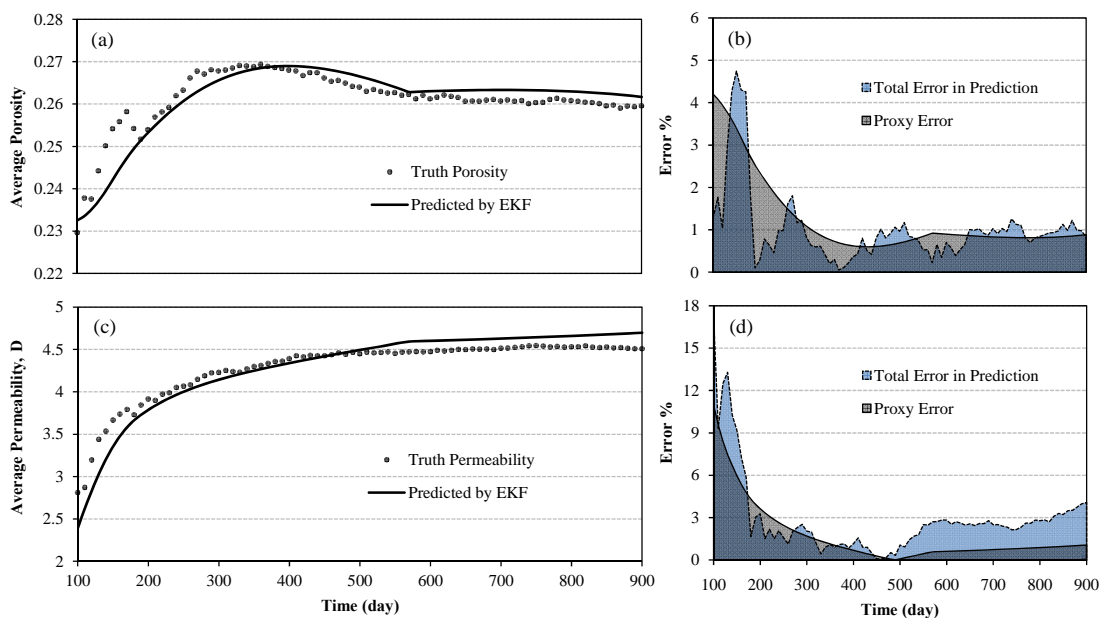
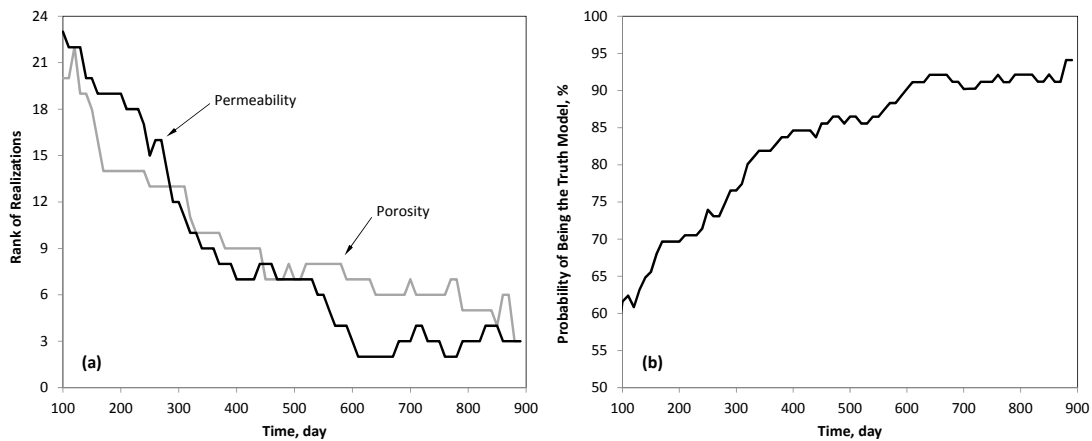


**Figure 16: Comparison of calculated average permeability and porosity based on the averaging assumption over reference models (a) in Zone 1 for porosity, and (c) in Zone 2 for permeability. Comparison between the total error and the proxy error (b) for porosity, and (d) for permeability.**

To quantify the error from the first source (i.e., the proxies), the coupled numerical simulator was run again with the same settings as the reference but with homogeneous models. Permeability and porosity were kept constant at 4500 mD and 0.26 (mean values from the histograms in Figure 10) respectively. This assures that the error is only generated by the proxies if we assume that only two sources exist. The difference between the estimated values and what is expected theoretically (constant values of permeability and porosity) can calculate the error. Figure 16b and

16d illustrate the total error containing errors from both sources and the error calculated using homogenous models. These two subplots show that the errors by the proxies are not essentially less than the total error. This might express that the errors from both sources has been canceled out in some time steps. We should also emphasize that the effect of changes in permeability and porosity is not linearly correlated with production and injection so that the heterogeneous and homogenous models might not be comparable. Moreover, the noise covariance that has been adjusted for the heterogeneous model might not work appropriately when the same matrix is used for homogeneous model. In general, it can be said that the averaging assumption is reasonable because it tightly tracks the predicted trend and the level of error is fairly low.

Secondly, the ranking methodology should be checked against the reference models. For this, the two reference models are placed in the stochastic model pool, and the algorithm is then applied to rank all of them at every time step.



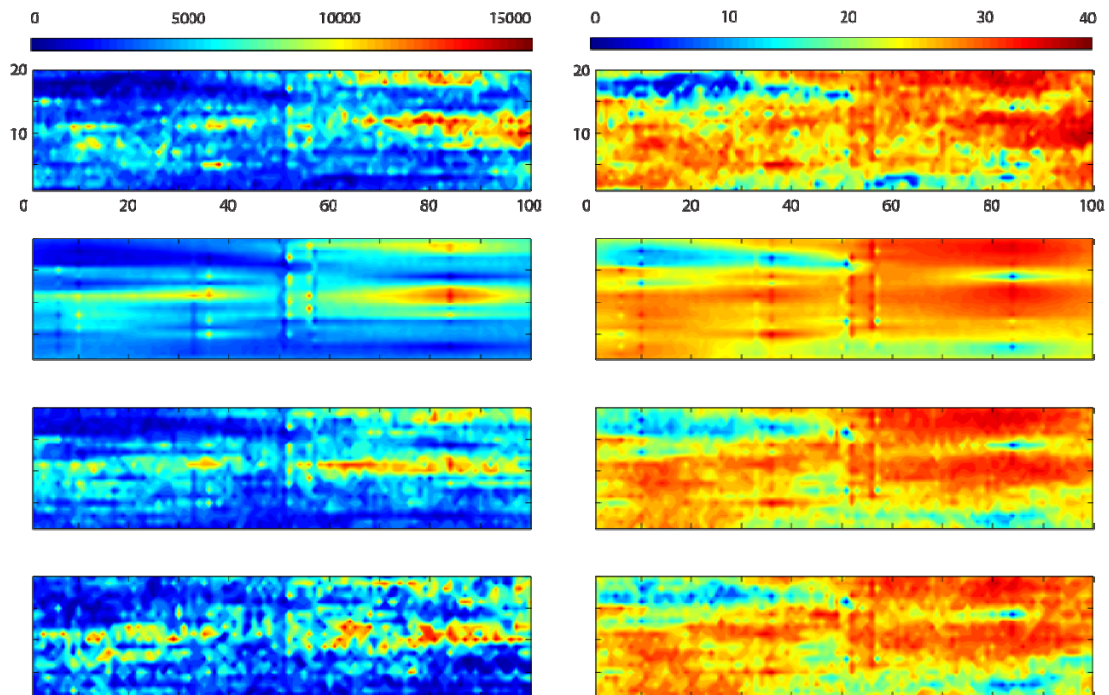
**Figure 17: (a) Ranking history of reference models, and (b) probability of being the truth model for reference models.**

Figure 17a tracks the rank of both reference models by time. It shows that the rank of the reference models is sharply reduced from around 25 to less than 10 after 250 days. As expected from Figure 16, the mismatch at the beginning prevents the algorithm from recognizing the reference model early in the process. The uncertainty analysis of the proposed algorithm is plotted in Figure 17b. Before applying the ranking algorithm,  $10^4$  combinations of the two sets of models have an equal chance to populate the reservoir. The probability of being the truth model for each combination

including the reference combination is  $1\% \times 1\% = 0.01\%$ . During the ranking process, the probability of any two models is calculated by multiplying their individual probabilities. Figure 17b shows that the probability of the reference models greatly increases to about 60% at the first step and quickly improves to 90% after 400 days.

### Data Assimilation – Dynamic Model Updating

Application of the EKF and the SAGD proxies is limited to estimating the average values and is not further applicable for dynamic updating. The EnKF is usually preferred for updating the models with a large number of variables and high nonlinearity (e.g., Zhang and Oliver, 2009, Phale and Oliver, 2010, Aanonsen et al., 2009).



**Figure 18: Data assimilation analysis for permeability models (left column in mD) and porosity models (right column in %). From top to bottom: reference models, E-type mean of initial models, E-type mean of updated models after 300 days, and E-type mean of updated models after 700 days.**

In simple words, the EnKF applies the fundamentals of the KF using statistical inverse modelling. In forward steps, the EnKF runs a simulator (system representative) for each ensemble member (each model) and returns the calculated parameters that are also monitored. These, in combination with the observation data,

are then used in a backward analysis to update the models. For processing real-time data, numerical simulators are too slow compared to proxies and take longer run time to complete each job. Also, numerical simulators should be furnished with a large number of inputs which are mostly uncertain at the primary stages and systematically amplify inaccuracies.

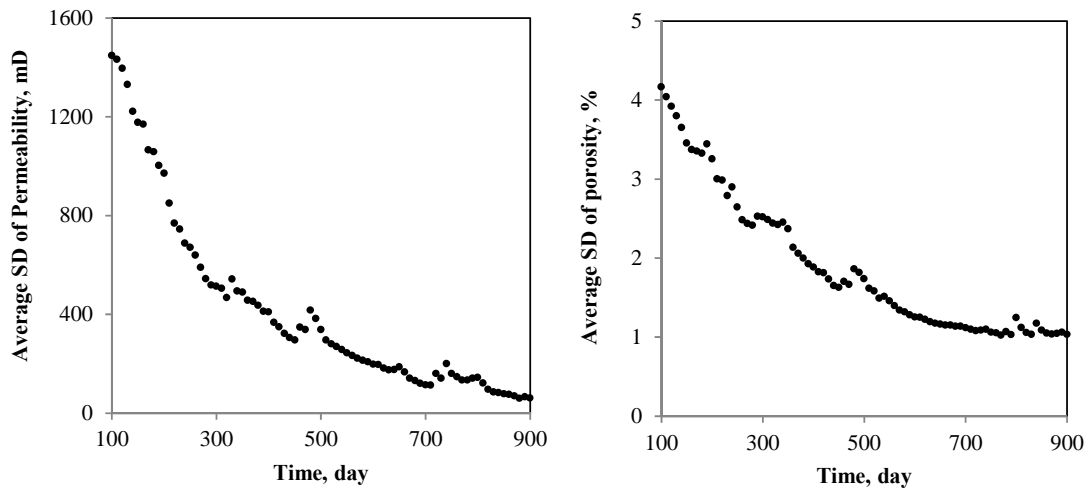


**Figure 19: Average standard deviation of E-type model for permeability (left) and porosity (right).**

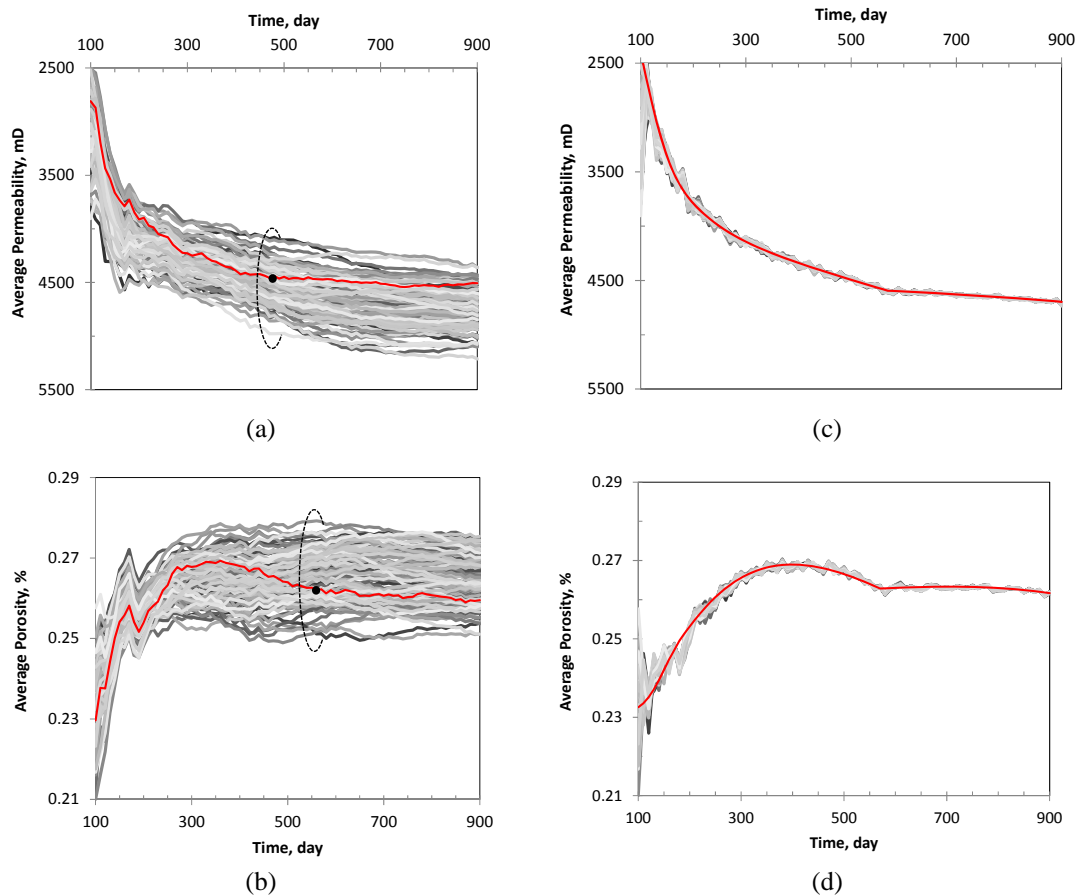
As explained before, this study is to facilitate the analysis time for short-term management. To accelerate the updating phase while using the advantages of the EnKF, the numerical simulation is bypassed, and instead, an observation vector whose elements are the calculated average permeability or porosity is replaced.

Figure 18 shows, respectively, the reference model, the E-type mean of the initial ensemble members, and the E-type means of the updated models after 300 and 700. The left column shows permeability maps in mD and the right column shows porosity.

The history of data fusion in Figure 18 reflects that the data assimilation algorithm has successfully updated the initial model into the models that mimic the references. Although in terms of extremes the updated models are dissimilar to the reference models, they sufficiently capture the structural features of the reservoir.

Other than visual investigation of the results presented in Figure 18, the models should be further examined through statistical quantifiers. Due to the large number of

variables cell to cell comparison would not characterize the overall quality of the updated models. For this reason, average standard deviation was selected to monitor the updating process. Standard deviation expresses the variability and measures confidence in statistical data in its original units. Standard deviation is calculated at each cell for each time step, and the average of the standard deviations of all cells is taken.



**Figure 20: (a) Average permeability and (b) average porosity of the truth model among other 99 models. (c) Average estimated permeability and (d) average estimated porosity by EKF among other 99 models assimilated using EnKF.**

Figure 19 plots the average standard deviation for permeability and porosity. The figure clearly confirms the reduction of global variance in the updated models. It shows that the ensemble members' dissimilarities are lowered as the updating phase progresses. It should be added that the reduction of global variance simply indicates that the populations of models collapses to essentially just one model (that in general

will be different from the truth model) and it does not necessarily mean that the error in the model estimation decreases as well.

The results of data assimilation by the EnKF have been also compared in Figure 20. The subplots in the left column compare the values of the average permeability and porosity of the truth model to those of the other models. These plots, basically, show the level of uncertainty before estimation. The average values are then estimated by the EKF that are plotted by black solid lines in the right column subplots among the average values of the models updated using the EnKF. These reveals that the update models tend to honor the data at least at the zones that averages are calculated.

## CONCLUSION

This paper addressed the idea of employing low-order proxies for handling real-time observation data in SAGD thermal recovery. A combination of the SAGD's analytical physics-based solutions was selected to form a unified proxy. Validation process using experimental and numerical data confirmed that the proxies can reasonably reproduce essential features of the steam chamber growth and production behavior with some limitations. A built-in technique was also implemented for geomechanical consideration and a mapping algorithm was adapted to link the single estimated rock property values by the proxies to the heterogeneous models. The EKF was then used to predict rock properties including porosity and permeability for ranking static models. In addition, ensemble Kalman filter was utilized for model updating combined to the proxies as fast simulators. Through a case study, the methodology and the idea were further expressed and the results were criticized. General observations derived from this study are:

- Analytical proxies can be adopted for the purpose of reservoir characterization. Because they imply essential features of the physics involved in a recovery process, they provide physical essence to numerical calculations. This would strongly support defining meaningful auxiliary links (the averaging assumption in this study) between the results and the real physics.

- Unlike full-physics numerical simulation, analytical proxy modelling is very fast and requires limited input parameters. This is very beneficial when data is provided in real time. Low-order modelling enables real-time data processing by removing large computational load at the expense of some resolution. This expense is worthwhile within a hierarchical simulation arrangement when the processed data accelerates high-order simulations.

## **ACKNOWLEDGEMENTS**

Authors would like to acknowledge Nathan Deisman for his contribution on reviewing this paper. His technical support and helpful comments are highly appreciated. We also thank Kelsey Wagner for editing the primary manuscript.

## APPENDIX A: EXTENDED KALMAN FILTER

A general stochastic process can be represented at time  $t$  by the state vector  $x_t$  and a nonlinear function  $f$  which describes the process in time (Equation A-1). The observation equation (Equation A-2) is used to determine the observation vector  $d_{obs}$  in relation to the process state vector  $x_t$  using another nonlinear function,  $h$ . The state vector for time  $t$  is determined through Equation A-2. On the other side, measurement relationship  $h$  can be used to determine the observation vector,  $d_{obs}$ , as reflected in Equation A-2.

$$x_t = f(x_{t-1}) + \omega_{t-1} \dots\dots\dots(A-1)$$

$$d_{obs,t} = h(x_t) + \epsilon_t \dots\dots\dots(A-2)$$

Random vectors  $\omega$  and  $\epsilon$  are process and measurement noises, respectively, and are assumed to be independent, white, and with normal probability distribution, as in Equations A-3 and A-4.

$$p(\omega) \sim N(0, Q) \dots\dots\dots(A-3)$$

$$p(\epsilon) \sim N(0, R) \dots\dots\dots(A-4)$$

Matrices  $Q$  and  $R$  are the covariance matrices defined for the noise vectors  $\omega$  and  $\epsilon$ , respectively. At each time step, process and measurement functions  $f$  and  $h$  are linearized locally about the working point and the following linear system and observation equations are established.

$$x_t \approx \tilde{x}_t + A(x_{t-1} - \hat{x}_{t-1}) + \omega_{t-1} \dots\dots\dots(A-5)$$

$$d_{obs,t} \approx \tilde{d}_{obs,t} + G(x_t - \tilde{x}_t) + \epsilon_t \dots\dots\dots(A-6)$$

In these equations,  $A$  and  $G$  are the Jacobian matrices with respect to  $x$  that are calculated at each time step  $t$  using Equations A-7 and A-8. Figure A-1 shows the solution flowchart for the filter after linearization.

$$A_{[i,j]} = \frac{\partial f_{[i]}}{\partial x_{[j]}}(\hat{x}_{t-1}) \dots\dots\dots(A-7)$$

$$G_{[i,j]} = \frac{\partial h_{[i]}}{\partial x_{[j]}}(\tilde{x}_t) \dots\dots\dots (A-8)$$

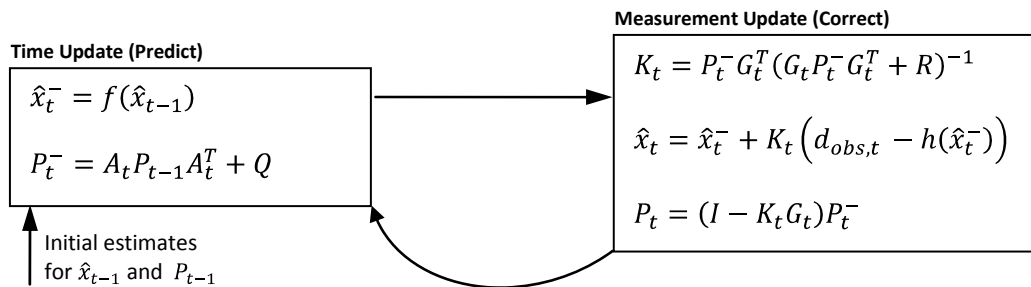


Figure A-1: Kalman filter workflow (after Welch and Bishop, 1995).

## APPENDIX B: ENSEMBLE-BASED UPDATING USING AN INDICATOR VECTOR

$\mathbf{X}$  is the ensemble containing  $N$  state vector (or  $N$  ensemble members). Each member has the model property vector ( $\mathbf{m}$ ) and an indicator,  $\omega$ .

$$\mathbf{X} = \begin{bmatrix} \mathbf{m}_i \\ \omega_i \end{bmatrix} = [\mathbf{x}_i] \dots\dots\dots (B-1)$$

If the model property vector reserves  $n$  dimension each for one cell in the model,  $\mathbf{X}$  is a  $(n+1)$  by  $N$  matrix as shown in Eq. B-2:

$$\mathbf{X} = \begin{bmatrix} \mathbf{m}_i \\ \omega_i \end{bmatrix} = \begin{bmatrix} m_{11} & \dots & m_{1N} \\ \vdots & \ddots & \vdots \\ m_{n1} & \dots & m_{nN} \\ \omega_1 & \dots & \omega_N \end{bmatrix} \dots\dots\dots (B-2)$$

The ensemble mean and covariance matrix can be written as Eq. B-3 and B-4, respectively.

$$E(\mathbf{X}) = \frac{1}{N} \sum_{i=1}^N \mathbf{x}_i = \begin{bmatrix} \bar{m}_1 \\ \vdots \\ \bar{m}_n \\ \bar{\omega} \end{bmatrix}_{(n+1) \times 1} \dots\dots\dots (B-3)$$

$$Cov(\mathbf{X}) = \frac{\mathbf{A}\mathbf{A}^T}{N-1} \dots\dots\dots (B-4)$$

where matrix  $\mathbf{A}$  is defined as below:

$$\mathbf{A} = \mathbf{X} - E(\mathbf{X}) = \mathbf{X} - \frac{1}{N}(\mathbf{X}\mathbf{e}_{N \times 1})\mathbf{e}_{1 \times N} \dots\dots\dots (\text{B-5})$$

and  $\mathbf{e}$  denotes the matrix of all ones. Then, the Kalman gain matrix is written as:

$$\mathbf{K} = \text{Cov}(\mathbf{X})\mathbf{H}^T(\mathbf{H}\text{Cov}(\mathbf{X})\mathbf{H}^T + \mathbf{R})^{-1} \dots\dots\dots (\text{B-6})$$

In Eq. B-6,  $\mathbf{H}$  is a 1 by  $(n+1)$  matrix of all zeros except for the  $(n+1)^{\text{th}}$  element of one, and  $\mathbf{R}$  is the noise covariance of the indicator vector. To simplify deriving an equation for model updating, we define the following parameters:

$$\mathbf{R} = r \sum_{i=1}^N (\omega_i - \bar{\omega})^2 \dots\dots\dots (\text{B-7})$$

$$\mathbf{C} = \begin{bmatrix} \sum_{i=1}^N (m_{1i} - \bar{m}_1)(\omega_i - \bar{\omega}) \\ \vdots \\ \sum_{i=1}^N (m_{ni} - \bar{m}_n)(\omega_i - \bar{\omega}) \end{bmatrix}_{n \times 1} \dots\dots\dots (\text{B-8})$$

If  $\omega^T$  is adapted as the truth indicator, then each ensemble member is updated using Eq. B-9. Superscripts  $p$  and  $u$  depict the prior and updated vectors:

$$\mathbf{m}_i^u = \mathbf{m}_i^p + \frac{(\omega^T - \omega_i)}{(1+r)} [\sum_{k=1}^N (\omega_k - \bar{\omega})^2]^{-1} \mathbf{C} \dots\dots\dots (\text{B-9})$$

For localization, the Schur product, which is an element-wise product of matrices with the same dimension, is used to reduce spurious correlation. If  $\Gamma$  is defined as the local support vector, then the updated member by covariance localization is calculated as:

$$\mathbf{m}_i^u = \mathbf{m}_i^p + \frac{(\omega^T - \omega_i)}{(1+r)} [\sum_{k=1}^N (\omega_k - \bar{\omega})^2]^{-1} (\mathbf{C} \circ \Gamma) \dots\dots\dots (\text{B-10})$$

The local support vector is a vector of zeros and ones that prevents updating in some locations which are assumed to be far from the monitoring or process data. The local data can also be selected of fractions between 0 and 1 for smoothing the predicted data.

## REFERENCES

- Aanonsen, S.I., Naevdal, G., Oliver, D.S., Reynolds, A.C., Valles, B. (2009): The ensemble Kalman filter in reservoir engineering - a review. *SPE Journal*, Vol. 14(3), 393-412.
- Akin, S. (2005): Mathematical modeling of steam-assisted gravity drainage. *SPE Reservoir Evaluation & Engineering*, SPE 86963-MS, Vol. 8(5), 372-376.
- Azad, A., Chalaturnyk, R.J. (2010): A mathematical improvement to SAGD using geomechanical modeling. *Journal of Canadian Petroleum Technology*, Vol. 49(10), 53-64.
- Azad, A., Chalaturnyk, R.J. (2011): Numerical study of SAGD: geomechanical-flow coupling for Athabasca oil sand reservoirs. In proceedings of the 45th US Rock Mechanics/Geomechanics Symposium, June 26-29, San Francisco.
- Butler, R.M., Stephens, D.J. (1981): The gravity drainage of steam-heated heavy oil to parallel horizontal wells, *The Journal of Canadian Petroleum Technology*, Vol. 20(2), 90-96.
- Butler, R.M. (1997): *Thermal Recovery of Oil and Bitumen*. Calgary, Canada, 528 p.
- Chalaturnyk, R.J. (1996): *Geomechanics of the Steam-Assisted Gravity Drainage Process in Heavy Oil Reservoirs*. PhD Thesis, University of Alberta, 576 p.
- Chilingarian, G.V., Mazzullo, S.J., and Rieke, H.H. (1996): *Carbonate Reservoir Characterization: A Geologic-Engineering Analysis - Part II*. Elsevier.
- Chung, K.H. & Butler, R.M. (1988): Geometrical effect of steam injection on the formation of emulsions in the steam-assisted gravity drainage process. *The Journal of Canadian Petroleum Technology*, 27(1), 36-42.
- Cokar, M., Kallos, M.S., Gates, I.D. (2011): A new thermogeomechanical theory for gravity drainage in SAGD. In *Proceedings of the World Heavy Oil Congress*, Edmonton, Canada, 6 p.
- Collins, P.M. (2007): Geomechanical effects on the SAGD process. *SPE Reservoir Evaluation & Engineering*. SPE 97905-PA, Vol. 10(4), 367-375.
- Davis, R.O., Selvadurai, A.P.S. (2002): *Plasticity and Geomechanics*. Cambridge University Press, New York, USA.
- Deutsch, C.V., Journel, A.G. (1997): *GSLIB: Geostatistical Software Library and User's Guide*. Oxford University Press, USA.
- Dusseault, M., Morgenstern, N. (1978): Shear strength of Athabasca oil sand. *Canadian Geotechnical Journal*. Vol. 15, 216-238.

- Edmunds, N.R., Kovalsky, J.A., Gittins, S.D., Pennacchioli, E.D. (1994): Review of phase A steam-assisted gravity-drainage test. SPE Reservoir Engineering. SPE 21529-PA, 9(2): 119-124.
- Edmunds, N.R., Chhina, N. (2001): Economic Optimum Operating Pressure for SAGD Projects in Alberta. Journal of Canadian Petroleum Technology. Vol. 40(12), 13-17.
- Evensen, G. (1994): Sequential Data Assimilation With a Nonlinear Quasigeostrophic Model Using Monte Carlo Methods to Forecast Error Statistics. Journal Geophysical Research, 99(C5), 10143–10162.
- Evensen, G. (2009): Data Assimilation: The Ensemble Kalman Filter. Springer, 2nd Edition.
- Gravdal, J.E., Lorentzen, R.J., Fjelde, K.K., Vefring, E.H. (2010): Tuning of computer model parameters in managed-pressure drilling applications using an unscented-Kalman filter technique, SPE Journal, SPE 97028-PA, Vol. 15(3), 856-866.
- Hetnarski, R.B., Eslami. M.R. (2008): Thermal Stresses – Advanced Theory and Applications. Springer, New York, USA.
- Kalman, R.E. (1960): A new approach to linear filtering and prediction problems. Journal of Basic Engineering, Vol. 82, 35-45.
- Li, P. (2006): Numerical Simulation of the SAGD Process Coupled with Geomechanical Behavior. Ph.D. dissertation, University of Alberta.
- Oliver, D.S., Reynolds, A.C., and Liu, N. (2008): Inverse Theory for Petroleum Reservoir Characterization and History Matching. Cambridge University Press.
- Phale, H.A., Oliver, D.S. (2010): Data Assimilation Using the Constrained Ensemble Kalman Filter. SPE Journal. SPE 125101-PA, Vol. 16(2), 331-342.
- Reis, J.C. (1992): A steam-assisted gravity drainage model for tar sands linear geometry. The Journal of Canadian Petroleum Technology, Vol. 31(10), 14-20.
- Tortike, W.S., Farouq Ali, S.M. (1993): Reservoir simulation integrated with geomechanics. The Journal of Canadian Petroleum Technology, Vol. 32(5), 28-37.
- Touhidi-Baghini, A. (1998): Absolute Permeability of McMurray Formation Oil Sands at Low Confining Stresses. Ph.D dissertation. Department of Civil Engineering, University of Alberta, 339 p.
- Vanegas P, J.W., Deutsch, C.V., and Cunha, L.B. (2008): Uncertainty assessment of SAGD performance using a proxy model based on Butler's theory, In the proceedings

of the SPE Annual Technical Conference and Exhibition, 21-24 September 2008, Denver, Colorado, USA, 21 p.

Welch, G., Bishop, G. (1995): An Introduction to the Kalman Filter, University of North Carolina, Department of Computer Science, TR 95-041.

Williams, G.J.J., Mansfield, M., MacDonald, D.G., and Bush, M.D. (2004): Top-down reservoir modeling. In proceedings of the SPE Annual Technical Conference and Exhibition, 26-29 September 2004, Houston, Texas, 8 p.

Zhai, D., Mendel, J.M., Liu, F. (2009): A new method for continual forecasting of interwell connectivity in waterfloods using an extended Kalman filter. SPE Western Regional Meeting, San Jose, California, 14 p.

Zhang, Y., Oliver, D.S. (2009): History Matching Using a Hierarchical Stochastic Model with the Ensemble Kalman Filter: A Field Case Study Authors. SPE Reservoir Simulation Symposium. SPE 118879-MS, 15 p.

Zubarev, D.I. (2009): Pros and cons of applying proxy-models as a substitute for full reservoir simulations. SPE Annual Technical Conference and Exhibition, SPE124815-MS, 23 p.

# CHAPTER 7: THE ROLE OF GEOMECHANICAL OBSERVATION IN CONTINUOUS UPDATING OF THERMAL RECOVERY SIMULATIONS USING THE ENSEMBLE KALMAN FILTER\*

## ABSTRACT

*In situ* thermal methods such as steam-assisted gravity drainage (SAGD) and cyclic steam stimulation (CSS) are widely employed in oil sand reservoirs. The physics of such thermal processes is generally well understood, and it has been shown that rock properties are highly influenced by the geomechanical behaviour of the reservoir during these recovery processes. Geomechanics improves the process dynamically, and its response can depict the progress of production within a reservoir. However, the potential of geomechanical monitoring for application to closed-loop reservoir optimization is not usually practiced. With increased implementation of highly instrumented wells and communication technologies providing real-time monitoring data from different sources, combining available data into reservoir-geomechanical simulations would improve updating numerical models and prediction process. This research explores effective uses of geomechanical observation data for history matching and types of geomechanical observation sources adequate for thermal recovery. The ensemble Kalman filter (EnKF), combined with an iterative geomechanical coupled simulator, has been chosen as the data assimilation algorithm to update the model continuously based on geomechanical observations. The results show that considering geomechanical modelling and observation improves the history matching process when geomechanics is an issue.

---

\* This paper was presented at the Canadian Unconventional Resources Conference held in Calgary, Alberta, Canada, 15–17 November 2011, SPE 146898-PP.

## INTRODUCTION

History matching usually refers to all adjustments applied to a reservoir simulation model to reproduce the reservoir's past behaviour. Although history matching is not the ultimate purpose of reservoir simulations, it is a crucial segment in closed-loop reservoir management. In reservoir engineering, production, injection, and pressure histories are generally claimed to be the effective features (objective functions) capturing the major elements of reservoir system behaviour. It is assumed that if these objective functions are closely matched, other adjusted parameters that are relatively impossible to monitor fully will be predicted with a good degree of confidence. Regardless of the employed history matching algorithm, inverse problems for highly nonlinear reservoir systems do not have a unique set of solutions. If the numerical adjustments, input population data, observation parameters, and type of simulation are chosen properly and closely constrained to the physics of the reservoir, the accuracy of the prediction is significantly improved.

When a thermal process is used for heavy oil recovery, the reservoir undergoes complex mechanisms that are apparently absent in conventional reservoirs. In addition to the flow process initiated by thermal conduction and convection, the reservoir experiences geomechanical changes in the same environment. The geomechanical behaviour of the reservoir causes stress-strain redistribution, reservoir deformation, ground surface heave, variation in rock properties, and deformation-disturbance in the caprock. These features occur parallel to the flow mechanism as components of the physics of the thermal process. Much research over the past thirty years has recognized the importance of geomechanics in steam-assisted gravity drainage (SAGD) and cyclic steam stimulation (CSS), which are both broadly employed in Canadian oil sand reservoirs. Extensive experimental studies by Dusseault and Morgenstern (1978), Agar et al. (1986), Scott and Seto (1986), Kosar et al. (1987), Oldakowski (1994), Scott et al. (1994), Chalaturnyk (1996), Samieh and Wong (1996), and Touhidi-Baghini (1998) established a very good understanding of the geomechanical behaviour of oil sand under thermal and non-thermal conditions and its influence on hydraulic properties such as absolute permeability and porosity.

These results opened the window for further studies in numerical modelling. Tortike (1991), Chalaturnyk (1996), Settari et al. (2001), Li (2006), and Du and Wong (2007) are amongst the researchers who investigated different aspects of coupling flow and geomechanics. They developed different methodologies including decoupled, iteratively coupled, and fully coupled simulations with reasonable agreement to real cases. Li and Chalaturnyk (2009) matched the histories resulting from an iteratively coupled simulation with those of the Underground Test Facility (UTF), a pilot project initiated in the mid-1980s. Because the physics is better honored in a geomechanical-flow simulation, they declared that the geomechanical consideration effectively improves the history matching process and, more importantly, explains the history of changes within the reservoir and the rock properties. Not only was the history better matched, but the system was better calibrated for future forecasting. Chalaturnyk and Scott (1995), Chalaturnyk and Li (2004), and Collins (2007) have provided guidance on geomechanical issues in thermal recovery processes.

Chang et al. (2010) studied the effect of geomechanical monitoring data on history matching processes using the EnKF. For thermal recovery, there are few public studies in closed-loop reservoir management. Chitralkha et al. (2010) and Gul et al. (2011) successfully applied the ensemble Kalman filter algorithm for the purpose of reservoir characterization and history matching. They demonstrated the efficiency of EnKF for history matching using several synthetically generated heterogeneous models under SAGD. However, the potential of geomechanical monitoring is not considered in their work. With the increased implementation of highly instrumented wells and communication technologies providing real-time monitoring data from different sources (e.g., pumps, observation wells, microseismic), combining available data in reservoir-geomechanical simulations would improve prediction processes and the updating of numerical models.

Consequently, this paper explores: (1) how geomechanical observation data can be used effectively for history matching and reservoir characterization purposes in thermal recovery and (2) types of geomechanical observation sources adequate for thermal recovery. The EnKF, combined with an iterative geomechanical coupled simulator, has been chosen as the data assimilation algorithm to update the model

continuously based on geomechanical and flow observations. This workflow is explored in a 2D SAGD model. Three schemes are considered for simulation: (1) Geomechanical coupled simulation with both types of data (flow and geomechanical); (2) Geomechanical coupled simulation with flow data only; and (3) Flow simulation with flow data only.

## **ITERATIVE FLOW-GEOMECHANICAL SIMULATION IN THERMAL RECOVERY**

Iterative (or sequential) simulation is one of the practical coupling techniques successfully used for modelling thermal processes in petroleum engineering (e.g., Tran et al., 2005). In this technique, a flow simulator is sequentially combined with a geomechanical solver. As shown in Fig. 1(a), at each time step within a simulation loop, temperature and pressure are extracted from the reservoir simulator results and translated to be readable by a geomechanical simulator. The geomechanical simulator takes the temperature and pressure values as inputs for the current time step and determines the volumetric strain. Volumetric strain is the source of the changes in permeability and porosity and is used for updating rock properties based on any empirical or theoretical assumptions. The changes, however, are not limited to permeability and porosity. Other rock properties such as relative permeability curves can also be updated. Usually two separate grids are generated for the reservoir model and the geomechanical model. Fig. 1(b) compares the dimensions of a geomechanical grid for a general problem with those of a reservoir grid.

Because geomechanics influence a region larger than the reservoir, an extended grid is required to capture the geomechanical changes. Depending on the purposes of the simulation, it is sometimes necessary to include all of the geological formations on top of the reservoir up to ground level, as well as the layers underneath the reservoir. However, for flow simulation, it is usually adequate to model the region inside the reservoir formation that has been affected by the thermal. Cell (block) sizes are not essentially the same in both grids. The reservoir cells are smaller than those depicted for a geomechanical simulation. Cell sizes are chosen to help the numerical solution phase, with the following considerations: (1) the cells should be small enough to

capture the physics of the problem in those regions where the changes are significant, (2) the cells should be large enough to save computational time, (3) the cell sizes should be in a range in which the numerical simulation does not encounter instability in convergence. More guidance on stability, accuracy, and efficiency of sequential methods is provided in Kim et al. (2011).

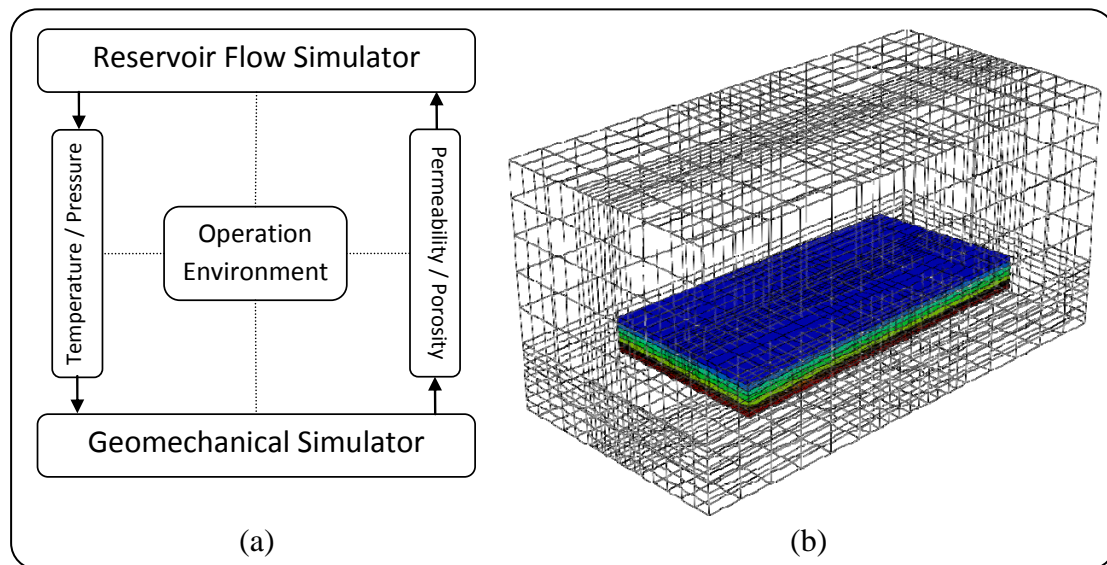


**Figure 1: (a) Iterative reservoir-geomechanical simulation loop, (b) position of reservoir grids surrounded by geomechanical grids.**

For thermal recovery simulation, this study uses the iterative flow-geomechanical coupling methodology previously presented by the authors (Azad and Chalaturnyk, 2011). The methodology sequentially couples two commercial simulators, considering changes in permeability and porosity only. For updating rock properties, it adopts the formulation proposed by Touhidi-Baghini (2008) established from experimental laboratory test results.

## **HISTORY MATCHING AND DATA ASSIMILATION USING THE ENKF**

With advances in smart technology, oil fields are expected to be intelligently managed using closed-loop reservoir optimization. The framework of this process consists of two elements: reservoir optimization and data assimilation. Prior to running optimization procedures to maximize production or minimize financial objective functions, data assimilation algorithms are utilized for history matching. Data assimilation adjusts the reservoir model consistent with the reality of the

geological model while honoring the historical behaviour of the reservoir. In other words, data assimilation attempts to update the geological model and reduce uncertainty in reservoir properties. Due to the complexity of fluid flow, especially when geomechanical effects are considered in a thermal process, it is never easy to determine a set of reservoir parameters to achieve a perfect match. However, great progress has been made recently in the area of inverse theories, and thus in the automation of history matching. Good history matching is now feasible for the cost of monitoring real-time data and multiple reservoir realization runs. As one of the various ensemble-based data assimilation tools, the EnKF offers a rigorous algorithm that is shown to be suitable (e.g., Nævdal et al., 2005, Gu and Oliver, 2006) for large-scale nonlinear dynamic systems. The EnKF is a sequential estimator that uses the Monte Carlo approach in which the covariance matrix (the correlation between reservoir response and reservoir variables) is estimated using the ensembles rather than the model. The EnKF algorithm has two major steps: (1) prediction, and (2) assimilation (or correction), in which the variables describing the state of the reservoir are estimated (or corrected) to honour the monitoring data.

Each ensemble (or state vector,  $y$ ) contains both static and dynamic variables such as permeability, porosity, bottom-hole pressure, production rates, etc. The collection of ensembles is denoted as  $Y$ , as suggested by Gu and Oliver (2006) in Eq. 1.

$$Y = [y_1, y_2, \dots, y_j, \dots, y_{N_e}] \dots \dots \dots (1)$$

in which:

$$y_j = [m_j^T, d_j^T]^T \dots \dots \dots (2)$$

where  $m$  is the model variable vector,  $d$  is the monitoring data vector, and  $N_e$  is the number of ensembles. The covariance matrix in the EnKF can then be calculated between ensembles using the standard covariance formulation as in Eq. 3:

$$C_Y^p = \frac{1}{N_e - 1} (Y^p - \bar{y}^p)(Y^p - \bar{y}^p)^T \dots \dots \dots (3)$$

where  $C$  is the prior (superscript  $p$ ) covariance matrix and  $\bar{y}$  is the mean of state vectors across the ensembles' members. At each time step, ensembles are updated

using the Kalman gain matrix,  $K$ , and the prior values are replaced by the updated (prescribe  $u$ ) values as:

$$y_j^u = y_j^p + K(d_j - Hy_j^p) \quad (j = 1, 2, \dots, N_e) \dots\dots\dots(4)$$

In Eq. 4,  $H$  is a trivial matrix whose components are 0 and 1 only. Gu (2006) has discussed more details of the EnKF theory and has provided a step-by-step calculation procedure.

Besides all of the advantages of the EnKF, the algorithm has some shortcomings that can lead to filter divergences. (1) When the covariance between the ensembles or between the variables is small, much noise is injected into the estimation process that reduces the algorithm's sensitivity to the observation data. This can lead to unrealistic estimations. (2) When the number of observations is large, the algorithm's performance is significantly reduced. This happens because the rank of the covariance matrix is less than or equal to the number of state variables. (3) Because of the approximation style of the EnKF, updates are built on a linear combination of the predicted ensembles. This limits the prediction to the space populated by the previous forecasts. (4) Use of finite ensemble size to calculate the error covariance produces spurious correlations in large-scale models or uncorrelated variables. This causes underestimations and nonphysical updates. More details on these techniques for improving the EnKF algorithm can be found in Chen (2008), and the leading state of the art information can be found in Evensen (2009).

### **CASE STUDY I: SHALLOW TRIPLE SAGD**

The first case study is of a shallow reservoir under the SAGD process. Three sets of injectors and producers are considered to mimic Phase A of the UTF pilot test (Edmunds et al., 1994). Two reservoir variables are assimilated in this problem: (1) permeability that is used in the flow simulator, and (2) modulus of elasticity that is used in the geomechanical simulator. The initial ensembles are stochastically generated and constrained to two sets of spatial synthetic data.

## Stochastic Realizations for Permeability and Modulus of Elasticity

In an area of 100 metres by 30 metres and 20 metres depth, nine wells were considered and two data sets were synthetically generated for each well, one for modulus of elasticity and the other for permeability. The well location map is very similar to that of the UTF-A pilot test. Fig. 2 shows histograms of the data sets, generated with real data (especially in the case of permeability) to keep them in a practical range approximating the rock properties of Canada's Athabasca oil sands. GSLIB (Journel and Deutsch, 1997) was used for the geostatistical study of the generated data.

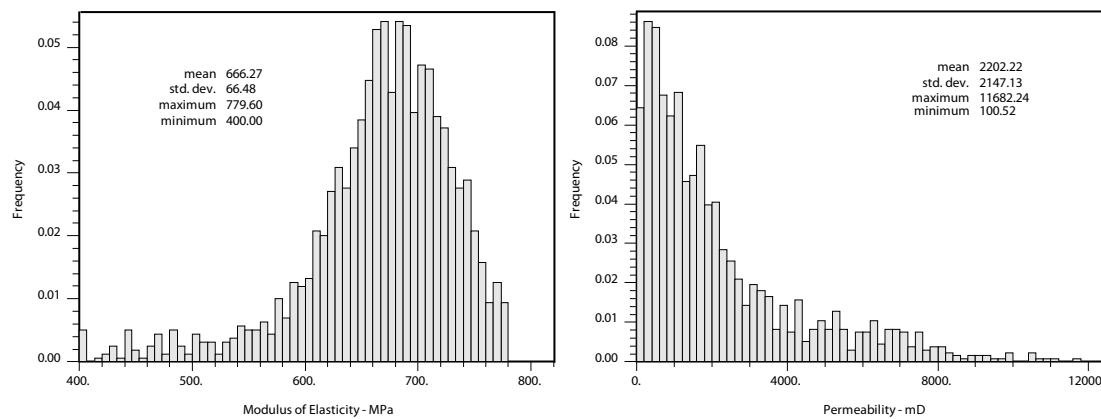


**Figure 2: Histograms of the synthetic data sets: modulus of elasticity (left) and permeability (right).**

Variograms were constructed in three principal continuity directions; the major and minor horizontal directions, and the vertical direction. Fig. 3 shows the semivariograms for each data set in normal score space. The variograms are quite similar in terms of range and nugget effects. However, the fitted structures (functions) are different, especially in major horizontal and vertical directions.

For each data set, 101 realizations were generated using the sequential Gaussian simulation technique. The E-type mean and variance of the first 100 realizations for each data set are plotted in a 3D model in Fig. 4 and 5 in the original data space. The E-type mean estimates the point-by-point average of the realizations, and the variance shows the variance of the conditional distribution.

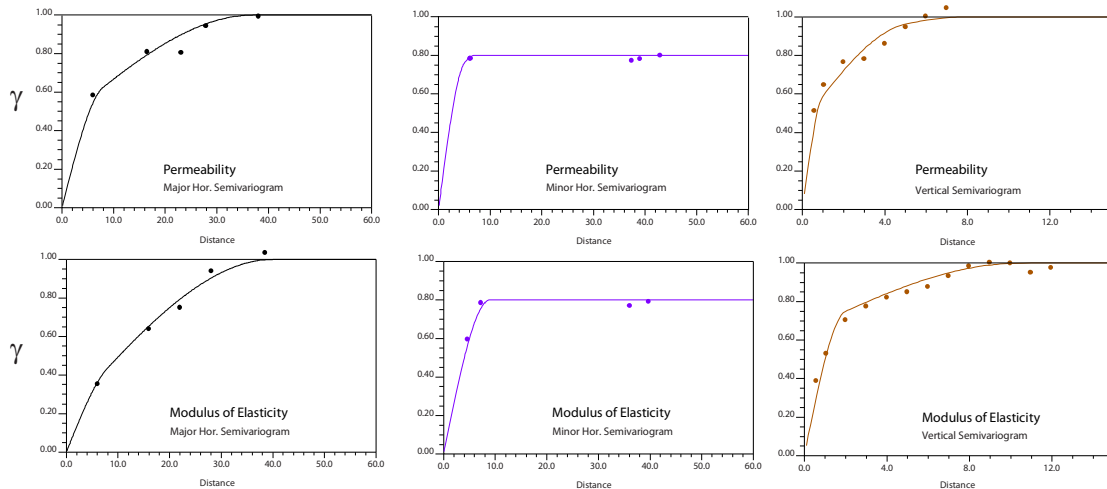


**Figure 3: Semivariograms for each data set in three principal continuity directions.**

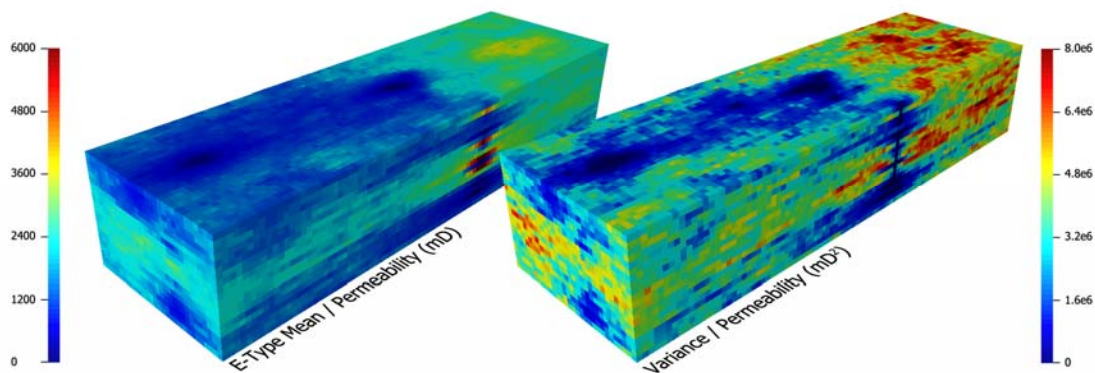


**Figure 4: E-type mean and variance of the 100 stochastic realizations for permeability.**

Variance is almost negligible at the well locations, showing the fact that there is no uncertainty in rock properties at those locations. The last realization from each data set (the 101<sup>st</sup>) is taken as the truth model and is used to generate the true production history. This means that the two rock properties estimated in this problem are constrained by the same prior geological data as are the true rock property populations.

In this study, it is assumed that permeability and modulus of elasticity are not correlated and that the synthetic data sets as well as the stochastic realization were not co-generated. In practice, an indirect relation between permeability and modulus of elasticity might be defined for specific known rocks. However, in general there is no theoretical correlation between these two rock properties.

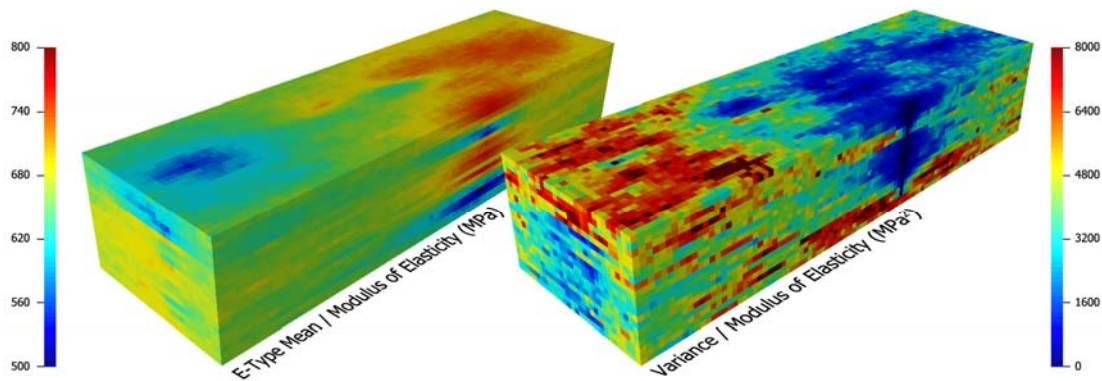


**Figure 5: E-type mean and variance of the 100 stochastic realizations for modulus of elasticity.**

### **Geomechanical flow simulation of the truth model**

The iterative flow-geomechanical technique was chosen for the case study to simulate the truth model. The problem was explored in a two-dimensional SAGD process with three borehole pairs. One vertical slice from each stochastic model (the 101<sup>st</sup> realization) was selected and the rock properties for each simulator were extracted. The reservoir is 100 metres wide and 20 metres thick. Fig. 6 shows the location of the reservoir grid boundary within a geomechanical model (usually known as the mechanical earth model, or MEM) with three layer-cake geological formations. Dimensions of the geomechanical and reservoir models were plotted on the same figure and selected to avoid any boundary effects. As soon as the model reactions (affected zone) near boundaries, simulation error increases. The boundaries of the flow model were chosen far from those of the largest probable steam chamber during the problem run time. For the geomechanical model, vertical displacement or stress concentration can be good criteria for boundary states. As long as vertical displacements at the boundaries are negligible, the model experiences the least error. Therefore, the geomechanical model designed wide enough as well as deep enough to catch the geomechanical changes all around the SAGD process and to avoid unrealistic results.

The three geological layers have been labeled in Fig. 6 by overburden, reservoir, and underburden. Overburden and underburden layers were considered to behave elastic. It means that no plastic deformation occurs in these two layers. This assumption

simplifies the model and prevents any failure in the caprock which is not the focus of this research. In real studies, more details of caprock and a realistic rock behavior are needed to be considered in the coupled simulation. The reservoir formation rests on a stiff Devonian limestone. It has been shown that oil sand behavior is strain-softening because of its interlocked grain structure. In this problem the Mohr-Coulomb model, an elastically-perfect plastic constitutive model, was chosen to represent the geomechanical behaviour of the oil sand (reservoir) formation.

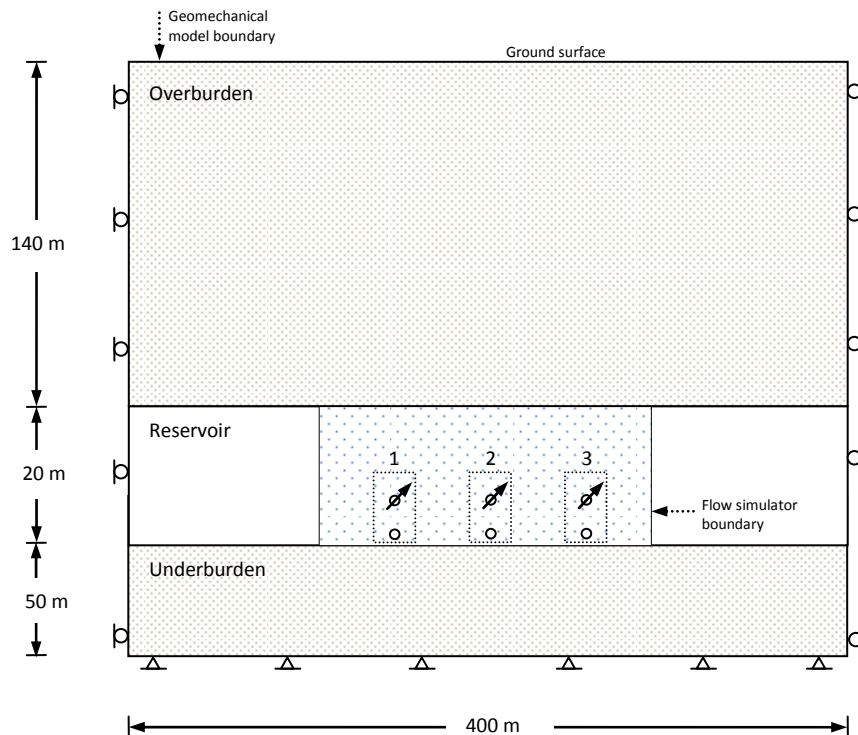


**Figure 6: Truth flow-geomechanical coupled model: dimensions and boundary conditions.**

Inside the part of the reservoir shared with the geomechanical grid, 2000 1×1-metre cells are equally distributed, occupying an area 100 cells along the horizontal direction and 20 cells in depth. At each time step, these cells interactively share temperature and pressure readings, exporting them into the geomechanical model. Permeability and porosity measurements are updated in return.

Physical properties of the geological layers shown in Fig. 6 are listed in Table 1. The information in Table 1 is used for geomechanical simulation. The minimum and

maximum horizontal stress gradients are also included. Some of the important properties of the flow simulation are listed in Table 2.

**Table 1: Physical properties of geological layers.**

	Parameter	Unit	Value
Overburden	Constitutive model	-	Linear elastic
	Bulk density	$kg/m^3$	2200
	Bulk modulus, $K$	$MPa$	667
	Shear modulus, $G$	$MPa$	308
	Module of elasticity, $E$	$MPa$	800
	Poisson's ratio, $\nu$	-	0.3
	Coefficient of linear thermal expansion	$^{\circ}K^{-1}$	$2 \times 10^{-5}$
Reservoir	Constitutive model	-	Elastoplastic – Mohr Coulomb
	Bulk density	$kg/m^3$	2200
	Module of elasticity, $E$	$MPa$	Stochastic realization
	Poisson's ratio, $\nu$	-	0.3
	Cohesion	$MPa$	0
	Friction angle	$^{\circ}$	60
	Dilation angle	$^{\circ}$	15
	Coefficient of linear thermal expansion	$^{\circ}K^{-1}$	$2 \times 10^{-5}$
Underburden	Constitutive model	-	Linear elastic
	Bulk density	$kg/m^3$	2200
	Bulk modulus, $K$	$MPa$	4167
	Shear modulus, $G$	$MPa$	1923
	Module of elasticity, $E$	$MPa$	5000
	Poisson's ratio, $\nu$	-	0.3
All	Coefficient of linear thermal expansion	$^{\circ}K^{-1}$	$2 \times 10^{-5}$
	Min. horizontal stress, ratio	-	1
	Max. horizontal stress, ratio	-	2
	Initial pore pressure	$kPa$	550

Histories of oil production and steam/oil ratio (SOR) over 800 days are plotted in Fig. 7. Each subplot in Fig. 7 compares the result of a coupled and an uncoupled (flow only) simulation, confirming that the production rate is higher in a coupled simulation than in an uncoupled simulation. As a result, when oil production is higher, SOR is lower and stays in a realistic range between 1.8 and 2.4.

The difference between the coupled and uncoupled simulation results can be explained by the geomechanical behaviour of the reservoir rock. Chalaturnyk (2006) showed that in a region close to and in advance of the steam chamber, horizontal stress is thermally induced and pore (fluid) pressure increases. These are the source of unbalanced force in the system that produces volumetric strains, mostly in front of the

steam chamber. In this region, permeability and porosity change, and the process rate (steam chamber growth) is improved.

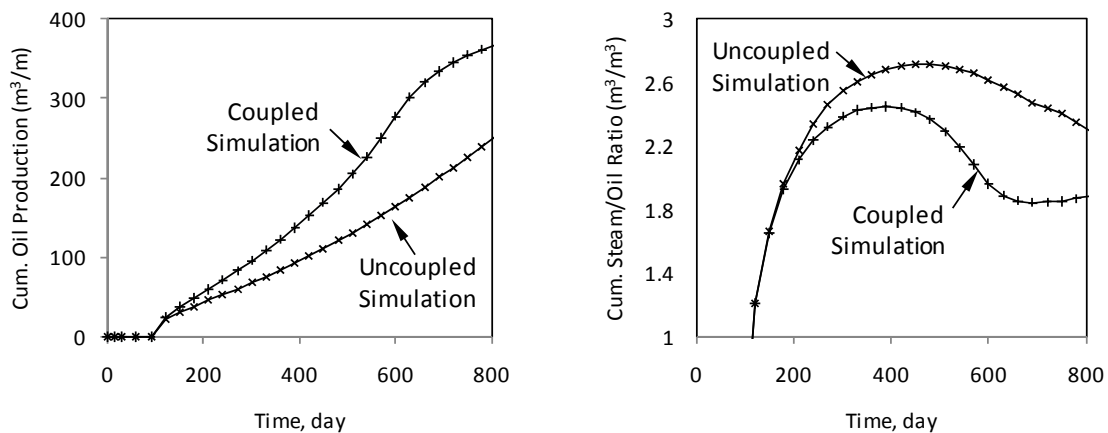


**Figure 7: Oil production (left) and steam/oil ratio (right) for the triple shallow SAGD case study: coupled and uncoupled results.**

In general, rock properties do not necessarily increase. However, due to the dilative behaviour of dense sands (in this case, oil sand) and the reduction in effective stress caused by the increase in pore pressure, dilation is most probably expected. This means that porosity and permeability usually improve in locations close to the steam chamber, and that the steam chamber occupies a larger area in a shorter period of time.

Fig. 8 compares the temperature profile after 300 days of simulation run inside the reservoir for coupled and uncoupled analyses. This clarifies that the steam chamber grows faster when improvements in rock properties are modelled through a geomechanical coupling simulation. The geomechanical behaviour of oil sand is not the only basis for improvement in rock properties. Chalaturnyk (2006) explained that in a zone between two steam chambers, horizontal stress is high enough to cause shear failures. While the steam chambers are growing, the shear failure zone gradually appears between every two injectors. The result of the triple SAGD plotted in Fig. 7 is relatively higher than that of the same process for single SAGD reported by Azad and Chalaturnyk (2011). This is mainly because of the shear failure zone between the well pairs, which hardly occurs in single SAGD processes.

From another point of view, the temperature profile of the coupled simulation in Fig. 8 is very similar to that of the UTF-A. Differences between the UTF-A and this

model (e.g., in well placement, operational schedule and duration, start-up phase) make conclusions difficult to draw. In reality, the UTF-A injection program is not continuous and simultaneous for the three injectors. However, similarities in the temperature profile confirm that the designed problem clearly represents the basics of the SAGD process for this case study.

**Table 2: Rock properties for reservoir simulation.**

Parameter	Unit	Reservoir
Porosity	%	32
Permeability	<i>mD</i>	Stochastic realization
Horizontal/Vertical permeability ratio	-	4
Initial oil saturation	%	85
Initial water saturation	%	15
Initial gas saturation	%	0
Initial temperature	°C	10
Rock compressibility	<i>1/kPa</i>	$5 \times 10^{-6}$
Rock expansion coefficient	$^{\circ}\text{C}^{-1}$	$3.84 \times 10^{-5}$
Rock heat capacity	<i>kJ/kg °K</i>	1865
Rock thermal conductivity	<i>W/m °K</i>	1.736
Initial reservoir pressure	<i>kPa</i>	550
Injection pressure	<i>kPa</i>	2500
Preheating and start-up duration	<i>day</i>	90
Steam quality	%	95
Steam trap difference	°C	10
Producer-Injector spacing	<i>m</i>	3
Injector spacing	<i>m</i>	25

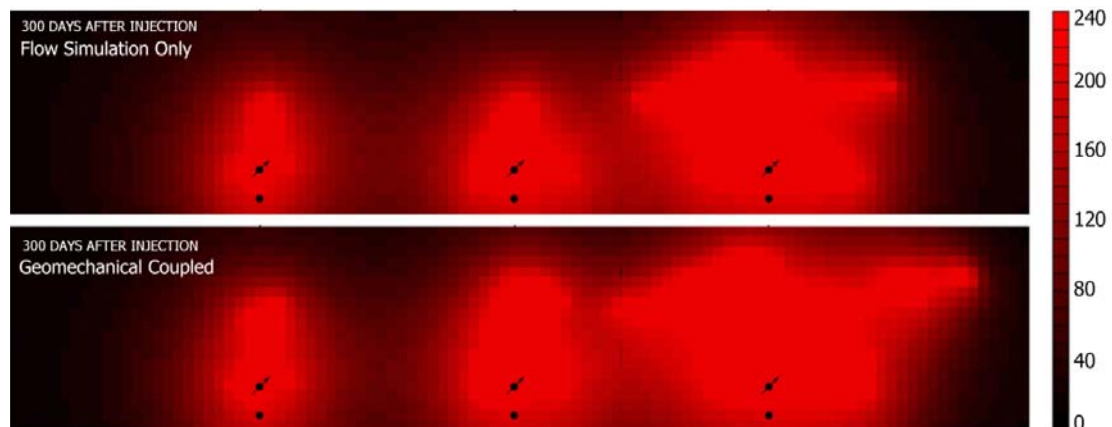


**Figure 8: Steam chamber growth after 300 days, temperature profile (°C): uncoupled simulation (top) and coupled simulation (bottom).**

### Solution Workflow and Settings

The output data from the coupled simulation that uses the true (reference) rock properties are referred to as monitoring data. The monitoring data for this problem falls in two categories: (1) oil production and steam injection rates for each borehole pair (flow observation data), and (2) vertical displacements at 14 locations that are equally distributed on the ground surface (geomechanical observation data). Hence, a total of 20 monitoring variables are defined. The first category is flow observation data and in the second category is geomechanical observation data. At the same time, permeability and modulus of elasticity are assimilated in 2000 cells, meaning that the model variable vector has 4000 elements. When all monitoring data is utilized and both rock properties are assimilated, the model variable and monitoring vectors are written as:

$$m_j^T = [\ln k_{j,1}, \dots, \ln k_{j,2000}, E_{j,1}, \dots, E_{j,2000}]_j^T \quad (j = 1, 2, \dots, 100) \quad \dots\dots\dots (5)$$

$$d_j^T = [q_{o,1}, q_{s,1}, q_{o,2}, q_{s,2}, q_{o,3}, q_{s,3}, \Delta H_1, \dots, \Delta H_{14}]_j^T \quad (j = 1, 2, \dots, 100) \quad \dots\dots\dots (6)$$

The model is run using three strategies: (1) flow simulation with flow monitoring data, (2) coupled simulation with flow monitoring data, and (3) coupled simulation with flow and geomechanical monitoring data. Therefore, the size of both the monitoring data vector and the model variable vector differ in each strategy. Monitoring data is obtained every 30 days, starting at Day 100 when uncoupled simulation is used. Because monitoring data usually contains different sources of measurement errors, a standard deviation was assumed for each item (Table 3).

Permeability and modulus of elasticity are dynamic properties and are updated at each cell during the process. Therefore, the dynamic values for both properties are assimilated at each update. This causes a conflict in the geomechanical modelling. The dynamic trend of the permeability is supposed to be defined by the result of geomechanical simulation, meaning that, permeability does not necessarily follow the volumetric strain at each update. More importantly, if it is updated in the middle of a geomechanical simulation, the initial tangent modulus of elasticity does not affect model behaviour.

Gu and Oliver (2006) reported a problem in which a part of the physics was not honoured for dynamic model properties. They showed that water saturation as a dynamic property is assimilated out of the physical range, and concluded that in stepwise assimilation, mass balance is not properly honoured. They suggested iterating the update at each step to remediate the problem.

**Table 3: Measurement errors for each monitoring data**

Monitoring item	Unit	Standard Deviation
Displacement	mm	5
Oil production rate	m <sup>3</sup> /day	0.01
Steam injection rate	m <sup>3</sup> /day	0.01

For the purposes of this study, only static properties are assimilated. At each time step, the initial permeability and modulus of elasticity are updated and the simulation is rerun from the beginning. Throughout this paper, this is called a flash back run. Flash back runs are not applicable when the uncoupled simulation is used and permeability is assimilated only. In this case, permeability is dynamically assimilated. In addition, localization technique or other modifications are not applied to improve history matching. This is essential for comparing the results of different strategies.

### History Matching Results

Production and injection histories of coupled simulations for the 100 ensembles are plotted in Fig. 9. For comparison, each subplot includes the history of the truth model shown in a bold solid line. Although the initial ensembles are constrained to the prior well data, they produce a wide range of uncertainty in production and injection for this particular model. Although the trend of the 100 histories in each subplot is quite similar to the truth model, in many cases, especially for boreholes pair 2, the results are relatively different from the truth model.

The EnKF history matching results are illustrated in Fig. 10 for the first strategy. Compared to the uncertainty that exists in initial ensembles, the EnKF has efficiently shifted the histories by updating permeability. In the first strategy, the flow data is monitored only and dynamic permeability is assimilated instead. Fig. 10 shows that the history can be matched closely to reality without considering geomechanics. Although the history matching has been done improperly in some time intervals in

subplots for borehole pairs 2 and 3, in general it is acceptable. Since the quality of history matching can be further improved using modification techniques and localizations, we evaluate the results visually for comparison. Moreover, some of the noise or mismatch in Fig. 10 comes from the amount of uncertainty in the initial ensembles. Compared to Fig. 9, the results of history matching using the first strategy can be assessed as reasonably accepted.

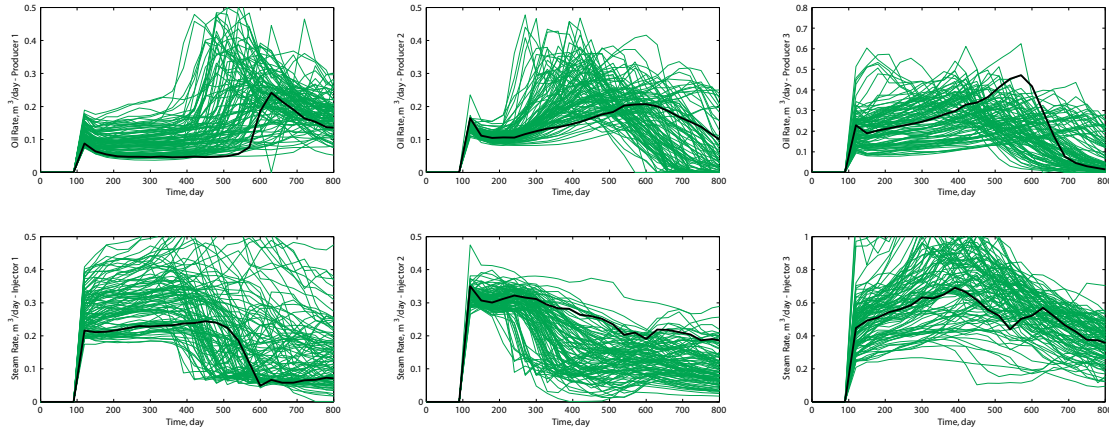


**Figure 9: Coupled flow-geomechanical simulation results using initial ensembles.**

On average, history matching results from the first and second strategies do not differ. All six histories are plotted in Fig. 11. No meaningful improvements are seen in the second strategy, and the histories deviate notably from the truth in the primary stages. Flow monitoring data is obtained in the second strategy as well as the first, but a coupled simulation is used with the EnKF to assimilate static properties. Such comparisons confirm that spending more for a coupled simulation does not improve the history matching process. Although geomechanics is supposed to lead the physics of simulation closer to reality, the assimilated data is twice more than the first strategy with the same monitoring data. Therefore, it is not beneficial to expend more computing effort for no improvement in history matching. There are significant improvements when coupled simulations are used with flow and geomechanical data while permeability and modulus of elasticity are assimilated by the EnKF algorithm. Fig. 12 reproduces all six plots for the third strategy. A visual comparison between the results of the three strategies clarifies that the histories are entirely matched in the third strategy without a serious deviation detected. In addition, the mismatches seen in the primary stages of the process in the other two strategies are effectively treated

by the EnKF in the third strategy (Fig. 12). Although history matching is just one part of the scenario, and the results of data assimilation should also be evaluated, it is clear that considering the geomechanical data, working with a coupled simulator has efficiently facilitated history matching without additional algorithm treatment.

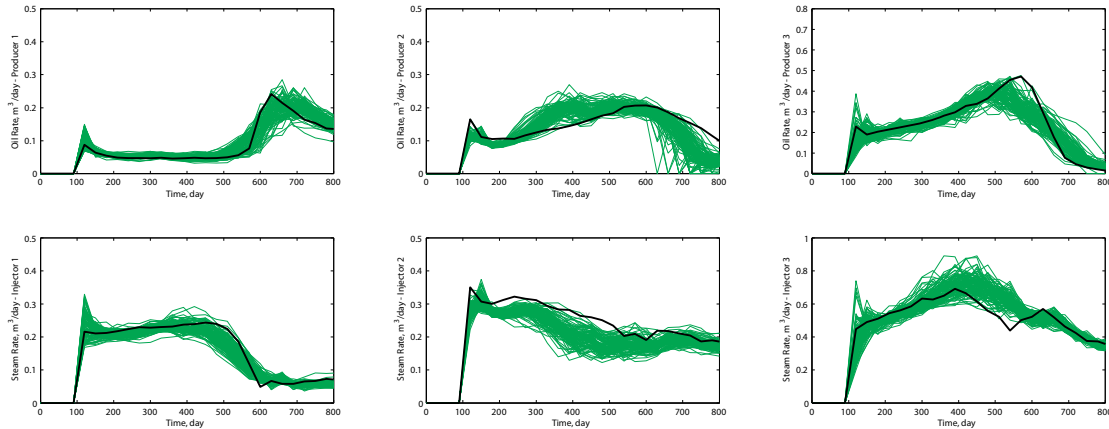


**Figure 10: History matching results for the first strategy: flow monitoring data and assimilation of dynamic permeability using only flow simulation.**

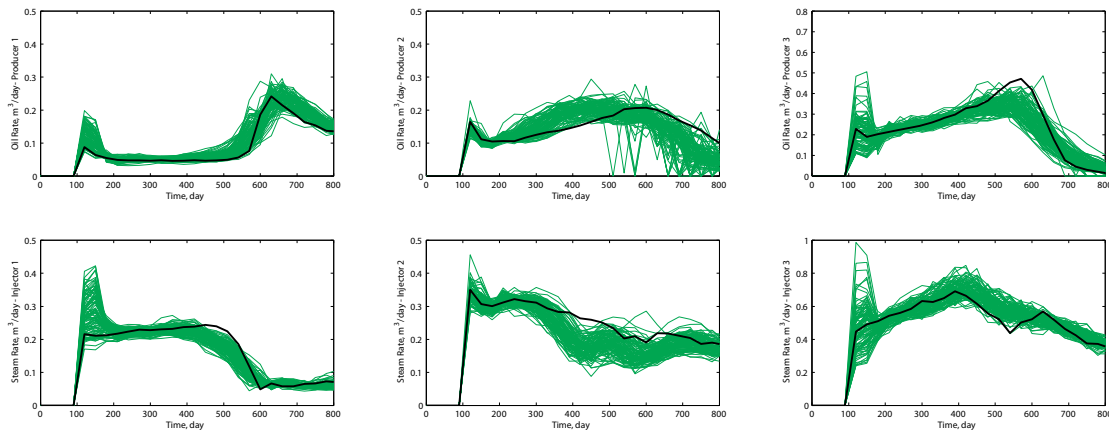


**Figure 11: History matching results for the second strategy: flow monitoring data and static assimilation of permeability and modulus of elasticity using flow-geomechanical coupled simulation.**

Results of the overall cumulative SOR and vertical displacements at the ground surface for the third strategy are plotted in Fig. 13. The two plots in the first row include the results of 100 coupled simulations using the initial ensembles. The effect of the history matching algorithm and monitoring data on these two parameters (variables) is illustrated in the second row in Fig. 13. SOR and vertical displacement histories are precisely matched. In Fig. 13, the displacement profile at the ground

surface is plotted at Day 700. The displacement profile at other time steps has quite the same trend. Generally, Fig. 13 shows that flow and geomechanics are well honoured at the same time.

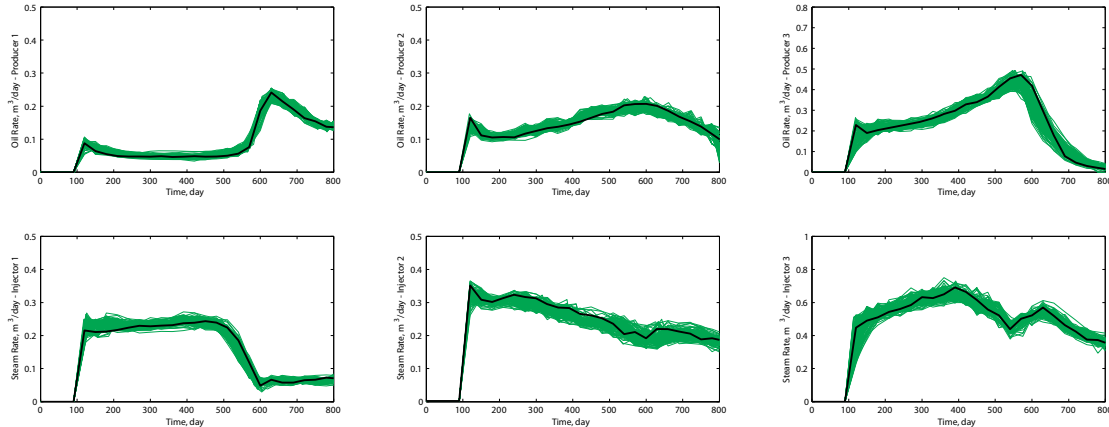


**Figure 12: History matching results for the third strategy: flow and geomechanical monitoring data and static assimilation of permeability and modulus of elasticity using flow-geomechanical coupled simulation.**

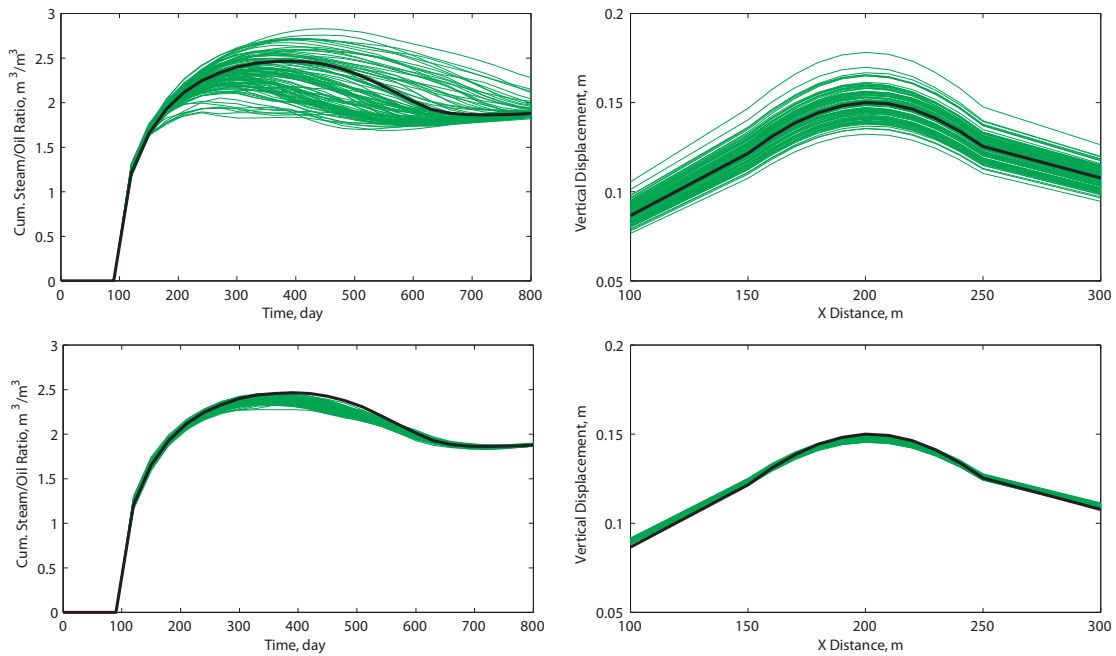


**Figure 13: History matching results: overall cumulative SOR (left) and vertical displacement profile (right) at ground surface at 700 days before (top) and after (bottom) applying the EnKF algorithm in the third strategy.**

The history matching results show the third strategy as the most efficient combination of monitoring data and simulation method of analysis. It seems that when geomechanical flow coupled simulation is run and static properties are assimilated

considering both sources of data, the EnKF can better control the history matching process. This judgment needs to be confirmed by assessing the assimilation results.

### Data Reproduction Results

While the history of the monitoring data is matched by the EnKF algorithm, rock properties are assimilated too. In general, even perfect history matching is not helpful if system variables are not properly predicted. At each time step, the 100 ensembles are adjusted (or predicted) for better history matching, while the correction results must be assessed. Although the truth model of this synthetic case study is available, comparing the predicted rock property population in the reservoir with the truth model is not quite simple and requires statistical study of dynamic models. Deterministic parameters alone are not usually practical to characterize the quality of assimilated data. Probabilistic analysis is required. For the current synthetic case study, however, the major purpose is to compare the prediction outcome of different strategies. Therefore, at any time step,  $t_k$ , a single indicator ( $\xi$  in Eq. 8) is introduced for each ensemble,  $j$ , to evaluate the error embedded in the predicted data as:

$$\delta_{i,j} = m_{i,j} - m_{truth,i} \quad (i = 1, 2, \dots, N_m \text{ and } j = 1, 2, \dots, N_e) \quad \dots\dots\dots(7)$$

$$\xi_j = \sqrt{\frac{1}{N_m} \sum_{i=1}^{N_m} (\delta_{i,j})^2} \quad (j = 1, 2, \dots, N_e) \quad \dots\dots\dots(8)$$

where  $\delta$  is the mismatch vector of the model variables,  $\xi$  is the error index value, and  $N_m$  is the number of ensemble elements. It should be noted that the error index is defined at each time step for each ensemble. However, the time dependence of the variables has been neglected for notational simplicity. Hence, the error index vector at  $t_k$  is written as:

$$\xi = [\xi_1 \quad \dots \quad \xi_j \quad \dots \quad \xi_{N_e}]_{t_k} \quad \dots\dots\dots(9)$$

The elements of the error index vector,  $\xi$ , represent the error value of each ensemble. At each time step, this vector is calculated and the mean and standard deviation of the vector elements are determined. These two values are chosen here to indicate the quality of data assimilation. These two values are supposed to become smaller by data

monitoring and the EnKF algorithm. It should be pointed out that the truth vector of model property,  $m_{truth}$ , is not constant in the first strategy. In this case, at each update time step the vector is dynamically replaced by the truth rock property of that time step. Consequently, the error index vector calculates the dynamic properties error rather than the static properties error.

Fig. 14 illustrates the variation of the mean and standard deviation of modulus of elasticity and permeability in the period of monitoring and history matching. Modulus of elasticity is predicted in the second and third strategies, while permeability is assimilated in all three strategies. From Fig. 14 two different trends are depicted: (1) When dynamic data is assimilated in the first strategy, the general trend of the mean and standard deviation is to deviate from the ideal value, 0. (2) In the second and third strategies, however, both the mean and standard deviation are reduced.

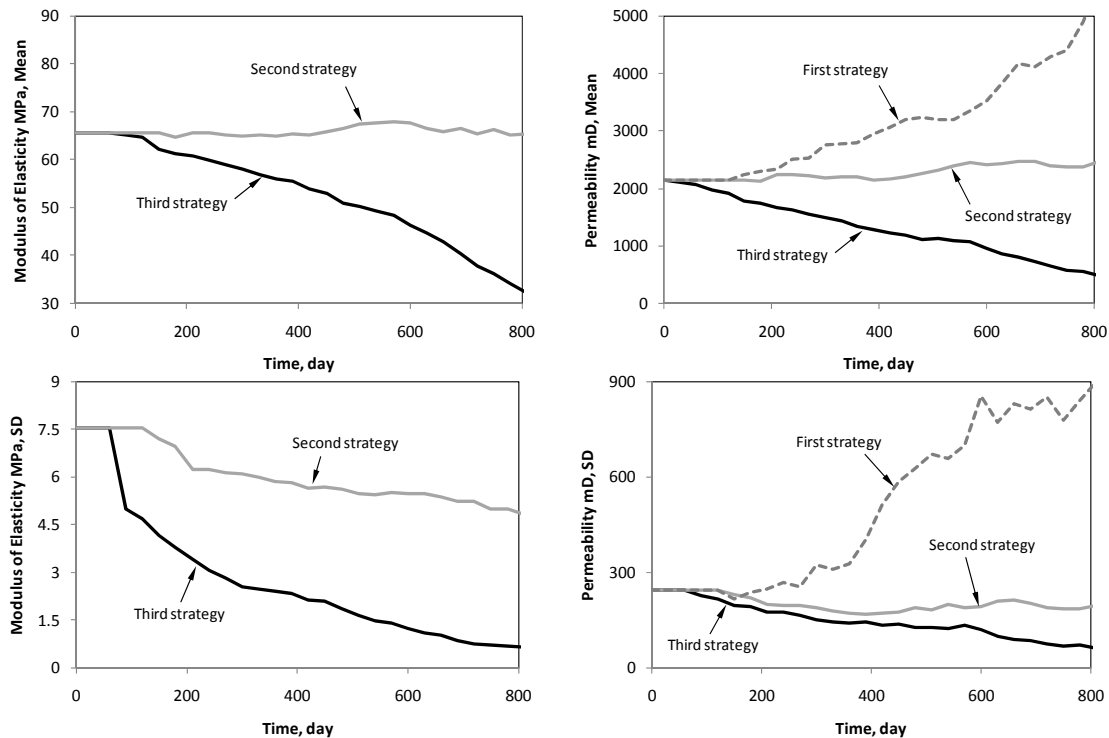


**Figure 14: Variation of mean (top) and standard deviation (bottom) of assimilation error: modulus of elasticity (left) and permeability (right).**

It is interesting to note the difference between the first and second strategies using error values defined in Eq. 9. While the history matching results are similar in the first and second strategies, the assimilation data analysis provides another aspect of

the estimation process. It seems that data is better predicted when flow data is monitored and a coupled simulator is used. Fig. 14 clarifies that the second strategy is beneficial when data assimilation is at a high level of importance. The second strategy is better when no geomechanical data is available. However, the results of the third strategy confirm that when both data sources are combined with a coupled simulator, both history matching and data assimilation perform considerably better than when geomechanical data is not monitored. This phenomenon is also reported by Chang et al. (2010).

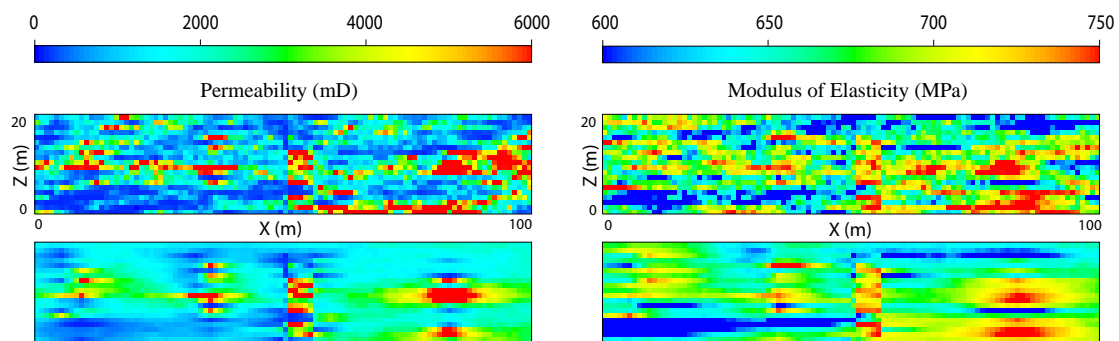


**Figure 15: Reference population (top) and E-type mean of the initial 100 stochastic realizations.**

Although visual inspection is not a fair criterion for evaluating data reproduction, some of the results are represented visually in 2D to show the progress of the prediction process in the adjusted data. Fig. 15 shows the E-type mean of the 100 stochastic realizations for both rock properties against the reference (truth) models. It is clear that the average of realizations (E-type mean) has been effectively modelled while honouring the well data. However, the truth model is too noisy and more effort is needed to build a similar model.

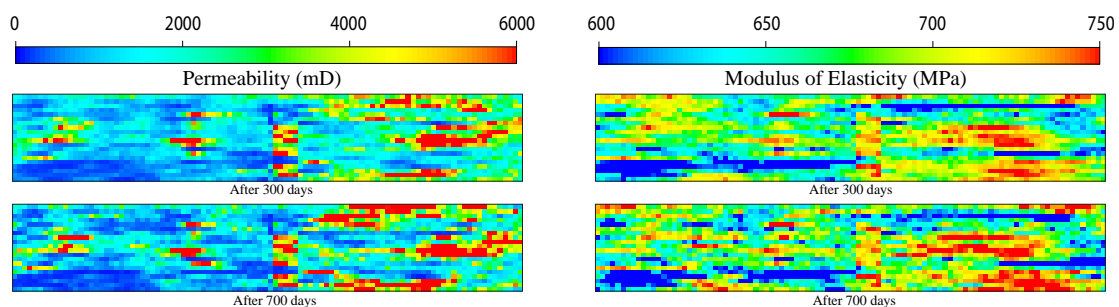


**Figure 16: Assimilated static data after 300 and 700 days in the third strategy: permeability (left) and modulus of elasticity (right).**

The pixel plots of the predicted permeability and modulus of elasticity are shown in Fig. 16 for two of the time steps. Fig. 16 is the result of data assimilation after 300 and 700 days when the third strategy is applied. These models should eventually be similar to the reference models in Fig. 15. The comparison between the reference models and assimilated models show that both data sets are predicted with higher resolution as the simulation proceeds. For the first strategy, however, the reference model changes over time.

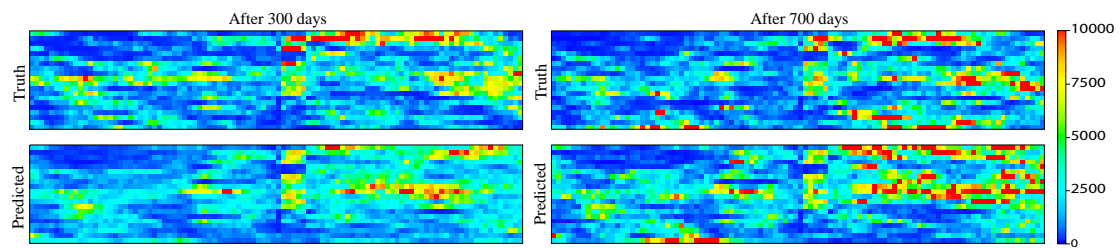


**Figure 17: Comparison between the truth and the assimilated dynamic data in mD after 300 and 700 days in the first strategy.**

Fig. 17 has plotted the assimilated dynamic data versus the truth of each time step for the first strategy. It is difficult to visually recognize the quality of assimilation, but generally speaking, the data is not far from what it should be. This means that depending on how much error or mismatch is accepted, the first strategy is always an option.

## CASE STUDY II: SINGLE SHALLOW SAGD

In the first case study, the focus was on the sources of data and the simulation technique. It was shown that the best results are produced when geomechanical and flow sources of data are used with a coupled simulator. Other combinations (the first and second strategies) are also helpful based on the purpose of the process. In the second case study, only the third strategy was employed. A shallow SAGD was simulated using stochastic models and operated with a single well pair. The objective of this case study was to assess the type of geomechanical data. There are many types of geomechanical data that can be observed, such as displacement, strain, stress, and geometry changes. However, to maintain consistency in this study, the EnKF was employed with displacement monitoring data, albeit in different locations. This case

study was meant to determine where and in which direction it is better to monitor displacement data.

### Problem Framework and Settings

Flow-geomechanical coupled simulations were used in this case study. The geometry and boundaries of the model were similar to those of the first case study, but borehole pairs 1 and 3 were removed from the model (see Fig. 6). The operation pressure and all the flow and geomechanical rock properties were identical to the first case study. This time, stochastic models were not constrained to the well data, and purely synthetic data was generated as a result. The other difference is that in this problem, only 25 realizations were stochastically simulated to save the computational time.

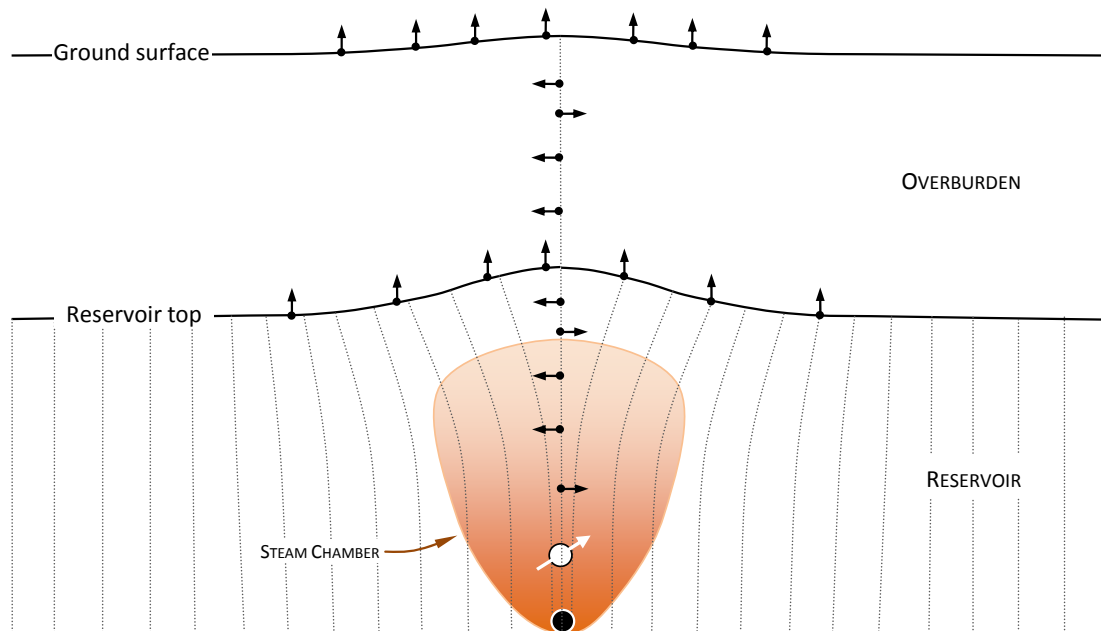


**Figure 18: Displacement monitoring at three locations: vertical displacement on the ground surface as well as the reservoir top and horizontal displacement at the centre line of the model.**

In total, 10 variables were obtained. Production and injection rates were monitored for the single well pair. On the other side, displacement was recorded in 8 locations. Three different scenarios were assigned for monitoring displacements to compare the effect of observing data on history matching and data assimilation: (1) vertical displacement on the ground surface, (2) vertical displacement on top of the reservoir, and (3) horizontal displacement at the horizontal line from the bottom of the reservoir

up to the ground surface. These sources are schematically illustrated in Fig. 18. It is clear that the reservoir top experiences larger vertical displacement than does the ground surface. Displacement trends were the same at both locations. In addition, there was a short time delay in geomechanical response on the ground surface compared to the reservoir top. Unlike vertical displacement, horizontal displacement does not follow a certain trend and can vary in magnitude and direction. Horizontal displacement response happens immediately in the reservoir and with a short delay in the overburden layer.

Costs related to providing data from the three locations described above are not equal. The locations also differ in terms of sensor devices responsible for monitoring. These are issues to be considered when comparing the results of such a case study, but are not covered in this paper.

### History Matching Results

Fig. 19 plots the primary flow histories resulting from the 25 stochastic realizations when the history matching algorithm is not applied. It can be seen that production and injection vary widely, most probably because of removal of the well data for stochastic model generation. It should be noted that only production and injection rates are monitored. The SOR is plotted using the other two curves and is not considered a variable in history matching.

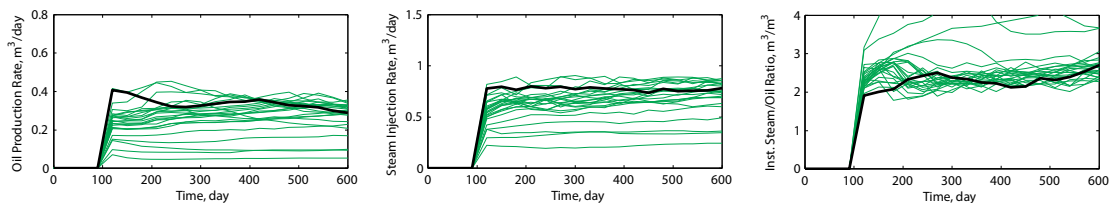


**Figure 19: Comparing the simulation results of the 25 stochastic realizations before history matching.**

Fig. 20 has included the results of the history matching algorithm using the EnKF. The best history matching is seen in the first column, for which vertical displacement data was monitored on the ground surface. For the second column, vertical displacement data was monitored at the reservoir top. The matching is clearly biased and can be generally accepted with lower accuracy. The results in the third column

are quite the same as the second column with some noise and spike. The third column is for cases in which horizontal displacement is monitored. In general, the EnKF has effectively matched all of the ensembles closely with the reference history. However, the type of monitoring data has evidently influenced the history matching process. The major differences between the data sources can be explained by the closeness of the sensors to the steam chamber, where most of the geomechanical changes occurred. Among the three sources, the vertical displacement on the ground surface is the least diverse during the SAGD process. The other two sources have sensors near the steam chamber, causing significant variations in the observations of those sensors.

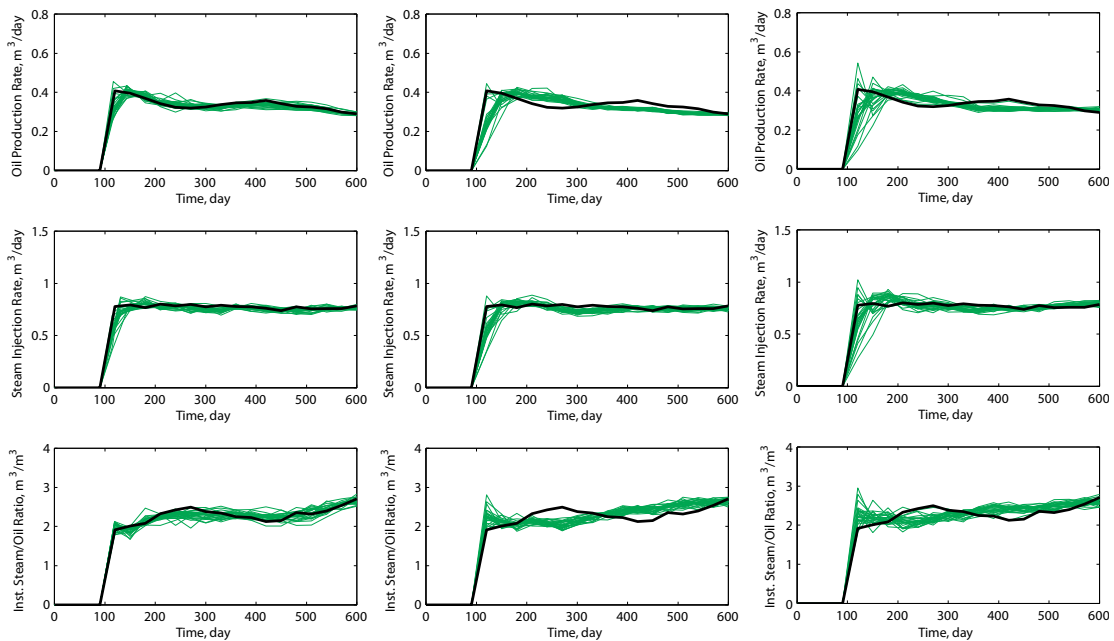


**Figure 20: Results of history matching using the EnKF. From left to right: with (1) vertical displacement data on the ground surface, (2) vertical displacement data at the reservoir top, and (3) horizontal displacement at the centre line.**

The variation of geomechanical responses with and without applying the EnKF algorithm and reservoir observation has been plotted in Fig. 21. The first row is the result history of displacement using the initial ensembles. It is obvious that the vertical displacement on the ground surface has a regular shape that has been reproduced in different runs. This trend is seen less on top of the reservoir, and in the horizontal displacement no clear trend can be depicted. Fig. 21 reflects that history matching with the large variation in the monitoring data has had the least success.

The results in Fig. 21, however, reveal that the EnKF more or less captured the trend or an average of the monitoring string data. The initial ensemble results with a high level of uncertainty were effectively re-estimated when the monitoring data was used. From Fig. 21, one can conclude that the response elements, i.e. the type of geomechanical monitoring data, play an important role in history matching.

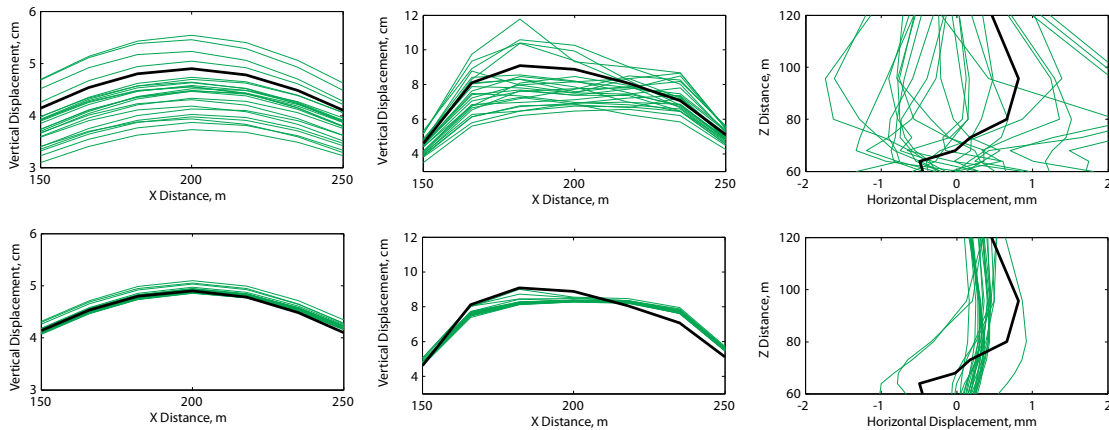


**Figure 21: Displacement histories before (top) and after (bottom) applying the EnKF algorithm. From left to right: vertical displacement on the ground surface, vertical displacement at reservoir top, and horizontal displacement after 700 days.**

While the EnKF does not have any limitations on the probabilistic distribution of the monitoring data, it seems that data that keeps its distribution shape at different stages of observation is better for monitoring. The quality of the history matching in the second column of Fig. 21 might be sufficiently improved using localization algorithms. However, it is hard to imagine modifications that could create better history matching in the horizontal displacement.

### Data Reproduction Results

Fig. 22 shows the results of data assimilation for each geomechanical monitoring data source in two columns, for permeability and porosity. For comparison, the figure also includes the reference models and cell-based average models of all of the initial realizations.

In data assimilation, again, the highest-quality results are those of the coupling simulation with the vertical displacement on the ground surface. The population of the modulus of elasticity is better reproduced, however, than that of permeability.

This difference is explained by the sensitivity of the physics of SAGD with these two properties. The geomechanical behavior of the reservoir is more sensitive to small variations in magnitude of modulus of elasticity; while small changes in permeability do not greatly change the flow process inside the reservoir. Therefore, the covariance matrix can better represent the geomechanical phase than the flow process. If it is assumed that the sensitivity assumption is the only effective parameter, using supplementary ensembles to increase the flow-related members in each individual ensemble would allow the algorithm to better capture the correlation between the response and the estimated properties. Otherwise, it would be useful to use nonlinear methods to construct the covariance matrix or to employ linearization and inflation techniques. Evensen (2009) is a good reference to diagnose the problem.

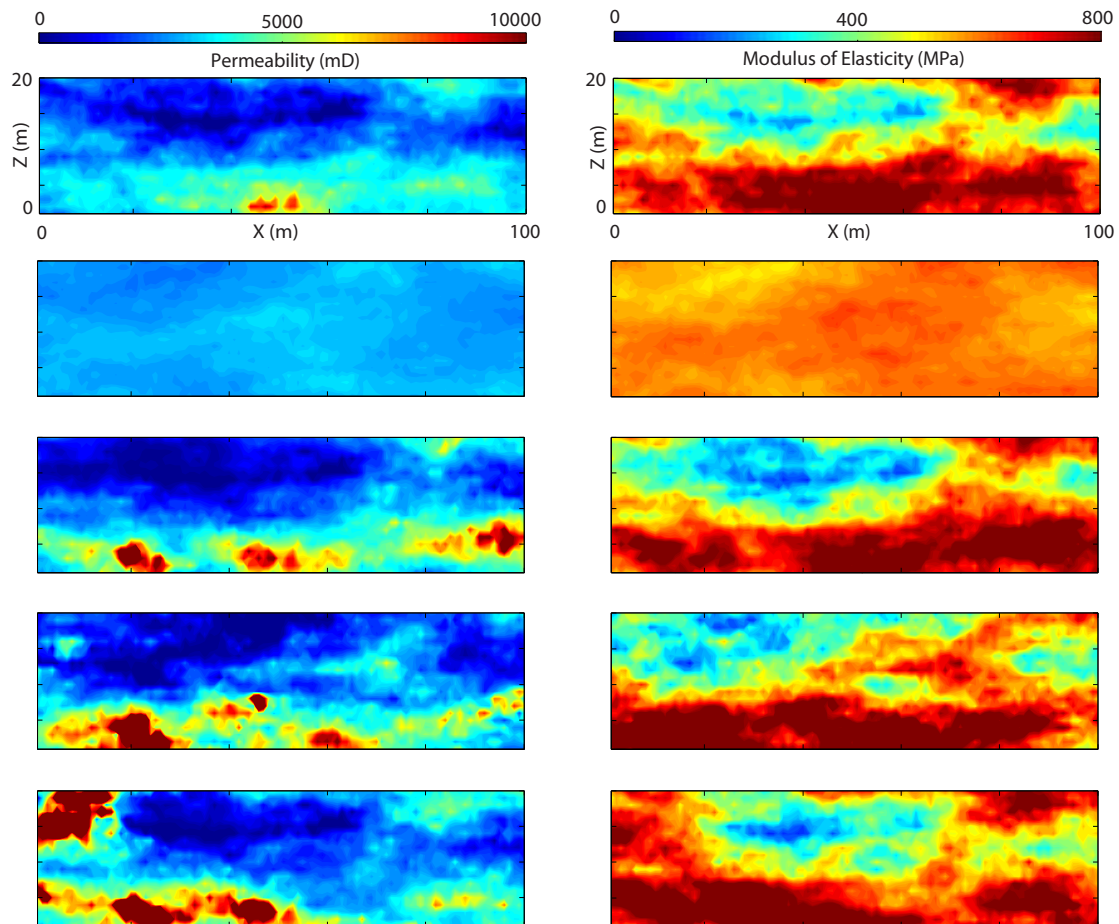


**Figure 22: Data assimilation results after 700 days of history matching; from top to bottom: reference model, E-type mean of the 25 stochastic models, data assimilation results using vertical displacement at ground surface, vertical displacement at reservoir top, and horizontal displacement.**

## SUMMARY AND CONCLUSIONS

Geomechanics is generally active in petroleum engineering parallel to the flow process, and influences recovery and operational strategies. In some cases, geomechanical behaviour of the reservoir critically affects production and reservoir performance. Hence, it must be considered and numerically modelled for reservoir treatment and decision making purposes. In some other cases, geomechanics is negligible. Regardless of the importance of geomechanics to the process, it is always part of the overall physics and reacts to any changes in the reservoir. For this reason, similar to the flow responses that are crucial for prior estimation and future forecasting, geomechanical observations can also provide valuable information on reservoir behaviour. Geomechanical observations address the intensity of the physical behaviour of the reservoir and implicitly display different aspects of the recovery process happening inside it.

In this study, the EnKF, an effective history matching algorithm was chosen to perform continuous (automatic) updating of reservoir simulation models to show the role of geomechanical observation in history matching. The EnKF is promising for petroleum engineering and needs minimal code development. An iterative flow-geomechanical coupled simulator was assembled using two commercial flow and geomechanical software packages and combined with the EnKF. Since geomechanical behaviour of reservoirs under thermal recovery processes is usually significant, two SAGD case studies were designed. The synthetic models generated closely matched results of a pilot test on unconventional reservoirs in Canada, UTF-A. In the first case study, three strategies were tested to understand the degree to which geomechanical observation can help both history matching and data assimilation (property estimation) processes. The second case study investigated which kind of geomechanical monitoring data is best among three displacement-based sources. In all of the analysis, no modifications were made to maintain consistency across results for comparison purposes. Acknowledging the limited analysis performed in the two case studies, the following conclusions are drawn from the study:

- Monitoring geomechanical data effectively improves history matching when proper numerical simulations are employed to consider flow and geomechanics at the same time.
- When a coupled simulation is used with a data assimilation algorithm, it is meaningful to forecast the recovery process at any time step, as at each step, the algorithm updates the static model and the coupled simulation provides the dynamic model. Therefore, using the latest updated static model, the coupled simulation can predict future production as well as the dynamic model of the reservoir.
- When a flow simulator is used, the dynamic model is estimated at each time step. The results show that in general, the accuracy of the predicted dynamic model is not as generally accepted as that of the coupled simulation. Because the dynamic nature of some rock properties is defined by geomechanical changes, an individual flow simulator cannot properly predict the future, even with the most accurate prior model.
- Geomechanical observation data have different values when in use with the data assimilation algorithm. Vertical displacement at the ground surface is shown to be a better option than horizontal displacement or vertical displacement at the reservoir top. Although further investigation is needed to understand physical reasons, from a mathematical point of view, we are suspicious of the trend between the geomechanical monitoring data. It seems that monitoring data with the smoothest historical deviation is probably more helpful when the EnKF is employed.

## **SUGGESTIONS AND FURTHER STUDIES**

In this study, the results of a flow-geomechanical simulation were taken as the truth model and the same simulator was employed to capture the truth model. In lack of real data, we were hoping to decrease the effect of this assumption by injecting noise into the data. For the next step, we suggest using real data. In that case, coupled simulation would not necessarily represent the physics of the problem, and immense

system noise would exist instead. Moreover, from a geomechanical perspective, algorithm modifications such as localization must be developed to improve the results when no ideal data or simulator is used. Another simplification made in this study was the rerunning of both simulators from the beginning of the process after each update. In place of the current procedure, a mechanism must be defined to handle the balance of efficiency and accuracy. Finally, a combined mathematical-experimental investigation is suggested to study and propose efficient geomechanical types of data for different recovery processes. These suggestions have been partially studied in the past five years but any ongoing worldwide research program is still in the primary stages.

## REFERENCE

- Agar, J.G., Morgenstern, N.R. and Scott, J.D. 1986. Shear strength and stress-strain behaviour of Athabasca oil sand at elevated temperatures and pressures. *Canadian Geotechnical Journal*. 24: 1-10.
- Azad, A. and Chalaturnyk, R.J. 2011. Numerical study of SAGD: geomechanical-flow coupling for Athabasca oil sands reservoirs, *Proc.*, the 45<sup>th</sup> US Rock Mechanics symposium, 1-14.
- Chalaturnyk, R.J. 1996. Geomechanics of the Steam-Assisted Gravity Drainage Process in Heavy Oil Reservoirs. PhD dissertation, University of Alberta, Edmonton, Canada.
- Chalaturnyk, R.J. and Li, P. 2004. When is it important to consider geomechanics in SAGD operations? *Journal of Canadian Petroleum Technology* 43(4): 53-61.
- Chalaturnyk, R.J. and Scott, J.D. 1995. Geomechanics Issues of Steam Assisted Gravity Drainage, Paper SPE 30280 presented at the International Heavy Oil Symposium, Calgary, Alberta, Canada, 19-21 June, doi: 10.2118/30280-MS.
- Chang, H., Chen, Y., and Zhang, D. 2010. Data Assimilation of Coupled Fluid Flow and Geomechanics Using the Ensemble Kalman Filter. *SPE Journal* 15(2): 382-394. SPE 118963-PA. doi: 10.2118/118963-PA.
- Chen, Y. 2008. Ensemble-Based Closed-Loop Production Optimization. PhD dissertation, University of Oklahoma, Norman, Oklahoma, USA.
- Chitrlekha, S.B., Trivedi, J.J. and Shah, S.L. 2010. Application of the Ensemble Kalman Filter for Characterization and History Matching of Unconventional Oil Reservoirs, SPE 137480-MS presented at the Canadian Unconventional Resources

and International Petroleum Conference, Calgary, Alberta, Canada, 19-21 October, doi: 10.2118/137480-MS.

Collins, P.M. 2007. Geomechanical effects on the SAGD process. *SPE Reservoir Evaluation & Engineering* 10(4): 367-375. SPE 97905-PA. doi: 10.2118/97905-PA.

Deutsch, C.V. and Journel, A.G. 1997. *GSLIB: Geostatistical Software Library and User's Guide*. Oxford University Press, USA.

Du, J. and Wong, R.C.K. 2007. Coupled geomechanics-reservoir simulation of UTF phase A project using a full permeability tensor. *Proc.*, the Petroleum Society's 8<sup>th</sup> Canadian International Petroleum Conference, 1-16.

Dusseault, M. and Morgenstern, N.R. 1978. Shear strength of Atabasca oil sand. *Canadian Geotechnical Journal* 15: 216-238.

Edmunds, N.R., Kovalsky, J.A., Gittins, S.D. and Pennacchioli, E.D. 1994. Review of phase A steam-assisted gravity-drainage test. *SPE Reservoir Engineering* 9(2): SPE 21529-PA. doi: 119-124. 10.2118/21529-PA.

Evensen, G. 2009. The ensemble Kalman filter for combined state and parameter. *IEEE Control Systems Magazine* 29(3): 82-104.

Gu, Y. 2006. History Matching Production Data Using the Ensemble Kalman Filter. PhD dissertation, University of Oklahoma, Norman, Oklahoma, USA.

Gu, Y. and Oliver, S.O. 2006. The ensemble Kalman filter for continuous updating of reservoir simulation models. *Journal of Energy Resources Technology* 128: 79-87.

Gul, A., Nejadi, S., Shah, S.L. and Trivedi, J.J. 2011. Make use of dynamic data - a constraint based EnKF for SAGD reservoir characterization and production management, *Proc.*, the 2011 World Heavy Oil Congress, 1-14.

Kim, J., Tchelepi, H.A. and Juanes, R. 2011. Stability, Accuracy, and Efficiency of Sequential Methods for Coupled Flow and Geomechanics. *SPE Journal* 16(2): 249-262. SPE 119084-PA. doi: 10.2118/119084-PA.

Kosar, K.M., Scott, J.D. and Morgenstern, N.R. 1987. Testing to determine the geotechnical properties of oil sands. *Proc.*, the 38<sup>th</sup> Annual Technical Meeting of the Petroleum Society of CIM, Calgary, 995-1010.

Li, P. 2006. Numerical Simulation of the SAGD Process Coupled With Geomechanical Behaviour. PhD dissertation, University of Alberta, Edmonton, Canada.

Li, P. and Chalaturnyk, R.J. 2009. History match of the UTF Phase A project with coupled reservoir geomechanical simulation. *The Journal of Canadian Petroleum Technology* 48(1): 29-35.

- Nævdal, G., Johnsen, L.M., Aanonsen, S.I. and Vefring, E.H. 2005. Reservoir Monitoring and Continuous Model Updating Using Ensemble Kalman Filter. *SPE Journal* 10(1): 66-74. SPE 84372-PA. doi: 10.2118/84372-PA.
- Oldakowski, K. 1994. Absolute Permeability of Oil Sands. PhD dissertation, University of Alberta, Edmonton, Canada.
- Samieh, A.M. and Wong, R.C.K. 1997. Deformation of Athabasca oil sand at low effective stresses under varying boundary conditions. *Canadian Geotechnical Journal* 34: 985-990.
- Scott, J.D., Proskin, S.A. and D.P. Adhikary. 1994. Volume and permeability changes associated with steam stimulation in an oil sands reservoir. *Journal of Canadian Petroleum Technology* 33(7): 44-52.
- Scott, J.D. and Seto, A.C. 1986. Thermal property measurements on oil sands. *Journal of Canadian Petroleum Technology* 25(6): 70-77.
- Settari, A., Walters, D.A. and Behie, G.A. 2001. Use of coupled reservoir and geomechanical modelling for integrated reservoir analysis and management. *Journal of Canadian Petroleum Technology* 40(12): 55-61.
- Tortike, W.S. 1991. Numerical Simulation of Thermal, Multiphase Fluid Flow in an Elastoplastic Deforming Oil Reservoir. PhD dissertation, University of Alberta, Edmonton, Canada.
- Touhidi-Baghini, A. 1998. Absolute Permeability of McMurray Formation Oil Sands at Low Confining Stresses. PhD dissertation, University of Alberta, Edmonton, Canada.
- Tran, D., Nghiem, L. and Buchanan, L. 2005. Improved Iterative Coupling of Geomechanics With Reservoir Simulation. SPE 93244-MS presented at the SPE Reservoir Simulation Symposium, The Woodlands, Texas, USA, 31 January-2 February, doi: 10.2118/93244-MS.

# CHAPTER 8: CONCLUSION AND RECOMMENDATIONS FOR FURTHER STUDIES

## **SUMMARY AND CONCLUSIONS**

The overall objective of this research work was to investigate the potential of geomechanical analysis and observation in SAGD process when real-time monitoring data is provided. Three conceptual methodologies were taken to tackle the goal:

- (1) Current geomechanical coupling practice for modelling a SAGD process suggests combining a numerical multiphase flow and a (geo)mechanical simulator. This technique, though reasonably correct and inclusive of full physics, is time-consuming for history matching purposes. When real-time monitoring data is available, it is almost impossible to update numerical models in real-time. Therefore, two low-order analytical models that can capture essential parts of physics with certain levels of divergence were developed for fast history matching. Method of slices was considered to improve the Butler/Reis drainage model. At the same time, the limit equilibrium method of analysis was utilized to consider geomechanics. The model, however, was modified further by circular steam chamber geometry and the geomechanical module was replaced by a multiplier coefficient, GIF. The final model was then used to show how the idea of replacing numerical coupling methods with an analytical coupling model can be effective for two case studies, UTF pilot test A and B. The advantage of this idea is that the fast speed run time is served by a physics-based theory, not a 'black-box' algorithm. This long term goal of this simulator is to join with an optimization methodology, providing a powerful

tool for fast on-line decision making stages in an ongoing project. Generally, history matching results showed that analytical physics-based models can be used as an alternative to numerical simulators. Since all of the variables have their own physical meaning, uncertainty analysis within the system or within the prediction is much more promising than other proxies. The required resolution and uncertainty of the results determines the application of the model in different stages of a SAGD project.

- (2) The application of analytical physics-based models was investigated as the second methodology of this research for reservoir characterization. The methodology benefitted from analytical proxy models for SAGD and adopted geomechanical considerations in modelling. In a synthetic case study with some random stochastic populations for modelling heterogeneity in rock properties, it was shown that EKF can be effectively employed as an estimation algorithm for ranking stochastic models. The simulation results confirmed that the application of analytical proxy models along with EKF is a promising and fast method to reduce uncertainty in reservoir characterization. The methodology can be used parallel to full physics reservoir simulations to enhance history matching.
- (3) The EnKF, an effective history matching algorithm was chosen to perform continuous (automatic) updating of reservoir simulation models to show the role of geomechanical observation in history matching. The EnKF is promising for petroleum engineering and needs minimal code development. An iterative flow-geomechanical coupled simulator was assembled using two commercial flow and geomechanical software packages and combined with the EnKF. Since geomechanical behaviour of reservoirs under thermal recovery processes is usually significant, two SAGD case studies were designed. The synthetic models generated closely matched results of a pilot test on unconventional reservoirs in Canada, UTF-A. It was concluded from the results that monitoring geomechanical data effectively improves history matching when proper numerical simulations are employed to consider flow and geomechanics at the same time. Also, it was observed that geomechanical observation data have different values when in use with the data assimilation algorithm.

## PROPOSED PROCEDURE FOR COMBINING MODELS

The original idea that has been followed in this thesis is combining models with different resolutions in a single simulation unit. Depending on the resolution of data and transfer interval, an appropriate model handles working with data interactively within the simulation unit. Although the methodology of this combination was never discussed and explored in details throughout this research due to the lack of data, the following procedure is proposed here. This can be taken as the foundation of further studies. As it is shown in Fig. 1, three circles have been assembled in a single processor each representing a single simulator.

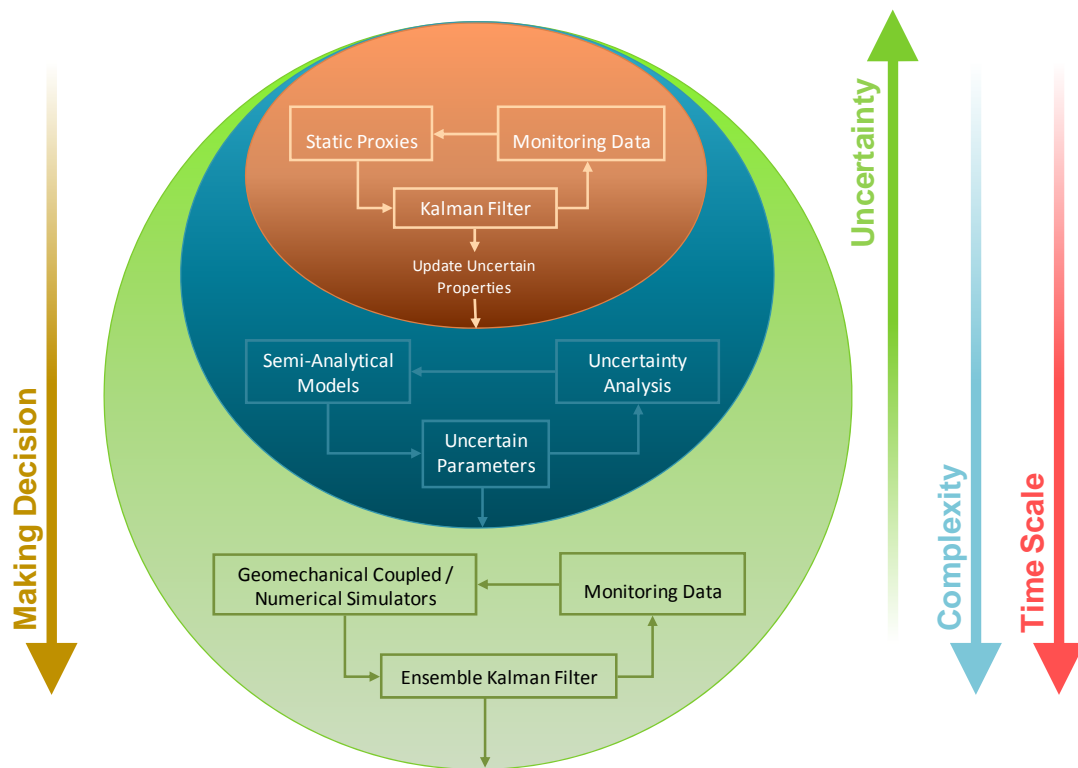


**Figure 1: arrangement of models with different resolutions in the simulation unit.**

From top to bottom, the arrows show that uncertainty is reduced while complexity is induced. Also, decisions are made at the numerical coupled simulation circle, third from the top, in longer time scale. The first circle is responsible for raking and updating the stochastic realizations. The updated realizations feed the second circle where uncertainty is quantified. These two stages are done so fast but in low

resolution. While these two stages are under run the third circle which is time consuming is updating the reservoir. The results of the third circle can periodically injected into the first and the second circle for fast uncertainty analysis mostly in operational evaluation. However, critical decisions are recommended to be made in at the bottom of the third circle.